DEVELOPMENT OF ROBUST BIOFUNCTIONAL INTERFACES

DEVELOPMENT OF ROBUST BIOFUNCTIONAL INTERFACES FOR APPLICATIONS IN SELF-CLEANING SURFACES, LAB-ON-A-CHIP SYSTEMS, AND DIAGNOSTICS

By AMID SHAKERI, B.Sc., M.Sc.

A Thesis Submitted to the School of Graduate Studies in Partial Fulfilment of the Requirements for the Degree Doctor of Philosophy

Doctor of Philosophy (2020), Department of Mechanical Engineering, McMaster University, Hamilton, Ontario

TITLE: Development of Robust Biofunctional Interfaces for Applications in Self-Cleaning Surfaces, Lab-On-A-Chip Systems, and Diagnostics

AUTHOR: Amid Shakeri**,** B.Sc., M.Sc**.**

SUPERVISOR: Dr. Tohid Didar

PAGES: xxvi, 257

Lay Abstract

The key goal of this thesis is to provide new strategies for preparation of robust and durable biointerfaces that could be employed for many biomedical devices such as self-cleaningcoatings, microfluidics, point-of-care diagnostics, biomedical assays, and biosensors in order to enhance their efficiency, sensitivity, and precision. The introduced surface biofunctionalization methods are straightforward to use and do not require multiple wet-chemistry steps and incubation times, making them suitable for mass production and high throughput demands. Moreover, the introduced surface coating strategies allow for creation of antibody/protein micro-patterns covalently bound onto a biomolecule-repellent surface. The repellent property of the surfaces is resulted from infusion of an FDA-approved lubricant into the surface of a chemically modified substrate. While the surface repellency can effectively prevent non-specific adhesion of biomolecules, the patterned antibodies can locally capture the desired analyte, making them a great candidate for biosensing.

Abstract

Biofunctional interfaces capable of anchoring biomolecules and nanoparticles of interest onto a platform are the key components of many biomedical assays, clinical pathologies, as well as antibacterial and antiviral surfaces. In an ideal biofunctional surface, bio-entities and particles are covalently immobilized on a substrate in order to provide robustness and long-term stability. Nonetheless, most of the reported covalent immobilization strategies incorporate complex wet-chemical steps and long incubation times hindering their implementation for mass production and commercialization. Another essential factor in the biointerface preparation, specially with regard to biosensors and diagnostic applications, is utilization of an efficient and durable blocking agent that can inhibit non-specific adsorption of biomolecules thereby enhancing the sensitivity of sensors by diminishing the level of background noise. Many of the commonly used blocking agents lack proper prevention of non-specific adsorption in complex fluids. In addition, most of these agents are physically attached to surfaces making them unreliable for long-term usage in harsh environments (*i.e.* where shear stresses above 50 dyn/cm^2 or strong washing buffers are involved).

This thesis presents novel and versatile strategies to covalently immobilize nanoparticles and biomolecules on substrates. The new surface coating techniques are first implemented for robust attachment of TiO_2 nanoparticles onto ceramic tiles providing self-cleaning properties. Further, we utilize similar strategies to covalently immobilize proteins and culture cells in microfluidic channels either as a full surface coating or as micropatterns of interest. The new strategies allow us to obtain adhesion of ~ 400 cells/mm^2 in microfluidic channels after only 1-day incubation, which is not

achievable by the conventional methods. Moreover, we show the possibility of covalently micropatterning of biomolecules on lubricant-infused surfaces (LISs) so as to attain a new class of biofunctional LISs. By integration of these surfaces into a biosensing platform, we are able to detect interleukin 6 (IL-6) in a complex biofluid of human whole plasma with a limit of detection (LOD) of 0.5 $pg.mL^{-1}$. This LOD is significantly lower than the smallest reported IL-6 LOD in plasma, 23 $pg\ mL^{-1}$, using a complex electrochemical system. The higher sensitivity of our developed biosensor can be attributed to the distinguish capability of biofunctional LISs in preventing non-specific adhesion of biomolecules compared to other blocking agents.

Acknowledgements

I would like to express my sincere gratitude to my supervisor, Dr. Tohid Didar, for giving me the opportunity to be a member of his research group and benefit from his precious guidance, full support, and persistent motivation and encouragement throughout my PhD study.

I wish to express my deepest regards to my lovely wife, Yasamin. Without her endless love and support, continued sacrifices and great patience along this journey, I would not be able to be in this place. My parents, Masoud and Farideh, deserve special thanks for their constant support and encouragement throughout my life.

Finally, I would like to recognize the invaluable assistance of my friends in Didar lab whose inputs enormously helped me to fulfill the goals of my project.

Table of Contents

List of Figures

List of Tables

List of all Abbreviations

1D: 1-dimensional

2D: 2-dimentional

4-AS: 4-Aminostyrene

AEAPTMS: N-[3-(Trimethoxysilyl)propyl]ethylenediamine

APTES: (3-aminopropyl)triethoxysilane

APTMS: (3-aminopropyl)trimethoxysilane

BSA: Bovine serum albumin

COC: Cyclic olefin copolymer

CPTES: (3-cyanopropyl)triethoxysilane

CVD: Chemical vapor deposition

DAP: 1,3-diaminopropane

DCC: N', N’-Dicyclohexyl carbodiimide

DIC: N,N'-Diisopropyl carbodiimide

EDC: 1-ethyl-3-(-3-dimethylaminopropyl) carbodiimide hydrochloride

GLYMO: Glycidyloxypropyl)trimethoxysilane

GMBS: N-γ-maleimidobutyryl-oxysuccinimide ester

HMD: Hexamethylenediamine

HPG: Hyperbranched polyglycerol

IFA: Immunofluorescence assays

IL-6: Interleukin 6

IPTMS: 3-isocyanatopropyltrimethoxysilane

LISs: Lubricant-infused surfaces

LOD: Limit of detection

LPD: Liquid phase deposition

MPTMS: 3-mercaptopropyl trimethoxysilane

NHS: N-hydroxysuccinimide

NSA: Non-specific adsorption

PAA: Poly(acrylic acid)

PAH: Poly(allylamine hydrochloride)

PAM: Polyacrylamide

PAN: Polyacrylonitrile

PC: Polycarbonates

PDMS: Polydimethylsiloxane

PEG: Poly(ethylene glycol)

PEG-DA: Poly(ethylene glycol) diacrylate

PEI: Polyethyleneimine

PMMA: Poly(methyl methacrylate)

PS: Polystyrene

PVA: Polyvinyl alcohol

SAM: Self-assembled monolayer

UVO: Ultraviolet/Ozone

Declaration of Academic Achievement

- Chapter 1, “Introduction”, was drafted by Amid Shakeri and reviewed to the final version by Dr. Tohid Didar.
- In chapter 2, “Biofunctionalization of Glass and Paper-based Microfluidic Devices; a Review”, Amid Shakeri performed the literature review and data gathering and wrote the initial draft of the review paper with help from Noor Abu Jarad and Ashlyn Leung under supervision of Dr. Tohid Didar. The manuscript was reviewed to the final version by Dr. Leyla Soleymani and Dr. Tohid Didar.
- In chapter 3, “Self-Cleaning Ceramic Tiles Produced via Stable Coating of TiO_2 Nanoparticles”, Dr. Tohid Didar conceived the research and supervised the experiments. Amid Shakeri performed the experiments, data validation, data visualization, and analysis with help from Darren Yip. Amid Shakeri wrote the manuscript with inputs from Dr. Tohid Didar and Dr. Mehdi Sanjari. Maryam Badv conducted the FT-IR tests. Sara M. Imani performed the AFM analyses.
- In chapter 4, “Plasma-induced Covalent Immobilization and Patterning of Bioactive Species in Microfluidic Devices”, Dr. Tohid Didar conceived the research and supervised the experiments. Amid Shakeri performed the experiments, data validation, data visualization, and analysis with help from Sara M. Imani, Eric Chen, Hanie Yousefi, and Raed Shabir. Amid Shakeri wrote the manuscript with input from Dr. Tohid Didar.
- In chapter 5, “Antibody Micropatterned Lubricant-infused Biosensors Enable Sub-picogram Immunofluorescence Detection of Interleukin 6 In Human Whole

Plasma", Dr. Tohid Didar conceived the research and supervised the experiments. Amid Shakeri performed the experiments, data validation, data visualization, and analysis with help from Noor Abu Jarad, Shadman Khan, and Ashlyn Leung. The image segmentation was performed with help from Simeng Chen. Amid Shakeri wrote the manuscript with input from Jeff Terryberry and Dr. Tohid Didar.

- Chapter 6, "Conclusions and Future Direction" was drafted by Amid Shakeri and reviewed to the final version by Dr. Tohid Didar.

Chapter 1: Introduction

1.1 Literature Review

1.1.1 Importance of Biofunctionalization

Nowadays, progression and viability of many state-of-the-art biomedical assays, clinical pathologies, and medical implants hinge upon one decisive factor; advancements in the design of bio-functional interfaces [1,2]. An appropriate method of conjugation of substrates and biological entities with functional groups substantially impact the efficacy of biological devices in various aspects including sensitivity and specificity, robustness and durability, as well as repeatability and multiplexing. Proper design of interfaces coated with biomolecules, cells, viruses and nanoparticles would result in developing interfaces with superior capabilities for drug delivery, anti-fouling, anti-chromogenicity, self-cleaning as well as evaluating and eliminating pollutants in environmental and agricultural applications [3–5]. Furthermore, in cellular and biochemical assays where cellular processes are detected and quantified, proper surface functionalization allows investigators to precisely control protein binding and guide cell growth [6,7].

Immunodiagnostic and biosensor industries are progressively looking for innovative approaches to modify the surface functionalization process for enhancing the sensitivity

and precision of sensors used in healthcare monitoring, on-chip screening for disease and point-of-care diagnostic devices. The global value of the immunoassays and analyzers market was estimated at 18.5 billion USD in 2019 with some experts projecting a value of 19.5 billion USD in 2020 [8]. Both the size and growth rate of this sector show the compelling opportunity for investment in technological development of this industry. New biofunctional interfaces capable of selectively anchoring the desired biomolecules onto a sensor enable the detection of target analytes in complex fluids such as blood, plasma and urine using low-cost and straightforward biosensing techniques [1,2,9]. Improved biointerfaces bring about higher precision and lower limits of detection (LODs) for target bio-species which is necessary for early diagnostics applications.

Biofunctional surfaces or more generically functional surfaces could also be utilized to covalently bind micro/nano particles as well as other functional entities to the substrates [10,11]. In particular, TiO_2 nanoparticles with great photocatalytic properties are widely employed in environmental and purification applications [12]. Creating a strong and durable TiO_2 coating on different substrates for outdoor usage, has always been a technical issue which can be well addressed by introducing cost-effective functional surfaces.

Moreover, novel biofunctional interfaces have been paved the way for implementation of microfluidic devices and lab-on-a-chip systems in the fast-evolving biomedical industry, bestowing simplicity, accuracy, and cost-effectiveness upon the conventional devices [13–21]. Microfluidic devices represent a breakthrough in hemostasis monitoring and point-of-care diagnostics owing to their exceptional superiorities such as ability for miniaturization and manipulation of fluids in microscale [22–25]. Moreover, fabrication of microfluidics with transparent materials enables researchers to incorporate simple optical or fluorescence imaging techniques for biological analyses [26,27]. Obtaining controlled immobilization of biomolecules inside the microchannels is highly challenging considering the size and complexity of the microchannels network as well as the aggressive conditions required for microfluidics fabrication (*e.g.* use of elevated temperatures, plasma etching, etc.) [28–31]. A robust interaction between the microchannel surface and the bioentity of interest could be achieved via chemically reactive groups induced inside the channels allowing for fabrication of durable point-of-care diagnostic devices as well as 2D or 3D cell culture for tissue- and organ-on-a-chip applications [32–41].

In general, an ideal biointerface amenable for biological applications should fulfill the following requirements: (1) specificity to the desired biomolecules and prevention of non-specific adsorption (NSA) via applying a proper blocking agent; (2) capability for

robust immobilization of biomolecule/nanoparticles which could be achieved by covalent attachments; (3) maintaining the transparency and optical properties of the device where optical microscopic techniques are to be used for analysis; (4) good stability at the operating temperatures.

1.1.2 Immobilization of the Biomolecules

In the non-covalent immobilization fashion, biomolecules can attach onto different substrates through electrostatic forces and hydrogen bonding [42,43], van der Waals forces as well as hydrophobic interactions in naturally hydrophobic substrates such as polydimethylsiloxane (PDMS) and poly(methyl methacrylate) (PMMA) [42,44,45]. Non-covalent immobilization could be obtained by simple incubation of the desired biomolecule on the substrate. However, engineering the surface wettability and surface charge is sometimes required to facilitate the non-covalent attachment. For instance, hydroxylation of the surface and amine treatment could promote electrostatic interactions by creating negatively charged and positively charged moieties on the substrates, respectively [43,46,47]. In an appropriate pH, the charged surfaces can absorb biomolecules with a net electrical charge such as negatively charged bovine serum albumin (BSA) or positively charged avidin. Physical entrapment of the biomolecules by creating biocompatible porous surfaces and embedded microwells [48–50] as well as use of magnetic field [51] are other reported approaches for non-

covalent immobilization. Although non-covalent attachment strategies are usually straightforward to be employed, they do not provide robust bio-interfaces and can increase the chance of biomolecules detachment. This could limit the applicability of these substrates for long-term usage in biosensors as well as microfluidics where high shear stresses (above 50 dyn/cm^2) could result in biomolecule dissociation. Moreover, in hydrophobic absorption methods, dehydration and denaturation of the absorbed biomolecules is plausible [42,52]. Another disadvantage associated with the hydrophobic immobilization technique is biomolecules NSA which could deteriorate the sensitivity in biosensor applications. In microfluidics, hydrophobicity of the substrate can also lead to air bubble formation. Furthermore, in hydroxylation and amine treatment techniques, there is a high chance that the substrate recover its initial surface energy after a short time, resulting in detachment of biomolecules if they have not been covalently linked to the surface [53,54].

These aforementioned issues emphasize the significance of covalent immobilization of biological entities to obtain highly robust bio-interfaces that can be utilized in different biological applications. The two main strategies that have frequently been used for covalent immobilization include grafting the substrates with amine groups and carboxylic groups.

One of the most-commonly used technique to introduce amine groups on substrates is silanization via trifunctional silane coupling agents of (3-aminopropyl)triethoxysilane (APTES) [23,55–58] and (3-aminopropyl)trimethoxysilane (APTMS) [59,60]. Prior to the silanization, substrates are usually required to be hydroxylated. This could be done via oxygen/air plasma treatment of the substrates [61–63], use of piranha etchant (a strong oxidizer mixture of hydrogen peroxide and sulfuric acid) [55,57], ultraviolet/Ozone (UVO) treatment [64,65], and corona discharge technique [27,66]. After inducement of the hydroxyl groups on a surface, APTES or APTMS silanization could be conducted via either chemical vapor deposition (CVD) [67–69] or liquid phase deposition (LPD) [70–72] methods. In CVD treatment, usually a proper amount of a neat silane solution is vaporized in an enclosed chamber through either heating the solution, vacuuming the chamber, or simultaneous use of heat and vacuum. In LPD method, the silane coupling agent is first diluted in a proper solvent (*e.g.* toluene, ethanol, or acetone) at low concentrations (~1 to 5%) and then incubated with the substrate. During this process, the head groups of the silane coupling agent are hydrolyzed forming silanol groups. The silanols will then be chemisorbed on to the substrate by reacting with the surface hydroxyl groups forming oxane bonds and releasing water as a by-product (Figure 1-1). In the course of polymerization and condensation, silane self-assembled monolayers (SAMs) are created by lateral cross linking of silanols and forming siloxane bonds. The amine groups at the tail groups of

APTES or APTMS could further be employed for covalent immobilization of biomolecules. Silanization is usually followed by a subsequent heat treatment step to promote the polymerization reactions. CVD treatment provides more uniform and denser SAMs compared to LPD due to its capability for precise control over humidity and hydrolysis reaction. However, CVD treatment requires more advanced equipment and utilization of CVD for some applications such as microfluidics could be challenging owing to the fact that the small scale and complexity of the microchannels can hinder the diffusion of silane vapor into the inner surface of the channels [55,69].

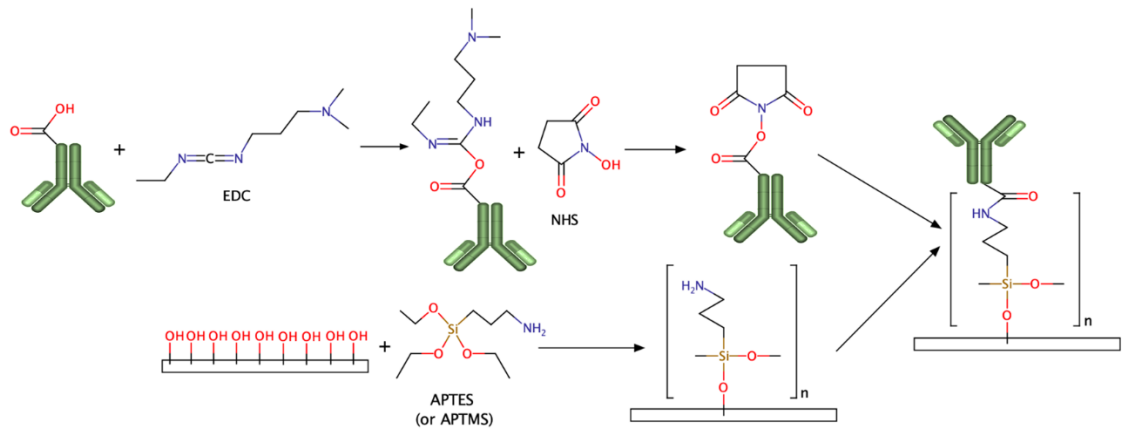

Figure 1-1. Schematic representation of APTES treatment of a substrate and covalent binding of biomolecules to the amine terminal groups via EDC-NHS chemistry.

Other silane coupling agents such as N-[3-(Trimethoxysilyl)propyl]ethylenediamine (AEAPTMS) [61] and Poly[dimethylsiloxane-co-(3-aminopropyl)methylsiloxane] [73] with amine tail groups, as well as 3-mercaptopropyl trimethoxysilane (MPTMS) [74–77], 3-isocyanatopropyltrimethoxysilane (IPTMS) [78], (3-

cyanopropyl)triethoxysilane (CPTES) [79], and glycidyloxypropyl)trimethoxysilane (GLYMO) [80] with other types of tail groups have also been reported for surface modification of different substrates. Silanization of GLYMO, in particular, creates epoxy terminal groups on the surface which can covalently bind to the amine groups of biomolecules through ring opening reactions (Figure 1-2 (a)). Furthermore, combination of MPTMS and n-γ-maleimidobutyryl-oxysuccinimide ester (GMBS) has been shown as a promising way to covalently bind the biomolecules through their amine groups [70,81]. Here, maleimide groups of GMBS can react with sulfhydryl groups of MPTMS creating thioether, and the NHS ester at the other end group of GMBS can react with amine groups of the biomolecules (Figure 1-2 (b)). Silanization technique is adaptable with many surfaces such as glass, polymers, silicon, and aluminium [82–86]. However, it needs several experimental steps and incubation times making it a time-consuming surface functionalization method.

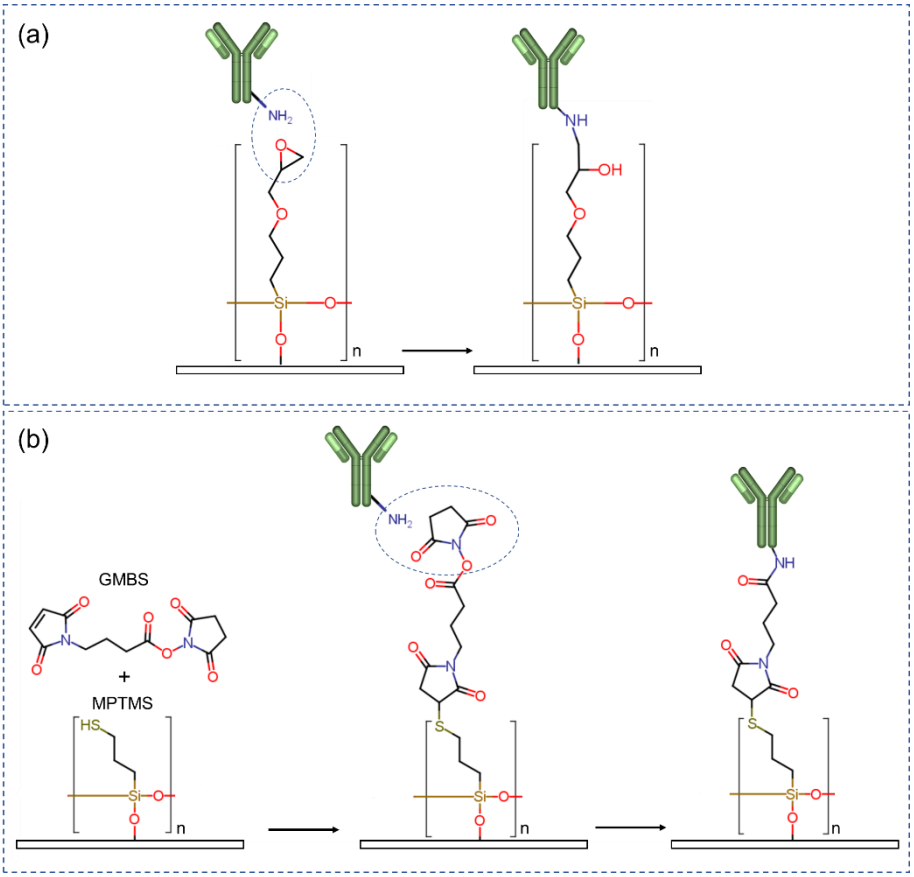

Figure 1-2. (a) Ring opening reactions of epoxy groups in a GLYMO treated surface can lead to covalent binding to biomolecules' amine groups. (b) Silanization of a surface with MPTMS can be used for covalent immobilization of biomolecules via GMBS crosslinker. Dash circles show the reacting functional groups at the biomolecule and surface.

In addition to the silane coupling agents, other chemicals and approaches that have been used to aminate the substrates include ammonia plasma activation [87], allylamine plasma treatment [43,88], 4,7,10-trioxa-1,13-tridecanediamine [89], polyethyleneimine (PEI) [90–93], amine terminated Polyacrylamide (PAM) [94], amine functional parylene [95], 4-aminostyrene (4-AS) [96], hexamethylene-diamine [97,98], as well as

poly(allylamine hydrochloride) (PAH), hexamethylenediamine (HMD), and 1,3-diaminopropane (DAP) [90]. Application of these chemicals could also add complexity to the surface bio-functionalization procedure.

Following the amine treatment of the substrates, amine terminals could link to the biomolecules using a proper crosslinker. Carbodiimide chemistry is one of the popular techniques for activation of the carboxylic groups of biomolecules and creating a covalent crosslink between the activated carboxylic groups and amine terminal groups at the surface. 1-ethyl-3-(-3-dimethylaminopropyl) carbodiimide hydrochloride (EDC) with solubility in aqueous buffers is the most frequently used carbodiimide that can react with the carboxylic groups of biomolecules producing O-acylisourea intermediates [23,30,67,99,100]. These intermediates immediately react with the amine terminals of the substrate and generate strong peptide bonds. Since EDC has a very high reaction rate, it is usually mixed with n-hydroxysuccinimide (NHS) or sulfo-NHS to become more stable and prevent aggregation of proteins. In this case, the O-acylisourea intermediates are replaced with more steady NHS esters which can subsequently react with the amine groups of biomolecules [23,101] (Figure 1-1). N', N’-dicyclohexyl carbodiimide (DCC) [96] and N,N'-diisopropyl carbodiimide (DIC) [89] with solubility in organic buffers are other well-known carbodiimides for activation of the carboxylic groups of proteins and antibodies. Carbodiimide crosslinking, even with utilization of

NHS, usually causes protein loss and un-uniformity in the surface coating. Since the biomolecules should first be mixed with the carbodiimides and then introduced to the surface, it is very challenging to prevent biomolecule aggregation due to the formation of crosslinks between the amine groups and carboxylic groups of adjacent biomolecules.

Glutaraldehyde is another crosslinker that is applied for coupling biomolecules to amine terminated surfaces [102,103]. Aldehyde groups can react with the amine groups of biomolecules and couple them with the amine terminal groups of a substrate. As the substrate can be incubated with glutaraldehyde prior to introducing the biomolecules, it does not result in protein aggregation. However, it should be noted that glutaraldehyde is highly toxic and can cause skin corrosion, eye damage, and throat and lung irritation. Thus, it is always accompanied with safety and healthcare issues.

The other approach for covalent immobilization of biomolecules is incorporation of carboxylic groups onto the substrate, which can subsequently bind to the amine groups of biomolecules. It has been shown that grafting hyperbranched polyglycerol (HPG) followed by addition of succinic anhydride and hydrolysis can create carboxylic groups at HPG [43]. Moreover, grafting poly(acrylic acid) (PAA) on PDMS surfaces have been declared as a promising way to achieve carboxylic groups [50,81,91,104]. Integrating alginate onto the substrate is another way for carboxylation of substrates [105].

Carboxylic groups of polyacrylonitrile (PAN)-made monolith is also utilized for covalent immobilization of biomolecules [106]. Carboxyl-terminated nanoparticles and magnetic beads are also frequently used for biomolecule immobilization benefiting from the large surface area of the particles for attachment [51,107]. Similar to the amine treatment, these strategies comprise complex experimental steps. The simpler way is UV treatment of some substrates such as cyclic olefin copolymer (COC), polystyrene (PS), PMMA, and polycarbonates (PC) to induce functional carboxylic groups [108–110]. This procedure, however, is not versatile and cannot be used for glass slides or types of substrates.

1.1.3 Blocking the Surface to prevent non-specific adsorption (NSA)

As mentioned earlier, seeking a durable and strong blocking agent is a crucial step in surface biofunctionalization for applications such as biosensors, bio-chemical assays, and implants. Many biological entities such as proteins, antibodies, and cells are naturally very prone to physically attach to the biointerfaces. This quality in biosensors, for instance, can cause background signals which are not distinguishable from the specific binding signals, and consequently decline the sensitivity and specificity of bio-chemical assays [111]. Non-grafted poly(ethylene glycol) (PEG), poly(acrylamide)s, poly(N-vinylpyrrolidone), BSA, serum, gelatin, milk powder, and Tween 20 are some of the common blocking agents used to prevent NSA [112–114]. While these blocking

agents have shown good potential in suppressing physisorption of biomolecules, there are serious drawbacks to them. For instance, one of the disadvantages of the blocking agents such as PEG, poly(acrylamide)s, and poly(N-vinylpyrrolidone) is inevitable formation of defects in the surface chemistry which leads to biomolecules attachment and biofouling [115]. Moreover, it has been shown that BSA, milk, and Tween 20 can sometimes disturb the sensitivity of the assays by interfering with immunochemical reactions or incomplete saturation [116–118]. Graft polymerization is another way to tailor the surface energy and anti-biofouling properties of different substrates. Since in this technique, the blocking agent is covalently bound to the surface, it provides more robust and efficient anti-biofouling properties compared to the physical attachment of the blocking agents stated above. For instance, silanization via 100% PEG-silane [119] or diluted PEG-silane [120], as well as UV-mediated grafting poly(ethylene glycol) diacrylate (PEG-DA) [52] have been proven to be effective methods to lower the contact angle of PDMS surfaces and increase the antifouling properties. Other common polymers used for inducing antifouling capability include P[NIPAAm-co-acrylic acid (AAc)] [52], PAA [81], PEI and PAA multilayers [91], multilayers of poly(diallyldimethylammonium chloride) [104], maleic anhydride copolymers [87], HPG [43], polyvinyl alcohol (PVA) polymer [121], and PAM polymer [94]. Grafting polymers could be performed via either “grafting from” or “grafting to” techniques. “Grafting from” techniques are usually performed via UV polymerization of the

polymer of choice using photoinitiators such as benzophenone [52,81,91]. In the "Grafting to" methods, pre-functionalization of the surface with functional groups such as amines and thiols is required in order for the polymer to bind to the surface [43,87].

Recently, lubricant-infused surfaces (LISs) [122], as another class of NSA coatings, have gained considerable attention for creating omniphobic surfaces that can repel all sorts of biological fluids, proteins, antibodies, bacteria, and blood cells, in a more effective way compared to other blocking agents [115,123–127]. This striking characteristic is resulted from a very thin layer of a lubricant that is locked within the surface layer of a substrate. In order to lock the lubricant on the surface, initial surface modification via either chemical approaches (*e.g.* by use of a fluorosilane) or physical techniques (*e.g.* by inducing porosity or surface roughness) should be conducted [122,128,129]. Since the lubricant can create a slippery interface, it is able to repel immiscible liquids as well as various biomolecules. Fluorinated LISs, as a perfect example, have proven to be a promising approach to induce surface omniphobicity and antifouling properties on biomedical surfaces [72,130]. This type of LISs are comprised of two main components; First, a fluorinated layer which can be CVD or LPD coated onto various substrates using chemicals such as 2-(Perfluorodecyl)ethyl acrylate and 1H,1H,2H,2H-perfluorodecanethiol, as well as fluorosilanes such as trichloro(1H,1H,2H,2H-perfluorooctyl)silane and 1H,1H,2H,2H-

Perfluorodecyltrimethoxysilane. Second, a compatible fluorocarbon based lubricant such as perfluorocarbon that is added and infused into the fluorinated layer (Figure 1-3). The fluorinated monolayer can lock a thin layer of the lubricant through van der Waals forces providing slippery properties. This technology has been employed for antibacterial coatings, and devices where thrombosis and infections could pose a threat [123,131–133]. However, LISs have not been utilized for biosensing industry as the immobilization of biomolecules on the omniphobic fluorinated layers is not attainable via conventional immobilization techniques. Nevertheless, implementation of this technology could be very advantageous for biosensors due to its potential to create a long-lasting blocking layer that can effectively prevent NSA.

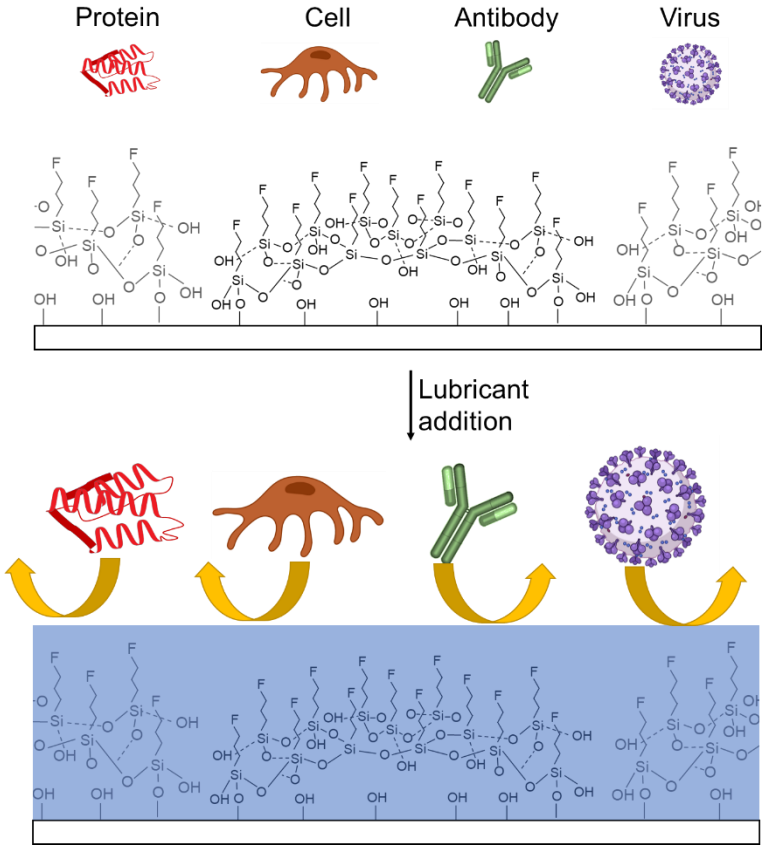

Figure 1-3. Schematic representation of umbrella-shape SAMs formed after CVD silanization of trichloro(1H,1H,2H,2H-perfluorooctyl)silane. Addition of the lubricant to the surface can bring about repellency against all sorts of biomolecules such as proteins, cells, antibodies, and viruses.

1.1.4 Surface Patterning

Precise patterning of a surface with the desired biomolecule plays an important role in selective screening in biosensors and biological assays. Micro/nano printing methods could provide us with access to separated biofunctional areas (microarrays) in order to investigate the status of multianalytes in high throughput systems [134–141]. Moreover, in tissue engineering, it is required to position biomolecules in distinct locations to

promote cell attachment on those area, while preventing cell attachment on undesired parts [134].

Non-contact printing method is one the commonly used technologies for creating microarrays of functional ligands [92,142]. Inkjet printers that are equipped with piezo dispense capillary nozzles are mostly utilized for non-contact printing [92]. Although effective, non-contact printing suffers from several disadvantages such as the need for advanced and costly equipment, the dependence of printed arrays' size on surface energy, and the long incubation times required for functionalization [143,144]. Photolithographic patterning is another widely used method to form biomolecules patterns [145]. The main advantages of this technique are the capability to covalently pattern biomolecules as well as the possibility for patterning inside the enclosed microfluidic channels. Photolithographic patterning requires a photosensitive layer, a photomask containing the patterns of interest as cavities, and UV light to activate a photosensitive linker. The substrate (which could be a microchannel) is first coated with a photosensitive linker and then irradiated by passing the UV light through a photomask. This results in cleavage of the linker at the irradiated areas and inducing localized reactive moieties. Afterwards, the biomolecules are associated with the substrates to covalently bind to the UV-induced reactive moieties [145]. This process is not as fast as non-contact printing and requires more reagents. In the constructive

photolithographic patterning technique, biomolecules can initially be mixed with the UV-sensitive linkers and then added to the substrate for irradiation [146–148]. This can shorten the patterning procedure time, however, it is not applicable to UV sensitive biomolecules.

Microfluidics have also been used to pattern a surface with 1-diminsional (1D) concentration gradient of biomolecules. In this case, the biomolecule concentration changes along either length or width of a microchannel. The simplest way to generate 1D concentration gradient is use of "source-sink" design in which the gradient is occurred by gradual diffusion of molecules from the inlet of the device as "source" to the outlet as "sink" (Figure 1-4 (a)) [149,150]. Another approach is using Y-shape junctions to create two parallel laminar flows composed of two different solutions in a straight microchannel [151,152]. Here, biomolecules can laterally diffuse from one flow stream to the adjacent one across their interface (Figure 1-4 (b)). Moreover, tree-shape designs of microfluidic channels have been proposed as an efficient way to create 1D concentration gradient [153,154]. This design has a large footprint size and the gradient is derived from a very complex channel network inducing multiple flow splitting and mixing stages (Figure 1-4 (c)). There are also a few numbers of microfluidic designs capable of creating 2-diminsional (2D) concentration gradients where the concentration of the desired biomolecule can change along both width and length of a microchamber,

simultaneously. This can be achieved by use of microwells [155], multifaceted tree-shape design [156], and multi-layer pressure balance systems [157]. These strategies are usually very complex and need external pumping and long diffusion times to operate. Moreover, they do not provide covalent binding between the biomolecules and the microchannel surface.

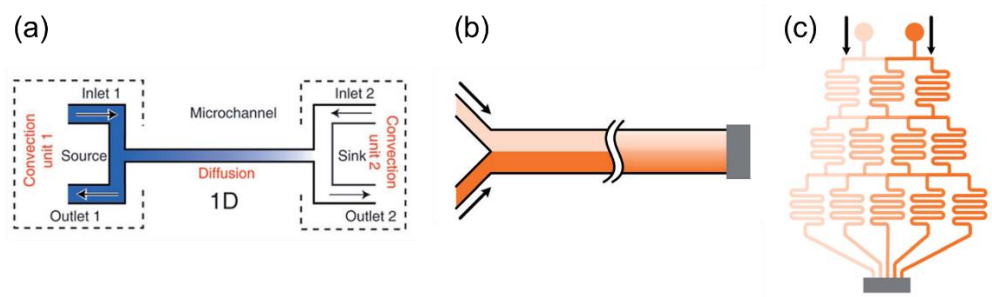

Figure 1-4. Common microfluidic 1D gradient generators; (a) Source-sink approach. Reprinted from Ref. [158] with permission from Royal Society of Chemistry (b) Y-shape junction method, (c) Tree-shape design. (b and c) are reprinted from Ref. [157] with permission from Royal Society of Chemistry.

Microcontact printing is an alternative approach to form various patterns on surfaces [41,159–164]. In this technique, a diluted biomolecule is first added to a stamp. The stamp is usually made of PDMS with the desired patterns as protrusions. After a proper incubation time (~10 min), the stamp is quickly blown with a strong blast of air or nitrogen leaving a thin semi wet layer of the biomolecule. The stamp is then pressed against a substrate leading to transferring of the biomolecules from the hydrophobic stamp to the more hydrophilic surface (Figure 1-5). Microcontact printing is a very simple and quick method and does not required advanced facilities. One major problem

with this technique is physical attachment of biomolecules to the surface. As a result, the created patterns cannot resist harsh *in vivo* and *in vitro* environments where high shear stresses (above 50 dyn/cm^2), for instant, can lead to detachment of biomolecules from the surface. Microcontact printing of APTES on plasma activated surfaces can be an alternative way to create a strong covalent bond between the amine terminated groups of the surface and carboxylic groups of the target bio-species [100,165]. This procedure, however, is very challenging and time consuming, and does not show good repeatability. The other issue with this technique is in creating multiplex patterns as well as scaling up for industrial application.

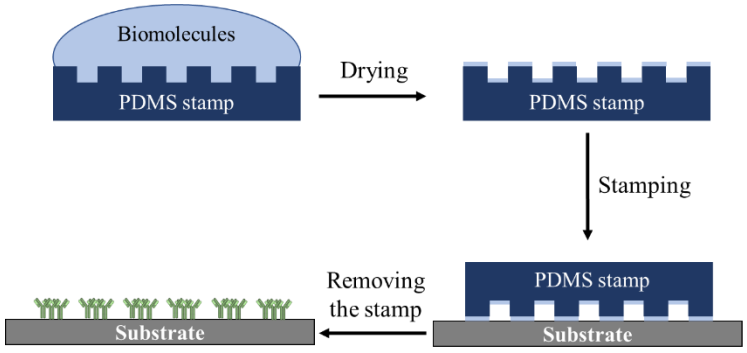

Figure 1-5. Schematic representation of microcontact printing protocol.

1.2 Objectives

In this thesis, several novel techniques are introduced to covalently bind nanoparticles and biomolecules on various platforms including ceramic tiles, microfluidic channels and diagnostic well plates. The key component of the introduced surface

functionalization techniques is use of CO_2 plasma treatment which can induce carboxylic groups as well as hydroxyl groups onto different substrates. Compared to the aforementioned surface functionalization strategies in the literature review section, this technique is very quick and straightforward allowing for inducing functional groups in one step without any need for wet chemistry. Furthermore, in our technique, activation of carboxylic groups could be conducted via EDC-NHS chemistry prior to introducing the antibodies, which can effectively prevent biomolecule aggregation and loss of proteins. In addition, we demonstrate the possibility of microcontact printing of EDC-NHS onto these CO_2 plasma activated surfaces in order to pattern biomolecules and cells. In this way, not only could we benefit from the simplicity of the microcontact printing method for biomolecule patterning, but we can also covalently immobilize the biomolecules patterns providing robust biointerfaces.

The other objective of this thesis is presenting a novel strategy by which, for the first time, one would be able to covalently pattern biomolecules on a lubricant-infused surface. As mentioned earlier, covalent immobilization of biomolecules on an omniphobic lubricant-infused platform could be highly beneficial for biosensor industries as it can effectively suppress NSA and consequently enhance the sensitivity of the sensor. To this end, we introduce a new type of bioink in which the antibody is initially conjugated with an epoxy-based silane coupling agent. In contrast to the

existing published methods for covalent attachment of antibodies and proteins on surfaces, where the substrate itself should first be entirely coated with chemical compounds, we coat the surface of the biomolecules with functional groups though silane chemistry. Thus, the biofunctional biomolecules can be covalently patterned onto fluorinated surfaces using simple microcontact printing techniques. The new biointerface enables biosensors to benefit from the durable repellency and omniphobicity properties of lubricant-infused surfaces while the patterned biomolecule can selectively detect the desired analytes in complex bio-fluids in a multiplex fashion.

1.3 Thesis Outline

The contents of each of the following chapters in the thesis are briefly described below.

Chapter 2: “Biofunctionalization of Glass and Paper-based Microfluidic Devices; a Review”. This chapter thoroughly reviews the biofunctionalization strategies that have been conducted to create biointerfaces in microfluidic devices made of glass substrates as well as paper-based microfluidics. *The review has been published in Advanced Materials Interfaces.*

Chapter 3: “Self-cleaning Ceramic Tiles Produced via Stable Coating of TiO_2 Nanoparticles”. This chapter introduces a CO_2 plasma treatment-based strategy to coat ceramic tiles with TiO_2 nanoparticles. As a proof of concept, the photocatalytic activity

of the TiO_2 coating is measured to show the capability of the coating layer for self-cleaning applications. A single step heat treatment method is also introduced for coating the ceramic tiles with TiO_2 nanoparticles. *The chapter has been published in Materials.*

Chapter 4: "Plasma-induced Covalent Immobilization and Patterning of Bioactive Species in Microfluidic Devices". This chapter demonstrates the utilization of CO_2 plasma treatment strategy to coat the surface of microfluidic channels with different proteins. It also shows the possibility of microcontact printing of carbodiimide crosslinker in order to covalently pattern the surface of the microfluidics with different proteins and cells. *The chapter has been published in Lab on a Chip*.

Chapter 5: "Antibody Micropatterned Lubricant-infused Biosensors Enable Sub-picogram Immunofluorescence Detection of Interleukin 6 in Human Whole Plasma". This chapter introduces a novel technique to covalently create patterns of interleukin 6 (IL-6) capture antibody on a lubricant-infused surface using functional bioink and microcontact printing techniques. The new strategy could dramatically enhance the LOD of IL-6 in complex biofluids such as human whole plasma and blood. *The chapter is under revision in Small.*

Chapter 6: "Conclusions and Future Direction". Finally, in this chapter some general conclusions are drawn and suggestions for future work are offered.

Appendix A: “Generating 2-dimensional Concentration Gradients of Biomolecules Using a Simple Microfluidic Design”. In this appendix, we introduce a novel method to simultaneously create 1D and 2D concentration gradients of biomolecules in a microfluidic platform with a small footprint size. The feasibility of the microfluidic gradient generating system is examined by finite element simulation analysis and fluorescently labelled IgG antibodies. *The appendix has been published in Biomicrofluidics*.

Appendix B: “Biofunctional Interfaces for Cell Culture in Microfluidic Devices”. This appendix includes a book chapter which introduces different strategies for accommodation of different cell lines in microfluidic channels. *The book chapter has been published in Woodhead Publishing Series in Electronic and Optical Materials as a chapter of “Bioelectronics and Medical Devices” book.*

1.4 References

[1] B. Kasemo, Biological surface science, Surf. Sci. 500 (2002) 656–677. doi:https://doi.org/10.1016/S0039-6028(01)01809-X.

[2] M. Van de Voorde, M. Werner, H. Fecht, The Nano-Micro Interface: Bridging the Micro and Nano Worlds, (2015).

[3] E. Sackmann, M. Tanaka, Supported membranes on soft polymer cushions:

fabrication, characterization and applications, Trends Biotechnol. 18 (2000) 58–64. doi:https://doi.org/10.1016/S0167-7799(99)01412-2.

[4] F. Frederix, K. Bonroy, W. Laureyn, G. Reekmans, A. Campitelli, W. Dehaen, G. Maes, Enhanced performance of an affinity biosensor interface based on mixed self-assembled monolayers of thiols on gold, Langmuir. 19 (2003) 4351–4357. doi:10.1021/la026908f.

[5] N. Tort, J.-P. Salvador, M.-P. Marco, Multimodal plasmonic biosensing nanostructures prepared by DNA-directed immobilization of multifunctional DNA-gold nanoparticles, Biosens. Bioelectron. 90 (2017) 13–22. doi:https://doi.org/10.1016/j.bios.2016.11.022.

[6] D. Zheng, K.G. Neoh, E.-T. Kang, Bifunctional coating based on carboxymethyl chitosan with stable conjugated alkaline phosphatase for inhibiting bacterial adhesion and promoting osteogenic differentiation on titanium, Appl. Surf. Sci. 360 (2016) 86–97. doi:https://doi.org/10.1016/j.apsusc.2015.11.003.

[7] M. Zychowicz, D. Dziedzicka, D. Mehn, H. Kozlowska, A. Kinsner-Ovaskainen, P.P. Stępień, F. Rossi, L. Buzanska, Developmental stage dependent neural stem cells sensitivity to methylmercury chloride on different biofunctional surfaces, Toxicol. Vitr. 28 (2014) 76–87. doi:https://doi.org/10.1016/j.tiv.2013.06.023.

[8] Immunoassay Instruments/Analyzers Market Revenue Analysis By Product (Chemiluminescence, Immunofluorescence Analyzers, Radioimmunoassay, Elisa), By Application (Oncology, Infectious Disease Testing, Autoimmune Disease), And Segment Forecasts To 2024, 2016.

[9] K.C. Ahn, H. Kim, M.R. Mccoy, S.J. Gee, D. Bruce, Immunoassays and Biosensors for Monitoring Environmental and Human Exposure to Pyrethroid Insecticides, J Agric Food Chem. 59 (2011) 2792–2802. doi:10.1021/jf1033569.Immunoassays.

[10] D. Roe, B. Karandikar, N. Bonn-Savage, B. Gibbins, J.-B. Roullet, Antimicrobial surface functionalization of plastic catheters by silver nanoparticles, J. Antimicrob. Chemother. 61 (2008) 869–876. http://dx.doi.org/10.1093/jac/dkn034.

[11] D. Shenoy, W. Fu, J. Li, C. Crasto, G. Jones, C. DiMarzio, S. Sridhar, M. Amiji, Surface functionalization of gold nanoparticles using hetero-bifunctional poly(ethylene glycol) spacer for intracellular tracking and delivery, Int. J. Nanomedicine. 1 (2006) 51–57. doi:10.2147/nano.2006.1.1.51.

[12] A. Fujishima, X. Zhang, D.A. Tryk, TiO_2 photocatalysis and related surface phenomena, Surf. Sci. Rep. 63 (2008) 515–582.

doi:10.1016/j.surfrep.2008.10.001.

[13] G. Velve-Casquillas, M. Le Berre, M. Piel, P.T. Tran, J. Urban, Microfluidic tools for cell biological research, Nano Today. 5 (2010) 28–47. doi:10.1016/j.nantod.2009.12.001.

[14] C.M.B. Ho, S.H. Ng, K.H.H. Li, Y.J. Yoon, 3D printed microfluidics for biological applications, Lab Chip. 15 (2015) 3627–3637. doi:10.1039/c5lc00685f.

[15] N.T. Nguyen, M. Hejazian, C.H. Ooi, N. Kashaninejad, Recent advances and future perspectives on microfluidic liquid handling, Micromachines. 8 (2017) 186. doi:10.3390/mi8060186.

[16] D. Holmes, S. Gawad, The Application of Microfluidics in Biology BT - Microengineering in Biotechnology, in: M.P. Hughes, K.F. Hoettges (Eds.), Humana Press, Totowa, NJ, 2010: pp. 55–80. doi:10.1007/978-1-60327-106-6_2.

[17] T.A. Duncombe, A.M. Tentori, A.E. Herr, Microfluidics: Reframing biological enquiry, Nat. Rev. Mol. Cell Biol. 16 (2015) 554–567. doi:10.1038/nrm4041.

[18] S.C.C. Shih, G. Goyal, P.W. Kim, N. Koutsoubelis, J.D. Keasling, P.D. Adams,

N.J. Hillson, A.K. Singh, A Versatile Microfluidic Device for Automating Synthetic Biology, ACS Synth. Biol. 4 (2015) 1151–1164. doi:10.1021/acssynbio.5b00062.

[19] A.M. Foudeh, T. Fatanat Didar, T. Veres, M. Tabrizian, Microfluidic designs and techniques using lab-on-a-chip devices for pathogen detection for point-of-care diagnostics, Lab Chip. 12 (2012) 3249–3266. doi:10.1039/C2LC40630F.

[20] T.F. Didar, M. Tabrizian, Adhesion based detection, sorting and enrichment of cells in microfluidic Lab-on-Chip devices, Lab Chip. 10 (2010) 3043–3053. doi:10.1039/C0LC00130A.

[21] T.F. Didar, K. Li, T. Veres, M. Tabrizian, Separation of rare oligodendrocyte progenitor cells from brain using a high-throughput multilayer thermoplastic-based microfluidic device, Biomaterials. 34 (2013) 5588–5593. doi:https://doi.org/10.1016/j.biomaterials.2013.04.014.

[22] M.L. Coluccio, G. Perozziello, N. Malara, E. Parrotta, P. Zhang, F. Gentile, T. Limongi, P.M. Raj, G. Cuda, P. Candeloro, E. Di Fabrizio, Microfluidic platforms for cell cultures and investigations, Microelectron. Eng. 208 (2019) 14–28. doi:https://doi.org/10.1016/j.mee.2019.01.004.

[23] Z.L. Zhang, C. Crozatier, M. Le Berre, Y. Chen, In situ bio-functionalization and

cell adhesion in microfluidic devices, Microelectron. Eng. 78–79 (2005) 556–562. doi:10.1016/j.mee.2004.12.071.

[24] H. Joo, E. Byun, M. Lee, Y. Hong, H. Lee, P. Kim, Biofunctionalization via flow shear stress resistant adhesive polysaccharide, hyaluronic acid-catechol, for enhanced in vitro endothelialization, J. Ind. Eng. Chem. 34 (2016) 14–20. doi:10.1016/j.jiec.2015.11.015.

[25] G. Luka, A. Ahmadi, H. Najjaran, E. Alocilja, M. DeRosa, K. Wolthers, A. Malki, H. Aziz, A. Althani, M. Hoorfar, Microfluidics Integrated Biosensors: A Leading Technology towards Lab-on-a-Chip and Sensing Applications, Sensors . 15 (2015). doi:10.3390/s151229783.

[26] A. Jain, A.D. van der Meer, A.L. Papa, R. Barrile, A. Lai, B.L. Schlechter, M.A. Otieno, C.S. Louden, G.A. Hamilton, A.D. Michelson, A.L. Frelinger, D.E. Ingber, Assessment of whole blood thrombosis in a microfluidic device lined by fixed human endothelium, Biomed. Microdevices. 18 (2016) 1–7. doi:10.1007/s10544-016-0095-6.

[27] M. Adiraj Iyer, D.T. Eddington, Storing and releasing rhodamine as a model hydrophobic compound in polydimethylsiloxane microfluidic devices, Lab Chip. 19 (2019) 574–579. doi:10.1039/C9LC00039A.

[28] J. Carpinelli, R. Krämer, E. Agosin, Metabolic Engineering of Corynebacterium glutamicum for Trehalose Overproduction: Role of the TreYZ Trehalose Biosynthetic Pathway, Appl. Environ. Microbiol. 72 (2006) 1949–1955. doi:10.1128/AEM.72.3.1949-1955.2006.

[29] Y. Zhao, X. Liu, J. Li, W. Qiang, L. Sun, H. Li, D. Xu, Microfluidic chip-based silver nanoparticles aptasensor for colorimetric detection of thrombin, Talanta. 150 (2016) 81–87.

[30] X. Guan, H.J. Zhang, Y.N. Bi, L. Zhang, D.L. Hao, Rapid detection of pathogens using antibody-coated microbeads with bioluminescence in microfluidic chips, Biomed. Microdevices. 12 (2010) 683–691. doi:10.1007/s10544-010-9421-6.

[31] G. Perozziello, G. Simone, N. Malara, R. La Rocca, R. Tallerico, R. Catalano, F. Pardeo, P. Candeloro, G. Cuda, E. Carbone, E. Di Fabrizio, Microfluidic biofunctionalisation protocols to form multi-valent interactions for cell rolling and phenotype modification investigations, Electrophoresis. 34 (2013) 1845–1851. doi:10.1002/elps.201300106.

[32] K. Gold, A.K. Gaharwar, A. Jain, Emerging trends in multiscale modeling of vascular pathophysiology: Organ-on-a-chip and 3D printing, Biomaterials. 196 (2019) 2–17. doi:https://doi.org/10.1016/j.biomaterials.2018.07.029.

[33] P. Valentina, R. Claudio, B. Benedikt, M. Sandro, R. Felix, B. Andreas, M. Lars, Abstract 012: Aorta-on-a-chip: a Tool to Gain Molecular and Translational Insight Into Vascular Diseases, Arterioscler. Thromb. Vasc. Biol. 38 (2018) A012–A012. doi:10.1161/atvb.38.suppl_1.012.

[34] N.K.R. Pandian, R.G. Mannino, W.A. Lam, A. Jain, Thrombosis-on-a-chip: Prospective impact of microphysiological models of vascular thrombosis, Curr. Opin. Biomed. Eng. 5 (2018) 29–34. doi:https://doi.org/10.1016/j.cobme.2017.12.001.

[35] J. Seo, D. Huh, Chapter 7 - Microphysiological models of human organs: A case study on microengineered lung-on-a-chip systems, in: J.T. Borenstein, V. Tandon, S.L. Tao, J.L.B.T.-M.C.C.S. (Second E. Charest (Eds.), Micro Nano Technol., Elsevier, 2019: pp. 187–208. doi:https://doi.org/10.1016/B978-0-12-813671-3.00007-4.

[36] X. Yang, K. Li, X. Zhang, C. Liu, B. Guo, W. Wen, X. Gao, Nanofiber membrane supported lung-on-a-chip microdevice for anti-cancer drug testing, Lab Chip. 18 (2018) 486–495. doi:10.1039/c7lc01224a.

[37] G.S. Ugolini, R. Visone, D. Cruz-Moreira, A. Mainardi, M. Rasponi, Chapter 4 - Generation of functional cardiac microtissues in a beating heart-on-a-chip, in:

J. Doh, D. Fletcher, M.B.T.-M. in C.B. Piel (Eds.), Microfluid. Cell Biol. Part A Microfluid. Multicell. Syst., Academic Press, 2018: pp. 69–84. doi:https://doi.org/10.1016/bs.mcb.2018.05.005.

[38] W. Ng, N. Howell, J.L. Newton, F.H. Van Der Westhuizen, N. Huebsch, B. Charrez, B. Siemons, S.C. Boggess, S. Wall, V. Charwat, K. Jaeger, F.L.T. Montiel, N.C. Jeffreys, N. Deveshwar, A. Edwards, J. Serrano, M. Snuderl, A. Stahl, A. Tveito, E.W. Miller, K.E. Healy, W. Ng, N. Howell, J.L. Newton, F.H. Van Der Westhuizen, Metabolically-Driven Maturation of hiPSC-Cell Derived Heart-on-a-Chip, BioRxiv. (2018) 485169. doi:10.1101/485169.

[39] S. Jalili-Firoozinezhad, R. Prantil-Baun, A. Jiang, R. Potla, T. Mammoto, J.C. Weaver, T.C. Ferrante, H.J. Kim, J.M.S. Cabral, O. Levy, D.E. Ingber, Modeling radiation injury-induced cell death and countermeasure drug responses in a human Gut-on-a-Chip article, Cell Death Dis. 9 (2018) 223. doi:10.1038/s41419-018-0304-8.

[40] A.R. Perestrelo, A.C.P. Águas, A. Rainer, G. Forte, Microfluidic organ/body-on-a-chip devices at the convergence of biology and microengineering, Sensors (Switzerland). 15 (2015) 31142–31170. doi:10.3390/s151229848.

[41] T.F. Didar, K. Bowey, G. Almazan, M. Tabrizian, A miniaturized multipurpose

platform for rapid, label-free, and simultaneous separation, patterning, and in vitro culture of primary and rare cells, Adv. Healthc. Mater. 3 (2014) 253–260. doi:10.1002/adhm.201300099.

[42] M. Jaffe, W. Hammond, P. Tolias, T.B.T.-C. of B. Arinzeh, eds., 6 - Studying molecular-scale protein–surface interactions in biomaterials, in: Charact. Biomater., Woodhead Publishing, 2013: pp. 182–223. doi:https://doi.org/10.1533/9780857093684.182.

[43] P.Y. Yeh, N.A.A. Rossi, J.N. Kizhakkedathu, M. Chiao, A silicone-based microfluidic chip grafted with carboxyl functionalized hyperbranched polyglycerols for selective protein capture, Microfluid. Nanofluidics. 9 (2010) 199–209. doi:10.1007/s10404-009-0535-1.

[44] N.C.A. Van Engeland, A.M.A.O. Pollet, J.M.J. Den Toonder, C.V.C. Bouten, O.M.J.A. Stassen, C.M. Sahlgren, A biomimetic microfluidic model to study signalling between endothelial and vascular smooth muscle cells under hemodynamic conditions, Lab Chip. 18 (2018) 1607–1620. doi:10.1039/c8lc00286j.

[45] P. Tengvall, 4.406 - Protein Interactions with Biomaterials, in: P.B.T.-C.B. Ducheyne (Ed.), Compr. Biomater., Elsevier, Oxford, 2011: pp. 63–73.

doi:https://doi.org/10.1016/B978-0-08-055294-1.00006-4.

[46] D. Maji, S.K. Lahiri, S. Das, Study of hydrophilicity and stability of chemically modified PDMS surface using piranha and KOH solution, Surf. Interface Anal. 44 (2012) 62–69. doi:10.1002/sia.3770.

[47] Y.A. Alzahid, P. Mostaghimi, A. Gerami, A. Singh, K. Privat, T. Amirian, R.T. Armstrong, Functionalisation of Polydimethylsiloxane (PDMS)- Microfluidic Devices coated with Rock Minerals, Sci. Rep. 8 (2018) 15518. doi:10.1038/s41598-018-33495-8.

[48] P. Kim, H.E. Jeong, A. Khademhosseini, K.Y. Suh, Fabrication of non-biofouling polyethylene glycol micro- and nanochannels by ultraviolet-assisted irreversible sealing, Lab Chip. 6 (2006) 1432–1437. doi:10.1039/b610503c.

[49] Y. Liu, W. Zhong, S. Meng, J. Kong, H. Lu, P. Yang, H.H. Girault, B. Liu, Assembly-controlled biocompatible interface on a microchip: Strategy to highly efficient proteolysis, Chem. - A Eur. J. 12 (2006) 6585–6591. doi:10.1002/chem.200501622.

[50] S.W. Han, E. Jang, W.G. Koh, Microfluidic-based multiplex immunoassay system integrated with an array of QD-encoded microbeads, Sensors Actuators, B Chem. 209 (2015) 242–251. doi:10.1016/j.snb.2014.11.115.

[51] C.H. Wang, C.J. Chang, J.J. Wu, G. Bin Lee, An integrated microfluidic device utilizing vancomycin conjugated magnetic beads and nanogold-labeled specific nucleotide probes for rapid pathogen diagnosis, Nanomedicine Nanotechnology, Biol. Med. 10 (2014) 809–818. doi:10.1016/j.nano.2013.10.013.

[52] M. Ebara, J.M. Hoffman, P.S. Stayton, A.S. Hoffman, Surface modification of microfluidic channels by UV-mediated graft polymerization of non-fouling and "smart" polymers, Radiat. Phys. Chem. 76 (2007) 1409–1413. doi:10.1016/j.radphyschem.2007.02.072.

[53] D.T. Eddington, J.P. Puccinelli, D.J. Beebe, Thermal aging and reduced hydrophobic recovery of polydimethylsiloxane, Sensors Actuators, B Chem. 114 (2006) 170–172. doi:10.1016/j.snb.2005.04.037.

[54] Y. Berdichevsky, J. Khandurina, A. Guttman, Y.H. Lo, UV/ozone modification of poly(dimethylsiloxane) microfluidic channels, Sensors Actuators, B Chem. 97 (2004) 402–408. doi:10.1016/j.snb.2003.09.022.

[55] W. Tan, T.A. Desai, Layer-by-layer microfluidics for biomimetic three-dimensional structures, Biomaterials. 25 (2004) 1355–1364. doi:10.1016/j.biomaterials.2003.08.021.

[56] D. Wu, B. Zhao, Z. Dai, J. Qin, B. Lin, Grafting epoxy-modified hydrophilic

polymers onto poly(dimethylsiloxane) microfluidic chip to resist nonspecific protein adsorption, Lab Chip. 6 (2006) 942–947. doi:10.1039/B600765A.

[57] J. Kim, E.C. Jensen, M. Megens, B. Boser, R. a Mathies, Integrated microfluidic bioprocessor for solid phase capture immunoassays, Lab Chip. 11 (2011) 3106–12. doi:10.1039/c1lc20407f.

[58] T.F. Didar, A.M. Foudeh, M. Tabrizian, Patterning multiplex protein microarrays in a single microfluidic channel, Anal. Chem. 84 (2012) 1012–1018. doi:10.1021/ac2025877.

[59] Z. Zhang, P. Zhao, G. Xiao, The fabrication of polymer microfluidic devices using a solid-to-solid interfacial polyaddition, Polymer (Guildf). 50 (2009) 5358–5361. doi:10.1016/j.polymer.2009.09.053.

[60] C. Séguin, J.M. McLachlan, P.R. Norton, F. Lagugné-Labarthet, Surface modification of poly(dimethylsiloxane) for microfluidic assay applications, Appl. Surf. Sci. 256 (2010) 2524–2531. doi:10.1016/j.apsusc.2009.10.099.

[61] K.H.K. Wong, A.E. Jensen, V. Thapar, D. Ting, M. Toner, S.L. Stott, P.T. Hammond, Enhanced Isolation and Release of Circulating Tumor Cells Using Nanoparticle Binding and Ligand Exchange in a Microfluidic Chip, J. Am. Chem. Soc. 139 (2017) 2741–2749. doi:10.1021/jacs.6b12236.

[62] H. Li, M. Zhao, W. Liu, W. Chu, Y. Guo, Polydimethylsiloxane microfluidic chemiluminescence immunodevice with the signal amplification strategy for sensitive detection of human immunoglobin G, Talanta. 147 (2016) 430–436. doi:10.1016/j.talanta.2015.10.018.

[63] M. Badv, S.M. Imani, J.I. Weitz, T.F. Didar, Lubricant-Infused Surfaces with Built-In Functional Biomolecules Exhibit Simultaneous Repellency and Tunable Cell Adhesion, ACS Nano. 12 (2018) 10890−10902. doi:10.1021/acsnano.8b03938.

[64] N.R. Glass, R. Tjeung, P. Chan, L.Y. Yeo, J.R. Friend, Organosilane deposition for microfluidic applications, Biomicrofluidics. 5 (2011) 1–7. doi:10.1063/1.3625605.

[65] H.Y. Chen, A.A. McClelland, Z. Chen, J. Lahann, Solventless adhesive bonding using reactive polymer coatings, Anal. Chem. 80 (2008) 4119–4124. doi:10.1021/ac800341m.

[66] H.J. Kim, D. Huh, G. Hamilton, D.E. Ingber, Human gut-on-a-chip inhabited by microbial flora that experiences intestinal peristalsis-like motions and flow, Lab Chip. 12 (2012) 2165–2174. doi:10.1039/c2lc40074j.

[67] H. Handa, S. Gurczynski, M.P. Jackson, G. Auner, J. Walker, G. Mao,

Recognition of Salmonella typhimurium by immobilized phage P22 monolayers, Surf. Sci. 602 (2008) 1392–1400. doi:10.1016/j.susc.2008.01.036.

[68] F. Zhang, K. Sautter, A.M. Larsen, D.A. Findley, R.C. Davis, H. Samha, M.R. Linford, Chemical vapor deposition of three aminosilanes on silicon dioxide: Surface characterization, stability, effects of silane concentration, and cyanine dye adsorption, Langmuir. 26 (2010) 14648–14654. doi:10.1021/la102447y.

[69] N.G. Batz, J.S. Mellors, J.P. Alarie, J.M. Ramsey, Chemical vapor deposition of aminopropyl silanes in microfluidic channels for highly efficient microchip capillary electrophoresis-electrospray ionization-mass spectrometry, Anal. Chem. 86 (2014) 3493–3500. doi:10.1021/ac404106u.

[70] W. Asghar, M. Yuksekkaya, H. Shafiee, M. Zhang, M.O. Ozen, F. Inci, M. Kocakulak, U. Demirci, Engineering long shelf life multi-layer biologically active surfaces on microfluidic devices for point of care applications, Sci. Rep. 6 (2016) 1–10. doi:10.1038/srep21163.

[71] M. Badv, I.H. Jaffer, J.I. Weitz, T.F. Didar, An omniphobic lubricant-infused coating produced by chemical vapor deposition of hydrophobic organosilanes attenuates clotting on catheter surfaces, Sci. Rep. 7 (2017) 11639. doi:10.1038/s41598-017-12149-1.

[72] M. Osborne, A. Aryasomayajula, A. Shakeri, P.R. Selvaganapathy, T.F. Didar, Suppression of Biofouling on a Permeable Membrane for Dissolved Oxygen Sensing Using a Lubricant-Infused Coating, ACS Sensors. 4 (2019) 687–693. doi:10.1021/acssensors.8b01541.

[73] B. Pečar, M. Možek, D. Vrtačnik, Thermoplastic - PDMS polymer covalent bonding for microfluidic applications, Inf. MIDEM. 47 (2017) 147–154.

[74] X. Cheng, D. Irimia, M. Dixon, K. Sekine, U. Demirci, L. Zamir, R.G. Tompkins, W. Rodriguez, M. Toner, A microfluidic device for practical label-free CD4+ T cell counting of HIV-infected subjects, Lab Chip. 7 (2007) 170–178. doi:10.1039/B612966H.

[75] C. Chen, J. Skog, C.-H. Hsu, R.T. Lessard, L. Balaj, T. Wurdinger, B.S. Carter, X.O. Breakefield, M. Toner, D. Irimia, Microfluidic isolation and transcriptome analysis of serum microvesicles, Lab Chip. 10 (2010) 505–511. doi:10.1039/B916199F.

[76] M. Xue, Z. Xie, L. Zhang, X. Ma, X. Wu, Y. Guo, W. Song, Z. Li, T. Cao, Microfluidic etching for fabrication of flexible and all-solid-state micro supercapacitor based on MnO2 nanoparticles, Nanoscale. 3 (2011) 2703–2708. doi:10.1039/C0NR00990C.

[77] J. Wu, R. Wang, H. Yu, G. Li, K. Xu, N.C. Tien, R.C. Roberts, D. Li, Inkjet-printed microelectrodes on PDMS as biosensors for functionalized microfluidic systems, Lab Chip. 15 (2015) 690–695. doi:10.1039/C4LC01121J.

[78] J.E. Baker, R. Sriram, B.L. Miller, Two-dimensional photonic crystals for sensitive microscale chemical and biochemical sensing, Lab Chip. 15 (2015) 971–990. doi:10.1039/C4LC01208A.

[79] C.-C. Wu, C.-Y. Yuan, S.-J. Ding, Effect of polydimethylsiloxane surfaces silanized with different nitrogen-containing groups on the adhesion progress of epithelial cells, Surf. Coatings Technol. 205 (2011) 3182–3189.

[80] S. Mccormick, Z. Tong, A. Ivask, M. Morozesk, N.H. Voelcker, E. Lombi, C. Priest, Optimization of binding B-lymphocytes in a microfluidic channel: surface modification, stasis time and shear response, Biofabrication. 10 (2018) 014101.

[81] C. Launiere, M. Gaskill, G. Czaplewski, J.H. Myung, S. Hong, D.T. Eddington, Channel surface patterning of alternating biomimetic protein combinations for enhanced microfluidic tumor cell isolation, Anal. Chem. 84 (2012) 4022–4028. doi:10.1021/ac2033408.

[82] I. Torres, L. Eland, C. Redfern, J. Hedley, Design Of a Mems Device for Studying Cell Migration and Differentiation, Sensors. 2 (2017) 17–19.

[83] G.C. Santini, C. Potrich, L. Lunelli, L. Vanzetti, S.L. Marasso, M. Cocuzza, F.C. Pirri, C. Pederzolli, miRNA purification with an optimized PDMS microdevice: Toward the direct purification of low abundant circulating biomarkers, Biophys. Chem. 229 (2017) 142–150. doi:10.1016/j.bpc.2017.04.009.

[84] A. Ofner, D.G. Moore, P.A. Rühs, P. Schwendimann, M. Eggersdorfer, E. Amstad, D.A. Weitz, A.R. Studart, High-Throughput Step Emulsification for the Production of Functional Materials Using a Glass Microfluidic Device, Macromol. Chem. Phys. 218 (2017) 1–10. doi:10.1002/macp.201600472.

[85] E. Hoque, J.A. Derose, P. Hoffmann, B. Bhushan, H.J. Mathieu, Alkylperfluorosilane self-assembled monolayers on aluminum: A comparison with alkylphosphonate self-assembled monolayers, J. Phys. Chem. C. 111 (2007) 3956–3962. doi:10.1021/jp066101m.

[86] A. V. Krasnoslobodtsev, S.N. Smirnov, Effect of water on silanization of silica by trimethoxysilanes, Langmuir. 18 (2002) 3181–3184. doi:10.1021/la015628h.

[87] A.L. Cordeiro, S. Zschoche, A. Janke, M. Nitschke, C. Werner, Functionalization of poly(dimethylsiloxane) surfaces with maleic anhydride copolymer films, Langmuir. 25 (2009) 1509–1517. doi:10.1021/la803054s.

[88] S.G. Im, K.W. Bong, C.H. Lee, P.S. Doyle, K.K. Gleason, A conformal nano-

adhesive via initiated chemical vapor deposition for microfluidic devices, Lab Chip. 9 (2009) 411–416. doi:10.1039/b812121d.

[89] G. Simone, P. Neuzil, G. Perozziello, M. Francardi, N. Malara, E. Di Fabrizio, A. Manz, A facile in situ microfluidic method for creating multivalent surfaces: Toward functional glycomics, Lab Chip. 12 (2012) 1500–1507. doi:10.1039/c2lc21217j.

[90] Y. Bai, C.G. Koh, M. Boreman, Y.-J. Juang, I.-C. Tang, L.J. Lee, S.-T. Yang, Surface modification for enhancing antibody binding on polymer-based microfluidic device for enzyme-linked immunosorbent assay, Langmuir. 22 (2006) 9458–9467.

[91] W.-C. Sung, H.-H. Chen, H. Makamba, S.-H. Chen, Functionalized 3D-Hydrogel Plugs Covalently Patterned Inside Hydrophilic Poly(dimethylsiloxane) Microchannels for Flow-Through Immunoassays, Anal. Chem. 81 (2009) 7967–7973. doi:10.1021/ac901138w.

[92] B. Feyssa, C. Liedert, L. Kivimaki, L.S. Johansson, H. Jantunen, L. Hakalahti, Patterned Immobilization of Antibodies within Roll-to-Roll Hot Embossed Polymeric Microfluidic Channels, PLoS One. 8 (2013) e68918. doi:10.1371/journal.pone.0068918.

[93] J. Horak, C. Dincer, E. Qelibari, H. Bakirci, G. Urban, Polymer-modified microfluidic immunochip for enhanced electrochemical detection of troponin I, Sensors Actuators, B Chem. 209 (2015) 478–485. doi:10.1016/j.snb.2014.12.006.

[94] T.T. Vu, M. Fouet, A.M. Gue, J. Sudor, A new and easy surface functionalization technnology for monitoring wettability in heterogeneous nano- and microfluidic devices, Sensors Actuators, B Chem. 196 (2014) 64–70. doi:10.1016/j.snb.2014.01.085.

[95] H.Y. Chen, Y. Elkasabi, J. Lahann, Surface modification of confined microgeometries via vapor-deposited polymer coatings, J. Am. Chem. Soc. 128 (2006) 374–380. doi:10.1021/ja057082h.

[96] J. Xu, K.K. Gleason, Conformal, amine-functionalized thin films by initiated chemical vapor deposition (iCVD) for hydrolytically stable microfluidic devices, Chem. Mater. 22 (2010) 1732–1738. doi:10.1021/cm903156a.

[97] G. Kulsharova, N. Dimov, M.P.C. Marques, N. Szita, F. Baganz, Simplified immobilisation method for histidine-tagged enzymes in poly(methyl methacrylate) microfluidic devices, N. Biotechnol. 47 (2018) 31–38. doi:10.1016/j.nbt.2017.12.004.

[98] M. Oshige, K. Yumoto, H. Miyata, S. Takahashi, M. Nakada, K. Ito, M. Tamegai, H. Kawaura, S. Katsura, Immobilization of His-Tagged Proteins on Various Solid Surfaces Using NTA-Modified Chitosan, Open J. Polym. Chem. 03 (2013) 6–10. doi:10.4236/ojpchem.2013.31002.

[99] R. Khnouf, D. Karasneh, B.A. Albiss, Protein immobilization on the surface of polydimethylsiloxane and polymethyl methacrylate microfluidic devices, Electrophoresis. 37 (2016) 529–535. doi:10.1002/elps.201500333.

[100] T.F. Didar, A.M. Foudeh, M. Tabrizian, Patterning multiplex protein microarrays in a single microfluidic channel, Anal. Chem. 84 (2012) 1012–1018. doi:10.1021/ac2025877.

[101] A. Shakeri, N.A. Jarad, A. Leung, L. Soleymani, T.F. Didar, Biofunctionalization of Glass- and Paper-Based Microfluidic Devices: A Review, Adv. Mater. Interfaces. 1900940 (2019) 1900940. doi:10.1002/admi.201900940.

[102] M.P. Nicholas, L. Rao, A. Gennerich, Covalent Immobilization of Microtubules on Glass Surfaces for Molecular Motor Force Measurements and Other Single-Molecule Assays, Methods Mol Biol. 1136 (2014) 137–169. doi:10.1007/978-1-4939-0329-0_9.

[103] F. Darain, P. Yager, K.L. Gan, S.C. Tjin, On-chip detection of myoglobin based

on fluorescence, Biosens. Bioelectron. 24 (2009) 1744–1750. doi:10.1016/j.bios.2008.09.004.

[104] S. Demming, G. Peterat, A. Llobera, H. Schmolke, A. Bruns, M. Kohlstedt, A. Al-Halhouli, C.P. Klages, R. Krull, S. Büttgenbach, Vertical microbubble column-A photonic lab-on-chip for cultivation and online analysis of yeast cell cultures, Biomicrofluidics. 6 (2012) 034106. doi:10.1063/1.4738587.

[105] C. Cha, E. Antoniadou, M. Lee, J.H. Jeong, W.W. Ahmed, T.A. Saif, S.A. Boppart, H. Kong, Tailoring hydrogel adhesion to polydimethylsiloxane substrates using polysaccharide glue, Angew. Chemie - Int. Ed. 52 (2013) 6949 –6952. doi:10.1002/anie.201302925.

[106] K. Mondal, A. Ali, S. Srivastava, B.D. Malhotra, A. Sharma, Electrospun functional micro / nanochannels embedded in porous carbon electrodes for microfluidic biosensing, Sensors Actuators B Chem. 229 (2016) 82–91.

[107] M.A. Ali, S. Srivastava, P.R. Solanki, V. Reddy, V. V. Agrawal, C. Kim, R. John, B.D. Malhotra, Highly efficient bienzyme functionalized nanocomposite-based microfluidics biosensor platform for biomedical application, Sci. Rep. 3 (2013) 1–9. doi:10.1038/srep02661.

[108] J. Schütte, C. Freudigmann, K. Benz, J. Böttger, R. Gebhardt, M. Stelzle, A

method for patterned in situ biofunctionalization in injection-molded microfluidic devices, Lab Chip. 10 (2010) 2551–2558. doi:10.1039/c005307d.

[109] Y. Li, Z. Wang, L.M.L. Ou, H.-Z. Yu, DNA detection on plastic: surface activation protocol to convert polycarbonate substrates to biochip platforms, Anal. Chem. 79 (2007) 426–433.

[110] Y. Liu, D. Ganser, A. Schneider, R. Liu, P. Grodzinski, N. Kroutchinina, Microfabricated polycarbonate CE devices for DNA analysis, Anal. Chem. 73 (2001) 4196–4201. doi:10.1021/ac010343v.

[111] J.Y. Lichtenberg, Y. Ling, S. Kim, Non-specific adsorption reduction methods in biosensing, Sensors (Switzerland). 19 (2019) 2488. doi:10.3390/s19112488.

[112] W.J. Yang, T. Cai, K.G. Neoh, E.T. Kang, S.L.M. Teo, D. Rittschof, Barnacle cement as surface anchor for "clicking" of antifouling and antimicrobial polymer brushes on stainless steel, Biomacromolecules. 14 (2013) 2041–2051. doi:10.1021/bm400382e.

[113] C. Rodriguez-Emmenegger, M. Houska, A.B. Alles, E. Brynda, Surfaces Resistant to Fouling from Biological Fluids: Towards Bioactive Surfaces for Real Applications, Macromol. Biosci. 12 (2012) 1413–1422. doi:10.1002/mabi.201200171.

[114] J. Jiang, L. Zhu, L. Zhu, H. Zhang, B. Zhu, Y. Xu, Antifouling and antimicrobial polymer membranes based on bioinspired polydopamine and strong hydrogen-bonded poly(n -vinyl pyrrolidone), ACS Appl. Mater. Interfaces. 5 (2013) 12895–12904. doi:10.1021/am403405c.

[115] A.K. Epstein, T.-S. Wong, R.A. Belisle, E.M. Boggs, J. Aizenberg, Liquid-infused structured surfaces with exceptional anti-biofouling performance, Proc. Natl. Acad. Sci. U. S. A. 109 (2012) 13182–13187. doi:10.1073/pnas.1201973109.

[116] M. Tanaka, E. Sackmann, Supported membranes as biofunctional interfaces and smart biosensor platforms, Phys. Status Solidi Appl. Mater. Sci. 203 (2006) 3452–3462. doi:10.1002/pssa.200622464.

[117] M.Á. Sentandreu, L. Aubry, F. Toldrá, A. Ouali, Blocking agents for ELISA quantification of compounds coming from bovine muscle crude extracts, Eur. Food Res. Technol. 224 (2007) 623–628. doi:10.1007/s00217-006-0348-3.

[118] J.W. Haycock, Polyvinylpyrrolidone as a blocking agents in immunochemical studies, Anal Biochem. 208 (1993) 397–399. doi:10.1006/abio.1993.1068.

[119] G. Sui, J. Wang, C.C. Lee, W. Lu, S.P. Lee, J. V. Leyton, A.M. Wu, H.R. Tseng, Solution-phase surface modification in intact poly(dimethylsiloxane)

microfluidic channels, Anal. Chem. 78 (2006) 5543–5551. doi:10.1021/ac060605z.

[120] K.M. Kovach, J.R. Capadona, A. Sen Gupta, J.A. Potkay, The effects of PEG-based surface modification of PDMS microchannels on long-term hemocompatibility, J. Biomed. Mater. Res. - Part A. 102A (2014) 4195–4205. doi:10.1002/jbm.a.35090.

[121] T. Trantidou, Y. Elani, E. Parsons, O. Ces, Hydrophilic surface modification of pdms for droplet microfluidics using a simple, quick, and robust method via pva deposition, Microsystems Nanoeng. 3 (2017) 16091. doi:10.1038/micronano.2016.91.

[122] T.-S. Wong, S.H. Kang, S.K.Y. Tang, E.J. Smythe, B.D. Hatton, A. Grinthal, J. Aizenberg, Bioinspired self-repairing slippery surfaces with pressure-stable omniphobicity, Nature. 477 (2011) 443–447. doi:10.1038/nature10447.

[123] D.C. Leslie, A. Waterhouse, J.B. Berthet, T.M. Valentin, A.L. Watters, A. Jain, P. Kim, B.D. Hatton, A. Nedder, K. Donovan, E.H. Super, C. Howell, C.P. Johnson, T.L. Vu, D.E. Bolgen, S. Rifai, A.R. Hansen, M. Aizenberg, M. Super, J. Aizenberg, D.E. Ingber, Donald E Ingber, A bioinspired omniphobic surface coating on medical devices prevents thrombosis and biofouling, Nat. Biotechnol.

32 (2014) 1134. doi:10.1038/nbt.3020.

[124] P. Kim, T.S. Wong, J. Alvarenga, M.J. Kreder, W.E. Adorno-Martinez, J. Aizenberg, Liquid-infused nanostructured surfaces with extreme anti-ice and anti-frost performance, ACS Nano. 6 (2012) 6569–6577. doi:10.1021/nn302310q.

[125] L. Xiao, J. Li, S. Mieszkin, A. Di Fino, A.S. Clare, M.E. Callow, J.A. Callow, M. Grunze, A. Rosenhahn, P.A. Levkin, Slippery liquid-infused porous surfaces showing marine antibiofouling properties, ACS Appl. Mater. Interfaces. 5 (2013) 10074–10080. doi:10.1021/am402635p.

[126] P.W. Wilson, W. Lu, H. Xu, P. Kim, M.J. Kreder, J. Alvarenga, J. Aizenberg, Inhibition of ice nucleation by slippery liquid-infused porous surfaces (SLIPS), Phys. Chem. Chem. Phys. 15 (2013) 581–585. doi:10.1039/C2CP43586A.

[127] P. Kim, M.J. Kreder, J. Alvarenga, J. Aizenberg, Hierarchical or not? Effect of the length scale and hierarchy of the surface roughness on omniphobicity of lubricant-infused substrates, Nano Lett. 13 (2013) 1793–1799. doi:10.1021/nl4003969.

[128] M. Villegas, Y. Zhang, N. Abu Jarad, L. Soleymani, T.F. Didar, Liquid-Infused Surfaces: A Review of Theory, Design, and Applications, ACS Nano. 13 (2019)

8517–8536. doi:10.1021/acsnano.9b04129.

[129] N. Vogel, R.A. Belisle, B. Hatton, T.S. Wong, J. Aizenberg, Transparency and damage tolerance of patternable omniphobic lubricated surfaces based on inverse colloidal monolayers, Nat. Commun. 4 (2013) 1–10. doi:10.1038/ncomms3176.

[130] M. Badv, C. Alonso-Cantu, A. Shakeri, Z. Hosseinidoust, J.I. Weitz, T.F. Didar, S.M. Imani, M. Badv, A. Shakeri, H. Yousefi, D. Yip, C. Fine, T.F. Didar, Biofunctional Lubricant-Infused Vascular Grafts Functionalized with Silanized Bio-Inks Suppress Thrombin Generation and Promote Endothelialization, ACS Biomater. Sci. Eng. 5 (2019) 6485–6496. doi:10.1021/acsbiomaterials.9b01062.

[131] J. Li, T. Kleintschek, A. Rieder, Y. Cheng, T. Baumbach, U. Obst, T. Schwartz, P.A. Levkin, Hydrophobic liquid-infused porous polymer surfaces for antibacterial applications, ACS Appl. Mater. Interfaces. 5 (2013) 6704–6711. doi:10.1021/am401532z.

[132] P. Wang, Z. Lu, D. Zhang, Slippery liquid-infused porous surfaces fabricated on aluminum as a barrier to corrosion induced by sulfate reducing bacteria, Corros. Sci. 93 (2015) 159–166. doi:10.1016/j.corsci.2015.01.015.

[133] S. Yuan, S. Luan, S. Yan, H. Shi, J. Yin, Facile Fabrication of Lubricant-Infused Wrinkling Surface for Preventing Thrombus Formation and Infection, ACS

Appl. Mater. Interfaces. 7 (2015) 19466–19473. doi:10.1021/acsami.5b05865.

[134] R.E. Saunders, B. Derby, Inkjet printing biomaterials for tissue engineering: bioprinting, Int. Mater. Rev. 59 (2014) 430–448. doi:10.1179/1743280414Y.0000000040.

[135] C. Tu, B. Huang, J. Zhou, Y. Liang, J. Tian, L. Ji, X. Liang, X. Ye, A microfluidic chip for cell patterning utilizing paired microwells and protein patterns, Micromachines. 8 (2017) 1–15. doi:10.3390/mi8010001.

[136] Z. Tong, A. Ivask, K. Guo, S. Mccormick, E. Lombi, C. Priest, N.H. Voelcker, Crossed flow microfluidics for high throughput screening of bioactive chemical–cell interactions, Lab Chip. 17 (2017) 501–510. doi:10.1039/c6lc01261b.

[137] H. Yousefi, M.M. Ali, H.-M. Su, C.D.M. Filipe, T.F. Didar, Sentinel Wraps : Real-Time Monitoring of Food Contamination by Printing DNAzyme Probes on Food Packaging, ACS Nano. 12 (2018) 3287–3294. doi:10.1021/acsnano.7b08010.

[138] R. Majumdar, I. Paprotny, Lithography-Free Self-Reconfigurable Post-Release Stress Engineering of Surface Micro-Machined MEMS Structures, J. Micro Electro Mech. Syst. 26 (2017) 671–678. doi:10.31438/trf.hh2016.67.

[139] R. Majumdar, V. Foroutan, I. Paprotny, Post-release stressengineering of surfacemicromachined MEMS structures using evaporated Chromium and in-situ fabricated reconfigurable shadow masks, in: Proc. 28th IEEE Int. Conf. Micro Electro Mech. Syst., 2015: pp. 296–299.

[140] S. Hussain, S. Ward, O. Mahdavipour, R. Majumdar, I. Paprotny, Untethered Microscale Flight: Mechanisms and Platforms for Future MEMS Aerial Microrobotics, in: Proc. SPIE - Int. Soc. Opt. Eng., 2015: pp. 94940F–12. doi:10.1117/12.2190851.

[141] S. Ward, V. Foroutan, R. Majumdar, O. Mahdavipour, S.A. Hussain, I. Paprotny, Towards Microscale Flight: Fabrication, Stability Analysis, and Initial Flight Experiments for 300μm × 300μm × 1.5μm Sized Untethered MEMS Microfliers, IEEE Trans. Nanobioscience. 14 (2015) 323–331. doi:10.1109/TNB.2015.2427837.

[142] X. Guo, Y. Chen, L. Zhang, W. Liu, An inkjet printing paper-based immunodevice for fluorescence determination of immunoglobulin G, Anal. Methods. 11 (2019) 3452–3459. doi:10.1039/C9AY00893D.

[143] T.N. Stewart, B.E. Pierson, R. Aggarwal, R.J. Narayan, Piezoelectric inkjet printing of a cross-hatch immunoassay on a disposable nylon membrane,

Biotechnol. J. 4 (2009) 206–209. doi:10.1002/biot.200800234.

[144] M.S. Hasenbank, T. Edwards, E. Fu, R. Garzon, T.F. Kosar, M. Look, A. Mashadi-Hossein, P. Yager, Demonstration of multi-analyte patterning using piezoelectric inkjet printing of multiple layers, Anal. Chim. Acta. 611 (2008) 80–88. doi:https://doi.org/10.1016/j.aca.2008.01.048.

[145] T. Vong, S. Schoffelen, S.F.M. Van Dongen, T.A. Van Beek, H. Zuilhof, J.C.M. van Hest, A DNA-based strategy for dynamic positional enzyme immobilization inside fused silica microchannels, Chem. Sci. 2 (2011) 1278–1285. doi:10.1039/c1sc00146a.

[146] A. Arora, G. Simone, G.B. Salieb-Beugelaar, J.T. Kim, A. Manz, Latest Developments in Micro Total Analysis Systems, Anal. Chem. 82 (2010) 4830–4847. doi:10.1021/ac100969k.

[147] T. Vong, J. ter Maat, T.A. van Beek, B. van Lagen, M. Giesbers, J.C.M. van Hest, H. Zuilhof, Site-Specific Immobilization of DNA in Glass Microchannels via Photolithography, Langmuir. 25 (2009) 13952–13958. doi:10.1021/la901558n.

[148] B. Renberg, K. Sato, K. Mawatari, N. Idota, T. Tsukahara, T. Kitamori, Serial DNA immobilization in micro- and extended nanospace channels, Lab Chip. 9

(2009) 1517–1523. doi:10.1039/b823436a.

[149] Y. Saka, M. Macpherson, C. V Giuraniuc, Generation and precise control of dynamic biochemical gradients for cellular assays, Physica A. 470 (2017) 132–145. doi:10.1016/j.physa.2016.11.134.

[150] X. Luo, T. Vo, F. Jambi, P. Pham, J.S. Choy, Microfluidic partition with in situ biofabricated semipermeable biopolymer membranes for static gradient generation, Lab Chip. 12 (2016) 513–521. doi:10.1039/C6LC00742B.

[151] M. Meier, E.M. Lucchetta, R.F. Ismagilov, Chemical stimulation of the Arabidopsis thaliana root using multi-laminar flow on a microfluidic chip, Lab Chip. 10 (2010) 2147–2153. doi:10.1039/c004629a.

[152] Y. Zhou, Y. Wang, T. Mukherjee, Q. Lin, Generation of complex concentration profiles by partial diffusive mixing in multi-stream laminar flow, Lab Chip. 9 (2009) 1439–1448. doi:10.1039/B818485B.

[153] H. Chen, T.K. Choo, J. Huang, Y. Wang, Y. Liu, M. Platt, A. Palaniappan, B. Liedberg, A.I.Y. Tok, Label-free electronic detection of interleukin-6 using horizontally aligned carbon nanotubes, Mater. Des. 90 (2016) 852–857. doi:10.1016/j.matdes.2015.11.029.

[154] K.-Y. Ko, I.-H. Kim, Aragonite crystallization in a Christmas-tree model microfluidic device with the addition of magnesium ions, Biotechnol. Bioprocess Eng. 21 (2016) 453–462. doi:10.1007/s12257-015-0796-3.

[155] Y.-H. Jang, M.J. Hancock, S.B. Kim, S. Selimović, W.Y. Sim, H. Bae, A. Khademhosseini, An integrated microfluidic device for two-dimensional combinatorial dilution, Lab Chip. 11 (2011) 3277–3286. doi:10.1039/c1lc20449a.

[156] G.A. Cooksey, C.G. Sip, A. Folch, A multi-purpose microfluidic perfusion system with combinatorial choice of inputs, mixtures, gradient patterns, and flow rates, Lab Chip. 9 (2009) 417–26. doi:10.1039/b806803h.

[157] X. Wang, Z. Liu, Y. Pang, Concentration gradient generation methods based on microfluidic systems, RSC Adv. 7 (2017) 29966–29984. doi:10.1039/c7ra04494a.

[158] J. Atencia, J. Morrow, L.E. Locascio, The microfluidic palette: A diffusive gradient generator with spatio-temporal control, Lab Chip. 9 (2009) 2707–2714. doi:10.1039/B902113B.

[159] P. Shi, S. Nedelec, H. Wichterle, L.C. Kam, Combined microfluidics/protein patterning platform for pharmacological interrogation of axon pathfinding, Lab

Chip. 10 (2010) 1005. doi:10.1039/b922143c.

[160] R. Lovchik, C. Von Arx, A. Viviani, E. Delamarche, Cellular microarrays for use with capillary-driven microfluidics, Anal. Bioanal. Chem. 390 (2008) 801–808. doi:10.1007/s00216-007-1436-3.

[161] L. Wong, J.D. Pegan, B. Gabela-zuniga, M. Khine, K.E. Mccloskey, Leaf-inspired microcontact printing vascular patterns, Biofabrication. 9 (2017) 021001.

[162] D.J. Graber, T.J. Zieziulewicz, D.A. Lawrence, W. Shain, J.N. Turner, Antigen binding specificity of antibodies patterned by microcontact printing, Langmuir. 19 (2003) 5431–5434. doi:10.1021/la034199f.

[163] T. Fatanat Didar, M. Tabrizian, Generating multiplex gradients of biomolecules for controlling cellular adhesion in parallel microfluidic channels, Lab Chip. 12 (2012) 4363–71. doi:10.1039/c2lc40233e.

[164] Y. Temiz, R.D. Lovchik, E. Delamarche, Capillary-Driven Microfluidic Chips for Miniaturized Immunoassays: Patterning Capture Antibodies Using Microcontact Printing and Dry-Film Resists BT - Microchip Diagnostics: Methods and Protocols, in: V. Taly, J.-L. Viovy, S. Descroix (Eds.), Springer New York, New York, NY, 2017: pp. 37–47. doi:10.1007/978-1-4939-6734-6_3.

[165] S. Sathish, S.G. Ricoult, K. Toda-Peters, A.Q. Shen, Microcontact printing with aminosilanes: creating biomolecule micro- and nanoarrays for multiplexed microfluidic bioassays, Analyst. 142 (2017) 1772–1781. doi:10.1039/C7AN00273D.

Chapter 2: Biofunctionalization of Glass and Paper-based Microfluidic Devices; a Review

Amid Shakeri, Noor Abu Jarad, Ashlyn Leung, Leyla Soleymani, Tohid F Didar*

Advanced Materials Interfaces 2019, 6, 1900940; doi: 10.1002/admi.201900940

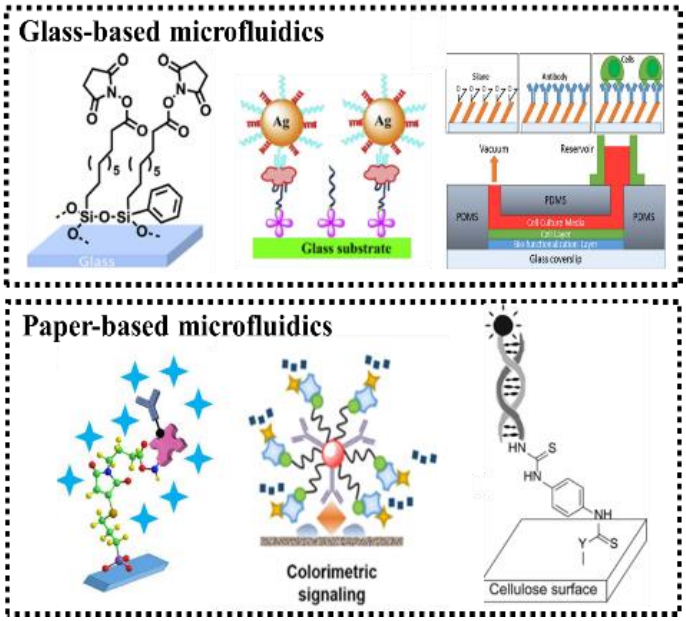

2.1 Abstract

Biofunctionalization of micro-channels is of great concern in the fabrication of microfluidic devices. Different substrates such as glass slides, papers, polymers, and beads require different biofunctionalization approaches granting the utilization of microfluidics in several biomedical applications. Covalent immobilization of biomolecules inside the microchannels is achieved by chemical modification of the surface such as silanization or introducing different coupling agents. Although creating biointerfaces that are covalently bonded to the microchannel surface necessitates multiple steps of surface modification and incubation times, it bestows a robust biointerface capable of withstanding high shear stresses and harsh conditions without dissipating the biofunctionality. Regarding the applications that do not require robustness and long-term stability, non-covalent attachment of biomolecules such as van der Waals and hydrophobic interactions are adequate to successfully create a functional biointerface. This review paper summarizes the various biofunctionalization approaches used in the most common microfluidic substrates: glass and paper. In addition, several biofunctionalization examples are proposed and described in detail along with their associated applications.

Keywords: microfluidics, biomolecules immobilization, silanization methods, paper-based microfluidics, glass substrates

2.2 Introduction

Microfluidic devices and lab-on-a-chip technology have been distinguished as a promising platform for ultrasensitive bioanalytical devices, point-of-care (POC) diagnostics and health monitoring systems, investigation of cell biology and tissue engineering, mixing and separation of bio-species, drug discovery, biohazard detection, as well as automating synthetic biology to create micro-organism and DNA foundries. [1–9] Incorporating microfluidics in different bioanalytical systems such as those based on fluorescence, colorimetric, electrochemical, and chemiluminescence readout, as well as mass spectrometry has significantly enhanced the limit of detection (LOD) of these assays. [10–19] In cell biology, microfluidics enables the integration of multiple cell lines to mimic "organs-on-chips" with the desired physiological conditions and hemodynamic forces. Lung-on-a-chip, gut-on-a-chip, vasculatures-on-a-chip, and heart-on-chip are some of the examples of this flourishing technology. [20–29]

In microfluidics, developing a biofunctional and biocompatible surface is a decisive step to make the microfluidic channel amenable to biological applications. The biofunctional channel facilitates the immobilization of the biomolecules such as proteins, antibodies, cells, DNAs, and enzymes to the channel surface. In microfluidic-based biosensors, for instance, a reliable immobilization technique can improve the efficiency of the bioreceptors in selectively capturing the sample analyte resulting in

high signals and lower limit of detections. [30] Moreover, in organs-on-chips, the right choice of surface functionalization method provides the means for culturing the desired cells in 2D or 3D and achieving fully confluent functional cells in a short time frame. [31] Biofunctionalization techniques in microfluidic channels determine the durability and stability of the final product against temperature, harsh chemical conditions and degradation as well as high shear forces. [32–34]

Immobilization of the biomolecules inside the microfluidic channels is not attainable unless the surface has either certain chemical properties or physical properties to anchor the biomolecules. An ideal biointerface should fulfill the following requirements: [35–37] (1) specificity to the desired biomolecule preventing non-specific adhesion and preserving the bioactivity of the biomolecule; (2) robust and stable immobilization; (3) sustainability to the optical properties of the device enabling optical readout techniques; (4) and temperature stability within the range used in the biological assays.

To make microfluidic channels biofunctional, the desired biomolecules can be covalently or non-covalently immobilized on the microchannel surface. Covalent immobilization is usually achieved by chemical modification of the substrate and chemisorption of the biomolecules on the surface. This needs more chemical reagents, incubation time, and surface modification steps compared to non-covalent immobilization. [38–41] However, the final biointerface would be more robust and can

withstand harsh environments such as high shear stresses which is usually the case for different microfluidic applications. In covalent immobilization, the biomolecules are usually bound to the functional groups of the surface through their amine moieties, carboxylic groups, or -CH_x terminates. Silanization process, generating a self assembled monolayer (SAM) of silane coupling agent, is the most commonly used method to obtain functional chemical groups specifically on the glass surfaces. This process results in the immobilization of the biomolecules via either their amine or carboxylic groups. [42–45] Use of succinimide esters is another way to chemically bind a protein to the surface. [37,46] In non-covalent immobilization, biomolecules are attached to the surface of the microfluidic channels by means of electrostatic interactions, hydrogen bonds, van der Waals interactions, and hydrophobic interactions. This is achieved by simple perfusion of the biomolecules into the channel followed by appropriate incubation. Non-covalent immobilization is weaker than covalent bonding resulting in lower efficiency of the immobilization process and higher chance of biomolecule detachment from the surface at high shear stresses. [47,48] In order to increase the yield of the immobilized proteins, the surface of the channels could be pre-treated using plasma etching or ultraviolent (UV) light which promotes the physical attachment of the proteins by changing the surface energy of the substrate.

Biocompatible substrates such as paper-based microfluidics [49–51] are also used for making biointerfaces. Paper-based microfluidics are usually well suited for biomolecule immobilization because of high physical absorption, bio-affinity, and bioactive ink entrapment. [52] Consequently, there is no need for further functionalization of the substrate. It is quite challenging to integrate paper substrates in an enclosed microfluidic channel as the porosity and hydrophilic nature of the majority of the papers can lead to leakage. Notably, 3D nature of paper fibers allow for 3D cell culture systems in microfluidics as well. [49] Extracellular Matrixes (ECMs) can also be incorporated in microfluidics as a 2D coating or a 3D structure. 2D ECMs such as fibronectin, collagen type I, and Matrigel are able to functionalize glass substrates. [53–56] To associate the surface with the 2D ECM, both covalent immobilization techniques such as silanization and physical attachment via simple ECM perfusion inside the channel are implemented.

There are several substrates that have been biofunctionalized and used in microfluidic systems such as glass slides, polymers, and paper. Each of these substrates could provide certain physical and chemical properties such as optical transparency, flexibility, mechanical strength, and chemical resistance. Choosing the proper method for functionalization of each substrate is important for developing various biological applications. This review paper revolves around the biofunctionalization of microfluidic devices, whereby the substrates are made of glass and paper. It initially elucidates the

silanization technique which is the most common biofunctionalization approach for covalent immobilization of biomolecules especially in glass-based microfluidic devices. Subsequently, we provide the most recent biofunctionalization examples along with their applications for glass and paper substrates in microfluidic channels.

2.3 Glass-based Microfluidic Devices

Glass is the most-commonly used material for microfluidic chip fabrication and surface functionalization. Glass has many advantages including high chemical stability, pressure resistance, hydrophilicity, and adaptability to many surface biofunctionalization techniques. [57] Hydroxylation of glass substrates are easy to achieve, (*e.g.* by oxygen plasma treatment) and the hydroxyl groups could remain active for a long time. Therefore, glass substrates are able to irreversibly bond to the plasma treated channel platform of the device (usually made of PDMS) by applying a gentle pressure. The hydroxyl groups in the channel permit several functionalization methods including silanization. The strong bond between the glass substrate and the polymeric layer makes it possible to fabricate multilayer microfluidic devices.

2.3.1 Silanization

Silanization of microfluidic substrates enables covalent immobilization of biomolecules on the microfluidic channels forming a robust and efficient biointerface. This process

has often been used to functionalize microfluidic channels with glass slides, [58,59] however it is also possible to use the same technique to functionalize the surface of the polymeric based channels which is not discussed in this review paper. Silane serves as a linker between the substrate and the biomolecule, and the termination of the silane needs to be selected depending on the type and conjugation of the biomolecule. Trimethoxysilane-based silanes such as 3-aminopropyltrimethoxysilane (APTMS), [42,60] (3-Glycidyloxypropyl)trimethoxysilane (GLYMO), [43] 3-methacryloxypropyl trimethoxysilane (MPTMS), [61,62] 3-mercaptopropyl trimethoxysilane (MPTMS), [63–66] 3-isocyanatopropyltrimethoxysilane (IPTMS), [67] as well as triethoxysilane-based silanes such as 3-aminopropyltriethoxysilane (APTES) [33,68–72] are the most commonly used silane coupling agents in microfluidics. Thermal stability (up to 250 ℃), mechanical and chemical stabilities, as well as capability to covalently anchor the ligands on the surface make the silane SAMs highly beneficial for generating a functional biointerface in microfluidics. [73–75]

A silane coupling agent is made of head groups, tail groups, and a backbone or spacer which provides a linkage between the tale and head groups **(**Figure 2-1**)**. Before performing the silanization, the substrate of interest is usually required to be hydroxylated to obtain OH groups. One approach to induce these hydroxyl groups is oxygen plasma treatment. [44,45,76–78] The other approach is using Piranha etching (a

mixture of sulfuric acid and hydrogen peroxide) to hydroxylate the surface. [68,70] These techniques also contribute to removing the impurities and residues from the surface which is an essential part of biological experiments. Ultraviolent (UV) irradiation with ozone is another conventional approach to hydroxylate the surface and simultaneously decontaminate it. [79] Washing the surface with water after the hydroxylation can also increase the efficiency of the process. [79] Hydroxylation of the microfluidic channels results in irreversible bonding of the microfluidic chip's layers (specifically when the device is made of PDMS or glass) due to the chemical reaction between the hydroxyl groups at the interface of the top and bottom layers. Since the hydroxylation techniques are adaptable with many surfaces such as glass, polymers including PDMS, silicon, and aluminium, a variety of substrates could be biofunctionalized using silane coupling agents. [80–84]

The silane coupling agent can be introduced to the surface for association with the hydroxylated layer through chemical vapor deposition (CVD) or liquid phase deposition (LPD) techniques, whereby a diluted silane solution (~1-5 volume percentages) is directly added to the substrate or perfused inside the channel. LPD is a simple and inexpensive process that does not rely on sophisticated equipment. [37,40,76,79,85] Optimizing the water content is critical as over-polymerization and formation of thick and disordered SAMs must be avoided. Moreover, insufficient amount of water leads

to partial polymerization which deteriorates the efficacy of functionalization. [79,86,87] CVD usually provides more packed and uniform SAM since the humidity and hydrolysis reactions could be accurately controlled. However, CVD treatment is more complex compared to LPD method and usually requires vacuum system and external pumps. Moreover, considering the closed system of microfluidics, it is usually difficult to silanize the inner surface of the channels. [68,88] CVD treatment could be conducted by either heating the silane solution in a closed system, use of vacuum, or employing heat and vacuum at the same time to fabricate the SAM more effectively at a shorter time period. [88–92] Silane CVD treatment could be followed by water CVD treatment to promote the SAM formation [92] through facilitating the hydrolysis reactions.

In both techniques, the head groups (methoxy and ethoxy groups) of the silane molecules undergo hydrolysis reactions leading to chemisorption of the silane coupling agent onto the substrate and formation of oxane bonds. [93] As the hydrolysis and condensation reactions continue, a crystalline or semi-crystalline self-assembled monolayer (SAM) of silane is formed on the surface through the lateral siloxane (Si—O—Si) polymerization, as well as interactions between the backbones caused by non-bonded reactions including electrostatic, van der Waals, steric, and repulsive forces. [94–97] The two models stated for creation of SAM layers include continuous growth model, whereby the disordered layer gradually converts to a crystalline SAM. The other model

is an island model, where localized SAM regions first nucleate and then grow to merge into each other creating a SAM. [84] The latter could occur when the water content of the reaction is high. [84,98]

The backbone of the silane agent and the interactions between the chains contribute to the robustness and mechanical properties of the SAM. [95,96,99] The tail groups of the silane coupling agent furnish the substrate with the desired physical or chemical characteristics. The kinetic of SAM formation is determined by ambient humidity, temperature, inter-molecular interactions, non-bonded interactions between adsorbates, as well as substrate-adsorbate and molecule-solvent interactions in LPD method. [97] The number of hydrolysable groups (head groups) in the silane coupling agent can also affect the kinetics and morphology of the SAM. Unlike the silane coupling agents with one head group, the bifunctional and trifunctional silanes such as APTES and GLYMO can possess multiple bonds to the substrates and create more packed and ordered SAM owing to the greater number of lateral siloxane linkages. [100,101] In multifunctional silanes – silanes with more than one head group – the silane coupling agent cannot always bind to the flat surface with all of its head groups because of the limitations in the silanol's bond length and angle. Therefore, some of the hydroxylated groups will remain functional for crosslinking and polymerization. When working with trifunctional silanes, one needs to precisely control the kinetics of the reaction.

Consequently, the multiple polycondensation reactions that lead to the formation of irregular, rough, and thick SAM can be precluded. [102]

In LPD method, APTES, APTMS, and GLYMO are usually diluted in toluene, ethanol, water, and acetone. [103–106] After introducing the silane solution to the microfluidic channel, an incubation time of 20 min to a couple of hours is required followed by washing steps to remove the excess amount of silane from the channel. The incubation time of silanization depends on the silane concentration and the substrate type. It is recommended to perform a heat treatment step afterwards to promote the oxane and siloxane formation and enhance the quality of SAMs. GLYMO induces epoxy terminal groups onto the modified surface. Epoxy rings are able to directly bind the amino groups of a protein or any amine-conjugated biomolecule. However, transforming the epoxy groups to the diol or thiol (Sulfhydryls) form could increase the efficiency of the reaction of the amino-groups of the biomolecules and bring about better immobilization. [107–109] APTES and APTMS treatment of the surface, on the other hand, provide amino tail groups on the surface. Amino groups can bind to the activated carboxylic groups of the proteins. Zero-length carbodiimide crosslinkers such as 1-ethyl-3-(-3-dimethylaminopropyl) carbodiimide hydrochloride (EDC or EDAC) [33,40,58,90,110] are usually used to activate the carboxylic groups by creating O-acylisourea intermediate. They react rapidly to the amino groups of the surface producing isourea as a by-product.

The other commonly used carbodiimide for crosslinking the carboxylic groups to the amino groups is diisopropylcarbodiimide (DIC). [111] O-acylisourea is very unstable, thus hydrolysis of the intermediate could result in regeneration of carboxylic groups by releasing N-unsubstituted urea. [112] N-hydroxysuccinimide (NHS) or sulfo-NHS are often used with EDC to stabilize the reaction for a few hours by forming NHS ester. The most efficient pH for the EDC crosslinking is 4.5 using 4-morpholinoethanesulfonic acid (MES) buffer. [113] EDC-NHS chemistry should be performed quickly because it can also result in crosslinking between amino groups of the protein to carboxylic groups of the adjacent protein thereby leading to aggregation of the antibody and loss of functionality. Immobilizing the antibodies through their carboxylic groups, which are mainly located on their fragment crystallizable region, (tail region, Figure 2-1c) can provide better antibody orientation compared to crosslinking the amino groups of the antibody to the surface. This is because the antigen-binding (Fab) fragment also contains amino groups. [112]

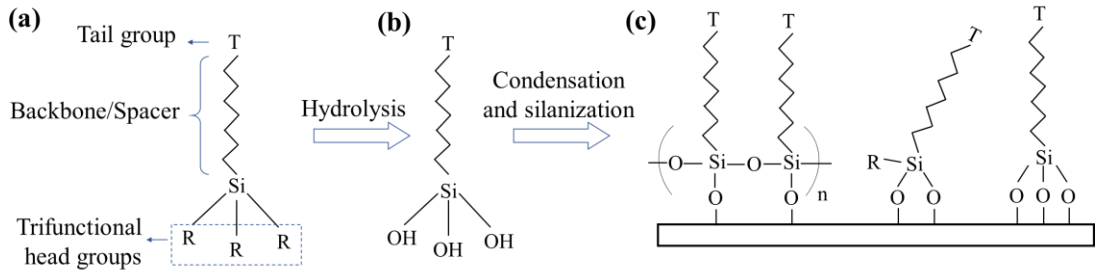

Figure 2-1. Schematic illustration of (a) a trifunctional silane coupling structure, (b) hydroxylation of the silane coupling agent, (c) three examples of various possibilities of silane bonding to a hydroxylated substrate.

2.3.2 Case Studies

Mccormick *et al.* [43] made a glass-PDMS microfluidic device to investigate the shear stress response on the HR1K B-lymphocytes cells. In this work, glass cover slips are first treated with 10% GLYMO diluted in distilled anhydrous toluene using LPD for 30 min to induce epoxy terminals on the surface. After washing and drying the surface, the glass substrate and PDMS layer were oxygen plasma treated to bond and form the channel. In order to protect the silanized layer of the substrate against etching by the plasma, a PDMS mask was used to cover the desired area during the plasma treatment and maintain its functionality after the device fabrication. This model was compared with a no-mask plasma treatment condition. After the device assembly, anti- CD20 antibody was flowed through the channel and incubated overnight at 4 ℃. The amino groups of the antibody covalently bind to the epoxy groups of the glass surface and form secondary amine bonds. The channels were seeded with the lymphocytes by pipetting the cells into the inlet port and withdrawing through the channel using a syringe pump (Figure 2-2a). In another study, Wong *et al.* [44] presented a glass-PDMS microfluidic platform to detect rare circulating tumor cells (CTCs) of the breast (MDA-MD-231) and prostate (PC3) in the blood. The device was composed of a PDMS layer containing multiple channels with herringbone-shape patterns that were bonded to a glass slide via oxygen plasma treatment. After the assembly, the channels were silanized with 1% N-[3-(Trimethoxysilyl)propyl]ethylenediamine (AEAPTMS) at room temperature to

create amino terminal groups on the surface. Next, NHS-functionalized Au nanoparticles diluted in ethanol were perfused in the channel to bind to the aminated surface with NHS esters. The channel was then incubated with NeutrAvidin. The amino groups of the lysines in the NeutrAvidin bind to the remaining free NHS groups of the Au particles. After the NeutrAvidin immobilization, biotinylated epithelial cell adhesion molecule (EpCAM) antibody was added to the channel and blocked with BSA. The device captured CTCs with high capture efficiency ranging between 96.4% ± 2.2 and 80.0% ± 1 and without damaging the cell viability.

Bavil *et al.* [114] used APTES treatment to functionalize a glass-PDMS microfluidic device for developing a microparticle-labeled immunoassay. In this work, a piranha cleaned glass slide was oxygen plasma treated with a PDMS mask on top so that only the desired areas were exposed to the plasma. Afterwards, the substrate was incubated in 5% APTES diluted in deionized water to form a SAM. The functionalized glass slide was bonded to an oxygen plasma treated PDMS layer to enclose the microchannels. They demonstrated the covalent immobilization of mouse IgG as well as monoclonal anti-cardiac troponin I through EDC-NHS activation technique. The device was implemented to detect cardiac Troponin I by a microparticle-labeled immunoassay (Figure 2-2b).

APTES treatment has also been utilized to functionalize glass beads and embed them in microfluidic channels. Microbeads significantly increase the available surface area which allows for more antibody immobilization. This enhances the sensitivity of the assay due to an increased antibody/target interaction. This technique is demonstrated in Guan *et al.*'s [40] work. Here, the device was made of a glass slide and PDMS channels, which were bonded together through UV treatment at 254 nm for 3 h, followed by a one day curing time at room temperature. To functionalize the glass beads, Piranha solution was used to etch the surface of the beads and induce hydroxyl groups. The beads were then APTES treated for 1 min using the LPD method. After washing, the beads were heated at 70 ℃ to dry them from the solutions. Next, anti-*E-coli* O157:H7 antibody was added to covalently attach to the amino groups of the beads using EDC/sulfo-NHS chemistry. The beads were also blocked with BSA to prevent non-specific adhesion. The device contained a microchamber in which only a monolayer of glass beads with the diameter of 50 μm could fit. This device was used for capture, enrichment, and quantification of *E. coli* in food samples. APTES treatment of the microfluidic channels is usually performed *in* situ after the preparation of the device platform. For instance, this method has been implemented in Zhang *et al.*'s [33] study to biofunctionalize the microfluidic channels *in situ*. They initially formed the microfluidic channels via plasma treatment technique to bond the PDMS platform containing the channels to a glass surface. The device was heated to further enhance the bond. Then, 2% APTES

solution diluted in 95% acetone was injected into the channels. To make the surface biofunctional, anti-fibronectin IgG antibody was activated via EDC-NHS and covalently bonded to the amino groups of the channel surface. The channel was also blocked with BSA to preclude non-specific attachment of the cells. They seeded the channel with murine cancer cells (S180 cells) for cell adhesion.

Although carbodiimide and NHS esters are usually used to activate the carboxylic groups and then crosslink it to the amine groups, Simone *et al.* [111] have introduced a new way to link NHS groups to the amine terminal groups of the surface. Their device was made of a glass substrate, a thin glass slide middle layer which was patterned using a CO_2 laser to create the layout of the channel and a poly(methylmethacrylate) (PMMA) top layer. After oxygen plasma treatment of the glass substrate, they bonded the device and incubated it with 30% APTES diluted in ethanol for 4 h. In order to induce succinimide terminal group on the amine groups, they introduced a mixture of 3% diisopropylcarbodiimide (DIC) and 3% NHS in dimethylformamide (DMF) to the surface and incubated it for 3 h. The channel was then incubated with 4,7,10-trioxa-1,13-tridecanediamine (3%) diluted in DMF for 3 h, and intruded the same solution of 3% DIC and 3% NHS in DMF to the channel for another 3 h. The channel was washed with DMS after each incubation step. The surface functional groups induced by this approach is shown in Figure 2-2(c-f). The created succinimide groups can covalently

link proteins, biomolecules, or any amine conjugated particle to the surface though their amine groups. Another technique to create amine to amine crosslinking is using glutaraldehyde. [115] In this case, glutaraldehyde binds to the amine tail of the silanized glass substrate, and the other end remains functional to bind to the amino groups of the desired antibody or biomolecule (Figure 2-2(g and h)). Notably, glutaraldehyde has acute toxicity and may cause throat and lung irritation, skin corrosion, and eye damage. Thus, special precaution such as respiratory protection and adequate ventilation should be considered.

Using biotin-streptavidin complex is a common method used for inducing biointerfaces on glass substrates. For example, De Vitis *et al.* [116] used this technique to functionalize the glass-PDMS microfluidic device with biotin, EDC, NHS, streptavidin and biotinylated anti-EpCAM to specifically capture proteins on the membrane of cancer cells to sort colon cancer cells (HCT-116) from healthy cells. After the microfluidic chamber was plasma treated and bonded, the micro-channels were treated with a solution of APTMS 30% in methanol for 1 h to obtain amino groups on the glass slide. Using the EDC-NHS activation, biotin was covalently bonded to the amine groups of the substrate. After that, streptavidin was introduced to the channel to bind to the immobilized biotin. In the next step, biotinylated anti-EpCAM was coupled with the biotin to capture the EpCAM proteins overexpressed on the tumor cell membrane.

Biotin-Streptavidin complex helps achieve an excellent alignment of the antibodies on the surface, thus the immobilization of antibody on the chip surface and the interactions between the surface and the cell membrane are enhanced. This method could be used to study the interaction between cell membrane and biomolecules, as well as isolate cancer cells in blood samples. As another example, we could mention the work done by Perozziello *et al.* [41]. In this study, microbeads were employed for celomic investigations, whereby the streptavidin-biotin interaction was used to couple antibodies to microfluidic devices. Here, they examined the cell rolling of mouse tumor cells MHC class I (MHC-I). The microfluidic chambers were assembled in PDMS and bonded to a glass slide by plasma radicalization. To covalently bind amino groups on the glass slide, a solution of 30% of APTMS in methanol was perfused inside the chamber and incubated for 1 h at room temperature. Further, through EDC-NHS reaction, a biotin was bridged to the surface after 2 h incubation at 4 ℃. Next, the microfluidic chamber was incubated with streptavidin-conjugated beads for 1 h. Biotinylated anti-mouse H-2Kb/H-2Db was then injected in the microfluidic chamber and incubated for 1 h at 4℃ to react with streptavidin (Figure 2-3a). Tumor cell lines were rolled across antibodies which are capable of forming complexes with MHC-I. The results showed that the cells treated with a bio-functionalized micro-beads had the lowest fluorescence intensity verifying the removal of MHC-I molecules.

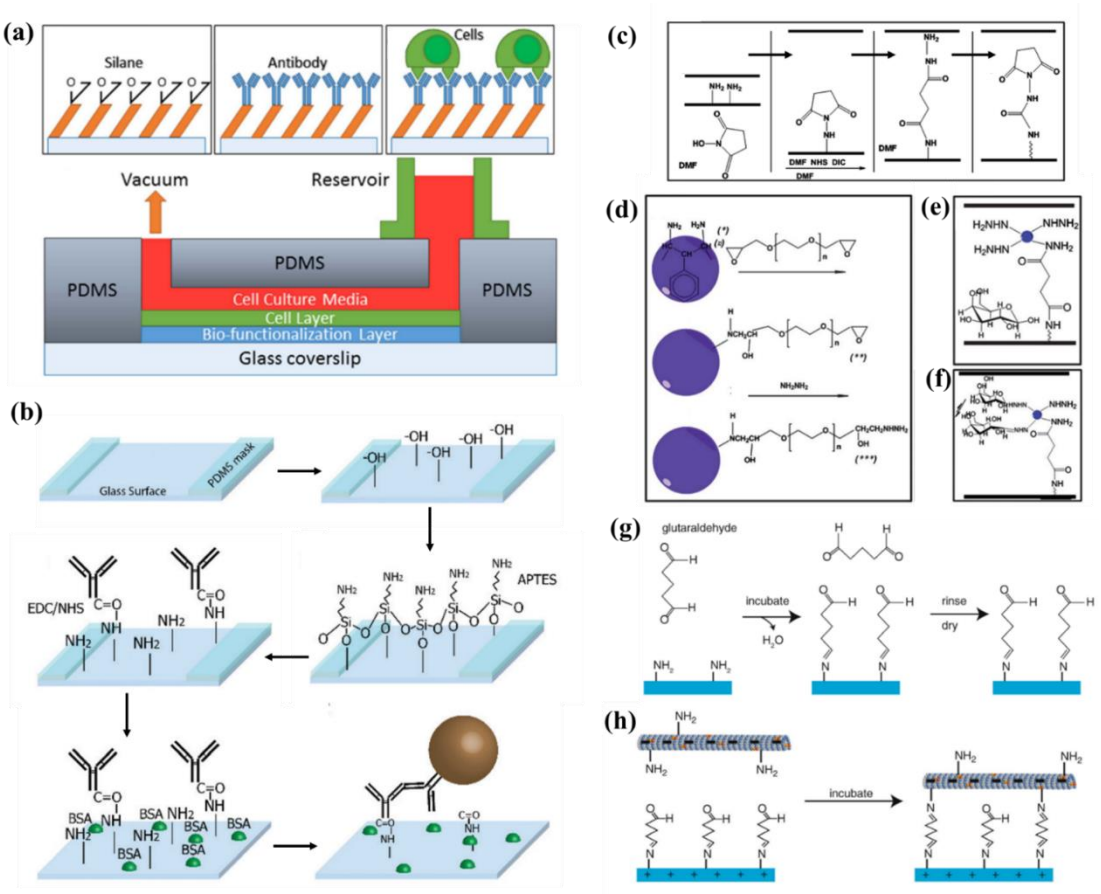

Figure 2-2. Schematic illustration of silanization in microchannels with a glass substrate: (a) 3-(glycidyloxypropyl)trimethoxysilane (GLYMO) treatment in a microfluidic channel. Reproduced with permission. [43] Copyright 2018, IOPscience. (b) 3-aminopropyltriethoxysilane (APTES) treatment. Biotinylated anti-mouse IgG conjugated with streptavidin-coated microparticles bound to the biofunctional microchannel coated with mouse IgG. Reproduced with permission. [114] Copyright 2018, Royal Society of Chemistry. (c) APTES treatment followed by succinimide group crosslinking, (d) Converting amine-conjugated microbeads to oxirane beads using diethylene glycol diglycidyl ether, and then to hydrazide beads using $NH_2NH_2{\cdot}H_2O$, (e) Perfusion of the hydrazide beads in the NHS-treated channel which results in chemically binding of the particles to the NHS groups of the glass surface. (f) using the remaining hydrazide groups on the particles to bind to monosaccharide carbohydrates. Reproduced with permission. [111] Copyright 2012, Royal Society of Chemistry. (g) Functionalization of the amine-treated glass with glutaraldehyde. (h) immobilization of amine-conjugated microtubes on the glutaraldehyde treated glass substrate. Reproduced with permission. [115] Copyright 2014, Springer.

In addition to nanoparticles, carbon nanotubes are also considered a good candidate to increase the surface area and to improve the biofunctionality of glass-based microfluidic systems. One of the best examples is the work done by Ali *et al.* [117] in which an electrochemical functionalization protocol is provided to integrate nickel oxide (NiO) nanoparticles and multi-walled carbon nanotubes (MWCNTs) with glass-PDMS microchannels. MWCNTs have a large surface area, very high tensile strength, as well as carrier mobility which lead to quantum electron transport. The presence of NiO is important as it prevents the MWCNT from aggregating. The functional groups and the large surface area are the main biofunctionalization aspects of this microfluidic device. The introduced biochip estimated the total cholesterol in the body. In this technique, the glass slide substrate was indium tin oxide (ITO) coated and a mixture of $H_2O_5 : H_2O_2 : NH_3$ (5:1:1) was used to hydrolyze it for bonding to the PDMS layer. The carboxyl-terminated MWCNTs and the NiO nanoparticles are negatively and positively charged resulting in increased electrostatic interactions. Functionalization was performed through the carboxylation and amidation of the nNiO-MWCNT nanocomposite. The carboxylic groups of the carbon nanotubes were activated through EDC-NHS to covalently bind to the amino groups of a bienzyme containing cholesterol oxidase (ChOx) and cholesterol esterase (ChEt). The formation of covalent (C-N) amide bonds was confirmed via X-ray photoelectron spectroscopy (XPS) studies. The large surface area of the MWCNTs and the presence of abundant functional groups improves

the stability and reproducibility of the system. The covalent functionalization onto MWCNT composite matrix was highly sensitive to cholesterol oxidation making the bio-enzyme chip a suitable platform for cholesterol monitoring.

Non-covalent immobilization of the biomolecules is also sometimes used to introduce biofunctionality to the surface. For instance, Tachikawa *et al.* [56] non-covalently attached laminin, the main component of ECM, to a glass substrate in order to provide bio-functionality in microfluidic channels. They used the device to investigate prostate cancer cell invasion by chemotaxis. The PDMS platform with multiple channels was fabricated through soft-lithography using a glass mold that was formed by three-dimensional stereoscopic exposure. The conventional oxygen plasma activation was also applied to bond the PDMS chip to the glass substrate (Figure 2-3b). In order to functionalize the glass substrate for cell attachment, they coated the channel with laminin before introducing the cancer cell suspension to the first channel. In their device, due to the hydrostatic pressure induced in the second channel and the small diameter of orifice channels crossing between the two channels, the cells were trapped in the orifice regions forming clusters. Thus, the cancer cell invasion effect was easily observed in the microfluidic channel, whereby intercellular interactions among the cells was studied.

A common problem with biofunctional interfaces used in microfluidics is that they need stringent storage conditions. Typically, these devices are stored at low temperatures (4-8 ℃ or less) in order to retain biofunctionality. However, this limits the access to point-of-care diagnostic and lab-on-a-chip technologies in settings where refrigeration and electricity are not available. [118,119] It could also increase the cost of transportation. To address this issue, Asghar *et al.* [37] have presented a multilayer surface preservation technique in microfluidic systems where multiple antibodies and proteins were conjugated together. Their biofunctional channels remained stable for 6 months at room temperature. Multi-layer immobilization technique can also bring about immobilized antibodies with preferred orientations. They used this technique to fabricate microfluidic devices for CD4 T cell counting. In the proposed protocol, oxygen plasma treated glass substrates were first silanized using 4% (3-Mercaptopropyl) trimethoxysilane in ethanol using LPD. Afterwards, the PMMA platform containing the channel cavity was attached to the glass slide using a double-sided adhesive. N-γ-maleimidobutyryl-oxysuccinimide ester (GMBS) was infused into the channel so that the maleimide groups of the GMBS react to sulfhydryl (–SH) terminal groups of the silanized glass and create thioether bond. The other maleimide end group of GMBS remain functional to covalently bind to the amino groups of the NeutrAvidin which was subsequently added to the channel. The next layer was biotinylated anti-CD4 antibody, which was added together with BSA as a blocking agent (Figure 2-3c). The channel was

incubated with Trehalose to preserve the biofunctionality. Trehalose is usually used to protect the biomolecules against heat, desiccation, and cold. [38] The preserved devices just needed to be washed with PBS for reactivation.

Functional nucleic acids are commonly used to create biofunctional interfaces in microfluidics. Zhao *et al.* [39] have developed microfluidic devices that use silver nanoparticles and aptamers to colorimetrically detect thrombin. The device was made by bonding a PDMS layer with the channel cavity to a glass substrate via oxygen plasma treatment. The channel was coated with streptavidin by overnight incubation at 4 ℃. There was no prior functionalization on the glass substrate, consequently, streptavidin non-covalently stuck to the channel surface. After proper washing, biotinylated 15- mer thrombin aptamer was passed through the channel to be functionalize on the surface for capturing thrombin. The colorimetric assay was performed by mixing thrombin with Ag nanoparticles conjugated with aptamer 29. The nanoparticles were properly blocked to prevent non-specific adhesion (Figure 3d). The mixture was constantly perfused through the channel for the purpose of detection. Considering the selectivity of the aptamer of choice, this method could be employed for detection of other biomolecules.

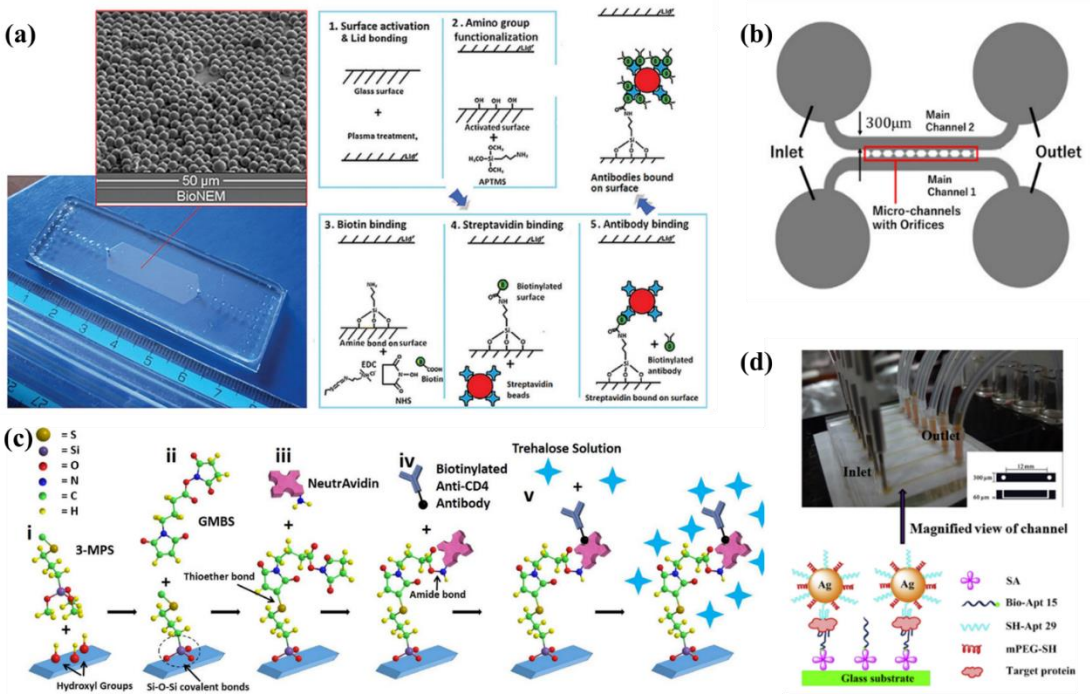

Figure 2-3. (a) Immobilization of streptavidin-conjugated beads on 3-aminopropyltrimethoxysilane (APTMS) treated surface coupled with a biotinylated antibody. Reproduced with permission. [41] Copyright 2013, Wiley. (b) Microfluidic design functionalized with laminin and used for the study of cancer cell invasion and intercellular interactions. Reproduced with permission. [56] Copyright 2019, Wiley. (c) Multilayer surface preservation technique on a (3-Mercaptopropyl) trimethoxysilane (3-MPS) treated glass using N-γ-maleimidobutyryl-oxysuccinimide ester (GMBS). Notably, the terminal groups of 3-MPS is S-H which is labeled with S-C in the reprinted figure by mistake. Reproduced under the terms of the CC BY 4.0 license. [37] Copyright 2016, Attribution 4.0 International (d) Functionalization of the channel with biotinylated 15- mer thrombin aptamer through non-covalent coating of the channel with streptavidin (ST). Reproduced with permission. [39] Copyright 2016, Elsevier.

In photolithographic patterning, the silanol groups of the substrate in a microfluidic channel is covalently bound with the certain patterns of the desired biomolecule after the fabrication of the microfluidic channels [120]. This technique usually involves the use of a photosensitive layer, masking a pattern, and UV light to activate a photosensitive linker. In these techniques, the microchannel is initially filled with a photosensitive

linker. Afterwards, by using UV light and a photomask with the desired pattern, one would be able to cleave the linker revealing localized reactive moieties on the surface. The biofunctional moieties can then couple with the biomolecules and enzymes. Vong *et al.* [57] have used UV-irradiation method to locally immobilize single stranded DNA (ss-DNA) in a closed fused silica microchannel. Fused silica was used here to ensure transparency in the UV-irradiation range. Here, the channel was filled with 2,2,2-tri-fluoroethylundec-10-enoate (TFEE) and irradiated for 10 h using a mask and mercury lamps. After that, amine-conjugated ss-DNA was added to the channel. Thus, during a carbonyl substitution reaction, the trifluoroethanol groups of the activated ester was replaced with the primary amino group of the ss-DNA. The immobilized ss-DNA could be used to immobilize other DNA-conjugated biomolecules. It is possible to reuse the device by dehybridization and hybridization of the DNA in order to remove one biomolecule and immobilize another one on the channel surface.

Another approach to create covalent patterns with UV-irradiation technique is a constructive method in which the ligand of interest is first mixed with the UV-sensitive linker, and then perfused inside the channel and exposed to the UV light. [121,122] Renberg *et al.* [123] have used this technique to covalently and locally immobilize DNA oligos on fused silica microfluidic channels formed via electron beam lithography technique. The channels were initially coated with 3% APTES by injecting the solution

inside the channel for 2 h at 5 ml/min. Furthermore, benzophenone-PEG12-COOH UV-linker was added to the channel. Using an active ester, the carboxylic groups of the surface couple with the amino groups of APTES and form amide bonds, while the benzophenone groups protrude outwards (Figure 2-4a). The hydrophilic PEG-spacer keeps the reactive benzophenones in a distance from the surface and makes the surface hydrophilic, thereby increasing the efficiency of the ligand immobilization. Afterwards, the biomolecule of choice was perfused through the channel, and the channel was then irradiated with UV light. UV results in formation of excited triplet state in benzophenone which binds the -CH_X groups of the biomolecules (Figure 2-4b). In this work, DNA oligomers were chosen as the biomolecule to be patterned on the surface. DNA oligos can be used to immobilize DNA-conjugated proteins and cells. [124,125] The disadvantages associated with such procedures are the high cost of chip fabrication, difficulty in channel bonding, and taking extreme precautions in the UV-irradiation step as it can decompose and denature the DNA and other biomolecules.

Recently, Carvalho *et al.* [126] presented a photolithography technique that does not require UV irradiation. Consequently, the microfluidic device is not required to be fabricated out of UV transparent materials, but rather can be made from standard commercial glass substrates. In order to locally functionalize the surface, a mixture of H-$SiPhCl_2$ and H-$SiCl_3$ in anhydrous cyclohexane was injected to the microchannels

made of borosilicate glass substrate. After 20 min incubation and proper washing, an NHS-terminated alkene was added to the channel and exposed to a pen lamp using a filter and a mask. H-$SiCl_3$ creates a hydrogen-terminated glass that can undergo hydrosilylation induced by light at $\lambda = 302$ nm. It is hypothesized that the phenyl ring of the phenylsilane (*i.e.* phenyldichlorosilane, H-$SiPhCl_2$) could lead to photochemical homolytic cleavage of Si−H bond at longer wavelengths by stabilization of intermediate Si· radicals and facilitation of the reaction (Figure 2-4c). Therefore, the wavelength required for the hydrosilytion increased to larger than 328 nm. The locally induced Si· radicals directly couple with NHS-functionalized ω-alkenes and form bio-functional patterns capable of bonding to any protein and biomolecule containing amino moieties. In this work paper, the immobilization of amino- terminated silicon nanoparticles and amino-terminated guanidine-rich DNA as a proof of concept has been demonstrated. In Table 2-1, different linkers used to introduce biointerface on the glass substrates have been summarized.

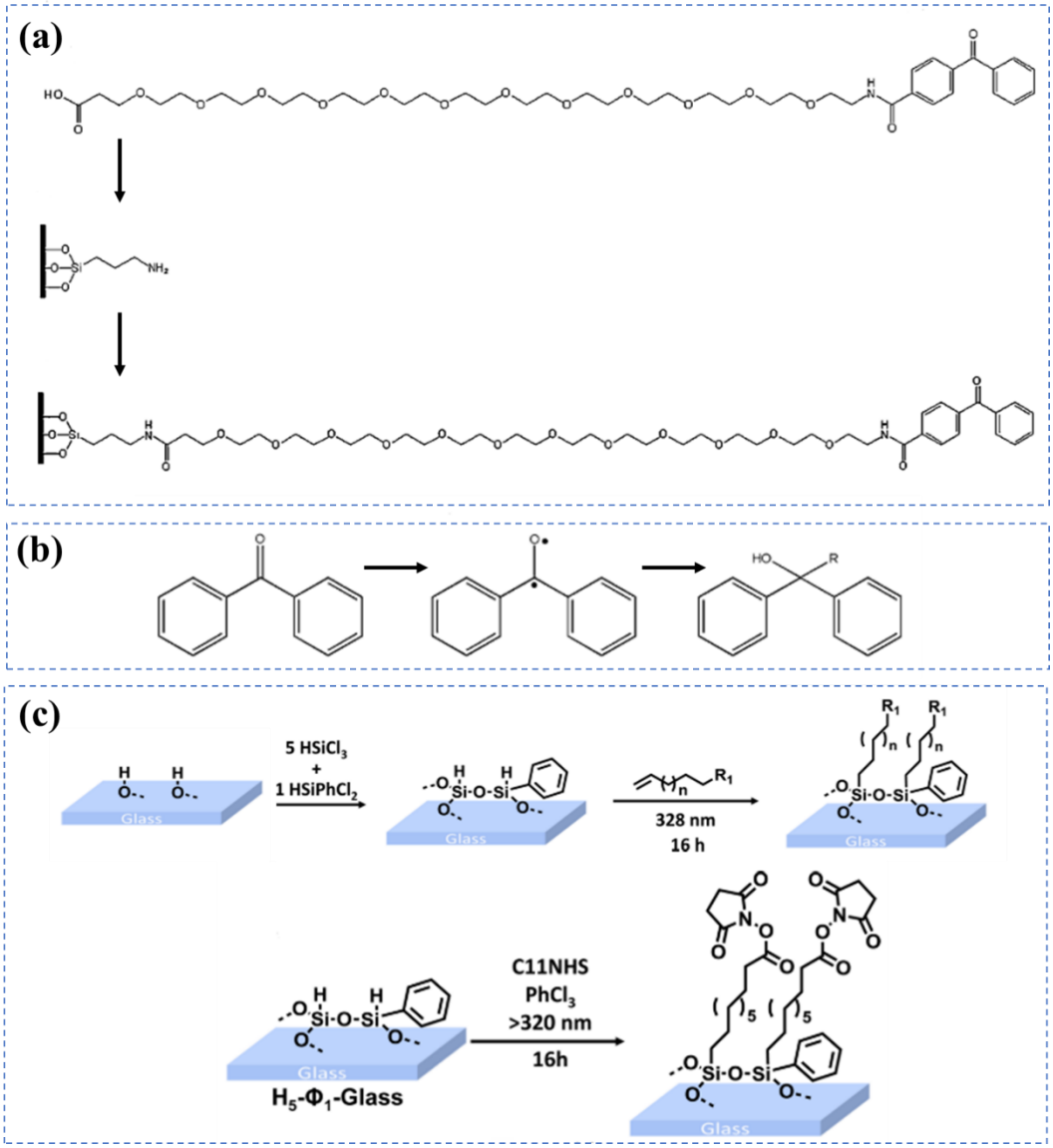

Figure 2-4. (a) Functionalization of the fused silica microfluidic channels with benzophenone through silanization of the substrate. (b) Formation of excited triplet state in benzophenone via UV exposure at 365 nm. Excited benzophenone reacts with -CHX groups of the biomolecules and forms covalent carbon–carbon bonds. Reproduced with permission. [123] Copyright 2009, Royal Society of Chemistry. (c) Functionalization of glass substrate with H-$SiPhCl_2$ and H-$SiCl_3$ followed by NHS-terminated alkene addition for photolithography patterning at λ = 328 nm. Reproduced with permission. [126] Copyright 2017, ACS publications.

Table 2-1. Biofunctionalization of the glass substrates in microfluidic channels

Coupling Method	Chemical Bonding	Immobilized Biomolecule	Application	Advantages	Disadvantages	Ref.
GLYMO + Anti- CD20 antibody	Covalent	HR1K B-lymphocytes cells	Investigation of shear stress on the cells	One-step chemical modification; possibility of patterning	Masking in plasma treatment step could be imprecise	[43]
AEAPTMS + NHS-functionalized Au nanoparticles + NeutrAvidin	Covalent	EpCAM antibody	Detecting rare circulating tumor cells of the breast and prostate	High efficiency in CTCs capturing and recovery	Complex functionalization method integrated with nanoparticles	[44]
APTES + EDC-NHS	Covalent	mouse IgG and monoclonal anti-cardiac troponin I	Detection of cardiac Troponin I via microparticle-labeled immunoassay	Simple surface modification; possibility of patterning	Masking in plasma treatment step could be imprecise	[114]
APTES + EDC/sulfo-NHS	Covalent	Anti-E-coli O157:H7 antibody	Detection of E.coli in food samples	High sensitivity in detecting E. coli	Use of nanoparticles made the procedure more challenging	[40]
APTES + EDC-NHS + Anti-fibronectin IgG	Covalent	murine cancer cells (S180)	Studying in-situ bio-functionalization and cell adhesion	Relatively simple functionalizati on	–	[33]
APTES + DIC-NHS + 4,7,10-trioxa-1,13-tridecanediamin e	Covalent	Colon tumor cells	Mimicking the cellular environment	Creating multivalent surfaces with high sensitivity and specificity	Complex and long functionalization technique	[111]

APTMS + EDC-NHS + Biotin + Streptavidin + Biotinylated anti-EpCAM	Covalent	EpCAM	Isolating of cancer cells from healthy cells	Great alignment of the antibodies on the surface		[116]
APTMS + EDC-NHS + biotin + streptavidin conjugated beads	Covalent	Biotinylated anti-mouse H-2Kb/H-2Db	Investigating of cell rolling of mouse tumor cells (MHC-I)	Creating multivalent surfaces in an assembled microchannel	Relatively long functionalization process integrated with use of nanoparticles	[41]
carboxyl-terminated nNiO-MWCNTs + EDC-NHS	Covalent	Bienzyme containing ChOx and ChEt	Monitoring cholesterol levels	High selectivity and sensitivity	More complex functionalization process with use of nanomaterial composite	[117]
Laminin	Non-covalent	Prostate cancer cells	Investigation of the cancer cell invasion	Simple and fast technique	Possibility of biomolecule removal due to lack of covalent bonds	[56]
(3-Mercaptopropyl) trimethoxysilane + GMBS	Covalent	Biotinylated anti-CD4 + Trehalose	CD4 T cell counting	Immobilization of the antibodies with preferred orientations; preserving antibodies	More chemical modification steps	[37]
Streptavidin + biotinylated 15-mer thrombin aptamer	Non-covalent	Thrombin mixed with aptamer 29-conjugated nanoparticles	Detecting thrombin via colorimetric assay	straightforward colorimetric detection	Possibility of biomolecule removal due to lack of covalent bonds; more complex functionalization method with use of nanoparticles	[39]

TFEE + UV irradiation	Covalent	amine-conjugated ss-DNA	Locally immobilizing ss-DNA	Possibility of *in situ* patterning	UV side effects; High cost of chip fabrication	[57]
APTES + Benzophenone-PEG12-COOH UV-linker	Covalent	DNA oligos + UV irradiation	Local immobilization of DNA-conjugated proteins and cells	Possibility of *in situ* patterning	UV side effects; High cost of chip fabrication	[123]
H-$SiPhCl_2$ and H-$SiCl_3$ + NHS-terminated alkene	Covalent	Amino-terminated silicon nanoparticles and amino-terminated guanidine-rich DNA	Local immobilization of biomolecules with amine moieties without UV irradiation	Possibility of *in situ* patterning	More chemical functionalization steps	[126]

2.4 Paper-based Microfluidics

Paper-based microfluidics are mostly used in combination with colorimetric and electrochemical readout for detecting biomolecules. [127–130] These devices are made of low-cost bioactive papers such as nitrocellulose membranes (*e.g.* Whatman BA85 Protran) or cellulose-based papers (*e.g.* chromatography paper). [131] Nitrocellulose membranes have a hydrophobic nature induced by their porous amorphous structure. [131] This hydrophobicity results in non-specific binding of hydrophobic biomolecules, which decreases their sensitivity. Post-processing such as adding surfactants is usually required to provide wettability on nitrocellulose. [132] Moreover, since capillary forces are not able to govern fluid movement in hydrophobic nitrocellulose, external equipment would be required for fluid pumping. Furthermore, to biofunctionalize the surface of the nitrocellulose membranes, the biomolecules are usually physiosorbed

(passive adsorption) to the membrane since there are only a few options for chemical immobilization. [133,134] It is hypothesized that the hydrophobic region of the biomolecules could interact with the hydrophobic carbon containing nitrocellulose resulting in the physical deposition of the biomolecules. [135] The other proposed mechanism is electrostatic interaction of the dipole nitrated groups and the biomolecule's dipoles. [136,137] The abovementioned disadvantages together with the breakability of the nitrocellulose makes it an unsuitable membrane for most of the lateral flow devices in microfluidics. On the other hand, cellulose-based papers are hydrophilic due to the higher pore size compared to the nitrocellulose surface [131] allowing the fluid to flow by capillary forces without any need for a syringe pump or other equipment. Whatman cellulose papers are made of cotton cellulose providing a higher degree of polymerization and crystallinity. [131]

In order to make a microchannel out of a paper sheet, it is possible to cut the sheet according to the shape and size of the desired channels using a computer-controlled cutter. Hydrophobic boundaries could also be created around the hydrophilic paper substrate to direct the liquid along the specific pathway towards the detection zone. There are a variety of techniques to create hydrophobic patterns on the paper sheet, including physical or chemical deposition of hydrophobic materials such as wax,

PDMS, and alkyl ketene dimer (AKD). These different methods are categorized in the review paper written by Li *et al.* . [138]

It is possible to immobilize biomolecules such as proteins, cells, and nucleic acids on paper using various techniques. As cellulose papers are biocompatible, researchers often physically immobilize the biomolecules on the paper by soaking the substrate with the biomolecule and reagents. This also allows for simple patterning of the paper with biomolecules via contact printing and non-contact printing (*e.g.* inkjet printing) techniques. [139] Depending on the porosity of paper, biomolecules will be trapped within the fibers. [50,140,141] The porosity of the paper is due to the voids between fibers, the retained lumen, and the inherent pores of the fiber walls. [139] Other than trapping inside the pores, the slightly negative charge of the cellulose surface can result in electrostatic attachment of the proteins form their cationic parts, as well as other ionic species via their positively charged moieties. [125,139]

Hong *et al.* [49] used a tree-shape design of channels to induce drug concentration gradients on a chromatography paper. They employed doxorubicin (DOX) as the model drug and investigated human epithelial cells response to the drug. In order to integrate the chromatography paper in microfluidic channels, they spin-coated a negative photoresist on the surface of the paper. After the paper was entirely soaked with the photoresist, they used conventional photolithographic technique to form the channels

on the photoresist. These hydrophilic microchannels within the hydrophobic photoresist-coated paper guide the fluid along the specified areas. The achieved paper microfluidic device was then placed between two PDMS layers containing the inlets and cell culture wells. They also tightened the device between two fixers at the top and bottom which are connected to each other by screws. After forming the drug gradient, they added the mixture of cells and collagen type I to the wells. The combination of collagen ECM and 3D paper fibers enabled them to perform 3D cell culture. Although this device was not easy to fabricate, it was claimed to be reusable.

One of the major problems with the open paper-based microchannels is evaporation of the fluid. This could be overcome by enclosing the paper sheet in a pre-made microfluidic channel to create a closed system by bonding the device. This technique has been used in the research done by Dou *et al.* [50] to simultaneously detect three types of bacterial meningitis including *Neisseria meningitidis*, Streptococcus pneumoniae, and *Haemophilus influenzae* type b. In this work, the papers were directly inserted inside the prefabricated PDMS layers. The device comprises a top PDMS layer with the channel cavity and inlets, a middle PDMS layer with the well-shaped zones for loop-mediated isothermal amplification process (LAMP) and a bottom glass substrate. The channels and wells were constructed with laser cutter and biopsy punches. The paper substrates that were cut using the laser cutter were placed inside the wells, and the

device was assembled using the oxygen plasma treatment (Figure 2-5a). Without doing any further functionalization, the paper disks were loaded with bacterial Hib DNA sequences and the LAMP mixture were added to the specified zones. The device could detect the pathogens with high sensitivity and long shelf life.

Moreover, Sanjay *et al.* [140] made a biosensor device using the same technique of chromatography paper embedded inside microfluidic channels. They have shown that the device is capable of detections of Immunoglobulin G (IgG) and Hepatitis B surface antigen with a limit of detection comparable to the conventional ELISA tests. In their design, the microchannels and wells were formed in a PMMA layer using a laser cutter. The paper sheet was placed on the PMMA layer with the funnel-shaped wells and cut with the laser cutter so that the paper disks fall into the wells (Figure 2-5b). For bonding the device, the assembly was clamped together and heated at 115–120 °C for 35 minutes. The primary antibodies or reagents can be directly immobilized onto the 3D micro-porous paper by passing through the paper along the wells. Further, the paper surface could be blocked with BSA and Tween 20 to prevent non-specific attachment of the secondary antibodies. Since the immobilization of the antibodies/antigens on the paper surface is very fast (about 10 minutes) and the device design eliminates the need for repeated micropipetting the reagents inside the wells, the immunoassay could be performed faster than conventional ELISA. In another work done by Huang *et al.* [142]

a paper-based analytical device (PAD) was used to detect prostate cancer biomarker (kallikrein-3, KLK3). Immobilization of KLK3 was done by printing 3 µl of the antibody solution onto PAD and waiting until it dries. The surface was also blocked with BSA. For the colorimetric sensing strategy, Au nanoparticles were coated with biotinylated poly(adenine) ssDNA conjugated with streptavidin-horseradish peroxidase (HRP), as well as anti-kallikrein-3 (aKLK3). The probe solution was then added to the KLK3 coated zones of the PAD (Figure 2-5c).

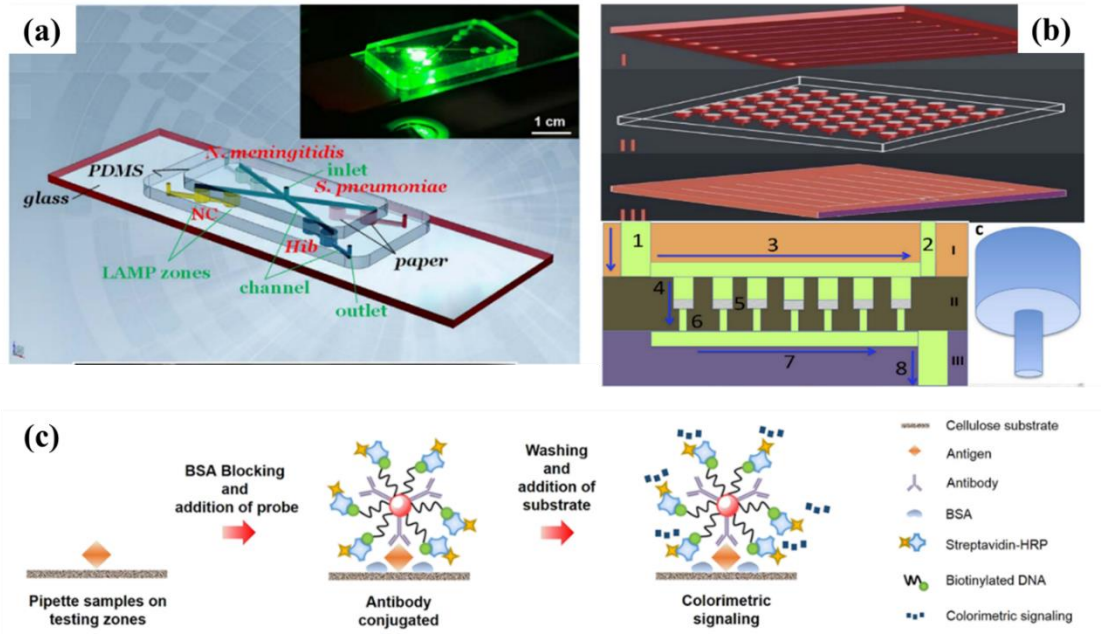

Figure 2-5. (a) Paper-based microfluidic design for loop-mediated isothermal amplification process (LAMP) detection of bacteria. Reproduced with permission. [50] Copyright 2017, Elsevier. (b) Chromatography papers embedded in the microfluidic device for rapid detections of Immunoglobulin G (IgG) and Hepatitis B surface antigen. Reproduced under the terms of the CC BY 4.0 license. [140] Copyright 2016, Attribution 4.0 International (c) Functionalization strategy of a paper-based analytical device (PAD) for prostate cancer biomarker diagnosis. Reproduced with permission. [142] Copyright 2018, ACS publications.

To improve the analytical performance of microfluidic paper–based devices (μPADs) and to eliminate washing, nanoparticles can be trapped within the porosity of the paper. [143,144] Figueredo *et al.* [145] have shown the modification of cellulose papers with Fe_3O_4 magnetic NPs (MNPs), multiwalled carbon nanotubes (MWCNT), and graphene oxide (GO) improve the limit of detection for glucose using μPADs. In carbon-based nanoparticles, electrostatic absorption and hydrogen bonding can enhance the attachment of the biomolecules. [146,147] Moreover, MWCNT and GO maximize the van der Waals forces as well as π–π stacking linkage of aromatic molecules. [148] In another work, Pelton *et al.* [149] used colloidal particles made of poly(N-isopropylacrylamide) (PNIPAM) microgels as a support for biomolecule immobilization. The prepared microgels contained carboxylic groups at their exterior surface. They used these carboxylic groups to couple Lissamine Rhodamine B ethylenediamine by EDC-NHS activation. In the same way, they conjugated the microgels with Streptavidin by which they coupled biotin-IgG and biotin-aptamer-fluorescein on their surface. The biomolecule-conjugated microgels were pipetted onto the cellulose layer and dried to become trapped within the porosity. It is also possible to covalently bind the biomolecules to the surface of some hydrogels to obtain better immobilization. PNIPAM conjugated with DNA aptamers, silica porous particles, and porous sol-gel particles that are conjugated with biomolecules are other examples for this strategy. [133]

The physical attachment of biomolecules onto surfaces increases their chance for detachment compared to the covalent modification routes. In some cases, it is necessary that the biomolecule is covalently bound to the surface to reduce desorption. [150] Chemical modifications could be done on the paper to induce covalent attachment of proteins. Cellulose naturally contains a number of hydroxyl groups, a few carboxylic groups induced by oxidation of the C6 hydroxyls, and oxidizing moieties at the end of cellulose chain. [133,139] The carboxylic groups could be activated by carbodiimide and used to bind to the amino groups of the proteins for covalent immobilization. However, the number of carboxylic groups are not enough to achieve a good biointerface. More functional groups can be found in papers containing hemicellulose, lignin, and other extractives. [133]

Although the hydroxyl groups of the cellulose are not reactive enough at low temperatures and mild conditions, they are used to form other functional groups such as aldehyde and epoxy groups. Leekrajang *et al.* [151] used these hydroxyl groups to graft a Whatman No. 1 filter paper with poly[glycidyl methacrylate-ran- poly(ethylene glycol)methacrylate] (P(GMA-ran-PEGMA)). In their procedure, an initiator which composed of 4,4-azobis(4-cyanovaleric acid) (ACVA), 4-(dimethylamino)pyridine (DMAP), and N,N'-dicyclohexylcarbodiimide (DCC) dissolved in dimethylformamide (DMF) was coupled with the hydroxyl groups using an incubation time of 20 h (Figure

2-6a). Furthermore, the paper was immersed in a mixture of ACVA and 4-cyano-4-(phenylcarbonothioylthio)pentanoic acid (CPD), GMA, and PEGMA in DMF and incubated at 70 ℃ for 3 h. The graft has epoxy groups which were employed to covalently bind peptide nucleic acid (PNA) with amine moieties. Araújo *et al.* [152] used amine-conjugated xyloglucan (XG-NH_2) to functionalize cellulose. After 24 h incubation with XG-NH_2, the surface was activated with 1,4-Phenylenediisothiocyanate (PDITC) which could bind to either amine groups of the XG-NH_2 or hydroxyl groups of the cellulose. The incubation time for this step was 12 h. The paper sheet was then used to immobilize amine-conjugated ssDNA (Figure 2-6b). Oxidization of the cellulose membrane using chemical reagents such as NaIO4 could be another way to functionalize the surface with aldehyde groups, [150] which can bind to amine-conjugated biomolecules and form imine bonds.

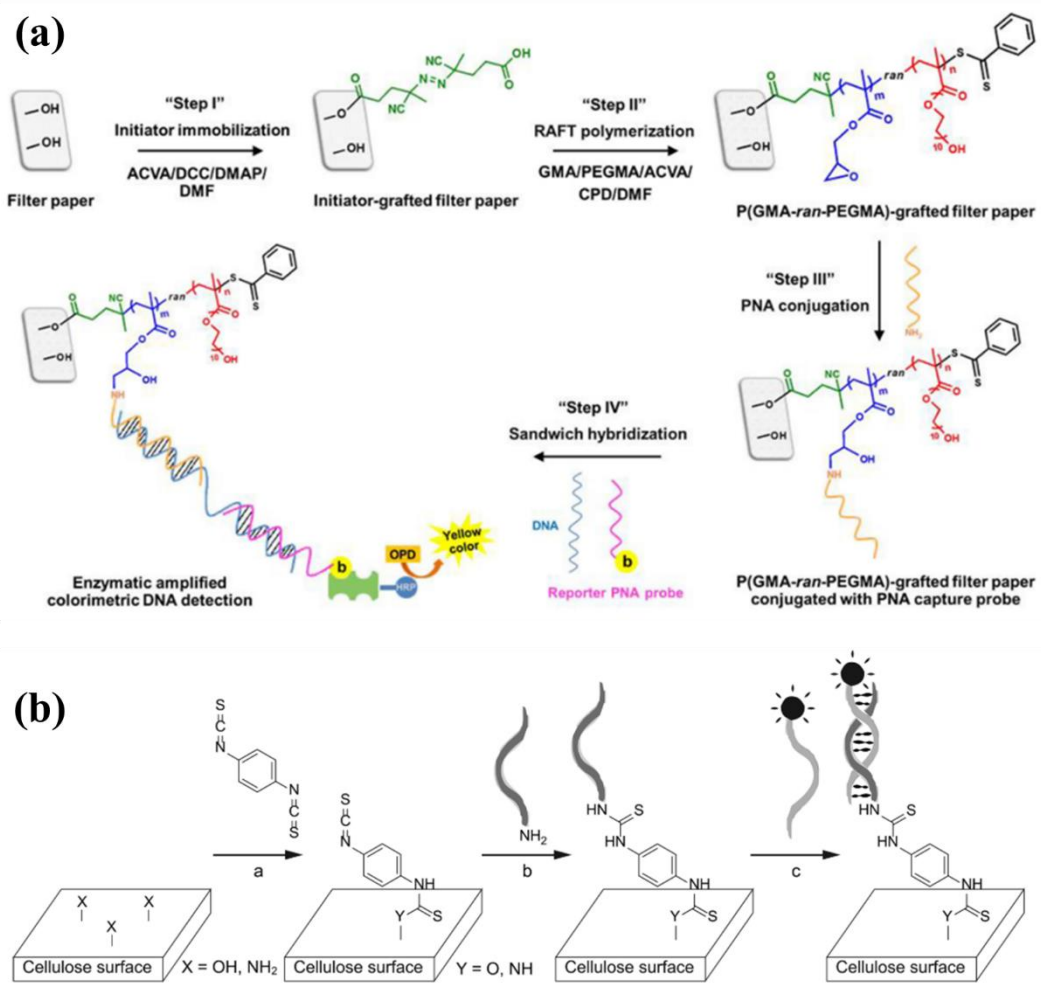

Figure 2-6. (a) Schematic of grafting a Whatman No. 1 filter paper with poly[glycidyl methacrylate-ran- poly(ethylene glycol)methacrylate] (P(GMA-ran-PEGMA)). Reproduced with permission. [151] Copyright 2019, Elsevier. (b) Functionalization of cellulose with 1,4-phenylenediisothiocyanate (PDITC) for DNA immobilization. Reproduced with permission. [152] Copyright 2012, ACS publications.

2.5 Conclusion and Future Outlook

Introducing biofunctional interfaces in microfluidic devices is essential for creating miniaturized bioanalytical devices and lab-on-a-chip systems. Biofunctionalization of

the micro-channels greatly depends on the surface characteristics of the substrate such as topography and surface area, surface energy and wettability properties, surface chemical groups, and biocompatibility. Moreover, the desired application of the microfluidic device plays an important role in selecting the best functionalization approach. Although most of the biofunctionalization techniques are applicable to different substrate types, finding the most efficient method that is simple yet stable and efficient is challenging for certain substrates and applications. Today, the general trend is towards covalent immobilization of biomolecules to achieve a robust biointerface. However, for the applications that do not require long-term stability and possess only mild flow rates, covalent bonding could be avoided. Interfaces such as chromatography papers are sufficiently biocompatible and do not require further functionalization for biomolecules immobilization. Chemical modification of these substrates could facilitate the biomolecule binding and enhance the efficacy of the biointerface layer. On the other hand, glass substrates are often required to be modified in order to obtain biofunctionality. Silanization method is one the most commonly used strategies to induce a variety of functional chemical groups such as amines, peroxides, and thiols. This technique could be utilized for many different substrates to covalently bind biomolecules onto the surfaces.

Currently, several chemical modification methods have been proposed to create covalently bonded biointerfaces in microfluidics made of a wide range of materials. Nevertheless, most of these techniques still need to be further modified in order to increase the yield of immobilized biomolecules, induce a preferred direction for the biomolecules, and enhance the chemical and physical stability of the biomolecules. Moreover, it is highly desirable to make the immobilization technique simplified and cost-effective allowing for high-throughput production of biofunctional microfluidics. In this respect, paper-based microfluidics are anticipated to become even more popular as the biomolecules can be non-covalently/physically bind to the surface eliminating the need for complex chemical functionalization of the channel. Furthermore, due to the capillary forces in paper-based devices there is no need for a syringe pump to perfuse the sample through the microchannels. Paper-based microfluidics also makes it possible to 3D culture cells which is turning to an essential factor in organs-on-chips technology. In addition, it appears that there is a high tendency to incorporate nanomaterials as 0D, 1D, and 2D structures in biofunctionalization of microfluidic channels so as to increase the surface area and intensify the device sensitivity. Patterning of the microfluidic channels (preferably in-situ patterning) is another flourishing technique since it enables the sensing of multiple analytes which is greatly beneficial in high-throughput applications. More research in the field of surface blocking is also required to be done with regard to surface blocking strategy in order to better prevent all non-specific

binding, thereby enhancing the efficacy of the final device. Fluorosilanization of the microchannels and use of surface wrinkling as well as lubricant-infused technologies [153] could be some potential alternative ways of blocking rather than the conventional blocking agents such as PEG or BSA.[154][155]

2.6 References

[1] G. Velve-Casquillas, M. Le Berre, M. Piel, P. T. Tran, J. Urban, *Nano Today* **2010**, *5*, 28.

[2] C. M. B. Ho, S. H. Ng, K. H. H. Li, Y. J. Yoon, *Lab Chip* **2015**, *15*, 3627.

[3] N. T. Nguyen, M. Hejazian, C. H. Ooi, N. Kashaninejad, *Micromachines* **2017**, *8*, 186.

[4] D. Holmes, S. Gawad, in (Eds.: M.P. Hughes, K.F. Hoettges), Humana Press, Totowa, NJ, **2010**, pp. 55–80.

[5] T. A. Duncombe, A. M. Tentori, A. E. Herr, *Nat. Rev. Mol. Cell Biol.* **2015**, *16*, 554.

[6] S. C. C. Shih, G. Goyal, P. W. Kim, N. Koutsoubelis, J. D. Keasling, P. D. Adams, N. J. Hillson, A. K. Singh, *ACS Synth. Biol.* **2015**, *4*, 1151.

[7] A. M. Foudeh, T. Fatanat Didar, T. Veres, M. Tabrizian, *Lab Chip* **2012**, *12*, 3249.

[8] T. F. Didar, M. Tabrizian, *Lab Chip* **2010**, *10*, 3043.

[9] T. F. Didar, K. Li, T. Veres, M. Tabrizian, *Biomaterials* **2013**, *34*, 5588.

[10] X. Cui, Y. Liu, D. Hu, W. Qian, C. Tin, D. Sun, W. Chen, R. H. W. Lam, *Lab Chip* **2018**, *18*, 522.

[11] R. R. G. Soares, D. R. Santos, I. F. Pinto, A. M. Azevedo, M. R. Aires-Barros, V. Chu, J. P. Conde, *Lab Chip* **2018**, *18*, 1569.

[12] M. He, B. Chen, H. Wang, B. Hu, *Appl. Spectrosc. Rev.* **2019**, *54*, 250.

[13] D. Wang, P. Mao, R. Gomez-Sjoberg, H.-T. Wang, P. Yang, *Microfluidic Devices for Liquid Chromatography-Mass Spectrometry and Microscopic Imaging*, **2019**, US 10 , 203 , 307 B2.

[14] X. Min, D. Fu, J. Zhang, J. Zeng, Z. Weng, W. Chen, S. Zhang, D. Zhang, S. Ge, J. Zhang, N. Xia, *Biomed. Microdevices* **2018**, *20*, 91.

[15] S. P. F. Costa, E. Cunha, A. M. O. Azevedo, S. A. P. Pereira, A. F. D. C. Neves, A. G. Vilaranda, A. R. T. S. Araujo, M. L. C. Passos, P. C. A. G. Pinto, M. L. M. F. S. Saraiva, *ACS Sustain. Chem. Eng.* **2018**, *6*, 6094.

[16] G. Kaur, M. Tomar, V. Gupta, *Sensors Actuators B Chem.* **2018**, *261*, 460.

[17] C. V Uliana, C. R. Peverari, A. S. Afonso, M. R. Cominetti, R. C. Faria, *Biosens. Bioelectron.* **2018**, *99*, 156.

[18] J. Choi, A. J. Bandodkar, J. T. Reeder, T. R. Ray, A. Turnquist, S. B. Kim, N. Nyberg, A. Hourlier-Fargette, J. B. Model, A. J. Aranyosi, S. Xu, R. Ghaffari, J. A. Rogers, *ACS Sensors* **2019**, *4*, 379.

[19] A. J. Bandodkar, P. Gutruf, J. Choi, K. Lee, Y. Sekine, J. T. Reeder, W. J. Jeang, A. J. Aranyosi, S. P. Lee, J. B. Model, R. Ghaffari, C.-J. Su, J. P. Leshock, T. Ray, A. Verrillo, K. Thomas, V. Krishnamurthi, S. Han, J. Kim, S. Krishnan, T. Hang, J. A. Rogers, *Sci. Adv.* **2019**, *5*, eaav3294.

[20] K. Gold, A. K. Gaharwar, A. Jain, *Biomaterials* **2019**, *196*, 2.

[21] P. Valentina, R. Claudio, B. Benedikt, M. Sandro, R. Felix, B. Andreas, M. Lars, *Arterioscler. Thromb. Vasc. Biol.* **2018**, *38*, A012.

[22] N. K. R. Pandian, R. G. Mannino, W. A. Lam, A. Jain, *Curr. Opin. Biomed. Eng.* **2018**, *5*, 29.

[23] J. Seo, D. Huh, in *Micro Nano Technol.* (Eds.: J.T. Borenstein, V. Tandon, S.L. Tao, J.L.B.T.-M.C.C.S. (Second E. Charest), Elsevier, **2019**, pp. 187–208.

[24] X. Yang, K. Li, X. Zhang, C. Liu, B. Guo, W. Wen, X. Gao, *Lab Chip* **2018**, *18*, 486.

[25] G. S. Ugolini, R. Visone, D. Cruz-Moreira, A. Mainardi, M. Rasponi, in *Microfluid. Cell Biol. Part A Microfluid. Multicell. Syst.* (Eds.: J. Doh, D. Fletcher, M.B.T.-M. in C.B. Piel), Academic Press, **2018**, pp. 69–84.

[26] W. Ng, N. Howell, J. L. Newton, F. H. Van Der Westhuizen, N. Huebsch, B. Charrez, B. Siemons, S. C. Boggess, S. Wall, V. Charwat, K. Jaeger, F. L. T. Montiel, N. C. Jeffreys, N. Deveshwar, A. Edwards, J. Serrano, M. Snuderl, A. Stahl, A. Tveito, E. W. Miller, K. E. Healy, W. Ng, N. Howell, J. L. Newton, F. H. Van Der Westhuizen, *bioRxiv* **2018**, 485169.

[27] S. Jalili-Firoozinezhad, R. Prantil-Baun, A. Jiang, R. Potla, T. Mammoto, J. C. Weaver, T. C. Ferrante, H. J. Kim, J. M. S. Cabral, O. Levy, D. E. Ingber, *Cell Death Dis.* **2018**, *9*, 223.

[28] A. R. Perestrelo, A. C. P. Águas, A. Rainer, G. Forte, *Sensors (Switzerland)* **2015**, *15*, 31142.

[29] T. F. Didar, K. Bowey, G. Almazan, M. Tabrizian, *Adv. Healthc. Mater.* **2014**, *3*, 253.

[30] G. Luka, A. Ahmadi, H. Najjaran, E. Alocilja, M. DeRosa, K. Wolthers, A. Malki, H. Aziz, A. Althani, M. Hoorfar, *Sensors* **2015**, *15*, DOI 10.3390/s151229783.

[31] S. N. Bhatia, D. E. Ingber, *Nat. Biotechnol.* **2014**, *32*, 760.

[32] M. L. Coluccio, G. Perozziello, N. Malara, E. Parrotta, P. Zhang, F. Gentile, T. Limongi, P. M. Raj, G. Cuda, P. Candeloro, E. Di Fabrizio, *Microelectron. Eng.* **2019**, *208*, 14.

[33] Z. L. Zhang, C. Crozatier, M. Le Berre, Y. Chen, *Microelectron. Eng.* **2005**, *78–79*, 556.

[34] H. Joo, E. Byun, M. Lee, Y. Hong, H. Lee, P. Kim, *J. Ind. Eng. Chem.* **2016**, *34*, 14.

[35] M. Arroyo-Hernández, R. J. Martı́n-Palma, J. Pérez-Rigueiro, J. P. Garcı́a-Ruiz, J. L. Garcı́a-Fierro, J. M. Martı́nez-Duart, *Mater. Sci. Eng. C* **2003**, *23*, 697.

[36] X. Chen, P. Sevilla, C. Aparicio, *Colloids Surfaces B Biointerfaces* **2013**, *107*, 189.

[37] W. Asghar, M. Yuksekkaya, H. Shafiee, M. Zhang, M. O. Ozen, F. Inci, M. Kocakulak, U. Demirci, *Sci. Rep.* **2016**, *6*, 1.

[38] J. Carpinelli, R. Krämer, E. Agosin, *Appl. Environ. Microbiol.* **2006**, *72*, 1949.

[39] Y. Zhao, X. Liu, J. Li, W. Qiang, L. Sun, H. Li, D. Xu, *Talanta* **2016**, *150*, 81.

[40] X. Guan, H. J. Zhang, Y. N. Bi, L. Zhang, D. L. Hao, *Biomed. Microdevices* **2010**, *12*, 683.

[41] G. Perozziello, G. Simone, N. Malara, R. La Rocca, R. Tallerico, R. Catalano, F. Pardeo, P. Candeloro, G. Cuda, E. Carbone, E. Di Fabrizio, *Electrophoresis* **2013**, *34*, 1845.

[42] C. Séguin, J. M. McLachlan, P. R. Norton, F. Lagugné-Labarthet, *Appl. Surf. Sci.* **2010**, *256*, 2524.

[43] S. Mccormick, Z. Tong, A. Ivask, M. Morozesk, N. H. Voelcker, E. Lombi, C. Priest, *Biofabrication* **2018**, *10*, 014101.

[44] K. H. K. Wong, A. E. Jensen, V. Thapar, D. Ting, M. Toner, S. L. Stott, P. T. Hammond, *J. Am. Chem. Soc.* **2017**, *139*, 2741.

[45] H. Li, M. Zhao, W. Liu, W. Chu, Y. Guo, *Talanta* **2016**, *147*, 430.

[46] T. Dong, N. M. M. Pires, *Biosens. Bioelectron.* **2017**, *94*, 321.

[47] N. C. A. Van Engeland, A. M. A. O. Pollet, J. M. J. Den Toonder, C. V. C. Bouten, O. M. J. A. Stassen, C. M. Sahlgren, *Lab Chip* **2018**, *18*, 1607.

[48] J. W. Song, W. Gu, N. Futai, K. A. Warner, J. E. Nor, S. Takayama, *Anal. Chem.* **2005**, *77*, 3993.

[49] B. Hong, P. Xue, Y. Wu, J. Bao, Y. J. Chuah, Y. Kang, *Biomed. Microdevices* **2016**, *18*, 21.

[50] M. Dou, S. T. Sanjay, D. C. Dominguez, P. Liu, F. Xu, X. J. Li, *Biosens. Bioelectron.* **2017**, *87*, 865.

[51] D. Mark, S. Haeberle, G. Roth, F. Von Stetten, R. Zengerle, in *Microfluid. Based Microsystems* (Eds.: S. Kakaç, B. Kosoy, D. Li, A. Pramuanjaroenkij), Springer Netherlands, Dordrecht, **2010**, pp. 305–376.

[52] F. Kong, Y. F. Hu, *Anal. Bioanal. Chem.* **2012**, *403*, 7.

[53] G. A. Giridharan, M.-D. D. Nguyen, R. Estrada, V. Parichehreh, T. Hamid, M. A. Ismahil, S. D. Prabhu, P. Sethu, *Anal. Chem.* **2010**, *82*, 7581.

[54] P. Shah, J. V. Fritz, E. Glaab, M. S. Desai, K. Greenhalgh, A. Frachet, M. Niegowska, M. Estes, C. Jäger, C. Seguin-Devaux, F. Zenhausern, P. Wilmes, *Nat. Commun.* **2016**, *7*, 11535.

[55] Y. Wang, L. Wang, Y. Guo, Y. Zhu, J. Qin, *RSC Adv.* **2018**, *8*, 1677.

[56] S. Tachikawa, S. Kaneda, M. Kumemura, R. Sato, T. Tsukamoto, T. Fujii, T. Suzuki, H. Fujita, *Electr. Eng. Japan (English Transl. Denki Gakkai Ronbunshi)* **2019**, *207*, 55.

[57] T. Vong, S. Schoffelen, S. F. M. Van Dongen, T. A. Van Beek, H. Zuilhof, J. C. M. van Hest, *Chem. Sci.* **2011**, *2*, 1278.

[58] T. F. Didar, A. M. Foudeh, M. Tabrizian, *Anal. Chem.* **2012**, *84*, 1012.

[59] T. F. Didar, M. J. Cartwright, M. Rottman, A. R. Graveline, N. Gamini, A. L. Watters, D. C. Leslie, T. Mammoto, M. J. Rodas, J. H. Kang, A. Waterhouse, B. T. Seiler, P. Lombardo, E. I. Qendro, M. Super, D. E. Ingber, *Biomaterials* **2015**, *67*, 382.

[60] Z. Zhang, P. Zhao, G. Xiao, *Polymer (Guildf).* **2009**, *50*, 5358.

[61] Y. Xu, M. Takai, T. Konno, K. Ishihara, *Lab Chip* **2007**, *7*, 199.

[62] F. Q. Nie, M. Yamada, J. Kobayashi, M. Yamato, A. Kikuchi, T. Okano, *Biomaterials* **2007**, *28*, 4017.

[63] X. Cheng, D. Irimia, M. Dixon, K. Sekine, U. Demirci, L. Zamir, R. G. Tompkins, W. Rodriguez, M. Toner, *Lab Chip* **2007**, *7*, 170.

[64] C. Chen, J. Skog, C.-H. Hsu, R. T. Lessard, L. Balaj, T. Wurdinger, B. S. Carter, X. O. Breakefield, M. Toner, D. Irimia, *Lab Chip* **2010**, *10*, 505.

[65] M. Xue, Z. Xie, L. Zhang, X. Ma, X. Wu, Y. Guo, W. Song, Z. Li, T. Cao, *Nanoscale* **2011**, *3*, 2703.

[66] J. Wu, R. Wang, H. Yu, G. Li, K. Xu, N. C. Tien, R. C. Roberts, D. Li, *Lab Chip* **2015**, *15*, 690.

[67] J. E. Baker, R. Sriram, B. L. Miller, *Lab Chip* **2015**, *15*, 971.

[68] W. Tan, T. A. Desai, *Biomaterials* **2004**, *25*, 1355.

[69] D. Wu, B. Zhao, Z. Dai, J. Qin, B. Lin, *Lab Chip* **2006**, *6*, 942.

[70] J. Kim, E. C. Jensen, M. Megens, B. Boser, R. a Mathies, *Lab Chip* **2011**, *11*, 3106.

[71] A. Shakeri, N. Sun, M. Badv, T. F. Didar, *Biomicrofluidics* **2017**, *11*, 044111.

[72] T. F. Didar, M. Tabrizian, *Lab Chip* **2012**, *12*, 4363.

[73] J. N. Ding, P. L. Wong, J. C. Yang, *Wear* **2006**, *260*, 209.

[74] U. Srinivasan, M. R. Houston, R. T. Howe, R. Maboudian, *J. Microelectromechanical Syst.* **1998**, *7*, 252.

[75] R. Helmy, A. Y. Fadeev, *Langmuir* **2002**, *18*, 8924.

[76] M. Badv, I. H. Jaffer, J. I. Weitz, T. F. Didar, *Sci. Rep.* **2017**, *7*, 11639.

[77] M. Badv, S. M. Imani, J. I. Weitz, T. F. Didar, *ACS Nano* **2018**, *12*, 10890−10902.

[78] A. Shakeri, D. Yip, M. Badv, S. M. Imani, M. Sanjari, T. F. Didar, *Materials (Basel).* **2018**, *11*, 1003.

[79] N. R. Glass, R. Tjeung, P. Chan, L. Y. Yeo, J. R. Friend, *Biomicrofluidics* **2011**, *5*, 1.

[80] I. Torres, L. Eland, C. Redfern, J. Hedley, *Sensors* **2017**, *2*, 17.

[81] G. C. Santini, C. Potrich, L. Lunelli, L. Vanzetti, S. L. Marasso, M. Cocuzza, F. C. Pirri, C. Pederzolli, *Biophys. Chem.* **2017**, *229*, 142.

[82] A. Ofner, D. G. Moore, P. A. Rühs, P. Schwendimann, M. Eggersdorfer, E. Amstad, D. A. Weitz, A. R. Studart, *Macromol. Chem. Phys.* **2017**, *218*, 1.

[83] E. Hoque, J. A. Derose, P. Hoffmann, B. Bhushan, H. J. Mathieu, *J. Phys. Chem. C* **2007**, *111*, 3956.

[84] A. V. Krasnoslobodtsev, S. N. Smirnov, *Langmuir* **2002**, *18*, 3181.

[85] M. Osborne, A. Aryasomayajula, A. Shakeri, P. R. Selvaganapathy, T. F. Didar, *ACS Sensors* **2019**, *4*, 687.

[86] M. Hu, S. Noda, T. Okubo, Y. Yamaguchi, H. Komiyama, *Appl. Surf. Sci.* **2001**, *181*, 307.

[87] Z.-Z. Liu, Q. Wang, X. Liu, J.-Q. Bao, *Thin Solid Films* **2008**, *517*, 635.

[88] N. G. Batz, J. S. Mellors, J. P. Alarie, J. M. Ramsey, *Anal. Chem.* **2014**, *86*, 3493.

[89] W. Wang, M. W. Vaughn, *Scanning* **2008**, *30*, 65.

[90] H. Handa, S. Gurczynski, M. P. Jackson, G. Auner, J. Walker, G. Mao, *Surf. Sci.* **2008**, *602*, 1392.

[91] F. Zhang, K. Sautter, A. M. Larsen, D. A. Findley, R. C. Davis, H. Samha, M. R. Linford, *Langmuir* **2010**, *26*, 14648.

[92] S. Fiorilli, P. Rivolo, E. Descrovi, C. Ricciardi, L. Pasquardini, L. Lunelli, L. Vanzetti, C. Pederzolli, B. Onida, E. Garrone, *J. Colloid Interface Sci.* **2008**, *321*, 235.

[93] S. Kango, S. Kalia, A. Celli, J. Njuguna, Y. Habibi, R. Kumar, *Prog. Polym. Sci.* **2013**, *38*, 1232.

[94] A. Hosseini, M. Villegas, J. Yang, M. Badv, I. W. Jeffrey, L. Soleymani, F. T. Didar, *Adv. Mater. Interfaces* **2018**, *5*, 1800617.

[95] H. Sellers, A. Ulman, Y. Shnidman, J. E. Eilers, *J. Am. Chem. Soc.* **1993**, *115*, 9389.

[96] M. Kind, C. Wöll, *Prog. Surf. Sci.* **2009**, *84*, 230.

[97] H. Cheng, Y. Hu, *Adv. Colloid Interface Sci.* **2012**, *171–172*, 53.

[98] T. Vallant, H. Brunner, U. Mayer, H. Hoffmann, T. Leitner, R. Resch, G. Friedbacher, *J. Phys. Chem. B* **1998**, *102*, 7190.

[99] M. Wang, K. M. Liechti, Q. Wang, J. M. White, *Langmuir* **2005**, *21*, 1848.

[100] A. N. Parikh, D. L. Allara, I. Ben Azouz, F. Rondelez, *J. Phys. Chem.* **1994**, *98*, 7577.

[101] J. B. Brzoska, I. Ben Azouz, F. Rondelez, *Langmuir* **1994**, *10*, 4367.

[102] V. Dugas, Y. Chevalier, *J. Colloid Interface Sci.* **2003**, *264*, 354.

[103] X. Tan, M. K. Khaing Oo, Y. Gong, Y. Li, H. Zhu, X. Fan, *Analyst* **2017**, *142*, 2378.

[104] L. Diéguez, M. A. Winter, K. J. Pocock, K. E. Bremmell, B. Thierry, *Analyst* **2015**, *140*, 3565.

[105] C.-H. Sang, S.-J. Chou, F. M. Pan, J.-T. Sheu, *Biosens. Bioelectron.* **2016**, *75*, 285.

[106] A. Jain, A. D. van der Meer, A. L. Papa, R. Barrile, A. Lai, B. L. Schlechter, M. A. Otieno, C. S. Louden, G. A. Hamilton, A. D. Michelson, A. L. Frelinger, D. E. Ingber, *Biomed. Microdevices* **2016**, *18*, 1.

[107] E. L. Kendall, E. Wienhold, O. D. Rahmanian, D. L. Devoe, *Sensors Actuators B. Chem.* **2014**, *202*, 866.

[108] J. Liu, C. Chen, C. Chang, D. L. Devoe, *Biosens. Bioelectron.* **2010**, *26*, 182.

[109] T. Jiang, R. Mallik, D. S. Hage, *Anal. Chem.* **2005**, *77*, 2362.

[110] R. Khnouf, D. Karasneh, B. A. Albiss, *Electrophoresis* **2016**, *37*, 529.

[111] G. Simone, P. Neuzil, G. Perozziello, M. Francardi, N. Malara, E. Di Fabrizio, A. Manz, *Lab Chip* **2012**, *12*, 1500.

[112] S. K. Vashist, *Diagnostics* **2012**, *2*, 23.

[113] "Carbodiimide Crosslinker Chemistry," can be found under https://www.thermofisher.com/ca/en/home/life-science/protein-biology/protein-biology-learning-center/protein-biology-resource-library/pierce-protein-methods/carbodiimide-crosslinker-chemistry.html, **n.d.**

[114] A. Khodayari Bavil, J. Kim, *Analyst* **2018**, *143*, 3335.

[115] M. P. Nicholas, L. Rao, A. Gennerich, *Methods Mol Biol.* **2014**, *1136*, 137.

[116] S. De Vitis, G. Matarise, F. Pardeo, R. Catalano, N. Malara, V. Trunzo, R. Tallerico, F. Gentile, P. Candeloro, M. L. Coluccio, A. Massaro, G. Viglietto, E. Carbone, J. P. Kutter, G. Perozziello, E. Di Fabrizio, *Microelectron. Eng.* **2014**, *124*, 76.

[117] M. A. Ali, S. Srivastava, P. R. Solanki, V. Reddy, V. V. Agrawal, C. Kim, R. John, B. D. Malhotra, *Sci. Rep.* **2013**, *3*, 1.

[118] H. Shafiee, S. Wang, F. Inci, M. Toy, T. J. Henrich, D. R. Kuritzkes, U. Demirci, *Annu. Rev. Med.* **2015**, *66*, 387.

[119] N. N. Watkins, U. Hassan, G. Damhorst, H. Ni, A. Vaid, W. Rodriguez, R. Bashir, *Sci. Transl. Med.* **2013**, *5*, 214ra170 LP.

[120] C. Priest, *Biomicrofluidics* **2010**, *4*, 32206.

[121] A. Arora, G. Simone, G. B. Salieb-Beugelaar, J. T. Kim, A. Manz, *Anal. Chem.* **2010**, *82*, 4830.

[122] T. Vong, J. ter Maat, T. A. van Beek, B. van Lagen, M. Giesbers, J. C. M. van Hest, H. Zuilhof, *Langmuir* **2009**, *25*, 13952.

[123] B. Renberg, K. Sato, K. Mawatari, N. Idota, T. Tsukahara, T. Kitamori, *Lab Chip* **2009**, *9*, 1517.

[124] E. S. Douglas, R. A. Chandra, C. R. Bertozzi, R. A. Mathies, M. B. Francis, *Lab Chip* **2007**, *7*, 1442.

[125] Y. Oku, K. Kamiya, H. Kamiya, Y. Shibahara, T. Ii, Y. Uesaka, *J. Immunol. Methods* **2001**, *258*, 73.

[126] R. R. Carvalho, S. P. Pujari, D. Gahtory, E. X. Vrouwe, B. Albada, H. Zuilhof, *Langmuir* **2017**, *33*, 8624.

[127] F. J. V. Gomez, P. A. Reed, D. Gonzalez Casamachin, J. Rivera De La Rosa, G. Chumanov, M. F. Silva, C. D. Garcia, *Anal. Methods* **2018**, *10*, 4020.

[128] X. Sun, H. Wang, Y. Jian, F. Lan, L. Zhang, H. Liu, S. Ge, J. Yu, *Biosens. Bioelectron.* **2018**, *105*, 218.

[129] M. Taghizadeh-Behbahani, B. Hemmateenejad, M. Shamsipur, *Chem. Pap.* **2017**, *72*, 1239.

[130] I. Ortiz-Gómez, A. Salinas-Castillo, A. G. García, J. A. Álvarez-Bermejo, I. de Orbe-Payá, A. Rodríguez-Diéguez, L. F. Capitán-Vallvey, *Microchim. Acta* **2017**, *185*, 47.

[131] M. N. Costa, B. Veigas, J. M. Jacob, D. S. Santos, J. Gomes, P. V. Baptista, R. Martins, J. Inácio, E. Fortunato, *Nanotechnology* **2014**, *25*, 094006.

[132] B. Li, D. R. Moore, *Porous Membranes Having a Hydrophilic Coating and Methods for Their Preparation and Use*, **2013**, US20130171669A1.

[133] R. Pelton, *TrAC Trends Anal. Chem.* **2009**, *28*, 925.

[134] J. Credou, H. Volland, J. Dano, T. Berthelot, *J. Mater. Chem. B* **2013**, *1*, 3277.

[135] R. Wong, H. Tse, *Lateral Flow Immunoassay*, Humana Press, **2009**.

[136] Millipore Co., **2008**.

[137] G. E. Fridley, C. A. Holstein, S. B. Oza, P. Yager, *MRS Bull.* **2013**, *38*, 326.

[138] X. Li, J. Tian, T. Nguyen, W. Shen, *Biomicrofluidics* **2012**, *6*, 011301.

[139] K. Yamada, T. G. Henares, K. Suzuki, D. Citterio, *Angew. Chemie - Int. Ed.* **2015**, *54*, 5294.

[140] S. T. Sanjay, M. Dou, J. Sun, X. Li, *Sci. Rep.* **2016**, *6*, 1.

[141] V. Hamedpour, G. J. Postma, E. van den Heuvel, J. J. Jansen, K. Suzuki, D. Citterio, *Anal. Bioanal. Chem.* **2018**, *410*, 2305.

[142] J.-Y. Huang, H.-T. Lin, T.-H. Chen, C.-A. Chen, H.-T. Chang, C.-F. Chen, *ACS Sensors* **2018**, *3*, 174.

[143] S. Liu, W. Su, X. Ding, *Sensors* **2016**, *16*, 2086.

[144] E. Evans, E. F. Moreira Gabriel, T. E. Benavidez, W. K. Tomazelli Coltro, C. D. Garcia, *Analyst* **2014**, *139*, 5560.

[145] F. Figueredo, P. T. Garcia, E. Cortón, W. K. T. Coltro, *ACS Appl. Mater. Interfaces* **2016**, *8*, 11.

[146] A. A. Shemetov, I. Nabiev, A. Sukhanova, *ACS Nano* **2012**, *6*, 4585.

[147] J. Zhang, F. Zhang, H. Yang, X. Huang, H. Liu, J. Zhang, S. Guo, *Langmuir* **2010**, *26*, 6083.

[148] M. M. Barsan, M. E. Ghica, C. M. A. Brett, *Anal. Chim. Acta* **2015**, *881*, 1.

[149] R. Pelton, S. Su, M. Ali, C. D. M. Filipe, Y. Li, *Biomacromolecules* **2008**, 935.

[150] S. Su, R. Nutiu, C. D. M. Filipe, Y. Li, R. Pelton, *Langmuir* **2007**, *23*, 1300.

[151] M. Leekrajang, P. Sae-ung, T. Vilaivan, V. P. Hoven, *Colloids Surfaces B Biointerfaces* **2019**, *173*, 851.

[152] A. C. Araújo, Y. Song, J. Lundeberg, P. L. Ståhl, H. Brumer, *Anal. Chem.* **2012**, *84*, 3311−3317.

[153] M. Villegas, Z. Cetinic, A. Shakeri, T. F. Didar, *Anal. Chim. Acta* **2018**, *1000*, 248.

[154] G. Wang, M. L. McCain, L. Yang, A. He, F. S. Pasqualini, A. Agarwal, H. Yuan, D. Jiang, D. Zhang, L. Zangi, J. Geva, A. E. Roberts, Q. Ma, J. Ding, J. Chen, D.-Z. Wang, K. Li, J. Wang, R. J. A. Wanders, W. Kulik, F. M. Vaz, M. A. Laflamme, C. E. Murry, K. R. Chien, R. I. Kelley, G. M. Church, K. K. Parker, W. T. Pu, *Nat. Med.* **2014**, *20*, 616.

[155] S. C. Low, R. Shaimi, Y. Thandaithabany, J. K. Lim, A. L. Ahmad, A. Ismail, *Colloids Surfaces B Biointerfaces* **2013**, *110*, 248.

2.7 Acknowledgements

This work was supported by Natural Sciences and Engineering Research Council of Canada (NSERC) Discovery Grant, Ontario Early Researcher Award Grant and McMaster start-up funds to T.F.D.

Chapter 3: Self-Cleaning Ceramic Tiles Produced via Stable Coating of TiO_2 Nanoparticles

Amid Shakeri, Darren Yip, Maryam Badv, Sara M. Imani, Mehdi Sanjari and Tohid F. Didar*

Materials 2018, 11, 1003; doi:10.3390/ma11061003

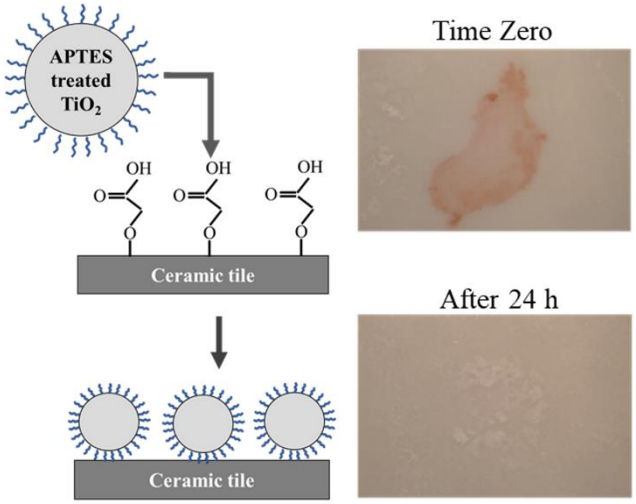

3.1 Abstract

The high photocatalytic power of TiO_2 nanoparticles has drawn great attention in environmental and medical applications. Coating surfaces with these particles enables us to benefit from self-cleaning properties and decomposition of pollutants. In this paper, two strategies have been introduced to coat ceramic tiles with TiO_2 nanoparticles, and the self-cleaning effect of the surfaces on degradation of an organic dye under ultraviolent (UV) exposure is investigated. In the first approach, a simple one-step heat treatment method is introduced for coating, and different parameters of the heat treatment process are examined. In the second method, TiO_2 nanoparticles are first aminosilanized using (3-Aminopropyl)triethoxysilane (APTES) treatment followed by their covalently attachment onto CO_2 plasma treated ceramic tiles via N-(3-Dimethylaminopropyl)-N0-ethylcarbodiimide hydrochloride (EDC) and N-Hydroxysuccinimide (NHS) chemistry. We monitor TiO_2 nanoparticle sizes throughout the coating process using dynamic light scattering (DLS) and characterize developed surfaces using X-ray photoelectron spectroscopy (XPS). Moreover, hydrophilicity of the coated surfaces is quantified using a contact angle measurement. It is shown that applying a one-step heat treatment process with the optimum temperature of 200 ℃ for 5 h results in successful coating of nanoparticles and rapid degradation of dye in a short time. In the second strategy, the APTES treatment creates a stable covalent coating,

while the photocatalytic capability of the particles is preserved. The results show that coated ceramic tiles are capable of fully degrading the added dyes under UV exposure in less than 24 h.

Keywords: TiO_2 nanoparticles; self-cleaning; photocatalyst; heat treatment; APTES treatment

3.2 Introduction

TiO_2 is one of the most well-known photocatalysts which has been widely used for photodegradation of organic compounds and decomposition of pollutants [1–3]. While TiO_2 with the bulk bandgap of ~3.2 eV (in anatase phase) is transparent to visible light, it could be activated under UV light illumination and create photo-generated charge carriers [4,5]. The electrons which are excited by UV absorption bring about reduction of oxygen molecules in air and produce superoxide radicals ($O_2^{\bullet -}$). The superoxide radicals are further reduced to form hydrogen peroxide (H_2O_2) and subsequently hydroxyl radicals ($OH^{\bullet}$) [6–8]. On the other hand, oxidation of water molecules by electron holes at the surface of the UV excited TiO_2 particles can also lead to the formation of hydroxyl radicals and hydrogen peroxide [7,9]. These reactive oxygen species can drive decomposition of organic pollutants and inactivation of micro-organisms such as *Escherichia coli* cell [10–12].

In addition to the photochemical power, TiO_2 has several other advantages such as chemical stability, nontoxicity, hydrophilicity, and cost which make it a promising candidate for many industrial and environmental applications including air purification, water purification, and creating self-cleaning tiles or glasses used in constructions [9,13–15]. From a biomedical perspective, photoexcited TiO_2 nanoparticles (NPs) have been utilized for cancer cell therapeutics [16,17], self-sterilizing of catheters [18], and antibacterial surfaces as well as photocatalytic disinfection [19,20].

So far various physical and chemical approaches have been employed in order to coat TiO_2 NPs onto different types of surfaces. One of the most commonly used coating methods is the sol-gel deposition technique which enables a uniform thin TiO_2 layer on different substrates [21–24]. Applying organic and inorganic binding agents capable of creating strong adhesion of TiO_2 is the other widely used strategy to directly coat different substrates with pre-synthesized TiO_2 particles [25]. Sopyan *et al.* have added TiO_2 particles to a paint-like sol composed of fluoropolymer resin and an organotitanium coupling agent. The sol was coated onto a glass substrate and cured at 120 ℃ [26]. Lin *et al.* have coated Polyvinyl Chloride (PVC) polymeric substrate with TiO_2 particles via dip-coating the substrate into Tetrahydrofuran (THF)-PVC-TiO_2 suspension [27]. In this method THF solvent can melt the PVC providing a strong physical attachment between TiO_2 particles and the substrate. In another research

carried out by Pal *et al.*, TiO_2 particles were combined with the inorganic binder of potassium silicate which can create chemical bonds with substrates by silicification process, and then applied onto the fired bricks [28].

Silanization of inorganic surfaces with (3-Aminopropyl)triethoxysilane (APTES) is a widely known procedure to functionalize the surfaces with amino terminal groups which could then be used to anchor different biomolecules (*i.e.* antibodies and proteins) via creating covalent peptide bonds [29–31]. Silanization process creates self-assembled monolayers (SAMs) of desired functional groups onto the surfaces and can be performed using chemical vapor deposition [32,33], liquid phase deposition (LPD)[34], and micro-contact printing [35–37]. APTES treatment has also been applied on TiO_2 particles for various purposes such as enhancement of proteins immobilization [38], preventing the UV photobleaching [39], and grafting with thermoresponsive polymers which enables TiO_2 particles to have self-flocculation and temperature-controlled switching photocatalytic properties [40]. However, so far, this method has not been utilized to coat construction materials such as ceramic tiles with TiO_2 particles.

Heat treatment is also a determining factor in many TiO_2 coating techniques. It is possible to precisely control the morphology, distribution, and size of the NPs in TiO_2 coating via adjusting the heat treatment parameters such as temperature and time [41–43]. In addition, heat treatment method has a prominent role in doping TiO_2 crystal

structure with different dopants such as nitrogen and carbon for the sake of photocatalytic activity [44,45].

In this paper, two different strategies are introduced to create a stable covalent coating of TiO_2 NPs onto ceramic tiles to induce self-cleaning capability. In the first approach, a single heat treatment step is used to make a strong physical bond between TiO_2 particles and the ceramic tile. In the second procedure, we used APTES treatment technique to functionalize TiO_2 particles and then the particles are covalently bonded to CO_2 plasma treated ceramic tiles. In both approaches, we have shown that the photocatalytic power of particles is preserved, the coating is stable, and the surfaces are able to thoroughly degrade the dye that is used as an organic pollutant.

3.3 Materials and Methods

3.3.1 Materials

TiO_2 particles grade SSP-20 (Sakai Chemical Industry Co.) with fully anatase crystal structure, pink food dye (A Preema Quality Product, Ingredients: Sodium Chloride and E122 Carmosine), Glazed ceramic tiles with the dimension of ~ 3 × 3 cm^2 (Home Depot, Canada), triethylamine (Sigma-Aldrich), ammonium hydroxide (Sigma-Aldrich), APTES (Sigma Aldrich, Canada), toluene (Sigma-Aldrich), N-(3-

Dimethylaminopropyl)-N′-ethylcarbodiimide hydrochloride (EDC) (Sigma-Aldrich), and N-Hydroxysuccinimide (NHS) (Sigma-Aldrich) are used as received.

3.3.2 Dye-degradation Measurements

Dye degradation experiments were conducted using a custom-made UV chamber (Figure 3-1)**.** We used a 10-watts UV lamp (Ster-L-Ray, Preheat Germicidal Ultraviolet Lamps, Atlantic Ultraviolet Corporation) with UV output total watts of 2.7, length of 21 cm, and diameter of ~1.5 cm. The chamber dimensions were 26 × 33 × 25 cm^3 and the distance from the lamp to the samples was around 3.5 cm. The chamber was covered with an aluminum foil to enhance the reflection.

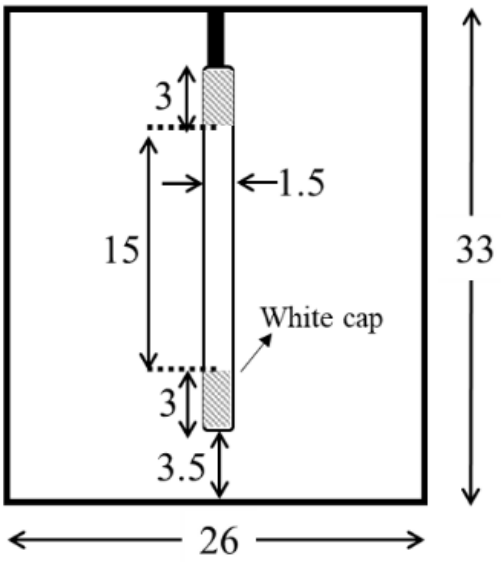

Figure 3-1. Schematic drawing of the costume-made UV chamber with a UV lamp at the center. All dimensions are in cm.

3.3.3 Dye-degradation Measurement of TiO_2 Nanoparticles

The Ultraviolet-Visible (UV-VIS) spectra of the dye was first measured to determine the optimal wavelength. This was done by using a 1.0 mg/mL concentration of the dye in deionized water and absorbance was read using a plate reader (Infinite M200 Pro, Tecan). The optimal wavelength was determined based on results obtained using a range of excitation wavelengths. This wavelength was then used to produce a calibration curve to determine the concentration of the dye during the process of cleaning. The calibration graph was produced by measuring the absorbances for dye concentrations at 1, 0.85, 0.70, 0.55, 0.40, 0.25, and 0.1 mg/mL. Then, TiO_2 NPs with a concentration of 1 mg/mL in deionized water were mixed with 1 mg/ml of the coloring dye. The suspension was then kept in the UV chamber while stirring to provide consistency with the reaction. A small sample was retrieved from the reaction at 5, 15, 30, 60, 180, and 360 minutes, and put into a microcentrifuge tube. The tube was then spun at 14800 rpm for 10 minutes to pellet the TiO_2 NPs out of the suspension. Next, 100 µl of the supernatant was gently pipetted from the microcentrifuge tube to the well plate. The well plate was then scanned using the plate reader and the data obtained was graphed and interpreted.

3.3.4 Coating TiO_2 Nanoparticles Using Heat Treatment Technique

30 µL of 1 mg/mL TiO_2 NPs suspension was added onto the ceramic tiles' surfaces and spread to cover the whole surface using a simple pipetting system, and then left to dry

at room temperature. The surfaces were then placed in a tube furnace or vacuum oven for lower temperatures. The heat treatments were done in different durations of 2 h and 5 h, and at different temperatures of 100, 200, 400, 500, 700, and 900 ℃. The rate of the temperature gradient in all experiments was 5°C/min. Following heat treatment, the surfaces were rinsed and wiped to remove any unattached particle (Figure 3-2a). 5µL of 1 mg/ml of dye was added onto each surface and placed in the UV chamber to examine the amount of dye degradation in different time intervals.

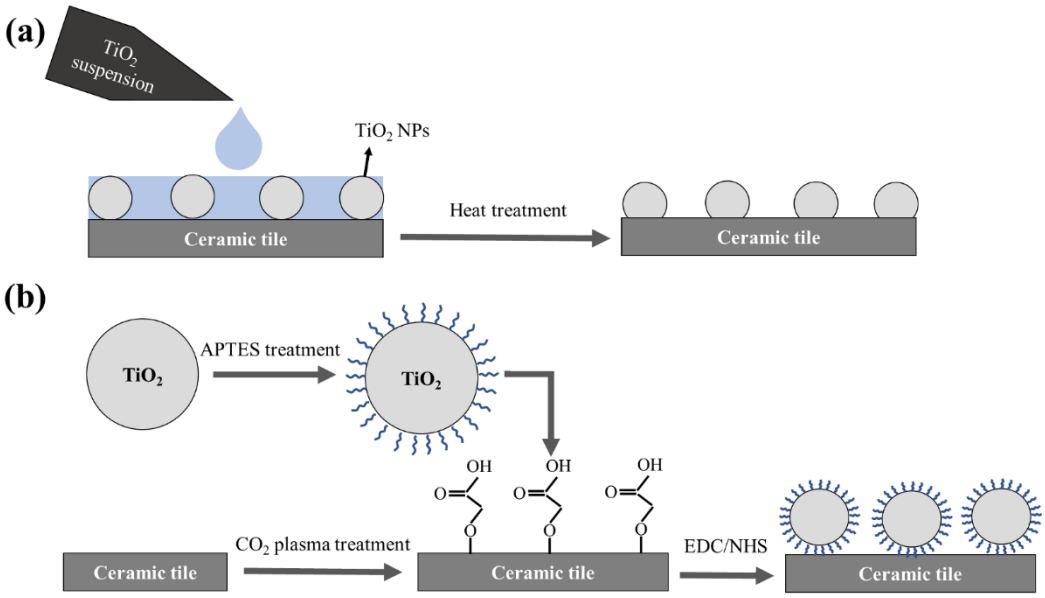

Figure 3-2. Schematic representation of (a) heat treatment method and (b) APTES treatment method for coating TiO_2 NPs on ceramic tiles.

3.3.5 APTES Treatment Technique

TiO_2 NPs were homogenized with triethylamine (for improving the particles dispersion [46]) and ethanol at 60°C. Further, ammonium hydroxide, DI water, and APTES (~1%)

was added to the suspension and left to stir overnight. [40]. Ammonium hydroxide as a catalyst can increase the rate of APTES hydrolysis reactions [47]. Finally, the suspension was centrifuged at 4500 rpm for 15 minutes. The supernatant was discarded, and the pellet was mixed with ethanol. The washing step was repeated 3 times and the obtained powder was stored in 50 mL of toluene.

In order to coat ceramic tiles with the APTES treated particles, the cleaned surfaces were CO_2 plasma treated (Harrick Plasma, Ithaca, NY, USA) to create carboxylic groups onto the surface. EDC-NHS chemistry (a molar ratio of EDC:NHS ~ 1:1) was used to activate the carboxylic groups on the surfaces. The solution was rinsed off the surface with DI water and then the APTES treated TiO_2 suspension was added to the surfaces and left for 2 hours. Finally, the surfaces were rinsed with DI water and dried at room temperature (Figure 3-2b). 5 uL of 1 mg/mL dye was added to the surfaces and left to dry. The surfaces were placed in the UV chamber and imaged at different time intervals.

3.3.6 Characterization Techniques

High-resolution XPS was used to investigate the amount of carboxylic groups induced by CO_2 plasma treatment of glass slides for different time durations. XPS measurements were carried out at binding energy between ~280 to ~300 (eV) to capture bond of O–C=O, C=O, C–C, and C–O as counts per second. The size distribution profile of the

TiO_2 NPs in suspension was determined using the dynamic light scattering method (DLS, Beckman Coulter, Indianapolis, IN, USA). In DLS analysis, 10 acquisitions were performed for every experiment, and each acquisition was 15 s long. All TiO_2 NPs were diluted in DI water with the concentration of 0.01 mg/mL and sonicated for 5 min. For the APTES treated sample, we took 5 µL of the suspension of NPs in toluene and diluted in DI water (10 mL) to achieve the desired concentration in order to exclude the effect of toluene in DLS measurements. Contact angles were measured by an optical contact angle (OCA 35) (Future Digital Scientific Corp., Garden City, NY, USA) using 5 µL droplet of DI water. Fourier-transform infrared spectroscopy (FT-IR) (Bruker, Karlsruhe, Germany) was used to confirm the presence of the TiO_2 coating on the ceramic tiles' surfaces after the washing steps as well as the effect of APTES treatment on the TiO_2 NPs. FT-IR was conducted on different samples and different spots on the surfaces for each experiment. ImageJ was utilized to quantify the photos achieved from the dye-degradation results. For better comparison, the graphs were normalized, so that all the graphs started at the same point. Atomic force microscopy (AFM) (BioScope Catalyst, Bruker, Milton, ON, Canada) was performed to analyze surface topography and roughness within the scan size of 1×1 µm^2. A ScanAsyst mode was utilized in the measurements using a probe with the spring constant of 0.4 N/m.

3.4 Results and Discussion

3.4.1 TiO_2 NPs Size Measurements

Figure 3-3 demonstrates the average particle sizes of untreated TiO_2 NPs and APTES treated TiO_2 NPs versus the particles population percentage. As is shown, the average radius of the untreated NPs was mostly distributed in two different sizes of 123 nm (24.3% of particle number) and 449 nm (75.7% of particle number). The existence of the larger particle sizes could be due to the NPs agglomeration even after the sonication. In Figure 3-3b, there were also two main particle size distributions associated with the APTES treated NPS. At the first peak, the average radius was almost the same as the untreated NPS. However, the number of NPs with that radius decreased, compared to the untreated NPs. Moreover, APTES treatment caused the second distribution to go up in terms of average radius as well as population density of the NPs. Consequently, APTES treatment of the particles caused a slight increase in the particles agglomeration, although this was not significant.

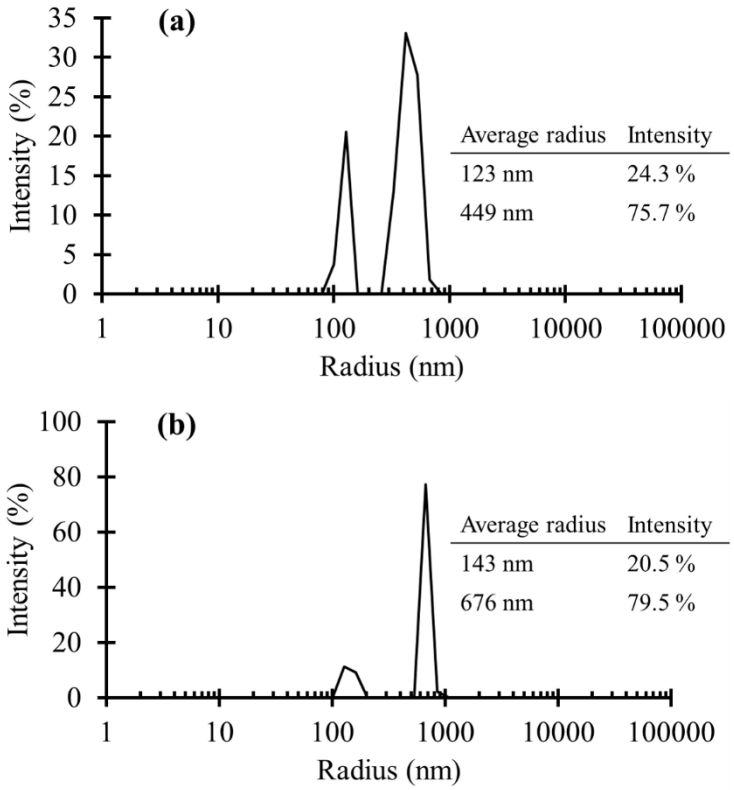

Figure 3-3. DLS results of the (a) untreated TiO_2 NPs and (b) APTES treated TiO_2 NPs. The vertical axes indicate the particle number percentages. The insect tables show the average radius of the NPs and related particle number intensities.

3.4.2 XPS Measurement of the CO_2 Plasma Treated Ceramic Tiles

The second approach that we employed to covalently bind TiO_2 NPs to the surface of ceramic tiles was aminosilanization of TiO_2 NPs and CO_2 plasma treatment of ceramic tiles. APTES treatment of TiO_2 NPs formed a monolayer of hydrolyzed and condensed APTES molecules on the surface providing free terminal NH_2 groups. Schematic presentation of this functionalization process is shown in Figure 3-2b. On the other hand, CO_2 plasma treatment of ceramic tiles can produce carboxylic groups (COOH)

on the surface, which can subsequently be activated using EDC/NHS chemistry. The functional carboxylic groups can go through a chemical reaction with amino groups of the APTES treated particles and form covalent peptide bonds. Consequently, we would be able to covalently bind the TiO_2 particles to the ceramic tiles.

To investigate the carboxylic group formation on the surface, a high-resolution XPS test was performed. Figure 3-4a depicts the XPS results of an untreated sample. XPS graphs of CO_2 plasma treated samples for different time periods are shown in Figure 3-4b–d. The peaks at binding energies around 288.66 (eV), 286.02 (eV), and 284.8 (eV) were assigned to O–C=O, C=O, and C–C as well as C–O, respectively [48]. Figure 3-4e demonstrates the variation in the amount of O–C=O groups by increasing the CO_2 plasma treatment time. It could be seen that after 2 min of plasma treatment, the O–C=O band area in XPS patterns has risen from 6.46% to 16.58%, indicating the well formation of carboxylic groups via the CO_2 plasma treatment. Increasing the plasma treatment time more than 2 min did not significantly change the O–C=O % area.

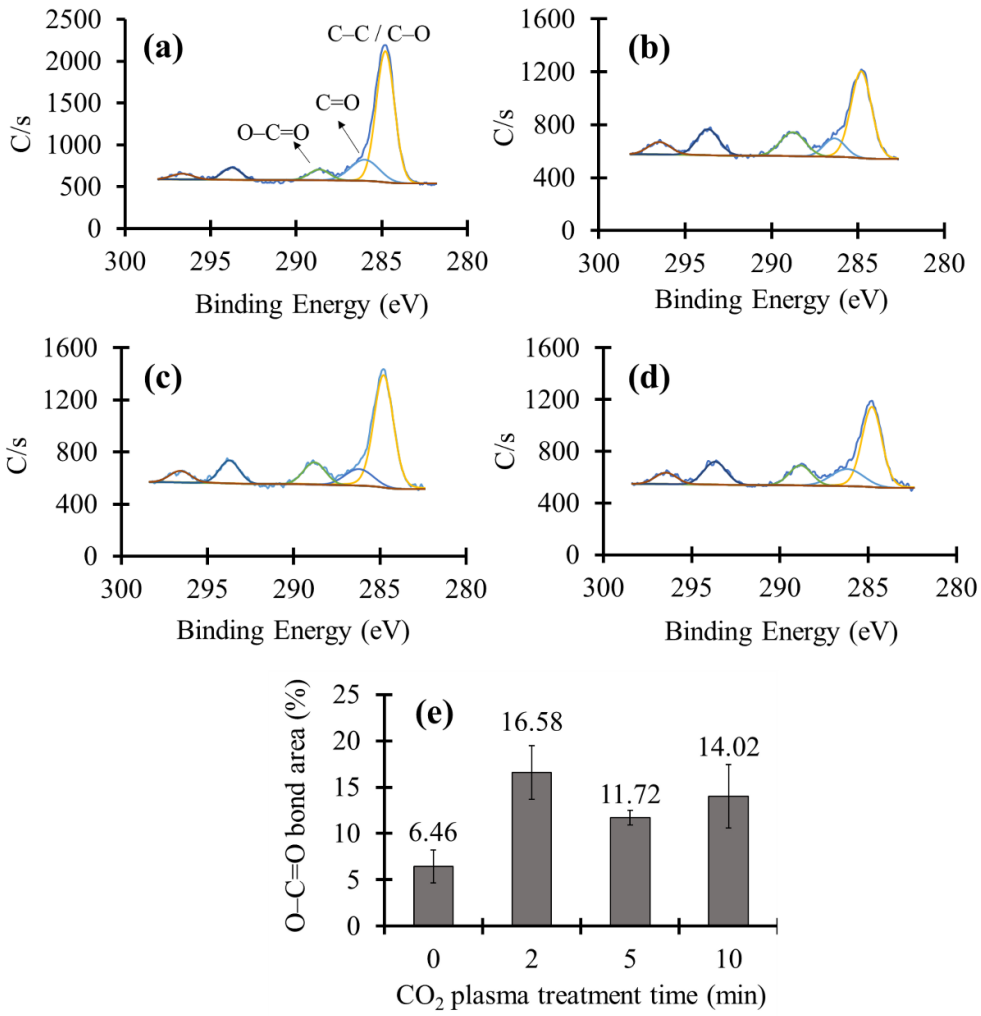

Figure 3-4. High resolution XPS plots of CO_2 plasma treated glass surfaces for (a) 0 min, (b) 2 min, (c) 5 min, and (d) 10 min. (e) variation of the amount of O–C=O bonds versus plasma treatment time.

3.4.3 FT-IR Studies of the TiO_2 Coated Tiles

FT-IR spectra of plain ceramic tiles, as well as the tiles coated with TiO_2 NPs using heat treatment and APTES treatment methods, are plotted in Figure 3-5. In FT-IR measurements, the surface of a plain ceramic tile was considered to be the background,

and all other spectra were normalized based on that. As a control, we applied untreated TiO_2 NPs on ceramic tiles and then performed the regular washing steps. It can be seen that the obtained spectrum was a flat line similar to the background, indicating a complete removal of the TiO_2 NPs during the washing process. Nevertheless, the spectra of the TiO_2 coated ceramic tiles using the heat treatment protocol had a number of peaks in the absorption band between 400 to 1200 cm^{-1}, mainly at 400 cm^{-1}, 790 cm^{-1}, and 900 cm^{-1}. This absorption band could be ascribed to the Ti–O stretching and Ti–O–Ti bridging stretching modes [49–53]. Thus, the results demonstrated the presence of TiO_2 NPs onto the surface of the tiles after performing the washing steps. This is due to the strong adhesion of TiO2 NPs to the surface induced via the heat treatment at 200 ℃ for 5 h (the optimum heat treatment condition based on the dye-degradation results in Figure 3-10). Figure 3-5 also depicts the same FT-IR spectra for the APTES treated NPs bonded to the plasma treated ceramic tiles. Moreover, the transmittance percentages of the peaks were almost the same as those of the heat-treated samples, which roughly illustrated the equal mass of TiO_2 coating. The results confirmed the stable bond formation between TiO_2 NPs and the substrate that retained the NPs onto the surface during the washing steps.

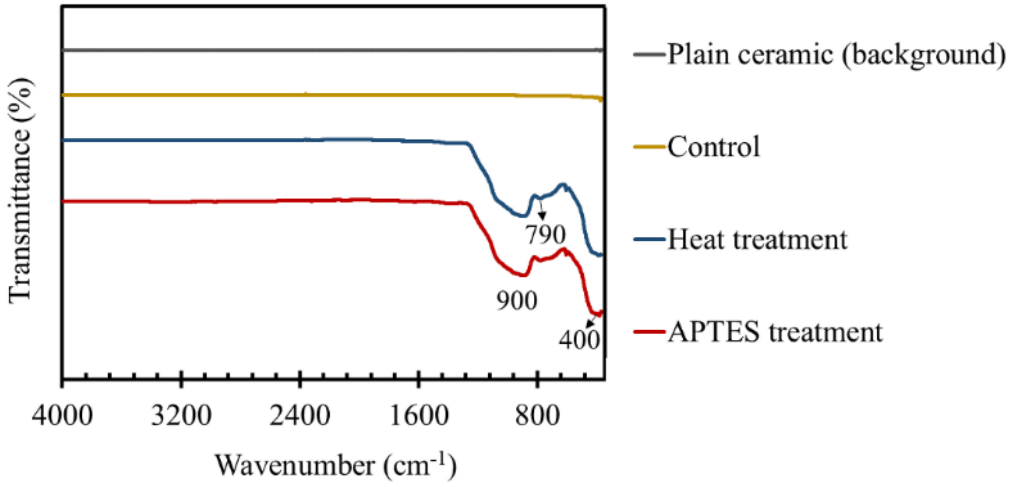

Figure 3-5. FT-IR spectra of plain ceramic tile indicated as the background, control ceramic tile in which untreated particles were applied to the substrate and then the washing steps were conducted, TiO_2 coated ceramic tile using heat treatment method at 200 ℃ for 5 h, and TiO_2 coated ceramic tile using APTES treatment protocol.

In Figure 3-6, the FT-IR spectra of APTES treated TiO2 NPs and untreated NPs were compared at the wavenumber between 2400 to 4000 cm^{-1} to confirm the efficacy of APTES functionalization. There are two main peaks at ~2900 and ~3300 in the transmittance spectrum of untreated TiO_2 NPs, which indicate the presence of hydroxyl groups on the surface of the NPs. The first peak could be associated with both symmetric and asymmetric CH2 stretching vibrations in –CH2–OH compound [54], and the second peak was attributed to hydroxyl group symmetric and asymmetric stretching vibrations in Ti–OH compounds [49]. The hydroxyl groups can be formed due to the chemical and physical adsorptions of atmosphere moisture on the surface of NPs [49,55]. As shown in Figure 3-6, for the APTES treated particles, the peaks related to hydroxyl groups

almost disappeared, and a broad peak between 2800 to 3600 cm^{-1} was formed in the spectrum of APTES treated NPs instead. This is because of the hydrolysis and condensation reactions of the silane head groups in APTES molecules and anchoring to the hydroxyl groups of the NPs surfaces to form oxane (Si–O–M) bonds [56]. The broad peak could be caused by OH stretching in silanol (Si–OH) groups (3200–3700 cm^{-1}) formed via hydrolysis of APTES, primary amine (3160–3450 cm^{-1}), as well as alkane C–H stretching vibrations in –CH3 and –CH2– (2840–2975 cm^{-1}) due to the presence of APTES molecules [54].

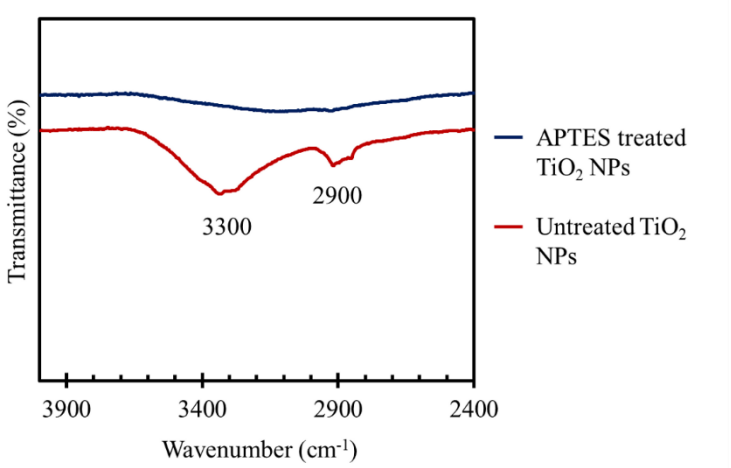

Figure 3-6. FT-IR spectra of the APTES treated TiO2 NPs compared to untreated NPs at the wavenumber between 2400 to 4000 cm^{-1}.

3.4.4 Hydrophilicity and Surface Topography of the TiO_2 Coated Tiles

The results of the contact angle measurement are shown in Figure 3-7. The contact angle of plain ceramic tiles was about 25.8 ± 4.0° indicating the hydrophilic behavior of the surfaces. By performing heat treatment, although surfaces remained hydrophilic, the

contact angle rose to 77.8 ± 3.2°. This unexpected increase in contact angle could be due to the surface roughness generated by partial diffusion of TiO_2 NPs into the surface, which can compensate for the inherent hydrophilicity of TiO_2 [57]. The APTES treatment method, on the other hand, resulted in more hydrophilic TiO_2 coated surfaces with the contact angle of less than 5°. A possible explanation for that is CO_2 plasma treatment step during the APTES treatment protocol, which can greatly increase hydrophilicity as well as the APTES coating on the surface of the NPs [58].

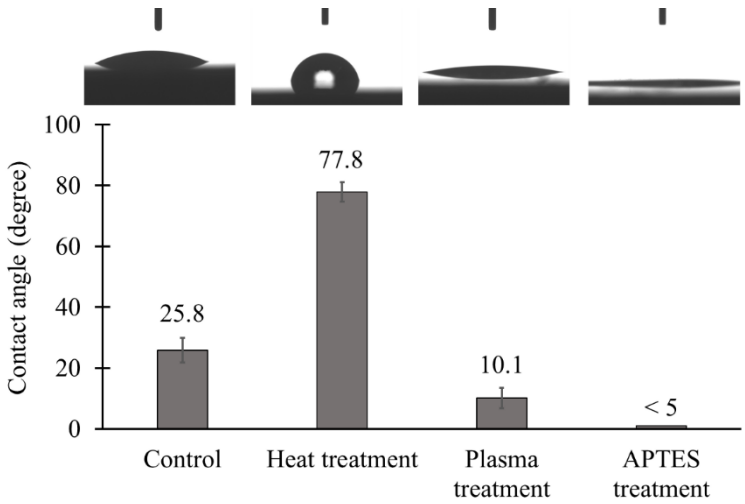

Figure 3-7. Contact angles of plain ceramic tiles (control), TiO_2 coated ceramic tiles via heat treatment method at 200 ℃ for 5 h, CO_2 plasma treated ceramic tiles, and TiO_2 coated ceramic tiles via APTES treatment method (n=3).

AFM images of the TiO_2 coated ceramic tiles are illustrated in Figure 3-8. The density of the NPs in the heat-treated sample (Figure 3-8a) was higher, compared to the sample coated with the APTES treatment protocol (Figure 3-8b). Furthermore, the root-mean-square (RMS) surface roughness of the ceramic tile increased from 0.676 nm for a plain

ceramic to 1.26 nm for TiO_2 coated ceramic using the APTES treatment method. The RMS parameter of the TiO_2 coated ceramic tiles with the heat treatment process was 1.82 nm, which was more than that for tiles with the APTES treatment protocol due to the higher number of NPs on the surface.

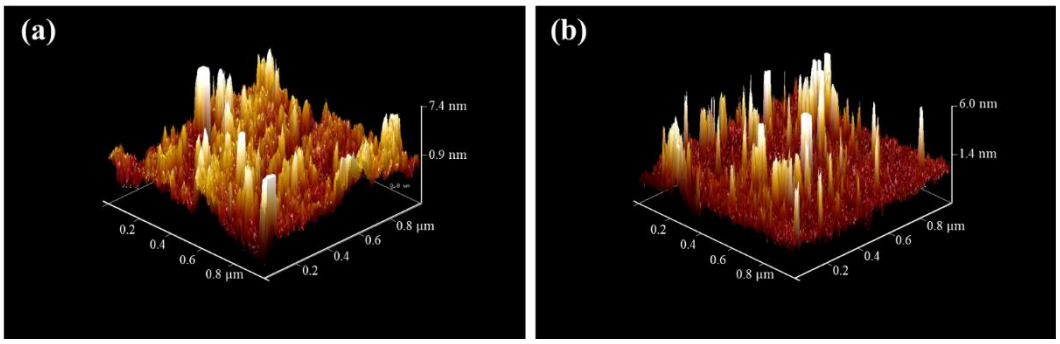

Figure 3-8. 3D AFM images of ceramic tile surfaces coated with TiO_2 NPs using (a) heat treatment at 200 ℃ for 5 h and (b) the APTES treatment method.

3.4.5 Dye Degradation of TiO_2 NPs in Suspension

In order to achieve the proper wavelength for reading the absorbances of the dye with a plate reader, the full absorbance spectra of 1 mg/mL concentration of the dye diluted in deionized water was measured. As shown in Figure 3-9a, the sharp peak at the wavelength of 512 nm, which can be easily distinguished, was used as a reference wavelength for the next absorbance measurements. The calibration curve for dye absorbance as a function of concentration at the wavelength of 512 nm is illustrated in Figure 3-9b. The obtained scatter diagram has a linear trend line. To measure the photocatalytic power of TiO_2 NPs, the particles were added to the 1 mg/mL dye solution and were kept in the UV light, under a constant stirring condition. The amount of dye-

degradation induced by TiO_2 photocatalyst could be calculated based on Figure 3-9b. The dye concentration results versus UV exposure time are shown in Figure 3-9c. As is shown, a considerable reduction in the dye concentration was achieved after 15 min where almost half of the dye was degraded, and the concentration reached 0.55 mg/mL. Afterwards, the rate of dye degradation became slower and after 1 day of UV irradiation, the dye concentration decreased down to 0.26 mg/mL. Thus, the TiO_2 nanoparticles possessed a considerable photocatalytic power in suspension. The reason why the expected exponential decay to zero was not observed in our sample could be attributed to the absorption of the partial degradation products on the photocatalyst surface and/or the pH variation of the suspension leading to deterioration in the dye-degradation process.

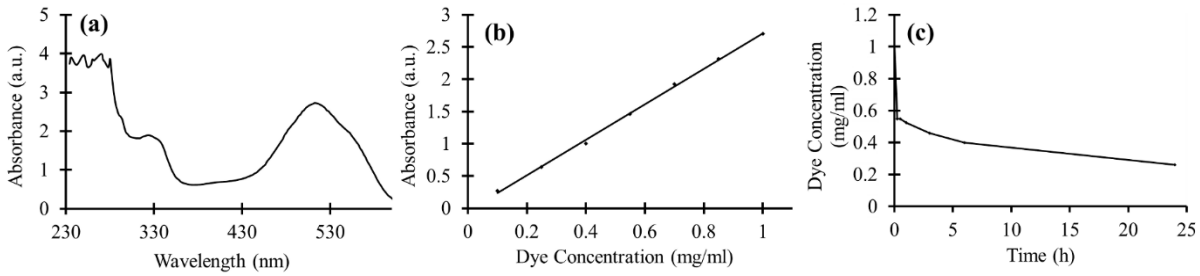

Figure 3-9. (a) UV–VIS spectra of 1 mg/ml concentration of the dye; (b) Absorbance curve as a function of dye concentration at the wavelength of 512 nm. (c) Dye concentration mixed with TiO_2 NPs suspension as a function of UV exposure time.

3.4.6 Dye Degradation on TiO_2 Coated Tiles Produced Using Heat Treatment

Figure 3-10 demonstrates the dye-degradation properties of ceramic tiles coated with TiO_2 nanoparticles using the heat treatment approach at different temperatures and

incubation time (1 and 5 h). Control ceramic tiles were incubated with a suspension of TiO_2 NPs with the same incubation time, but no heat treatment was involved (labeled by "no heat treatment" in Figure 3-10). Following the washing step, all TiO_2 NPs were detached from the surface of control tiles and therefore, no dye degradation was observed. Moreover, when the samples were heat treated for 1 h (Figure 3-10a), no dye-degradation properties were recorded at any heat treatment temperatures. One major problem with high temperatures of 700 ℃ and 900 ℃ is that since the temperatures were above the phase transition temperature of TiO_2 from anatase to rutile [59–62], the formed rutile phase could have deteriorated the photocatalytic activity of the TiO_2 particles even if the particles were successfully attached to the ceramic tiles. It has been proved that TiO_2 exhibits a higher photocatalytic activity in anatase phase compared to fully rutile phase, which may be due to larger band gap in anatase compared to rutile TiO_2 [4]. Thus, the optimal temperature for heat treatment should not change the structure of TiO_2. According to the composite phase diagram of TiO_2, the anatase-rutile phase transition takes place at around 600 ℃ at atmospheric pressure [59].

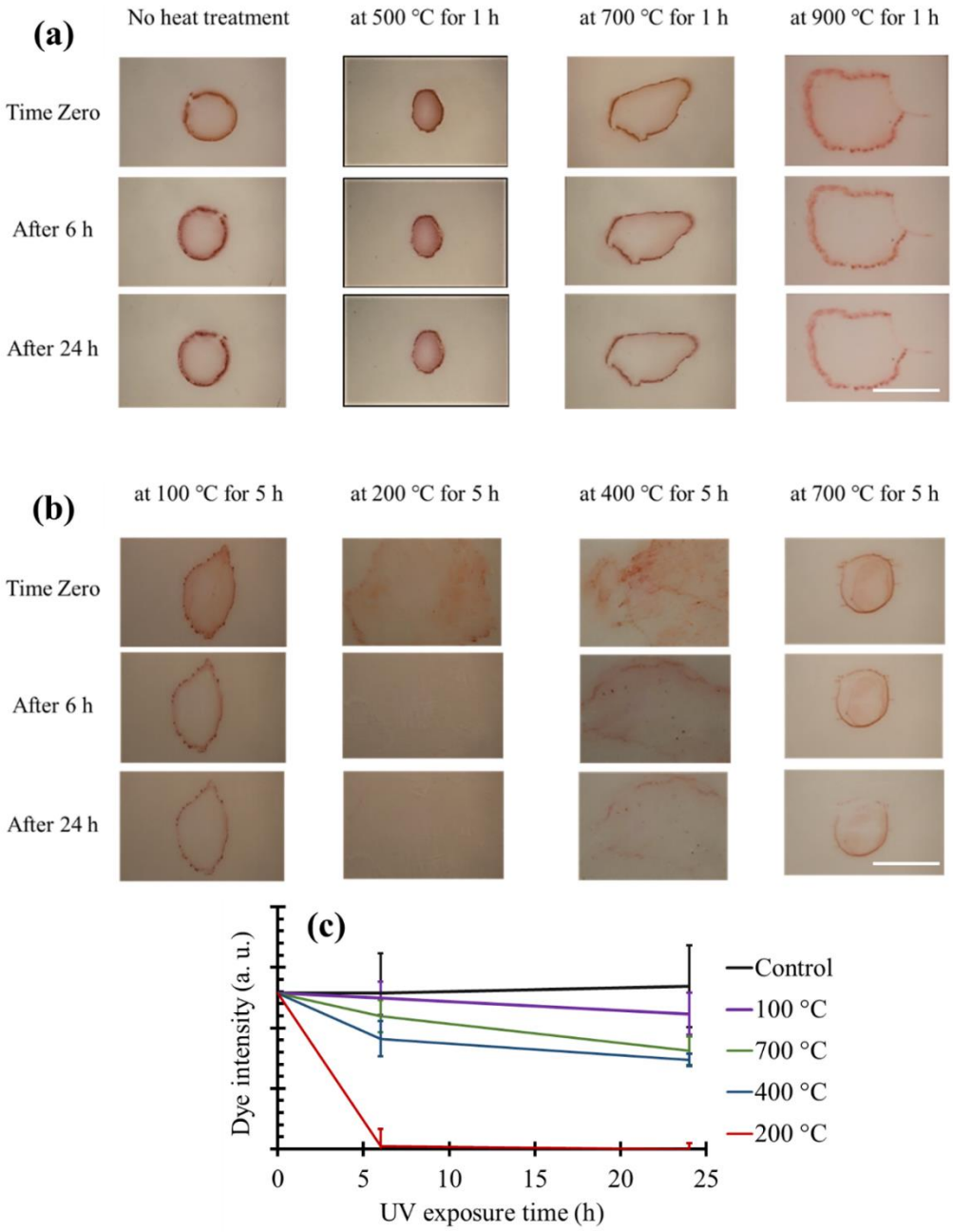

Figure 3-10. Dye degradation results of the heat-treated ceramic tiles under UV exposure. Heat treatment was performed at different temperatures for 1 h, (a) and 5 h (b). Scale bars are 1 cm. (c) Quantification of the dye-degradation on the samples heat treated for 5 h at different temperatures and the control sample without any heat treatment.

Therefore, we increased the heat treatment duration from 1 h to 5 h to investigate the effect of heat treatment time on the coating process, specially the possibility of successful and functional coating at lower temperatures. Figure 3-10b exhibits the dye-degradation trend for the ceramic tile samples, which were heat treated at varying temperatures for 5 h. In Figure 3-10c, the results were also quantified for better comparison. The samples that were heat treated at 400 ℃ degraded the dye at a lower rate than heat treatment at 200 ℃, although both temperatures were below the anatase-rutile phase transition temperature. This can be caused by slightly more agglomeration of the TiO_2 NPs at 400 ℃ in comparison to 200 ℃, leading to a small increase in the average particle size and a reduction in the overall surface area of the particles, thereby diminishing the photocatalytic power. The other possible explanation could be attributed to the higher diffusion of NPs inside the glossy surface of the ceramic tiles at 400 ℃. Therefore, the smaller area of the particles would get in touch with the dye, causing a decrease in the dye-degradation rate. Performing the heat treatment at a more cost-effective temperature of 200 ℃ caused the dye to be fully degraded after 6 h. Nevertheless, 100 ℃ heat treatment for 5 h appeared to be not enough for the TiO_2 particles to be completely attached to the surface of ceramic tiles, thereby resulting in less dye degradation under UV exposure. Therefore, a 5 h heat treatment at 200 ℃ provided the best dye-degradation properties for the ceramic tiles.

3.4.7 Dye Degradation on TiO_2 Coated Tiles Produced Using Aminosilanization

Figure 3-11a illustrates the dye-degradation results of the ceramic tiles coated with the APTES treatment method. Quantifications of the obtained results are plotted in Figure 3-11b. We applied untreated TiO_2 particles onto the ceramic tiles as control samples. Most of the particles were removed from the surface during the washing process, and the dye was not degraded after 1 day in control samples. However, when APTES treated particles were used, the dye was almost invisible after 24 h, demonstrating excellent effectivity of the APTES treatment process for coating ceramic tiles with TiO_2 NPs. In comparison to the heat treatment at 200 ℃ for 5 h, coating the surfaces via the APTES treatment resulted in a lower rate of dye degradation due to two main reasons: a smaller number of particles on the surface which was confirmed with AFM test, and covering the particles via a silane coupling agent which can reduce the photoactivity of the particles [63]. Nevertheless, using the APTES treatment protocol has two important advantages. First, the method for functionalization using APTES is much simpler and does not require high temperatures compared to the heat treatment. Second, since this technique creates covalent bonds between TiO_2 NPs and surfaces, the durability of the coating durability of the coating would be higher in the long term.

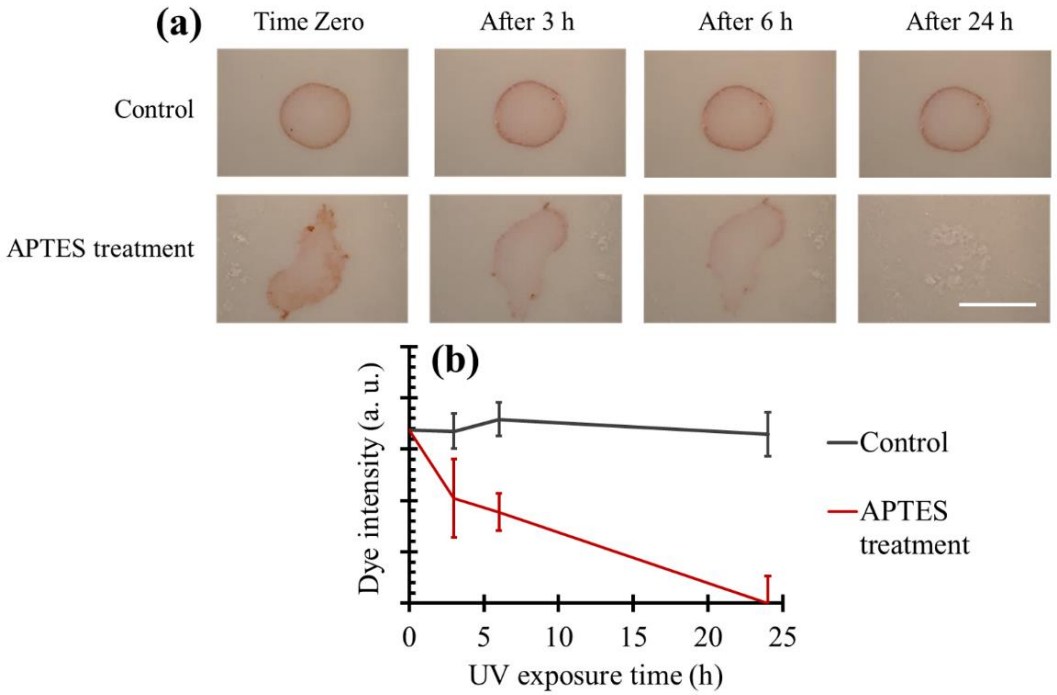

Figure 3-11. (a) Dye degradation results of the ceramic tiles coated with TiO_2 particles using APTES treatment technique. Scale bar is 1 cm. (b) Quantification of the dye-degradation images.

3.5 Conclusions

The photocatalytic power of TiO_2 NPs measured inside the suspension showed a proper dye-degradation effect under UV exposure. We introduced two strategies to coat ceramic tiles with the TiO_2 NPs. Both protocols led to transparent TiO_2 coating on ceramic tiles without any adverse effect on the tile's physical appearance. In the heat treatment approach, it was shown that applying a simple one-step heat treatment with the optimum temperature of 200 ℃ for 5 h resulted in rapid degradation of dye in a short time. In the second strategy, the APTES treatment method was employed to covalently

bond the TiO_2 particles to the CO_2 treated ceramic tiles, while the photocatalytic power of the particles was preserved. The success of the covalent bonding protocol suggests a possible longer duration of the coating in harsh environments. In future, we will focus on enhancement of the self-cleaning behavior, as well as studying the durability of the coating by performing proper weathering tests.

3.6 References

1. Dong, H.; Zeng, G.; Tang, L.; Fan, C.; Zhang, C.; He, X.; He, Y. An overview on limitations of TiO_2-based particles for photocatalytic degradation of organic pollutants and the corresponding countermeasures. *Water Res.* **2015**, *79*, 128–146, doi:https://doi.org/10.1016/j.watres.2015.04.038.

2. Weon, S.; Kim, J.; Choi, W. Dual-components modified TiO_2 with Pt and fluoride as deactivation-resistant photocatalyst for the degradation of volatile organic compound. *Appl. Catal. B Environ.* **2018**, *220*, 1–8, doi:https://doi.org/10.1016/j.apcatb.2017.08.036.

3. Li, S.; Ishikawa, S.; Huang, C.; Zhang, W.; Tanizaki, T.; Higuchi, T.; Haraga, H. Production of active intermediates and decomposition behaviors of organic compounds in the ultraviolet ray / supersonic wave reactions with TiO2 photocatalyst. *Sustain. Environ. Res.* **2015**, *25*, 67–72.

4. Luttrell, T.; Halpegamage, S.; Tao, J.; Kramer, A.; Sutter, E.; Batzill, M. Why is anatase a better photocatalyst than rutile? - Model studies on epitaxial TiO2films. *Sci. Rep.* **2015**, *4*, 1–8, doi:10.1038/srep04043.

5. Hashimoto, K.; Irie, H.; Fujishima, A. TiO2 Photocatalysis: A Historical Overview and Future Prospects. *Jpn. J. Appl. Phys.* **2005**, *44*, 8269–8285, doi:10.1143/JJAP.44.8269.

6. Nosaka, Y.; Nosaka, A.Y. Identification and Roles of the Active Species Generated on Various Photocatalysts. In *Photocatalysis and Water Purification*; Wiley-VCH Verlag GmbH & Co. KGaA, 2013; pp. 1–24 ISBN 9783527645404.

7. Fujishima, A.; Zhang, X.; Tryk, D.A. TiO_2 photocatalysis and related surface phenomena. *Surf. Sci. Rep.* **2008**, *63*, 515–582, doi:10.1016/j.surfrep.2008.10.001.

8. Fujishima, A.; Rao, T.N.; Tryk, D.A. Titanium dioxide photocatalysis. *J. Photochem. Photobiol. C Photochem. Rev.* **2000**, *1*, 1–21, doi:10.1016/S1389-5567(00)00002-2.

9. Nakata, K.; Fujishima, A. TiO2 photocatalysis: Design and applications. *J. Photochem. Photobiol. C Photochem. Rev.* **2012**, *13*, 169–189, doi:10.1016/j.jphotochemrev.2012.06.001.

10. Marugán, J.; van Grieken, R.; Pablos, C.; Satuf, M.L.; Cassano, A.E.; Alfano, O.M. Photocatalytic inactivation of Escherichia coli aqueous suspensions in a fixed-bed reactor. *Catal. Today* **2015**, *252*, 143–149, doi:https://doi.org/10.1016/j.cattod.2014.10.031.

11. Liu, H.-L.; Yang, T.C.-K. Photocatalytic inactivation of Escherichia coli and Lactobacillus helveticus by ZnO and TiO_2 activated with ultraviolet light. *Process Biochem.* **2003**, *39*, 475–481, doi:https://doi.org/10.1016/S0032-9592(03)00084-0.

12. Padervand, M.; Vossoughi, M.; Yousefi, H.; Salari, H.; Gholami, M.R. An experimental and theoretical study on the structure and photoactivity of XFe2O4 (X = Mn, Fe, Ni, Co, and Zn) structures. *Russ. J. Phys. Chem. A* **2014**, *88*, 2451–2461, doi:10.1134/S0036024414130184.

13. Banerjee, S.; Dionysiou, D.D.; Pillai, S.C. Self-cleaning applications of TiO_2 by photo-induced hydrophilicity and photocatalysis. *Appl. Catal. B Environ.* **2015**, *176–177*, 396–428, doi:https://doi.org/10.1016/j.apcatb.2015.03.058.

14. Klein, M.; Grabowska, E.; Zaleska, A. Noble metal modified TiO_2 for photocatalytic air purification. *Physicochem. Probl. Miner. Process.* **2015**, *Vol. 51*, *i*, 49–57, doi:10.5277/ppmp150105.

15. Song, J.; Wang, X.; Yan, J.; Yu, J.; Sun, G.; Ding, B. Soft Zr-doped TiO_2 Nanofibrous Membranes with Enhanced Photocatalytic Activity for Water Purification. *Sci. Rep.* **2017**, *7*, 1636, doi:10.1038/s41598-017-01969-w.

16. Imani, R.; Dillert, R.; Bahnemann, D.W.; Pazoki, M.; Apih, T.; Kononenko, V.; Repar, N.; Kralj-Iglič, V.; Boschloo, G.; Drobne, D.; et al. Multifunctional Gadolinium-Doped Mesoporous TiO_2 Nanobeads: Photoluminescence, Enhanced Spin Relaxation, and Reactive Oxygen Species Photogeneration, Beneficial for Cancer Diagnosis and Treatment. *Small* **2017**, *13*, 1–11, doi:10.1002/smll.201700349.

17. Seo, J.W.; Chung, H.; Kim, M.Y.; Lee, J.; Choi, I.H.; Cheon, J. Development of water-soluble single-crystalline TiO_2 nanoparticles for photocatalytic cancer-cell treatment. *Small* **2007**, *3*, 850–853, doi:10.1002/smll.200600488.

18. Ohko, Y.; Utsumi, Y.; Niwa, C.; Tatsuma, T.; Kobayakawa, K.; Satoh, Y.; Kubota, Y.; Fujishima, A. Self-sterilizing and self-cleaning of silicone catheters coated with TiO_2 photocatalyst thin films: A preclinical work. *J. Biomed. Mater. Res.* **2001**, *58*, 97–101, doi:10.1002/1097-4636(2001)58:1<97::AID-JBM140>3.0.CO;2-8.

19. Suketa, N.; Sawase, T.; Kitaura, H.; Naito, M.; Baba, K.; Nakayama, K.;

Wennerberg, A.; Atsuta, M. An antibacterial surface on dental implants, based on the photocatalytic bactericidal effect. *Clin. Implant Dent. Relat. Res.* **2005**, *7*, 105–11, doi:10.1111/j.1708-8208.2005.tb00053.x.

20. Kim, D.S.; Kwak, S.-Y. Photocatalytic inactivation of E. coli with a mesoporous TiO2 coated film using the film adhesion method. *Environ. Sci. Technol.* **2009**, *43*, 148–151, doi:10.1021/es801029h.

21. Behpour, M.; Mehrzad, M.; Hosseinpour-Mashkani, S.M. TiO_2 Thin Film: Preparation, Characterization, and its Photocatalytic Degradation of Basic Yellow 28 Dye. *J. Nanostructures* **2015**, *5*, 183–187, doi:10.7508/jns.2015.02.014.

22. Vera, M.L.; Leyva, G.; Litter, M.I. Simple TiO2 Coatings by Sol–Gel Techniques Combined with Commercial TiO2 Particles for Use in Heterogeneous Photocatalysis. *J. Nanosci. Nanotechnol.* **2017**, *17*, 4946–4954, doi:10.1166/jnn.2017.13430.

23. Justicia, I.; Garcia, G.; Vázquez, L.; Santiso, J.; Ordejón, P.; Battiston, G.; Gerbasi, R.; Figueras, A. Self-doped titanium oxide thin films for efficient visible light photocatalysis: An example: Nonylphenol photodegradation. *Sensors Actuators, B Chem.* **2005**, *109*, 52–56, doi:10.1016/j.snb.2005.03.021.

24. Justicia, I.; Ordejón, P.; Canto, G.; Mozos, J.L.; Fraxedas, J.; Battiston, G.A.; Gerbasi, R.; Figueras, A. Designed self-doped titanium dioxide thin films for Efficient Visible-Light Photocatalysis. *Adv. Mater.* **2002**, *14*, 1399–1402, doi:10.1002/1521-4095(20021002)14:19<1399::AID-ADMA1399>3.0.CO;2-C.

25. Yemmireddy, V.K.; Farrell, G.D.; Hung, Y.C. Development of Titanium Dioxide (TiO_2) Nanocoatings on Food Contact Surfaces and Method to Evaluate Their Durability and Photocatalytic Bactericidal Property. *J. Food Sci.* **2015**, *80*, N1903–N1911, doi:10.1111/1750-3841.12962.

26. Sopyan, I.; Watanabe, M.; Murasawa, S.; Hashimoto, K.; Fujishima, A. A film-type photocatalyst incorporating highly active TiO_2 powder and fluororesin binder: photocatalytic activity and long-term stability. *J. Electroanal. Chem.* **1996**, *415*, 183–186, doi:https://doi.org/10.1016/S0022-0728(96)01007-8.

27. Lin, H.; Xu, Z.; Wang, X.; Long, J.; Su, W.; Fu, X.; Lin, Q. Photocatalytic and antibacterial properties of medical-grade PVC material coated with TiO2 film. *J. Biomed. Mater. Res. - Part B Appl. Biomater.* **2008**, *87*, 425–431, doi:10.1002/jbm.b.31120.

28. Pal, S.; Contaldi, V.; Licciulli, A.; Marzo, F. Self-Cleaning Mineral Paint for

Application in Architectural Heritage. *Coatings* **2016**, *6*, 48, doi:10.3390/coatings6040048.

29. Gunda, N.S.K.; Singh, M.; Norman, L.; Kaur, K.; Mitra, S.K. Optimization and characterization of biomolecule immobilization on silicon substrates using (3-aminopropyl)triethoxysilane (APTES) and glutaraldehyde linker. *Appl. Surf. Sci.* **2014**, *305*, 522–530, doi:10.1016/j.apsusc.2014.03.130.

30. Landoulsi, J.; Genet, M.J.; Kirat, K. El; Richard, C.; Pulvin, S.; Rouxhe, P.G. Silanization with APTES for Controlling the Interactions Between Stainless Steel and Biocomponents: Reality vs Expectation. *Biomater. - Phys. Chem.* **2011**, *5*, 99–126, doi:978-953-307-418-4.

31. Li, G.; Yang, P.; Qin, W.; Maitz, M.F.; Zhou, S.; Huang, N. The effect of coimmobilizing heparin and fibronectin on titanium on hemocompatibility and endothelialization. *Biomaterials* **2011**, *32*, 4691–4703, doi:https://doi.org/10.1016/j.biomaterials.2011.03.025.

32. Badv, M.; Jaffer, I.H.; Weitz, J.I.; Didar, T.F. An omniphobic lubricant-infused coating produced by chemical vapor deposition of hydrophobic organosilanes attenuates clotting on catheter surfaces. *Sci. Rep.* **2017**, *7*, 11639, doi:10.1038/s41598-017-12149-1.

33. Villegas, M.; Cetinic, Z.; Shakeri, A.; Didar, T.F. Fabricating smooth PDMS microfluidic channels from low-resolution 3D printed molds using an omniphobic lubricant-infused coating. *Anal. Chim. Acta* **2018**, *1000*, 248–255, doi:https://doi.org/10.1016/j.aca.2017.11.063.

34. Didar, T.F.; Cartwright, M.J.; Rottman, M.; Graveline, A.R.; Gamini, N.; Watters, A.L.; Leslie, D.C.; Mammoto, T.; Rodas, M.J.; Kang, J.H.; et al. Improved treatment of systemic blood infections using antibiotics with extracorporeal opsonin hemoadsorption. *Biomaterials* **2015**, *67*, 382–392, doi:https://doi.org/10.1016/j.biomaterials.2015.07.046.

35. Didar, T.F.; Tabrizian, M. Generating multiplex gradients of biomolecules for controlling cellular adhesion in parallel microfluidic channels. *Lab Chip* **2012**, *12*, 4363–4371, doi:10.1039/C2LC40233E.

36. Didar, T.F.; Bowey, K.; Almazan, G.; Tabrizian, M. A miniaturized multipurpose platform for rapid, label-free, and simultaneous separation, patterning, and in vitro culture of primary and rare cells. *Adv. Healthc. Mater.* **2014**, *3*, 253–260, doi:10.1002/adhm.201300099.

37. Shakeri, A.; Sun, N.; Badv, M.; Didar, T.F. Generating 2-dimensional concentration gradients of biomolecules using a simple microfluidic design.

Biomicrofluidics **2017**, *11*, 044111.

38. Kim, W.J.; Kim, S.; Lee, B.S.; Kim, A.; Ah, C.S.; Huh, C.; Sung, G.Y.; Yun, W.S. Enhanced protein immobilization efficiency on a TiO_2 surface modified with a hydroxyl functional group. *Langmuir* **2009**, *25*, 11692–11697, doi:10.1021/la901615e.

39. Cheng, F.; Sajedin, S.M.; Kelly, S.M.; Lee, A.F.; Kornherr, A. UV-stable paper coated with APTES-modified P25 TiO_2 nanoparticles. *Carbohydr. Polym.* **2014**, *114*, 246–252, doi:10.1016/j.carbpol.2014.07.076.

40. Gong, Z.; Tang, D.; Guo, Y. The fabrication and self-flocculation effect of hybrid TiO2 nanoparticles grafted with poly(N-isopropylacrylamide) at ambient temperature via surface-initiated atom transfer radical polymerization. *J. Mater. Chem.* **2012**, *22*, 16872, doi:10.1039/c2jm32168h.

41. Xu, Z.; Shang, J.; Liu, C.; Kang, C.; Guo, H.; Du, Y. The preparation and characterization of TiO_2 ultrafine particles. *Mater. Sci. Eng. B* **1999**, *63*, 211–214, doi:https://doi.org/10.1016/S0921-5107(99)00084-7.

42. Yu, J.-G.; Yu, H.-G.; Cheng, B.; Zhao, X.-J.; Yu, J.C.; Ho, W.-K. The Effect of Calcination Temperature on the Surface Microstructure and Photocatalytic Activity of TiO_2 Thin Films Prepared by Liquid Phase Deposition. *J. Phys.*

Chem. B **2003**, *107*, 13871–13879, doi:10.1021/jp036158y.

43. Lopez, N.; Nørskov, J.K.; Janssens, T.V.W.; Carlsson, A.; Puig-Molina, A.; Clausen, B.S.; Grunwaldt, J.-D. The adhesion and shape of nanosized Au particles in a Au/TiO_2 catalyst. *J. Catal.* **2004**, *225*, 86–94, doi:https://doi.org/10.1016/j.jcat.2004.03.036.

44. Kang, I.-C.; Zhang, Q.; Yin, S.; Sato, T.; Saito, F. Preparation of a visible sensitive carbon doped TiO_2 photo-catalyst by grinding TiO_2 with ethanol and heating treatment. *Appl. Catal. B Environ.* **2008**, *80*, 81–87, doi:https://doi.org/10.1016/j.apcatb.2007.11.005.

45. Yamada, K.; Yamane, H.; Matsushima, S.; Nakamura, H.; Ohira, K.; Kouya, M.; Kumada, K. Effect of thermal treatment on photocatalytic activity of N-doped TiO_2 particles under visible light. *Thin Solid Films* **2008**, *516*, 7482–7487, doi:https://doi.org/10.1016/j.tsf.2008.03.041.

46. Widegren, J.; Bergström, L. The effect of acids and bases on the dispersion and stabilization of ceramic particles in ethanol. *J. Eur. Ceram. Soc.* **2000**, *20*, 659–665, doi:10.1016/S0955-2219(99)00199-5.

47. Kardys, A.Y.; Bharali, D.J.; Mousa, S.A. Amino-functionalized silica nanoparticles: In vitro evaluation for targeted delivery and therapy of pancreatic

cancer. *J. Nanotechnol.* **2013**, *2013*, ID 768724, doi:10.1155/2013/768724.

48. Chen, L.-X.; Zheng, J.-N.; Wang, A.-J.; Wu, L.-J.; Chen, J.-R.; Feng, J.-J. Facile synthesis of porous bimetallic alloyed PdAg nanoflowers supported on reduced graphene oxide for simultaneous detection of ascorbic acid, dopamine, and uric acid. *Analyst* **2015**, *140*, 3183–3192, doi:10.1039/C4AN02200A.

49. Praveen, P.; Viruthagiri, G.; Mugundan, S.; Shanmugam, N. Structural, optical and morphological analyses of pristine titanium di-oxide nanoparticles - Synthesized via sol-gel route. *Spectrochim. Acta - Part A Mol. Biomol. Spectrosc.* **2014**, *117*, 622–629, doi:10.1016/j.saa.2013.09.037.

50. Lu, H. Bin; Zhou, Y.Z.; Vongehr, S.; Tang, S.C.; Meng, X.K. Effects of hydrothermal temperature on formation and decoloration characteristics of anatase TiO_2 nanoparticles. *Sci. China Technol. Sci.* **2012**, *55*, 894–902, doi:10.1007/s11431-011-4706-4.

51. Watson, S.; Beydoun, D.; Scott, J.; Amal, R. Preparation of nanosized crystalline TiO_2 particles at low temperature for photocatalysis. *J. Nanoparticle Res.* **2004**, *6*, 193–207, doi:Doi 10.1023/B:Nano.0000034623.33083.71.

52. Chen, Y.F.; Lee, C.Y.; Yeng, M.Y.; Chiu, H.T. The effect of calcination temperature on the crystallinity of TiO_2 nanopowders. *J. Cryst. Growth* **2003**,

247, 363–370, doi:10.1016/S0022-0248(02)01938-3.

53. Chellappa, M.; Anjaneyulu, U.; Manivasagam, G.; Vijayalakshmi, U. Preparation and evaluation of the cytotoxic nature of TiO_2 nanoparticles by direct contact method. *Int. J. Nanomedicine* **2015**, *10*, 31–41, doi:10.2147/IJN.S79978.

54. Socrates, G. *Infrared and Raman characteristic group frequencies*; Third.; 2001; ISBN 978-0-470-09307-8.

55. Olurode, K.; Neelgund, G.M.; Oki, A.; Luo, Z. A facile hydrothermal approach for construction of carbon coating on TiO2 nanoparticles. *Spectrochim. Acta Part A Mol. Biomol. Spectrosc.* **2012**, *89*, 333–336, doi:https://doi.org/10.1016/j.saa.2011.12.025.

56. Kango, S.; Kalia, S.; Celli, A.; Njuguna, J.; Habibi, Y.; Kumar, R. Surface modification of inorganic nanoparticles for development of organic-inorganic nanocomposites - A review. *Prog. Polym. Sci.* **2013**, *38*, 1232–1261, doi:10.1016/j.progpolymsci.2013.02.003.

57. Yoshimitsu, Z.; Nakajima, A.; Watanabe, T.; Hashimoto, K. Effects of surface structure on the hydrophobicity and sliding behavior of water droplets. *Langmuir* **2002**, *18*, 5818–5822, doi:10.1021/la020088p.

58. Han, J.-B.; Wang, X.; Wang, N.; Wei, Z.-H.; Yu, G.-P.; Zhou, Z.-G.; Wang, Q.-Q. Effect of plasma treatment on hydrophilic properties of TiO_2 thin films. *Surf. Coatings Technol.* **2006**, *200*, 4876–4878, doi:https://doi.org/10.1016/j.surfcoat.2005.04.036.

59. Nie, X.; Zhuo, S.; Maeng, G.; Sohlberg, K. Doping of TiO_2 Polymorphs for Altered Optical and Photocatalytic Properties. *Int. J. Photoenergy* **2009**, *2009*, 1–22, doi:10.1155/2009/294042.

60. Ren, R.; Yang, Z.; Shaw, L.L. Polymorphic transformation and powder characteristics of TiO2 during high energy milling. J. Mater. Sci. 2000, 35, 6015–6026.

61. Mei, Z.-G.; Wang, Y.; Shang, S.; Liu, Z.-K. First-principles study of the mechanical properties and phase stability of TiO_2. Comput. Mater. Sci. 2014, 83, 114–119.

62. Hanaor, D.A.H.; Sorrell, C.C. Review of the anatase to rutile phase transformation. J. Mater. Sci. 2011, 46, 855–874.

63. Zhao, J.; Milanova, M.; Warmoeskerken, M.M.C.G.; Dutschk, V. Surface modification of TiO2 nanoparticles with silane coupling agents. Colloids Surfaces A Physicochem. Eng. Asp. 2012, 413, 273–279.

Chapter 4: Plasma-induced Covalent Immobilization and Patterning of Bioactive Species in Microfluidic Devices

Amid Shakeri, Sara M. Imani, Eric Chen, Hanie Yousefi, Raed Shabbir, Tohid F Didar*

Lab on a Chip, 2019, 19, 3104–3115

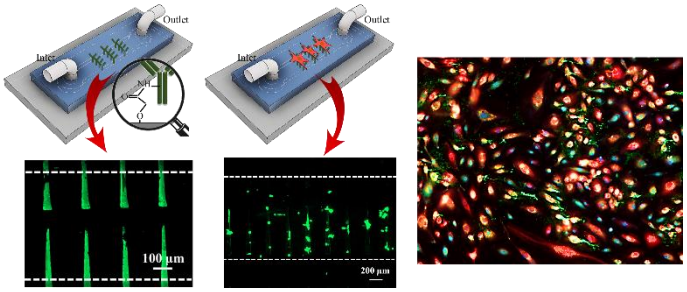

4.1 Abstract

Here, we present a straightforward technique to create bio-functional microfluidic channels using CO_2 plasma to induce both carboxylic and hydroxyl groups onto the channel surface. Consequently, not only does the surface allow for irreversible covalent bonding to an oxygen plasma treated PDMS for microfluidic device fabrication, but it also provides functionality for biomolecular immobilization. Furthermore, we demonstrate integration of this technique with microcontact printing to covalently micropattern functional biomolecules inside microfluidic channels. The bio-functionality and efficacy of the microcontact printed antibodies is demonstrated for both bioassays as well as patterning and culturing different cell lines. Results show that the introduced method can be an excellent candidate for cell culture studies in microfluidics. With the new printing method, full cell confluency (~400 cells/mm^2) was achieved after incubation for only 1 day, which is significantly greater than other conventional cell culture techniques inside microfluidic devices. As a proof of concept, we demonstrated the endothelial cells functionality by stimulating von Willebrand Factor secretion under shear stress. This is done via perfusion of histamine through the channel and performing immunofluorescence labeling to observe the inflammatory response of the cells. The developed method eliminates the need for wet chemistry and

significantly simplifies producing bio-functional chips which can be used for biosensing, organs-on-chips and tissue engineering applications.

Keywords: Microfluidics, plasma treatment, covalent immobilization, surface patterning, cell culture, Biofunctional microchannels

4.2 Introduction

Recently, microfluidic systems capable of controlling and manipulating laminar flows with volumes ranging from microliters to picolitres have been widely used in biosensors and biomedical applications [1–4]. These systems have been used for the miniaturization and parallelization of common lab tasks with lab-on-a-chip devices, mimicry of physiological responses of organs with organs-o-chip devices, execution of point of care diagnostics, and for bio [5–13].

With the rise of high resolution 3D printed molds and soft lithographic techniques, creating smooth microfluidic channels with polymers such as polydimethylsiloxane (PDMS) is easy to accomplish [14–16]. The polymeric platform can irreversibly be bonded to a substrate which could be either a glass surface or another polymeric membrane, by means of an oxygen plasma activation technique [17]. In this technique, partially ionized oxygen gas induces silanol groups onto the surface of the material via inelastic collisions between free electrons and ground state atoms. This atomic interaction results

in the formation of reactive hydroxyl radicals on the surface[18,19]. The silanol-modified surfaces can be brought together to induce covalent bond formation via condensation of the silanol groups. The PDMS-glass bond formed through the oxygen plasma treatment technique was experimentally found to withstand up to 74 psi units of pressure [20]. In addition, plasma treatment is an advantageous technique that can be used for other applications such as for surface cleaning and sterilization (which is of a great importance for biological assays and cell culture), and for inducing polar functional groups on the surface of hydrophobic materials, including PDMS. Induction of polar functional groups in such cases results in increased hydrophilicity and wettability, which reduces the possibility of air bubble formation inside microchannels [21].

Implementing microfluidic devices for chemical and biological assays often requires the existence of a bio-functional surface inside the microchannels[22]. This could be achieved either by perfusion of a desired biomolecule inside the channel which brings about physical attachment of the biomolecule, or by covalent immobilization of bio-species onto the channel surface. The latter offers greater efficacy by providing a higher yield of immobilized biomolecules on the channel, and better robustness and longevity, especially when working with high flow rates that could detach non-covalent interactions due to high amounts of wall shear stress [23,24]. The usage of organosilane chemistry is an effective technique for facilitating covalent bond formation between

organic and inorganic surfaces by creating self assembled monolayers (SAMs) on the microchannel's hydroxylated surfaces. Aminosilanes such as 3-aminopropyltrimethoxysilane (APTMS) and 3-aminopropyltriethoxysilane (APTES) are the most commonly used silane coupling agents for the immobilization of biomolecules [24–27]. Silanization of the microfluidic channels is conventionally performed via liquid phase deposition method (LPD) after the oxygen plasma treatment of the device's layers and usually subsequent to the channel assembly. The plasma induced hydroxyl groups inside the channel are utilized to create SAMs of the silane molecule of choice through the hydrolysis and condensation reactions. This could be done by perfusion of a diluted silane coupling agent though the microfluidic channels for a specific period of time (usually for a couple of hours) followed by proper washing and heat treatment steps [26,28,29]. Submerging the channels' layers inside the silane solution before the channel assembly is another way for LPD silanization [30–32].

Following silanization with APTES or APTMS, the carboxyl groups of the desired biomolecules should be activated using 1-ethyl-3-(-3-dimethylaminopropyl) carbodiimide hydrochloride (EDC) and N-hydroxysuccinimide (NHS) chemistry [33–44]. Silane SAMs are mechanically and chemically robust, and each organofunctional group gives unique chemical properties for a certain application. However, silanization of microfluidic channels is time-consuming and adds an extra step for surface

functionalization. Thus, eliminating silanization out of the procedure can result in both time and cost savings. Moreover, producing homogeneous SAMs is challenging and mixing biomolecules with EDC-NHS could result in self-crosslinking between biomolecules via their carboxylic and amino groups. Therefore, this process leads to protein loss and non-uniformity in surface coating due to the aggregation of proteins.

Furthermore, precise micro/nano patterning of the microchannel's surface is of considerable importance for selective screening in biosensors, biological assays or cell studies [45–52]. Microcontact printing is one of the most simple and straightforward techniques used to form various patterns on different surfaces [53–58]. In this technique, typically, biomolecules are physically attached to the surface. This configuration can result in gradual elimination of the patterns and detachment of the biomolecules from the surface over time, when the surface is exposed to harsh flow rates and high shear stress. Microcontact printing of silane coupling agents such as APTES on hydroxylated surfaces is suggested as an alternative approach to covalently pattern biomolecules [59,60]. Nevertheless, obtaining distinct patterns with this procedure could be quite challenging and time consuming.

The aforementioned issues of the conventional surface functionalization and patterning methods stimulate a great demand for seeking a more convenient and efficient strategy to provide localized biofunctionality inside the microfluidic channels. Here, we

introduce a robust and versatile technique to create bio-functional microfluidic channels by means of CO_2 plasma activation of the surface rather than conventional O_2 plasma treatment and silanization process. The new strategy offers the following advantages:

(i) The carboxylic groups induced by CO_2 plasma activation of the substrate can directly be employed to immobilize the biomolecules. Thus, it eliminates the need for silanization or any other wet chemistry in order to provide functionality. This accelerates the surface functionalization process and makes it more straightforward.

(ii) Since the carboxylic groups of the surface can covalently bind to the amino groups of the biomolecules, the created biofunctional interface will possess long-term stability and robustness against harsh physical conditions such as high flow rates and shear stresses.

(iii) CO_2 plasma treatment can also induce hydroxyl groups in addition to the carboxylic groups onto the substrate. The hydroxyl groups allow for irreversible bonding with an oxygen plasma treated polymeric platform. Therefore, only a single step plasma treatment is required to assemble the microfluidic channel as well as provide functionality for biomolecules immobilization.

(iv) The carboxylic groups of the channel could be activated via introducing EDC-NHS before the perfusion of antibodies. Since here there is no need to mix EDC-NHS with

the antibody, self-crosslinking and protein aggregation, and consequent wasting of the biomolecules will be prevented by the new protocol.

(v) The proposed technique also enables covalent mico-patterning of the microfluidic channels with the desired biomolecules. This could be achieved through contact printing of EDC-NHS on the CO_2 plasma activated surface.

As a proof of concept, we performed cell culture experiments demonstrating significant differences in the number of cells adhered on the immobilized fibronectin patterned channels via applying our approach compared to the conventional methods.

4.3 Experimental Procedure

4.3.1 Materials and Equipment

Materials and reagents used for device fabrication and antibody immobilization included: Polydimethylsiloxane (PDMS) (Dow SYLGARD™ 184 Silicone Encapsulant, Ellsworth Adhesives, Stoney Creek, ON, Canada), Trichloro(1H,1H,2H,2H-perfluorooctyl)silane (Sigma-Aldrich, Oakville, ON, Canada), N-(3-Dimethylaminopropyl)-N′-ethylcarbodiimide hydrochloride (EDC) (Sigma-Aldrich, Oakville, ON, Canada), N-Hydroxysuccinimide (NHS) (Sigma-Aldrich, Oakville, ON, Canada), Albumin–fluorescein isothiocyanate conjugate (BSA-FITC) (Sigma-Aldrich, Oakville, ON, Canada), Poly(L-lysine) - poly(ethylene glycol)

(PLL(20)-g[3.5]- PEG(2), SuSoS surface technology, Dübendorf, Switzerland), CD34 Monoclonal Antibody (4H11[APG]), Alexa Fluor® 488 conjugate (ThermoFisher Scientific, ON, Canada), Alexa Fluor® 594-conjugated AffiniPure Goat Anti-Mouse IgG (H+L) (Jackson ImmunoResearch Laboratories, Inc., West Grove, PA, USA), Tris-buffered saline mixed with 0.005% Tween® 20 (TBST) (Sigma-Aldrich, Oakville, ON, Canada)

Cell culture experiments were performed using: Fibronectin from human plasma (Sigma-Aldrich, Oakville, ON, Canada), Green fluorescent protein transfected NIH 3T3 (GFP-NIH 3T3) cell line (ATCC, Manassas, VA, USA), Red fluorescent protein transfected human umbilical vein endothelial cells (RFP-HUVECs) (ATCC, Manassas, VA, USA), Supplemented Endothelial Cell Growth Basal Medium-2 (EBM^{TM}-2) (Lonza, Mississauga, ON, Canada), Dulbecco's Modified Eagle Medium (DMEM) supplemented with 10% FBS and 1% PenStrep (ThermoFisher Scientific, ON, Canada), Trypsin-EDTA (0.25%) (Thermo Fisher Scientific, Waltham, MA, USA), Trypsin neutralizer (Cedarlane, Burlington, ON, Canada), Pierce™ 16% Formaldehyde (w/v), Methanol-free (ThermoFisher Scientific, ON, Canada), Invitrogen™ Molecular Probes™ Hoechst 33342, Trihydrochloride, Trihydrate (Fisher scientific, Ottawa, ON, Canada), histamine (≥97.0%, Sigma-Aldrich, Oakville, ON, Canada), polyclonal Rabbit Anti-Human Von Willebrand Factor (Agilent, ON, Canada), goat anti-Rabbit

IgG (H+L) Cross-Adsorbed Secondary Antibody, Alexa Fluor 488 (ThermoFisher Scientific, ON, Canada).

4.3.2 Overview of the Procedure

The proposed protocol involves CO_2 plasma activation of a glass substrate which induces both carboxylic groups and hydroxyl groups onto the surface. The glass substrate was then covalently bonded to an oxygen plasma treated PDMS containing the channels geometries to form the microfluidic device. The remaining carboxylic groups inside the channel were activated via EDC-NHS followed by proper washing steps. Afterwards, the desired biomolecule was perfused through the channel to covalently bind to the activated carboxylic groups of the surface via the biomolecule's amino groups.

In order to pattern the biomolecules in the microchannels, EDC-NHS was contact printed onto the CO_2 plasma activated glass substrate to locally activate the carboxylic groups. The printing step should be performed before the PDMS bonding and channel assembly. After printing the EDC-NHS, the biomolecule of interest could either be perfused inside the channel or contact printed (double printing protocol) on the EDC-NHS printed area.

4.3.3 CO_2 Plasma Induced Functionalization

PDMS was first mixed at a ratio of 10:1 (elastomer : curing agent), degassed and cured in a 3D-printed mold to form the PDMS platform of the microfluidic device with the channel's cavity. The mold was 3D-printed by Stratasys Objet 24 (Javelin Technologies) using Stratasys VeroWhitePlus FullCure 835 for the build, and Polyjet Support Material FullCure 705 for the support resin. The 3D-printed mold was fluorosilanized through chemical vapor deposition (CVD) of Trichloro(1H,1H,2H,2H-perfluorooctyl)silane for 1 hour followed by overnight heat treatment at 60 °C. This facilitates the PDMS casting and peeling off process and increase the accuracy of the channels' dimensions. The channel dimensions were 52 μm in height, 2 cm in length, with the width varying between 0.2 mm to 2 mm. Fabrication of the microfluidic channels began with 5 min CO_2 plasma treatment (Harrick Plasma) of a glass slide which induced CO_2 and O_2 groups onto the substrate. Three different approaches were employed to immobilize bio-species on the functional surfaces of the channels. In the first technique, the entire channel was coated with the biomolecule of interest. The other two techniques were implemented to create micropatterns of biomolecules covalently bonded to the substrate of the microfluidic channels (Figure 4-1).

4.3.4 Non-patterning Functionalization

PDMS platform was oxygen plasma treated for 2 minutes and then placed onto the CO_2 plasma treated glass slide for irreversible bonding. EDC and NHS with the molar ratio of EDC/NHS: ~1/1 were diluted in MES buffer (pH = 4.5) with an EDC concentration of 40 mg/ml. The EDC-NHS solution was perfused inside the channel (flow rate = 20 µl/min, dispensed volume = 100 µl) using a syringe pump (NE-1000 Programmable Single Syringe Pump, New Era Pump Systems Inc.). After incubation for 15 min, the channel was rinsed with distilled water (flow rate = 100 µl/min, dispensed volume = 300 µl). Two different proteins were immobilized in the channels; BSA-FITC and fibronectin. Immobilization of BSA-FITC was performed by perfusion of BSA-FITC (250 µg/ml diluted in PBS) at a flow rate of 100 µl/min, followed by incubation in a stationary condition for 90 min. Next the channel was washed by TBST (flow rate = 100 µl/min, dispensed volume = 600 µl).

Fibronectin immobilization was conducted through perfusion of fibronectin (1:25 diluted in PBS) followed by 30 min incubation in the stationary state. Then, the microchannels were washed with PBS (flow rate = 300 µl/min, dispensed volume = 300 µl) and TBST buffer (flow rate = 300 µl/min, dispensed volume = 300 µl).

4.3.5 Single Step Micro-contact Printing

Before microcontact printing, PDMS stamps were sonicated in ethanol bath for 10 min. 100 µl of EDC-NHS solution (EDC/NHS molar ratio: ~1/1, EDC concentration of 40 mg/ml, diluted in MES with pH : 4.5) was added to a patterned PDMS stamp. After 2 min, the stamp was blown dry by nitrogen blast, and was immediately placed on the CO_2 plasma treated glass slide. A small amount of weight was added on top of the stamp to ensure the patterns were completely in touch with the surface. After 15 min, the stamp was removed, and the oxygen plasma treated PDMS platform (with microfluidic channels) was placed on the substrate while ensuring that the patterned area crossed the microchannel. Next, fluor® 488-conjugated CD34 antibody (1:50 diluted in PBS) was flowed through the channel at a flow rate of 25 µl/h for 2 hours. Finally, the channel was washed with PBS (flow rate = 100 µl/min, dispensed volume = 250 µl) and TBST (flow rate = 100 µl/min, dispensed volume = 250 µl).

4.3.6 Double Step Micro-contact Printing

100 µl of EDC-NHS solution (EDC/NHS molar ratio: ~1/1, EDC concentration of 40 mg/ml, diluted in MES with pH : 4.5) was added to a flat PDMS stamp without any pattern. The stamp was dried with a strong blast of air for 2 min, and placed onto the CO_2 plasma treated glass substrate with a weight on top. The stamp was left for 15 min to let the EDC-NHS activate the carboxylic groups underneath. The next step was to

print the desired antibody with a patterned stamp. The second printing was performed with fluor® 488-conjugated CD34 antibody (1:50 diluted in PBS) and fibronectin (1:25 diluted in PBS). For both experiments, 20 µl of the desired protein was added to a patterned stamp and an oxygen plasma treated cover slip was placed on top in order to spread the solution on the entire surface of the stamp. After 10 min, the stamp was briefly washed with PBS and distilled water and dried with a blast of nitrogen gas. The patterned stamp was placed onto the surface of the glass slide which was previously activated with EDC-NHS, and left for two minutes with a small weight on top. Finally, the substrate was bonded with the O_2 plasma treated PDMS platform to form the microfluidic device such that the patterns were located within the channel area.

In the CD34 experiment, the bio-functionality of the antibody was also evaluated via perfusion of Alexa Fluor® 594-conjugated Goat Anti-Mouse IgG (1:500 diluted in PBS), which had an affinity for the patterned CD34 antibody. For this purpose, the channel was first washed with PBS (flow rate = 100 µl/min, dispensed volume = 300 µl) and blocked by perfusing PLL-PEG (0.1 mg/ml diluted in PBS) at a flow rate of 0.1 ml/h for 30 min. Then, the channel was again rinsed with PBS (flow rate = 100 µl/min, dispensed volume = 300 µl) and the Fluor® 594-conjugated Goat Anti-Mouse IgG antibody was perfused through the channel (flow rate = 100 µl/min, dispensed volume = 200 µl).

Double step printing of fibronectin was also compared with conventional printing methods, where the patterned stamp was placed onto a glass substrate that underwent oxygen plasma treatment for 5 min. The protocol was the same as the new procedure, except the EDC-NHS printing step was not conducted.

4.3.7 Cell Culture

Before culturing cells inside the microfluidic devices, the channels were blocked via incubation of PLL-PEG (0.1 mg/ml diluted in PBS) in the channels for 1 hour. Furthermore, the channels were washed with PBS (flow rate = 200 µl/min, dispensed volume = 300 µl) and warmed cell medium (flow rate = 100 µl/min, dispensed volume = 200 µl). Cell culture experiments were performed with two different cell lines: GFP-NIH 3T3 grown in DMEM and RFP-HUVECs grown in EBM^{TM}-2. Cell incubation was done at 37 °C in 5% CO_2-humidified air atmosphere. Trypsin-EDTA and trypsin neutralizer were used for cell passaging. The microchannels were seeded with the desired cells at a concentration of ~ 10^7 cells/ml followed by incubation for 1 day. During the incubation period, syringes filled with the medium were placed at the inlets and outlets to supply the cultured cells. After 1 day, dead cells were flushed out (flow rate = 600 µl/h, dispensed volume = 100 µl) and fresh media were replaced at the inlets and outlets. This process was repeated at each incubation time step.

4.3.8 RFP-HUVECs Stimulation and Immunofluorescence Labelling

After achieving the fully confluent endothelial cells in the microfluidic device, histamine (50 uM diluted in PBS) was perfused through the channel (flow rate = 600 ul/h) for 10 min inside the incubator in order to stimulate von Willebrand factor (VWF) secretion. Then, the cells were immediately fixed by perfusion of 150 µl 4% methanol-free formalin (achieved by dilution of 16% methanol-free formaldehyde in PBS) at the flow rate of 600 µl/h, and incubation for 15 min at room temperature. The microchannels were then washed with PBS (flow rate = 600 µl/h, dispensed volume = 100 µl).

Afterwards, Rabbit Anti-Human von Willebrand Factor (1:125 v/v diluted in PBS) was perfused inside the channel (flow rate = 600 ul/h, dispensed volume = 100 ul), and the device was incubated for 30 min at room temperature. Following the PBS washing of the channel, Alexa 488–labeled goat anti-rabbit immunoglobulin G (1:250 v/v diluted in PBS) was used for indirect immunofluorescence staining of the secreted VWF (flow rate = 600 ul/h, dispensed volume = 100 ul). After half an hour incubation, the device was washed with PBS. Furthermore, Hoechst334 (1:1000 diluted in PBS) was perfused and incubated for 15 min to stain the cells' nuclei. Finally, the microchannels were washed with PBS (flow rate = 600 µl/h, dispensed volume = 100 µl).

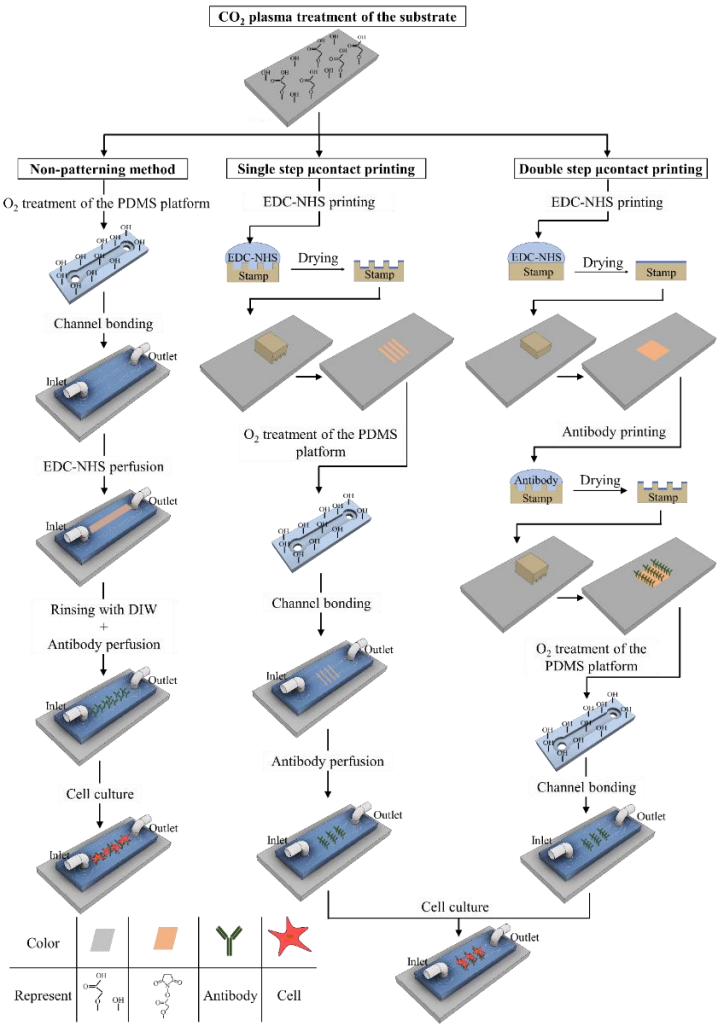

Figure 4-1. Schematic representation of microfluidic fabrication. CO_2 plasma treatment of the substrate induces both carboxylic groups and hydroxyl groups onto the glass slide surface. In the Non-patterning method, the PDMS platform is O_2 plasma treated to induce covalent bond formation on the substrate. The channel is activated with EDC-NHS and rinsed with DIW. Afterwards, the antibody is covalently immobilized onto the activated carboxylic groups to functionalize the surface for cell adherence. In the Single step µcontact printing method, EDC-NHS is micro-contact printed onto the CO_2 treated substrate to locally functionalize the surface. Then, the channel is bonded, and the antibody is perfused through the channel in order to bind with the activated areas and induce micro patterns of the antibody. In the Double step µcontact printing method, first EDC-NHS is printed on the surface using a flat stamp to activate the CO_2 group on a certain region. Then, the desired antibody is micro-contact printed onto the activated region, and then the channel is bonded. Both microcontact printing methods allow for micro patterning of cells inside the channels.

4.4 Results and Discussion

4.4.1 Characterization of CO_2 Plasma Treated Surfaces

Wide-scan and high resolution XPS (HR-XPS) tests were conducted on the CO_2 plasma treated glass slides to demonstrate the presence of carboxylic and hydroxyl groups on the surface following plasma activation. The wide-scan spectra of the CO_2 plasma treated glass slides are shown in Figure 4-2 (a) at different exposure times. CO_2 plasma treatment led to the formation of a peak at ~680 eV attributed to fluorine and an increase in the O1s and O KLL peaks at ~530 eV and ~980 eV, respectively. The appearance of a fluorine peak after plasma activation could be a result of the physical or chemical absorption of residues remaining after the hydrofluoric acid cleansing treatment of glass substrates[61,62]. The intensity variation of O1s peak is plotted in Figure 4-2 (b) as a function of plasma treatment time. This peak is mainly composed of $Si(-O)_2$, $Si(-OH)_x$ and $Si(-O)_4$ groups at 531.9, 531.1 and 532.9 eV, respectively [62]. According to Figure 4-2 (b), CO_2 plasma treatment for 2 min to 5 min induced the maximum amount of hydroxylation. Moreover, 5 min CO_2 plasma activation gives smaller whiskers (*i.e.* highest and lowest observations), indicating higher uniformity in the distribution of hydroxyl groups over the surface. In 10 min, however, the amount of hydroxyl groups deteriorated. This may be due to the over exposure time, and consequent etching of the pre-existing hydroxyls.

HR-XPS results in Figure 4-2 (c) and (d) illustrate different carbon bonds created on the CO_2 plasma activated substrate. The O–C=O bond could be detected at a binding energy of 288.7 eV. The other peaks at binding energies of 286 eV and 284.8 eV are attributed to C=O, and C–C / C–O, respectively [63]. Figure 4-2 (d) depicts an increase in the O–C=O bond area percentage, which confirms the presence of CO_2-plasma induced groups after 2 minutes treatment. No significant variation in the amount of CO_2 bonds was observed at higher plasma treatment times. Therefore, 5 min CO_2 plasma treatment time was selected as the optimum time to achieve a robust bond with PDMS, while inducing adequate amount of carboxylic groups for further activation with EDC-NHS. It is worth mentioning that the XPS measurements were performed 1-2 days after the CO_2 plasma treatment. This shows the stability of carboxylic groups on the glass substrates within a couple of days.

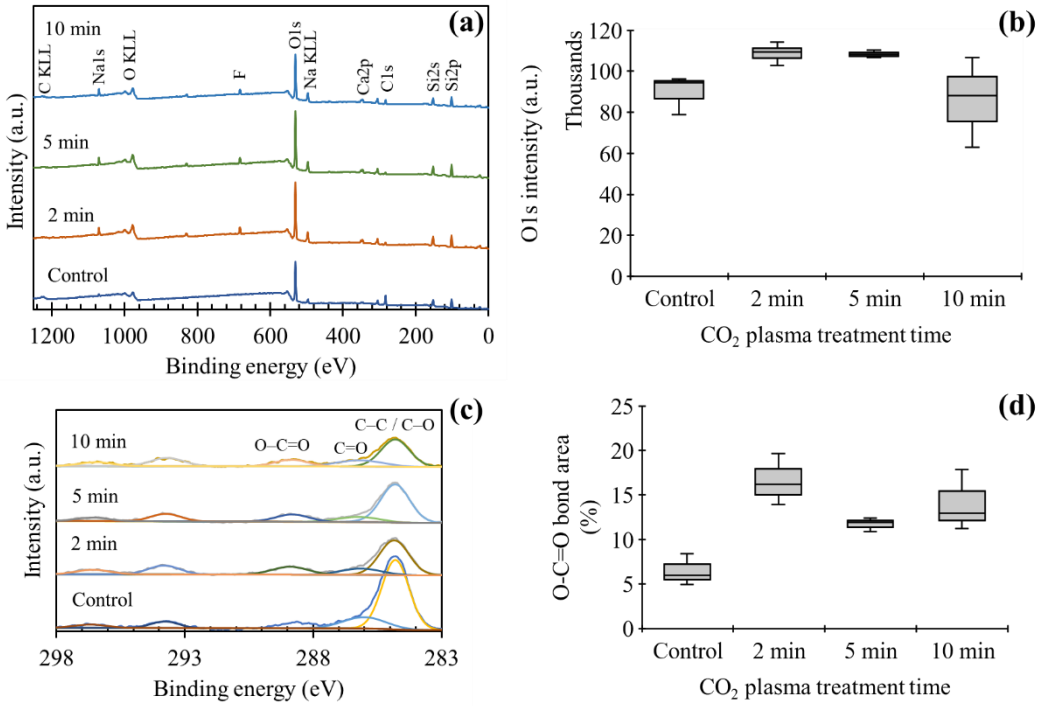

Figure 4-2. XPS spectra of CO_2 plasma treated glass slides; (a) Wide-scan spectra of CO_2 treated glass slides for 2 min, 5 min, and 10 min. The control shows the XPS spectrum of a plain glass slide without any treatment. (b) Box and whisker plot of O1s peak intensity in different CO_2 plasma treatment times. At 2 and 5 min, the maximum amounts of hydroxyl groups are created during the plasma treatment. (c) High-resolution XPS spectra of CO_2 treated samples at various times of treatment. (d) Carboxylic group bond area percentage vs CO_2 plasma treatment time showing the formation of CO_2 groups at 2 min.

4.4.2 Biofunctionalization of CO_2 Plasma Treated Microfluidic Devices

Following the CO_2 plasma activation of the glass substrate, an oxygen treated PDMS platform containing the microchannel cavity was brought together with the glass substrate. This formed an irreversible bond due to the covalent interactions between silanol groups of the PDMS surface and those of the CO_2 treated glass substrate. Afterwards, it was possible to separately activate the remaining carboxylic groups on

the microchannel surface via perfusion of EDC-NHS before applying the biomolecule of choice. Therefore, in contrast to conventional immobilization of bio-species where the biomolecule is mixed with carbodiimide compounds or silane coupling agents, there was no need to prepare a mixture that could cause aggregation and considerable loss of biomolecules caused by self-crosslinking between amino and carboxylic groups of the proteins. In order to investigate the effect of CO_2 treated bio-functional microchannels on immobilization of the biomolecules, BSA-FITC was applied to measure the fluorescence intensity of the channel. In Figure 4-3 (a), a CO_2 plasma treatment method was used to bond the channel, which then underwent subsequent activation with EDC-NHS. In Figure 4-3 (b), conventional O_2 plasma treatment was performed on both the glass slide and PDMS part to bond the channel. BSA-FITC was injected in both channels and was then heavily washed with TBST after 1.5 hour incubation time. The fluorescence intensities of both channels and a plain glass slide are compared in Figure 4-3 (c). As seen, there is a significant difference between the fluorescence intensities of the CO_2 treatment and O_2 treatment techniques. Perfusion of BSA-FITC in the O_2 treated channel only led to a small adsorption of the protein, which likely occurred due to the highly adhesive nature of BSA against glass. However, in the channel with the activated carboxylic groups, amino moieties of BSA could crosslink to the functional groups on the channel, thus creating stable covalent bonds which prevented protein detachment from the surface during the washing period. It should be mentioned that

there was no sign of leakage on the CO_2 plasma treated channels during the harsh washing steps. Since during the CO_2 plasma treatment, sufficient amount of hydroxyl groups is created on the glass substrate, the bonding strength of O_2 plasma treated PDMS to the CO_2 plasma treated glass slides is high enough to withstand the reasonable range of flow rates, similar to the conventional O_2 plasma treatment strategy.

4.4.3 Patterning of CO_2 Plasma Treated Microfluidic Devices Using Microcontact Printing

We used two different methods to microcontact print CO_2 plasma treated devices as following:

4.4.3.1 Single-step Patterning via Microcontact Printing EDC-NHS:

In the single-step microcontact printing approach, EDC-NHS was printed on a CO_2 plasma treated glass slide to locally activate the carboxylic groups on the surface using two different PDMS stamps with stripes and triangle patterns. After forming the microfluidic device, Alexa Fluor® 488-conjugated CD34 antibody was perfused through the entire channel. Figure 4-4 (a) exhibits the attachment of CD34 on the distinct EDC-NHS activated areas. Since there was no specificity between EDC-NHS microprinted regions and the antibody of choice, it could be concluded that the antibody was covalently bonded to the NHS esters on the pattern areas through its primary amines. Conventional microcontact printing methods create physical attachment

between biomolecules and substrates while here we achieve covalent patterning by printing EDC-NHS. One issue with the single step microcontact printing is the background fluorescence intensity caused by non-specific adhesion of the antibody on the areas between the patterns. Since the antibody is perfused inside the whole channel, it is likely that it sticks to the unpatterned areas as well.

4.4.3.2 Double-step Patterning via Microcontact Printing EDC-NHS:

In order to prevent the non-specific attachment of the antibody, we developed a double step microcontact printing method. In this method, a certain area of the CO_2 plasma treated glass slide was first activated by contact printing of EDC-NHS using a flat stamp without a pattern. Afterwards, the antibody was microcontact printed with a patterned stamp onto the EDC-NHS activated area to form covalent antibody patterns. Employing this technique, Alexa Fluor® 488-conjugated CD34 antibody was patterned onto the CO_2 treated glass slide (Figure 4-4 (b)). As the microchannel is bonded after printing the antibody, a faint trace of the pattern could be seen beyond the channel boundary underneath the PDMS platform bonded to the glass substrate. However, it was determined that this did not have an impact on channel bonding. This finding could be due to the fact that only a very small yield of antibody (most probably a monolayer) was achieved by the microcontact printing method [64], and consequently the patterned

antibody does not shield all the hydroxyl groups available for covalent bonding to PDMS.

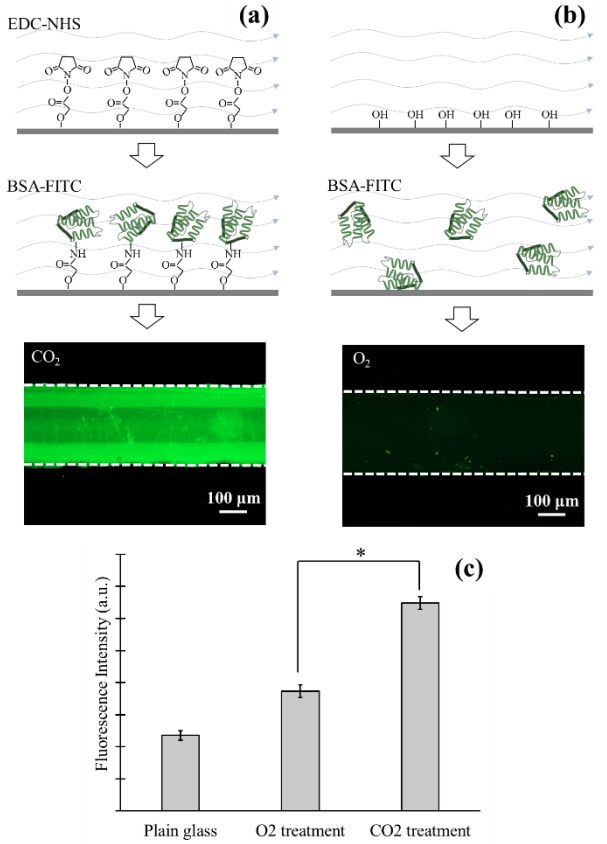

Figure 4-3. Immobilization of BSA-FITC on a bio-functional channel compared to a normal channel; (a) CO_2 plasma treated channel was first activated via perfusion of EDC-NHS through the channel. Next, BSA-FITC was perfused in the channel resulting in covalent bonding of the protein to the activated carboxylic groups through its amino moieties. (b) Microfluidic channel bonding was conducted through typical O_2 plasma treatment technique. After the perfusion of BSA-FITC, only a small portion of the proteins were non-specifically attached to the channel surface. Dashed lines represent the channel boundaries (c) Comparison between the fluorescence intensities of a plain glass slide, and immobilized BSA-FITC in the microchannel using typical O_2 treatment and the new CO_2 treatment techniques. Data are shown as mean ± SD. There is a significant difference in the BSA-FITC fluorescence intensities with *P ≪ 0.0001.

Figure 4-4 (c) assesses the bio-functionality of the CD34 antibody micropatterned via the double step printing method. In this experiment, after microcontact printing CD34 and bonding the channel, PEG was used to block the unpatterned regions of the channel. Next, Alexa Fluor® 594-conjugated Goat Anti-Mouse IgG (as a secondary antibody with affinity to CD34) was perfused in the channel. The presence of the red fluorescent antibody at the CD34 stripes confirms that the new microcontact printing method does not impose an adverse influence on the bio-functionality of the antibody. Furthermore, there was no evidence that the secondary antibody penetrated underneath PDMS or bound to any CD34 patterns outside of the channel, which indicates the PDMS platform was well bonded to the substrate after the double step microcontact printing.

4.4.4 Cell Culture and Patterning

The efficacy of the developed bio-functionalization methods was examined in microfluidic cell culture systems. In the first trial, the non-patterning method was utilized to associate the surface of microchannels with fibronectin glycoprotein. Similar to the experiment that utilized BSA-FITC protein, EDC-NHS was used to activate the CO_2 plasma treated channels. The channels were then lined with fibronectin via perfusion of the protein through the channel and by consequent crosslinking with the NHS esters. Furthermore, the channels were blocked with PLL-PEG, and fluorescently labelled human endothelial cells (RFP-HUVEC) were flowed through the channels. The

results are illustrated in Figure 4-5 and compared to devices made by conventional oxygen plasma treatment, and then fibronectin perfusion. Using the conventional O_2 treatment method (Figure 4-5 a), no trace of RFP-HUVECs was observed inside the channel. This finding indicates fibronectin was completely removed from the channel during rinsing with TBST buffer, due to the lack of robust covalent bonding on the surface. Figure 4-5 (a) also implies that PEG, as expected, had effectively blocked the channel surface since there were no non-specifically attached cells in the channel. However, CO_2 plasma treatment of the substrate and activation with EDC-NHS beforehand resulted in a greater amount of covalently bonded fibronectin on the surface. When the new technique was used, RFP-HUVECs adhered to the fibronectin matrix inside the channel (Figure 4-5 (b)). Higher magnification images of the cell morphologies on day 1 are provided in Figure 4-5 (g) indicating that the cells were well adhered to and spread on the fibronectin layer. As the incubation time extended to 2 days, the cells grew inside the devices and become fully confluent. Importantly, at each new incubation interval, the microchannels were washed to eliminate any floating dead cells, and new EBM^{TM}-2 was perfused in the channel.

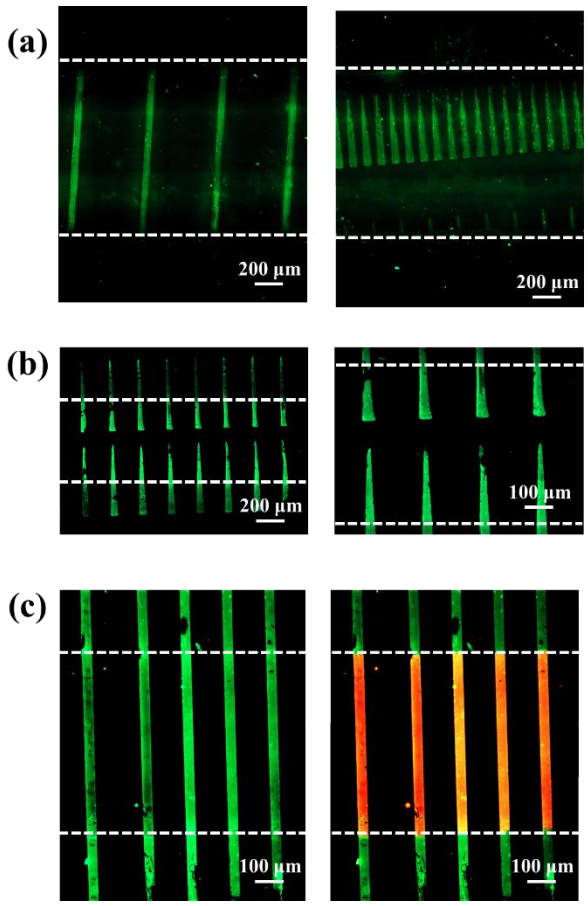

Figure 4-4. Micropatterns of CD34 inside the microfluidic channels; (a) When the single step microcontact printing method was used to pattern the antibody. The background fluorescence shows nonspecific attachment of the antibody. (b) When the double step microcontact printing method was employed. There is no background intensity between the patterns. (c) CD34 (green) printed using double the step method, and anti-CD34 patterns (red) perfused inside the device showing functionality of CD34. Dash lines represent the channel's boundaries.

In order to show the functionality of the cultured RFP-HUVECs, we performed VWF stimulation assay on the cells. This was done by perfusion of histamine through the channel for 10 min and immediate fixing with 4% methanol-free formalin. Rabbit Anti-Human VWF and Alexa 488–labeled goat anti-rabbit IgG were used to indirectly stain

the secreted VWF through an immunofluorescence labeling technique. In Figure 4-5 (d and e), ultra-large VWF (ULVWF) multimers are shown as green fluorescent strings. The ULVWFs were secreted from the Weibel-Palade (WP) bodies of the endothelial cells and expanded along the flow direction. This demonstrates the good response of the cells to the inflammatory mediator of histamine. Moreover, Figure 4-5 (d and e) shows the distribution of the rod-shaped WP bodies with green color along the endothelial cells. The stimulated RFP-HUVECs were stained with Hoechst 33342 (Figure 4-5 (f, h and i)) to show the nuclei. The cell counting results are plotted in Figure 4-5 (j). There is a significant difference between the number of cells per mm^2 in the O_2 treated microfluidic devices and CO_2 treated ones. Furthermore, the significant difference in the number of cells present after 2 days compared to 1 day indicates appropriate cell growth inside the device.

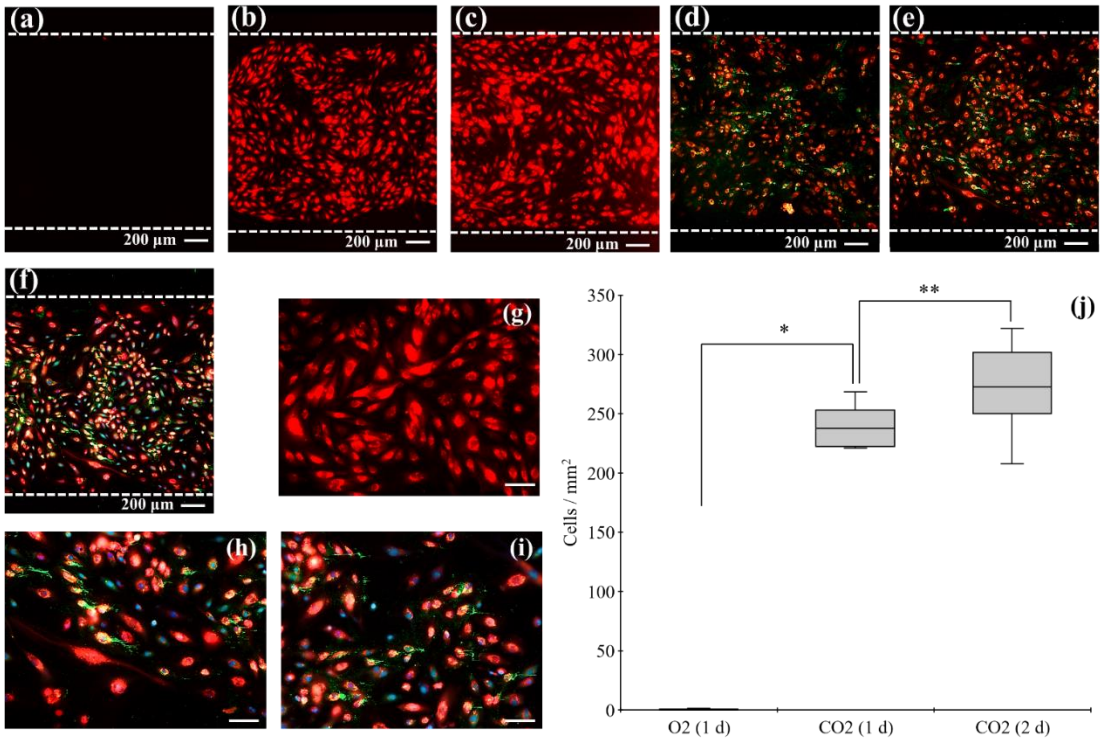

Figure 4-5. Cell culture results on the fibronectin lined channel which was blocked with PEG; (a) the microfluidic channel was bonded with the typical O_2 plasma treatment method. No cell was attached to the surface due to the complete removal of fibronectin in the washing step. (b) CO_2 plasma treatment with the non-patterning technique was used to coat the channel with fibronectin through covalent bonding with activated carboxylic groups. The image shows the adhered cells after 1 day of incubation. (c) The cell population result after 2 days of incubation. (d) and (e) The cells were stimulated with histamine to secrete VWF and then fixed and indirectly stained using anti-VWF and Alexa 488–labeled anti-rabbit IgG. The stretched bodies with green fluorescent color indicate the ULVWF strings. The green rod-shaped bodies show WP distribution in the cells. (f) Hoechst 33342 was used to stain the cells' nuclei. Blue color shows the nucleus of the cell. Dashed lines represent the channel boundaries. (g) Cells morphologies in day 1 with higher magnification. (h) and (i) Stained cells in day 2 with higher magnification showing the ULVF strings. (j) Cell counting results corresponding to different incubation time periods. There is a significant difference in the number of cells in O_2 treatment vs CO_2 treatment, as well as 1-day incubation time vs 2-day incubation time with *$P < 0.0001$ and **$P < 0.05$, respectively.

We then examined the efficiency of the new microcontact printing method for cell culture studies and compared the results to the conventional microcontact printing method (Figure 4-6). As shown in Figure 4-6 (a), the conventional microcontact printing method was used to print fibronectin on an O_2 plasma treated glass slide. A flat PDMS stamp was used to print the protein in these experiments, in order to target the number of live cells achieved for each protocol. Subsequently, the channel was bonded with an O_2 treated PDMS platform and blocked with PEG to prevent non-specific attachment of the cells. The fluorescent images after 1-day incubation period with RFP-HUVECs illustrate that only a few cells adhered to and spread within the channel.

In Figure 4-6 (b), the double-step microcontact printing method was used to coat the channels with fibronectin. After CO_2 treatment of the substrate, EDC-NHS was printed to activate the carboxylic groups, and then fibronectin was printed to the same area. The channels were bonded on the printed area such that only half of the channels were coated with fibronectin. The region inside the dashed box in the fluorescent image in Figure 4-6 (b), shows the fibronectin coated area indicating significantly greater number of cells attached to the fibronectin printed area compared to the other half of the channel. In Figure 4-6 (c) and (d), the dense population of the cells within the fibronectin printed area are shown. Taking into consideration that this large mass of adhered cells could be achieved after only 1 day of incubation, it is evident that the new contact printing

method has a superior capacity for cell culture in microfluidic devices. Compared to the conventional microcontact printing method, this new technique provides a higher volume of fibronectin transferred to the substrate from the stamp, causing increased cell adhesion and growth inside the channels. Moreover, as the protein is covalently bonded to the surface, it is unlikely to be removed by the washing buffer. As a result, the yield of printed fibronectin is significantly greater when compared to the normal printing method.

The double step microcontact printing technique could also be utilized to pattern cells inside microfluidic channels. In this case, fluor® 488-conjugated CD34 antibody was first patterned inside the channels followed by perfusion of PLL-PEG to block non-specific binding. Figure 4-6 (f) and (g) illustrate the alignment of GFP-NIH 3T3 with the CD34 patterns after a 1 day incubation period. It can be seen that the unpatterned regions are mostly occupied with dead cells and round shaped cells with no junction, whereas on the micropatterns of CD34, the cells tend to stretch along the triangles. These results support the bio-functionality of the microcontact printed antibody in terms of cell capturing. In Figure 4-6 (e), fibronectin was microcontact printed instead of CD34 by the double step printing method, using the same stamp containing triangle patterns. Then, the channel was blocked with PLL-PEG, and RFP-HUVECs were seeded. As our employed fibronectin is not fluorescently labeled, the initial patterns of

fibronectin are not visible in Figure 4-6 (e). Nevertheless, the cells patterned across the channel and perpendicular to the channel direction can be clearly distinguished.

In Figure 4-6 (h), the cell count results of the conventional microcontact printing and the new double-step microcontact printing are plotted. The cell counts of the channels functionalized via non-pattering method after 2 days incubation time was also added to the same plot for better comparison. As seen, there is a significant difference between the number of cells achieved via the new contact printing method versus the conventional method. Furthermore, the new double step printing technique had a greater number of cells adhered to the channel compared to non-patterning technique even after 2 days of incubation. Thus, the new contact printing method allows for achieving full confluency after only 1 day, which is dramatically faster and more efficient than the previously mentioned methods.

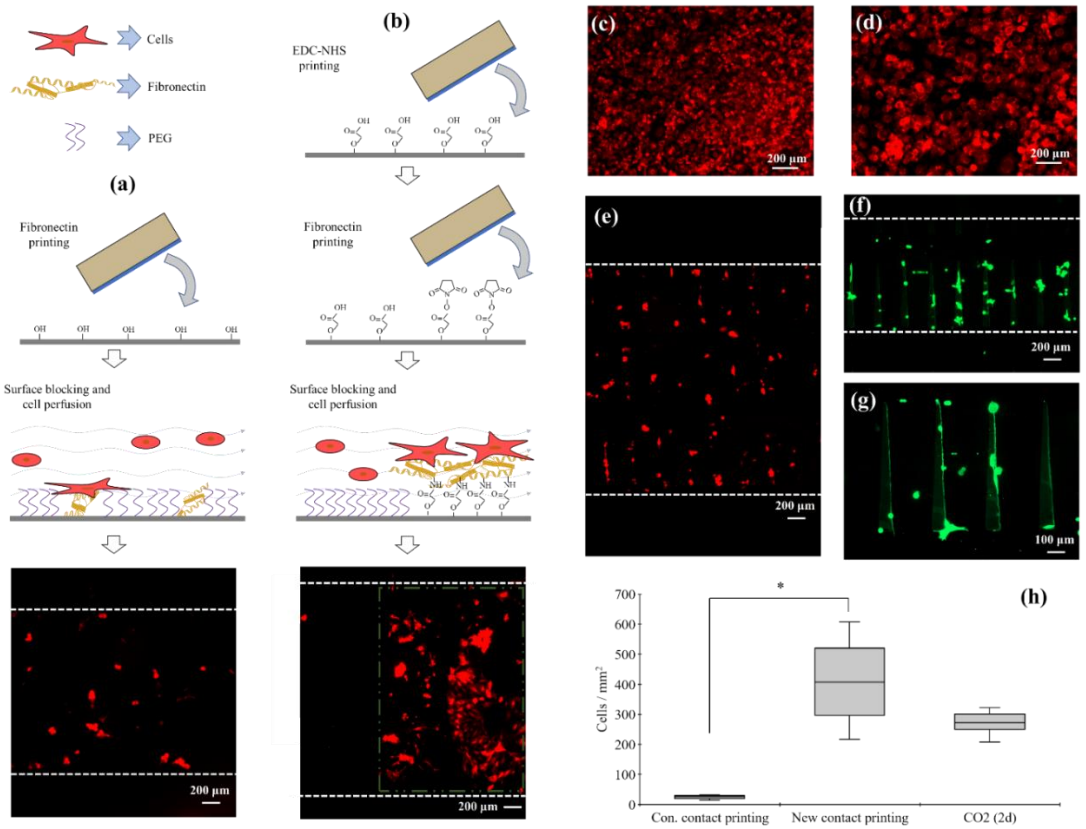

Figure 4-6. Cell culture results of the double step microcontact printing technique; (a) Conventional microcontact printing with a flat stamp was used to coat the channel with fibronectin. Only a small number of cells were attached to the printed area. Schematics represent the process done to functionalize the channel. The channel was washed and blocked with PEG prior to cell culture perfusion (b) Double step microcontact printing technique was used to print fibronectin on the right half of the channel using flat stamps. Dashed box indicates the printed area. (c) and (d) cell morphology and population within the patterned area using double step microcontact printing method. (e) RFP-HUVECs micropatterned on the CD34 printed via the double step microcontact printing method. Fibronectin was patterned using a similar stamp to the one which used for CD34 patterning. The cells are aligned along the fibronectin patterns perpendicular to the channel direction. (f) and (g) GFP-NIH 3T3 cells micropatterned on the CD34 printed via the double step microcontact printing method. The results show the bio-functionality of the CD34 patterns. (h) Cell count results of conventional microcontact printing method in (a), new double step microcontact printing method in (b), as well as non-patterning method with CO_2 plasma treatment after 2 days of incubation. There is significant cell count difference between the new contact printing method and the conventional one with $*P < 0.05$.

4.5 Conclusions

Plasma modification of glass substrates with CO_2 gas exposure induced hydroxyl and carboxylic groups onto the surfaces. The hydroxyl groups enabled the substrate to perfectly bond with an oxygen plasma treated PDMS, and the fabricated microchannel did not show any sign of leakage. It was found that the carboxylic groups on the channel surface could easily be activated through perfusion of EDC-NHS inside the channel. Single step microcontact printing results showed the possibility to locally activate the carboxylic groups of the surface through EDC-NHS microcontact printing. This procedure resulted in covalent patterning of the antibody which is not achievable via conventional microcontact printing. Furthermore, double step microcontact printing was introduced as an alternative way by which the antibody can be microprinted onto an EDC-NHS activated region. The bio-functionality of the printed antibody was confirmed via specific attachment of anti IgG antibody as a secondary antibody with affinity to CD34 patterns. An additional cell culture study demonstrated a high yield of fibronectin immobilized inside the channel which resulted in a greater number of cells adhered on the channel surface compared to the typical immobilization techniques. With double-step microcontact printing method, full confluency inside the microchannels was achieved only after 1 day of incubation.

4.6 Future Trend

The finding of this work suggests that the high efficiency of this novel method can be beneficial for use in different biomedical applications. For instance, in cell studies and organs-on-chips technology, one could apply the introduced protocol to prepare a microchannel with high affinity for cell attachment. The new strategy facilitates the biofunctionalization process of the microfluidic channels, and enables achieving full confluency of cells inside the microfluidic channel in a very short period of time which is a very important leverage in organs on a chip systems. Moreover, regarding the applications of microfluidics in the biosensor industries, the new protocol provides the capability for covalently micropatterning the inner surface of the microfluidic channels with the antibodies. The final product would be very robust for long term usage and increase the efficiency of different bioassays in microfluidic devices. Also, as the procedure is relatively simple and does not need silanization or other wet chemistries, it allows for cost-effective high-throughput production of the biosensors.

4.7 Acknowledgements

This work was supported by Natural Sciences and Engineering Research Council of Canada (NSERC) Discovery Grant, Ontario Early Researcher Award Grant and McMaster start-up funds to T.F.D.

4.8 References

1 Y.-X. Huang, C.-L. He, P. Wang, Y.-T. Pan, W.-W. Tuo and C.-C. Yao, *Biosens. Bioelectron.*, 2018, **101**, 66–74.

2 F. Yu, N. D. Selva Kumar, D. Choudhury, L. C. Foo and S. H. Ng, *Drug Discov. Today*, 2018, **23**, 815–829.

3 A. Bein, W. Shin, S. Jalili-Firoozinezhad, M. H. Park, A. Sontheimer-Phelps, A. Tovaglieri, A. Chalkiadaki, H. J. Kim and D. E. Ingber, *Cell. Mol. Gastroenterol. Hepatol.*, 2018, **5**, 659–668.

4 G. M. Whitesides, *Nature*, 2006.

5 P. Abgrall and A.-M. Gué, *J. Micromech. Microeng*, 2007, **17**, 15–49.

6 Z. Wang, R. Samanipour, K.-I. Koo and K. Kim, *Sensors Mater.*, 2015, **27**, 487–506.

7 K. Ronaldson-Bouchard and G. Vunjak-Novakovic, *Cell Stem Cell*, 2018, **22**, 310–324.

8 U. Hassan, T. Ghonge, B. Reddy Jr., M. Patel, M. Rappleye, I. Taneja, A. Tanna, R. Healey, N. Manusry, Z. Price, T. Jensen, J. Berger, A. Hasnain, E. Flaugher, S. Liu, B. Davis, J. Kumar, K. White and R. Bashir, *Nat. Commun.*, 2017, **8**, 15949.

9 D. Erickson and D. Li, *Anal. Chim. Acta*, 2004, **507**, 11–26.

10 E. K. Sackmann, A. L. Fulton and D. J. Beebe, *Nature*, 2014, 507, 181–189.

11 G. ; Du, Q. Fang, J. M. J. Den Toonder, A. C. Acta, G. Du, Q. Fang and J. M. J. Den Toonder, , DOI:10.1016/j.aca.2015.11.023.

12 S. Musah, A. Mammoto, T. C. Ferrante, S. S. F. Jeanty, M. Hirano-Kobayashi, T. Mammoto, K. Roberts, S. Chung, R. Novak, M. Ingram, T. Fatanat-Didar, S. Koshy, J. C. Weaver, G. M. Church and D. E. Ingber, *Nat. Biomed. Eng.*, 2017, **1**, 69.

13 T. F. Didar, K. Li, T. Veres and M. Tabrizian, *Biomaterials*, 2013, **34**, 5588–5593.

14 M. Villegas, Z. Cetinic, A. Shakeri and T. F. Didar, *Anal. Chim. Acta*, 2018, **1000**, 248–255.

15 N. Bhattacharjee, A. Urrios, S. Kang and A. Folch, *Lab Chip*, , DOI:10.1039/c6lc00163g.

16 J. C. McDonald, D. C. Duffy, J. R. Anderson, D. T. Chiu, H. Wu, O. J. A. Schueller and G. M. Whitesides, *Electrophoresis*, 2000, **21**, 27–40.

17 S. Bhattacharya, A. Datta, J. M. Berg and S. Gangopadhyay, *J. MICROELECTROMECHANICAL Syst.*, , DOI:10.1109/JMEMS.2005.844746.

18 J. Zhou, A. V. Ellis and N. H. Voelcker, *Electrophoresis*, 2010, **31**, 2–16.

19 E. M. Liston, L. Martinu and M. R. Wertheimer, *J. Adhes. Sci. Technol.*, 1993, **7**, 1091–1127.

20 C. W. Beh, W. Zhou and T.-H. Wang, *Lab Chip*, 2012, **12**, 4120–4127.

21 S. H. Tan, N.-T. Nguyen, Y. C. Chua and T. G. Kang, *Biomicrofluidics*, 2010, **4**, 032204.

22 J. Wu, Z. He, Q. Chen and J.-M. Lin, *TrAC Trends Anal. Chem.*, 2016, **80**, 213–231.

23 J. M. Goddard and D. Erickson, *Anal. Bioanal. Chem.*, 2009, **394**, 469–479.

24 J. Pivetal, F. M. Pereira, A. I. Barbosa, A. P. Castanheira, N. M. Reis and A. D. Edwards, *Analyst*, 2017, **142**, 959–968.

25 T. F. Didar, M. J. Cartwright, M. Rottman, A. R. Graveline, N. Gamini, A. L. Watters, D. C. Leslie, T. Mammoto, M. J. Rodas, J. H. Kang, A. Waterhouse, B. T. Seiler, P. Lombardo, E. I. Qendro, M. Super and D. E. Ingber, *Biomaterials*, 2015, **67**, 382–392.

26 A. Siddique, T. Meckel, R. W. Stark and S. Narayan, *Colloids Surfaces B Biointerfaces*, 2017, **150**, 456–464.

27 C. Geng, C. Li, W. Li, W. Yan and J. Li, *J. Micromechanics Microengineering Pap.*, 2018, **28**, 115011.

28 A. Shakeri, S. Rahmani, S. M. Imani, M. Osborne, H. Yousefi and T. F. Didar, in *Woodhead Publishing Series in Electronic and Optical Materials*, eds. K. Pal, H.-B. Kraatz, A. Khasnobish, S. Bag, I. Banerjee and U. B. T.-B. and M. D. Kuruganti, Woodhead Publishing, 2019, pp. 635–699.

29 K. H. K. Wong, A. E. Jensen, V. Thapar, D. Ting, M. Toner, S. L. Stott and P. T. Hammond, *J. Am. Chem. Soc.*, 2017, **139**, 2741–2749.

30 S. Mccormick, Z. Tong, A. Ivask, M. Morozesk, N. H. Voelcker, E. Lombi and C. Priest, *Biofabrication*, 2018, **10**, 014101.

31 A. Khodayari Bavil and J. Kim, *Analyst*, 2018, **143**, 3335–3342.

32 I. R. Ausri, E. M. Feygin, C. Q. Cheng, Y. Wang, Z. Y. (William) Lin and X. (Shirley) Tang, *MRS Commun.*, 2018, **8**, 474–479.

33 Z. L. Zhang, C. Crozatier, M. Le Berre and Y. Chen, *Microelectron. Eng.*, 2005, **78**–**79**, 556–562.

34 H. Handa, S. Gurczynski, M. P. Jackson, G. Auner, J. Walker and G. Mao, *Surf. Sci.*, 2008, **602**, 1392–1400.

35 A. Shakeri, N. Sun, M. Badv and T. F. Didar, *Biomicrofluidics*, 2017, **11**, 044111.

36 M. Badv, S. M. Imani, J. I. Weitz and T. F. Didar, *ACS Nano*, 2018, **12**, 10890−10902.

37 R. Khnouf, D. Karasneh and B. A. Albiss, *Electrophoresis*, 2016, **37**, 529–535.

38 X. Guan, H. J. Zhang, Y. N. Bi, L. Zhang and D. L. Hao, *Biomed. Microdevices*, 2010, **12**, 683–691.

39 J.-P. Chen and J.-Y. Chen, *J. Mol. Catal. B Enzym.*, 1998, **5**, 483–490.

40 M. J. B. Wissink, R. Beernink, J. S. Pieper, A. A. Poot, G. H. M. Engbers, T. Beugeling, W. G. van Aken and J. Feijen, *Biomaterials*, 2001, **22**, 151–163.

41 S. Sam, L. Touahir, J. S. Andresa, P. Allongue, J.-N. Chazalviel, A. C. Gouget-Laemmel, C. Henry De Villeneuve, A. Moraillon, F. Ozanam, N. Gabouze and S. Djebbar, *Langmuir*, 2010, **26**, 809–814.

42 M. J. E. Fischer, eds. N. J. Mol and M. J. E. Fischer, Humana Press, Totowa, NJ, 2010, pp. 55–73.

43 H. Yousefi, H.-M. Su, M. Ali, C. D. M. Filipe and F. D. Tohid, *Adv. Mater. Interfaces*, 2018, **5**, 1800659.

44 A. Shakeri, D. Yip, M. Badv, S. M. Imani, M. Sanjari and T. F. Didar, *Materials (Basel).*, 2018, **11**, 1003.

45 R. E. Saunders and B. Derby, *Int. Mater. Rev.*, 2014, **59**, 430–448.

46 C. Tu, B. Huang, J. Zhou, Y. Liang, J. Tian, L. Ji, X. Liang and X. Ye, *Micromachines*, 2017, **8**, 1–15.

47 Z. Tong, A. Ivask, K. Guo, S. Mccormick, E. Lombi, C. Priest and N. H. Voelcker, *Lab Chip*, 2017, **17**, 501–510.

48 H. Yousefi, M. M. Ali, H.-M. Su, C. D. M. Filipe and T. F. Didar, *ACS Nano*, 2018, **12**, 3287–3294.

49 R. Majumdar and I. Paprotny, *J. Micro Electro Mech. Syst.*, 2017, **26**, 671–678.

50 R. Majumdar, V. Foroutan and I. Paprotny, in *in Proc. 28th IEEE Int. Conf. Micro Electro Mech. Syst. (MEMS)*, 2015, pp. 296–299.

51 S. Hussain, S. Ward, O. Mahdavipour, R. Majumdar and I. Paprotny, in *Proceedings of SPIE - The International Society for Optical Engineering*, 2015, pp. 94940F–12.

52 S. Ward, V. Foroutan, R. Majumdar, O. Mahdavipour, S. A. Hussain and I. Paprotny, *IEEE Trans. Nanobioscience*, 2015, **14**, 323–331.

53 P. Shi, S. Nedelec, H. Wichterle and L. C. Kam, *Lab Chip*, 2010, **10**, 1005.

54 R. Lovchik, C. Von Arx, A. Viviani and E. Delamarche, *Anal. Bioanal. Chem.*, 2008, **390**, 801–808.

55 L. Wong, J. D. Pegan, B. Gabela-zuniga, M. Khine and K. E. Mccloskey, *Biofabrication*, 2017, **9**, 021001.

56 D. J. Graber, T. J. Zieziulewicz, D. A. Lawrence, W. Shain and J. N. Turner, *Langmuir*, 2003, **19**, 5431–5434.

57 T. Fatanat Didar and M. Tabrizian, *Lab Chip*, 2012, **12**, 4363–71.

58 T. F. Didar, K. Bowey, G. Almazan and M. Tabrizian, *Adv. Healthc. Mater.*, 2014, **3**, 253–260.

59 S. Sathish, S. G. Ricoult, K. Toda-Peters and A. Q. Shen, *Analyst*, 2017, **142**, 1772–1781.

60 T. F. Didar, A. M. Foudeh and M. Tabrizian, *Anal. Chem.*, 2012, **84**, 1012–1018.

61 W. Kern, *ECS J. Solid State Sci. Technol.*, 1990, **137**, 1887–1892.

62 A. U. Alam, M. M. R. Howlader and M. J. Deen, *ECS J. Solid State Sci. Technol.*, 2013, **2**, 515–523.

63 L.-X. Chen, J.-N. Zheng, A.-J. Wang, L.-J. Wu, J.-R. Chen and J.-J. Feng, *Analyst*, 2015, **140**, 3183–3192.

64 C. D. James, R. C. Davis, L. Kam, H. G. Craighead, M. Isaacson, J. N. Turner and W. Shain, *Langmuir*, 1998, **14**, 741–744.

Chapter 5: Antibody Micropatterned Lubricant-infused Biosensors Enable Sub-picogram Immunofluorescence Detection of Interleukin 6 In Human Whole Plasma

Amid Shakeri, Noor Abu Jarad, Jeff Terryberry, Shadman Khan, Ashlyn Leung, Simeng Chen, Tohid F Didar*

The chapter has been reviewed in Small

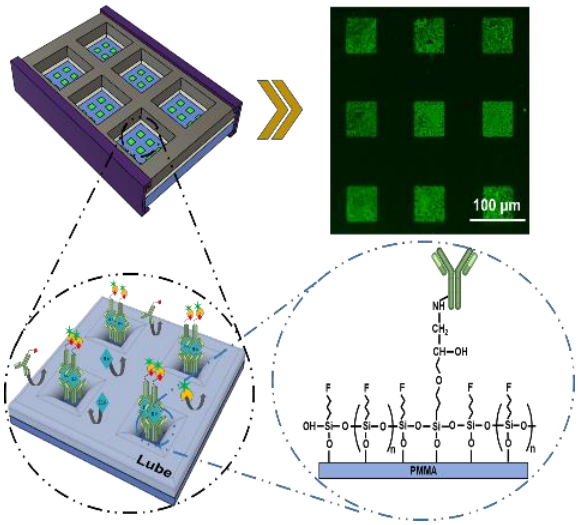

5.1 Abstract

Recent studies have shown a correlation between elevated interleukin 6 (IL-6) concentrations and the risk of respiratory failure in COVID-19 patients. Therefore, detection of IL-6 at low concentrations permits early diagnosis of worst-case outcome in viral respiratory infections. Here, a versatile bio-interface is presented that eliminates non-specific adhesion and thus enables immunofluorescence detection of IL-6 in whole human plasma or whole human blood during coagulation, down to a limit of detection of 0.5 pg mL^{-1}. The sensitivity of the developed lubricant-infused biosensor for immunofluorescence assays in detecting low molecular weight proteins such as IL-6 is facilitated by (i) producing a bioink in which the capture antibody is functionalized by an epoxy-based silane for covalent linkage to the fluorosilanized surface, and (ii) suppressing non-specific adhesion by patterning the developed bioink into a lubricant-infused coating. The developed biosensor addresses one of the major challenges for biosensing in complex fluids, namely non-specific adhesion, therefore paving the way for highly sensitive biosensing in complex fluids.

Keywords: lubricant-infused surfaces, biosensing in plasma, immunofluorescence assays, interleukin 6 detection, bioink

5.2 Introduction

Human interleukin-6 (IL-6) is a multifunctional, pro-inflammatory cytokine that has been found to be overexpressed in viral infections, inflammatory conditions and several cancer types such as lung, colorectal, breast, and prostate cancers [1–7] as well as in respiratory infections caused by Severe Acute Respiratory Syndrome Corona Virus 2 (SARS-CoV-2).[8–10] The level of expression in plasma typically reflects severity of the disease, where significantly elevated levels indicate aggressive tumor growth or viral load and poor prognosis in patients.[2,10] Additionally, IL-6 is an important anti-inflammatory cytokine that induces acute responses in chronic inflammatory pathologies. As such, there has been an increasing interest in the use of IL-6 as a biomarker for the diagnosis of early stages of viral infections, cancer, and chronic inflammation.[9–11] A practical IL-6 biosensor should provide a low limit of detection (LOD) ($\leq$5 pg mL^{-1}) and acceptable linear dynamic range (1pg mL^{-1} to 100 pg mL^{-1}) in complex fluids, in addition to accuracy, facile operation, and amenable to mass production.[11,12]

There are a large number of different IL-6 detection techniques that have been reported in the literature including electrochemical sensors,[13–22] surface plasmon resonance (SPR),[23–25] chemiluminescence immunoassay (CLIA),[26–29] and immunofluorescence assays (IFA),[30–33] Utilizing zero- and one-dimensional materials such as carbon

nanotubes (CNTs),[14,16] nanoparticles and nanowires,[13,19] as well as porous nanoparticles,[15] optical fibers,[32] and microfluidic platforms,[28] have enabled higher sensitivity in IL-6 detection and to date, electrochemical methods have proven to be the most promising candidate for detection of IL-6 at very low concentrations (0.33 pg mL^{-1} in buffer) with a wide linear dynamic range.[22] While reported IL-6 biosensors have demonstrated satisfactory LODs in buffer or processed serum, their performance in human whole plasma declines significantly, leading to higher LOD's and/or false positive results. In electrochemical sensors, for example, the non-specific attachment of biological entities in plasma or blood can interfere with the resistivity at the electrodes thereby deteriorating their sensitivity for detection of IL-6 at clinically relevant concentrations.[34] So far, the lowest theoretical LOD for IL-6 detection in plasma was reported by Sabaté del Río *et al.*.[13] This method utilized a complex system composed of 3D BSA nanocomposite, CNTs/Au-nanoparticles, and Au-nanowires and electrochemical detection to obtain an LOD of 23 pg mL^{-1} in human plasma, which exceeds the typical sensitivity requirements of $\leq$5 pg mL^{-1}.

Omniphobic lubricant-infused surfaces (LISs),[35] have aroused interest as anti-biofouling coatings in recent years due to their ability to repel bacteria, blood cells, proteins, as well as their non-wetting properties to different fluids.[36–39] This property is caused by a slippery or low surface tension interface between a monolayer of

lubricant, locked into a porous or rough surface and the biofluid or immiscible liquid to be repelled.[40] The omniphobic LIS technology has been employed for antibacterial applications, as well as medical implants and devices where thrombosis and infections could pose a threat;[41–44] however, they have not been implemented as blocking agents for biosensing and we hypothesize that the superior repellency offered by such slippery surfaces may prove to decrease LOD for IL-6 detection in complex fluids.

To verify our hypothesis, we chose an IFA as the sensing platform. IFA's typically fall behind electrochemical sensors in achieving low LOD in buffer and plasma, but they are simple, cost effective and more amenable for point of care diagnostics. Using bead or nanoparticle-based enzyme-linked immunosorbent assay IFA (ELISA-IFA), can enhance the LOD and sensitivity of IFAs for IL-6 detection in buffer, but adds more complexity, and increases the cost.[31–33] Two key aspects that can be modified in ELISA-IFA to further improve its performance and functionality are the proper immobilization of capture biomolecules and the use of optimal surface blocking agents to reduce the background noise often associated with fluorescence-based assays.[45–47] For immobilization of biorecognition elements, contact printing and non-contact printing strategies have been widely used to generate microarrays of biorecognition elements (*e.g.* antibodies) using desired chemical linkers (*e.g.* amine or carboxyl groups).[48–50] The microarrays shape, diameter, thickness, homogeneity, and binding

mechanism are important attributes to evaluate the efficacy of different microarray biosensing surface strategies.[51] Although several conventional blocking agents are widely used to prevent non-specific binding, they still result in defects leading to non-specific attachment and biofouling, and reduce the sensitivity of assays by interfering with immunochemical reactions or specific signal generation.[52,53] Polymers such as Poly(ethylene glycol) (PEG), poly(N-vinylpyrrolidone) (PVP), proteins such as bovine serum albumin (BSA), milk powder, casein, gelatins, sugars such as sucrose, and trehalose and surfactants like Tween 20 are some of the these commonly used blocking agents.[54–56]

In this work, we combined two technologies – microcontact printing of a bioink and lubricant-infusion of a fluorosilanized surface – to develop a new biosensing interface for covalently attaching IL-6 capture antibody onto a poly(methyl methacrylate) (PMMA) substrate. To further promote the stabilization of the patterned antibodies through microcontact printing, covalent printing of the capture antibodies was performed via the introduced functional bioinks. Prior to printing onto the surface, the capture antibodies are functionalized via an epoxy-based silane coupling agent that then covalently bind to the free hydroxyl groups on a functionalized surface through the terminal hydroxyl groups of the epoxy-based silane. This provides a robust and stable immobilized capture antibody, that enhances the selectivity and reproducibility of an

IL-6 IFA. Applying the LIS anti-fouling coating to the bioink printed PMMA surfaces produced a robust, simple and cost-effective IFA that allowed detection of IL-6 in human whole plasma with an LOD as low as 0.5 pg mL^{-1} and enabled detection in citrated human whole blood during its coagulation induced by calcium chloride. Therefore, the advantages and novelty of our work include: (i) Significantly higher sensitivity for detection of IL-6 in complex biofluids such as human whole blood and plasma, (ii) Simplicity of the design via using an ELISA based IFA, eliminating any need for use of nanoparticles, nanotubes, nanowires, fibers, and microfluidics. Consequently, the proposed method is low cost and can be mass produced in a short run. (iii) Robustness of the device through the covalent immobilization of the capture antibodies onto the FS treated surfaces and (iv) Potential capability for multiplex detection of cytokines via creation of microarrays of different biorecognition elements.

5.3 Results and discussion

Antibody embedded lubricant-infused surfaces were created on PMMA, a low-priced polymer with many advantages such as optical transparency, durable chemical and mechanical properties, and recyclability.[57,58] PMMA surfaces were first oxygen plasma treated to induce hydroxyl groups on the surface, and then fluorosilanized via chemical vapor deposition (CVD) of trichloro(1*H*,1*H*,2*H*,2*H*-perfluorooctyl)silane followed by heat treatment at 90 ℃ to promote the hydrolysis and condensation

reactions. Immediately after the plasma treatment, the hydrophilicity of the surface can cause adsorption of water molecules on the surface. During the CVD treatment, the adsorbed water is recruited for oligomerization of trichloro(1*H*,1*H*,2*H*,2*H*-perfluorooctyl)silane prior to its engagement with the plasma induced functional groups. In consequence of the former oligomerization of the trichlorosilane due to the rapid hydrolysis rate of its head groups and the presence of the adsorbed water, stochastically distributed dense self-assembled monolayers (SAMs) of fluorosilane (FS) with an umbrella-shape structure can form across the PMMA substrate **(**Figure 5-1).[59-64]

Our developed bioink was prepared by serial dilution of (3-Glycidyloxypropyl)trimethoxy-silane (GLYMO) in PBS and mixing the silane solution with the IL-6 capture antibody as explained in Methods. Following the FS treatment of the PMMA, the GLYMO-conjugated bioink was patterned onto the surface via microcontact printing using polydimethylsiloxane (PDMS) stamps (50×50 μm^2 arrays of protruded squares). The produced positional microarrays provides improved repeatability of the assay by providing numerous sample replicates inside each well. This plays an important role in the assay performance, as well as its adaptability to high throughput applications. Moreover, since the GLYMO-conjugated capture antibody can covalently bind to the surface, the developed biointerface on the PMMA substrates are

very robust. The biofunctional PMMA microarrays were fitted into a superstructure which provides wells for IFA (Figure 5-1). The wells were subsequently lubricated via perfluoroperhydrophenanthrene (PFPP), a fluorinated lubricant that infuses into the FS SAM and is locked through van der Waals forces on the fluorine groups of FS SAM creating the LIS. This provides the surface with anti-fouling properties against biofluids and proteins thereby diminishing the non-specific absorption and enhancing the sensitivity of the biosensor. The developed biosensing surfaces were then used for IFA assays for IL-6 detection

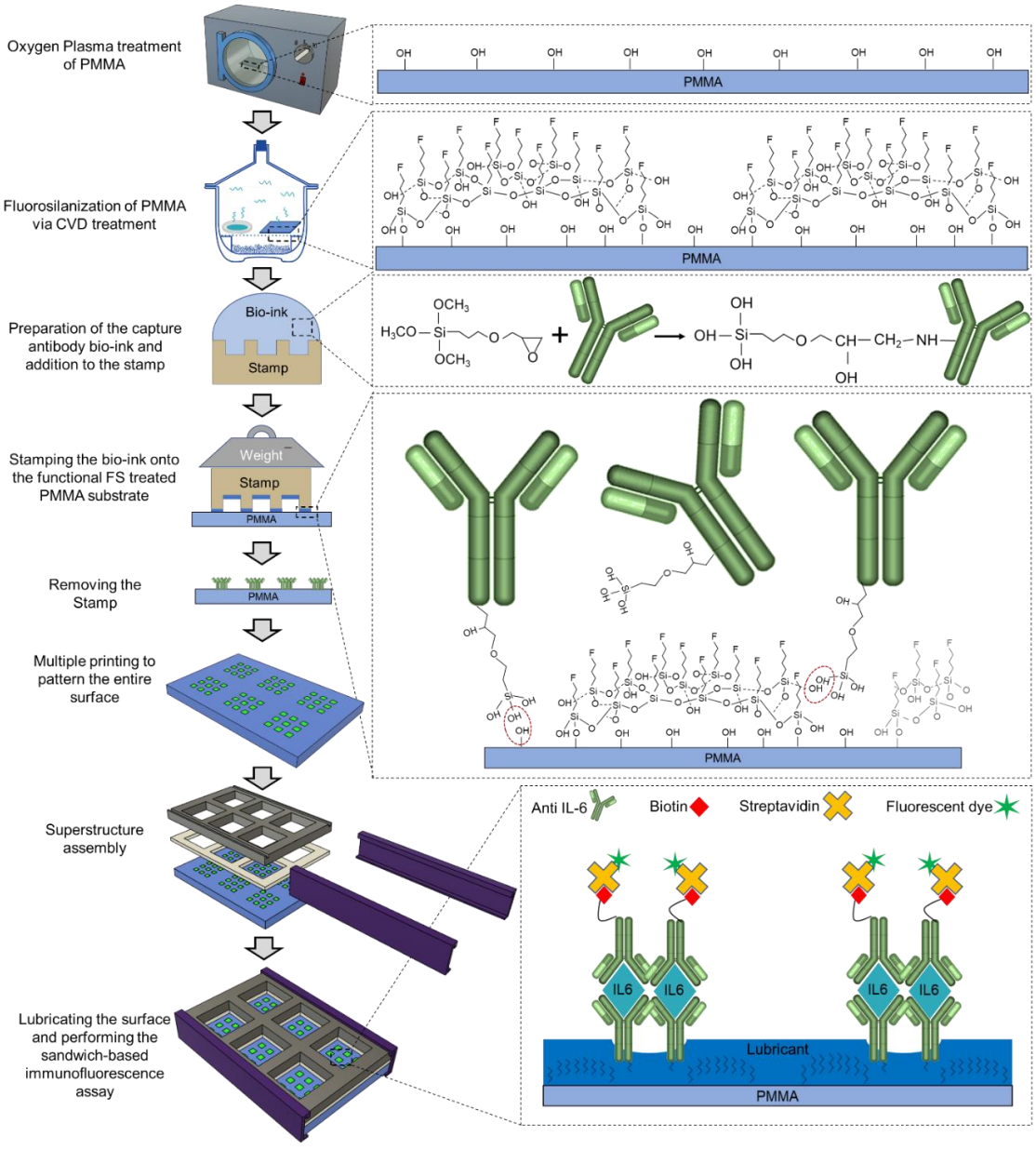

Figure 5-1. Schematic representation of the process for producing PMMA-based antibody embedded lubricant-infused sensors for IL-6 detection. During the microcontact printing, The IL-6 capture antibody can crosslink to the surface through the reaction between one of the hydroxyls at the head groups of the conjugated epoxy-based silane and the hydroxyl groups remaining after the incomplete FS treatment of the surface (red dash circles).

In order to examine the chemical bonds created after fluorosilanization of PMMA, we conducted high resolution XPS analysis on plain, plasma treated, and FS treated surfaces. Figure 5-2 demonstrates deconvoluted spectra of C1s, O1s, and F1s for each sample. The typical deconvolution of PMMA C1s spectra is illustrated in Figure 5-2 (a) - "plain sample" which consists of a hydrocarbon peak C─C/C─H at 284.57 (±0.1) eV, a beta carbon peak C─C═O at 285.42 (±0.16) eV, C─O bond in methoxy groups at 286.47 (±0.14) eV, and a carboxyl carbon O─C═O peak at 288.58 (±0.2) eV.[65,66] The peak area (%) of C1s components are shown in Table 5-1. As seen, oxygen plasma treatment raised the carboxyl carbon peak area from 12.71% to 18.91%, which could be correlated with oxidation of PMMA and formation of carboxyl groups through plasma induced oxygen radicals.

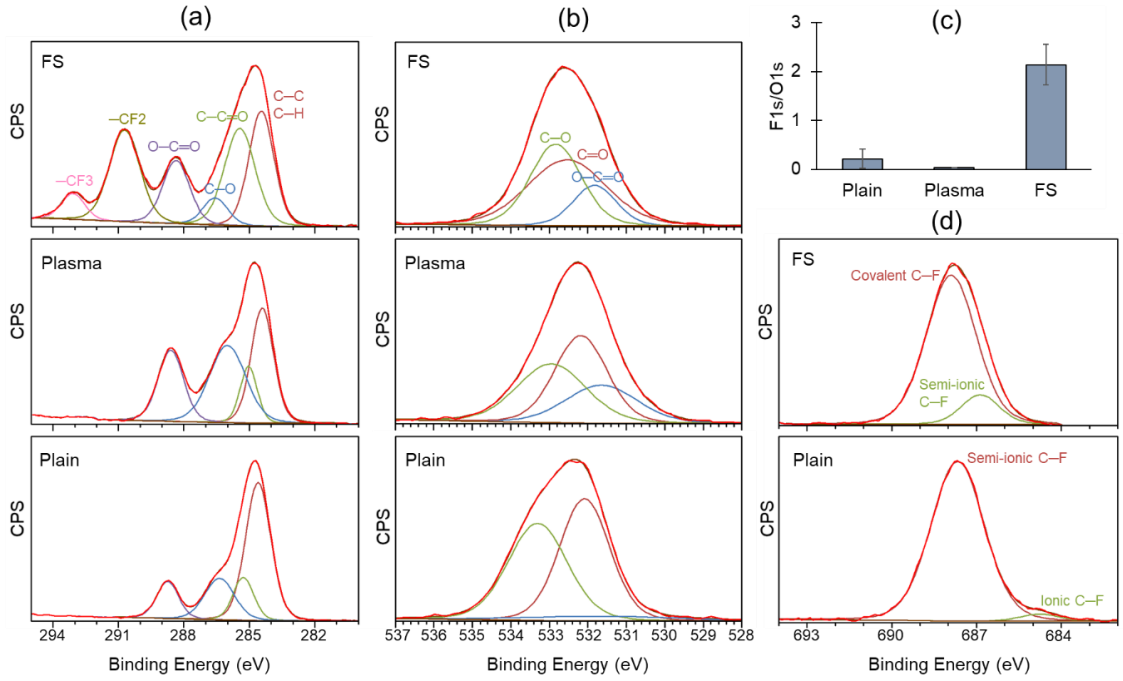

Figure 5-2. Deconvoluted high resolution XPS spectra of (a) C1s, (b) O1s, and (d) F1s, for the PMMA surface before plasma treatment (plain), after the plasma treatment (plasma), and after fluorosilanization (FS). (c) F1s/O1s peak area ratio before and after PMMA surface modification. Data are shown as mean ± SD.

Table 5-1. Quantification of the peak area percentages of C1s spectra for PMMA surfaces before and after the surface modification. Data are shown as mean ± SD

Binding energy (eV)	*284.57 (±0.1)*	*285.42 (±0.16)*	*286.47 (±0.14)*	*288.58 (±0.2)*	*290.69 (±0.06)*	*293.05 (±0.06)*
Chemical bond	C─C/C─H	C─C═O	C─O	O─C═O	─CF2	─CF3
	Peak area (%)					
Plain PMMA	56.41 (±1.18)	14.45 (±2.73)	15.42 (±2.83)	12.71 (±0.45)	0	0
Plasma treatment	49.83 (±5.96)	16.59 (±2.52)	14.67 (±4.71)	18.91 (±3.3)	0	0
FS treatment	23.58 (±1.06)	23.48 (±4.3)	6.97 (±1.62)	14.19 (±0.98)	26.25 (±3.44)	5.52 (±0.64)

According to Table 5-1, the ratio of C-O:O-C=O bonds was also changed from 15.42:12.71 for the plain PMMA surface to 14.67:18.91 for the plasma treated PMMA surface and then down to 6.97:14.19 after the FS treatment. The C-O percentage of plain PMMA shown in the Cs1 spectra could be due to the methyl groups of PMMA. During plasma treatment, these methyl groups on PMMA (highlighted with a circle in Figure S 5-1) are partially reduced. At the same time, plasma induced C-OH groups can be created on the surface. Thus, the resulting effect is minimal change in the abundance of

C-O groups before and after plasma treatment. Simultaneously, plasma treatment can increase the amount of carboxyl groups on the surface as discussed previously. As a result, there is a slight shift in the C-O:O-C=O ratio towards O-C=O bonds. During the fluorosilanization of the surface, the broken C-O groups can be replaced by FS groups. Moreover, the heat treatment step conducted after FS treatment can result in partial hydrophobic recovery of the PMMA surface. Thus, hydroxylated PMMA can lose its hydrophilic C-OH and O-C=OH groups induced by the initial plasma treatment. This could be the reason for slight reduction of O-C=OH groups after FS treatment. However, regarding C-O groups, there is relatively more reduction in the area percentage of C-O groups even compared to the plain PMMA surface due to the hydrophobic recovery of the plasma induced C-O groups as well as the replacement of the methyl groups of PMMA by FS groups during the silanization.

Although fluorosilanization of PMMA surfaces reduced the percentage of carboxyl groups to 14.19%, there was an increase in carboxylic groups compared to the control. The remaining carboxylic groups with functional OH moieties on the surface could be as a result of short CVD and heat treatment durations we employed in this study (*i.e.* 30 min for each step) which led to incomplete polymerization of FS SAMs. Furthermore, the incomplete polymerization can provide functional hydroxyl groups at the umbrella-shape SAMs. The unreacted silanol groups at FS SAMs could also be a consequence of

the reasonable values of bond lengths and angles that silanol bonds can only take.[67,68] The remaining hydroxyl groups provide functionality for further immobilization of anti-IL6 antibody bioink. In fact, at higher CVD durations, we were unable to properly microcontact print the capture antibody onto the treated PMMA surfaces which could be attributed to lack of OH groups on the surface.

In microcontact printing, the IL-6 capture antibody can physically attach to the hydrophobic surface via hydrophobic interactions. By conjugating the capture antibody with GLYMO, covalent attachment of the antibody increases, leading to a higher yield of antibody immobilization. As illustrated in Figure 5-1, the epoxy moiety at the tail group of GLYMO could first couple with the primary and secondary amines of the antibody throughout the bioink formation. During the microcontact printing, we hypothesized the possibility for any of the OH head groups of epoxy silane in the bioink to randomly react with the OH groups of FS SAMs remained after the incomplete fluorosilanization of the surface. For instance, in the umbrella structure of FS, the hydrolyzed head groups of GLYMO can react with the OH groups tethering on the sides of the FS umbrella causing small buckling/bending of siloxanes. Moreover, given the fact that the surface is not fully covered with FS umbrella SAMs, The trifunctional GLYMO can bind to the remaining OH groups located potentially between the areas covered by FS SAMs (Figure 5-1), creating C–O–Si bonds. In Figure 5-1, the schematic

related to the covalent attachment of GLYMO-conjugated antibodies exhibits potential reactions that can happen between the OH groups of GLYMO and the FS treated surface.

In Figure 5-2 (a), fluorosilanization of PMMA resulted in the appearance of two new peaks in the C1s spectrum at 290.69 eV and 293.05 eV which are associated with ─CF2 and ─CF3, respectively.[69,70] These peaks confirm the formation of FS layer with the linear formula of $CF_3(CF_2)_5CH_2CH_2SiCl_3$ as the precursor. The O1s spectrum of plain PMMA surface in Figure 5-2 (b) can be deconvoluted into primarily two peaks of C─O at ~533.3 eV and C═O at 532 eV.[71–73] Plasma treatment of the surface advanced a peak at ~531.6 eV attributed to O─C═O bond [74] which remained in the O1s spectrum after fluorosilanization of the surface, indicating the presence of functional OH groups on the FS treated PMMA surfaces. The peak area ratio of F1s/O1s is plotted in Figure 5-2 (c) which reveals a substantial increase in the amount of fluorine atoms on PMMA surfaces through the FS treatment. The F1s spectra of plain PMMA surface (Figure 5-2 (d)) consisted of semi-ionic C─F bond at ~ 687.5 eV, as well as ionic C─F bond at ~684.5 eV.[75] These bonds were completely etched and removed via oxygen plasma treatment of the surface. Fluorosilanization of the PMMA surface resulted in the emergence of covalent C─F bond at ~688 eV [76] which depicts the robust FS SAM created onto the PMMA substrate. Notably, we performed the XPS test a month after the surface

functionalization to confirm the stability of the functional groups onto the PMMA surfaces.

The omniphobic properties of the fluorosilanized PMMA surfaces were quantified using contact angle and sliding angle measurements (Figure 5-3). The contact angle and sliding angle of plain PMMA surfaces before any treatment were estimated at 71.5° and >90°, respectively. After 15 mins of oxygen plasma treatment, the contact angle dropped to 42° due to formation of hydroxyl groups. Fluorosilanization of the PMMA surfaces for half an hour via CVD technique significantly increased the contact angle to 109°. It is worth mentioning that higher surface hydrophobicity and contact angles can hinder printing the antibodies through microcontact printing protocol with PDMS stamps. Measuring the angular slip of the LIS estimated its interfacial tension and omniphobicity.[77,78] For this purpose, PFPP lubricant was added to the surface and the excess amount of lubricant was removed by tilting the substrate. Infusing the lubricant into the surface can change the surface energy of the substrate and create a slippery interface on which water-based solutions and biofluids can easily slide off by a tremble. The thin layer of the lubricant trapped onto the FS treated surfaces reduced the sliding angle to less than 5°. When the lubricant was added to a plain PMMA surface, due to the absence of FS groups, the lubricant completely came off the surface after tilting the substrate, resulting in no slippery properties. Notably, printing of the antibodies did not

significantly impact the average contact angle and hydrophobicity of the PMMA surfaces as the antibody arrays occupy only a small portion of the substrate. However, due to the fact that droplets can be pinned at the printed areas, which is desirable considering the applicability of the surface for IFA, the sliding angle of the surface changed after patterning, and the droplets could not slide off the entire PMMA surface. The high contact angle and low angular slip of the FS treated PMMA surfaces indicate repellent behavior of the surfaces against different proteins and biomolecules in solution, a key characteristic to prevent non-specific adhesion for biosensing. It should be mentioned that after even 5 minutes of FS CVD treatment of the PMMA surfaces, we were still able to get high contact angles comparable to the 30-min CVD treatment time due to the rapid formation of nano-sized FS SAMs on the surface. However, the samples that were treated for shorter CVD times did not exhibit proper sliding properties which could be because of the inadequate FS groups on the PMMA surface for locking a sufficient amount of lubricant on the surface.

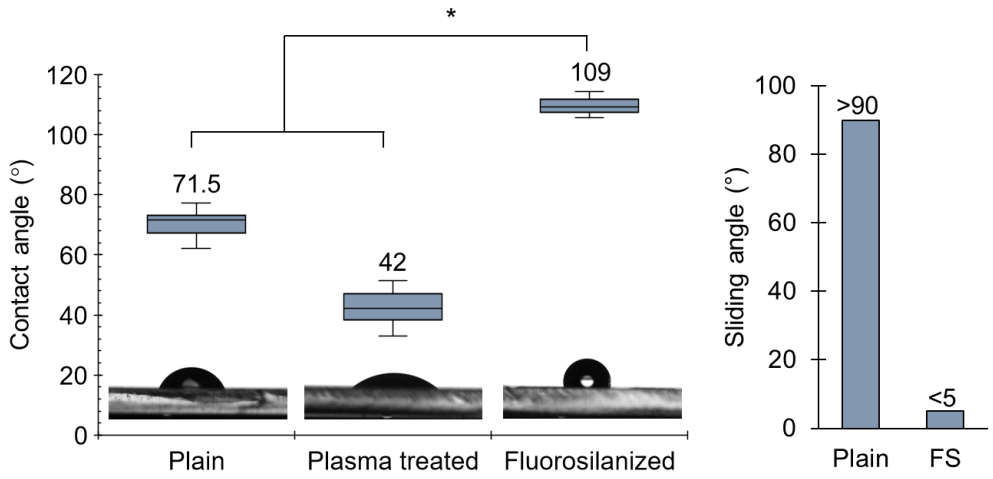

Figure 5-3. Contact angle and sliding angle results of PMMA surfaces before and after the surface modification. Error bars represent the standard deviation. There is a significant difference in the contact angles with $*P \ll 10^{-7}$.

In order to confirm the robust attachment of the IL-6 capture antibody onto the FS treated surfaces, we microcontact printed fluorescently labeled BSA-FITC conjugated with GLYMO and compared the results with unconjugated BSA-FITC sample as a control. As shown in Figure S 5-2, conjugating BSA-FITC with GLYMO before printing can bring about a higher yield of BSA-FITC patterned on the surface. This shows the positive effect of epoxy conjugation on the efficacy of the printed proteins via microcontact printing. Moreover, in order to show the printed proteins do not wash off throughout the washing steps in the assay, we submerged the samples in the buffer of tris-buffered saline mixed with Tween 20 (TBST) which we used in the IL-6 detection assay. In addition, we shook the samples at 100 RPM inside the buffer for 24 hours. After imaging the samples, we noticed that there was no significant difference in

the fluorescence intensity of the patterns achieved via BSA-FITC conjugated with GLYMO, while in the control sample, the patterns were almost completely washed off (Figure S 5-2).

To detect IL-6 using IFA, recombinant IL-6 present in either buffer or plasma was added to the antibody printed lubricant-infused PMMA sensors at various concentrations ranging from 0 to 2500 pg mL^{-1}. Since the unprocessed human whole plasma contains several interfering biological entities such as clotting factors, hormones, albumins, and fibrinogen, detection of IL-6 in such a complex biofluids can attest to the enhanced sensitivity of the biosensor. The sandwich assay was followed by addition of a biotinylated IL-6 detector antibody and a fluorescently labeled streptavidin (Figure 5-4 (a) and (b)). Representative images of the detection fluorescent arrays at different IL-6 concentrations in buffer and plasma are shown in Figure S 5-3 and Figure S 5-4, indicating the microarrays of IL-6 are clearly distinguishable in both plasma and buffer at the concentration of 0.5 pg mL^{-1}. FiJi ImageJ software [79] was utilized to process and quantify the mean fluorescent intensity (MFI) of each printed square. As a confirmatory method to FiJi Image J, Chan-Vese segmentation [80,81] image processing in Python was performed for quantification of results in buffer. Figure 5-4 (c) and (d), illustrates representative fluorescence images of the microarrays of IL-6 at a concentration of 312.5 pg mL^{-1} before and after the Chan-Vese segmentation. Results of Chan-Vese

segmentation processing on the other sample concentrations can be seen in Figure S 5-5.

Table 5-2 illustrates the results of the IL-6 IFA in both buffer and plasma. Two separate and individually processed imaging methods were used to confirm equivalent MFI results in buffer. The more sophisticated Chan-Vase Python approach reduces the influence of artifacts and outliers. The error values corresponding to each result is indicated as coefficient of variation (CV%) in Table 5-2. The LIS IL-6 IFA yielded a functional LOD of 0.5 pg mL^{-1} which was significantly differentiated ($p < 5\times10^{-6}$) from the 0 pg mL^{-1} control for both raw and background-subtracted MFI values in buffer and plasma (Table S 5-1 and Table S 5-2).

Table 5-2. Standard curve MFI values and precision for the LIS IL-6 IFA in buffer and plasma using two image processing methods

	Buffer					Plasma	
Concentration pg/mL	Background Subtracted MFI FiJi ImageJ	%CV Raw FiJi ImageJ	Background Subtracted MFI Chan-Vese Python	%CV Raw Chan-Vese Python	% Robust CV Background Subtracted Chan-Vese Python	Background Subtracted MFI FiJi ImageJ	%CV Raw FiJi ImageJ
2500	12278	14.0	12658	13.6	17.1	9576	15.0
312.5	8156	10.9	7938	10.9	23.8	5523	7.4
156	3499	10.1	3495	10.2	17.0	4291	9.5
40	2622	10.7	2737	10.8	31.2	3184	8.7
5	2310	8.1	2107	8.7	28.6	2439	4.4
1	1538	5.3	1465	5.7	32.2	1634	11.3
0.5	804	2.3	755	2.6	25.2	1207	3.5
0	150	1.4	19	1.3	N/A	338	3.0

Figure 5-4 (e) shows the linear dynamic range of MFI as a function of concentration. The linear range obtained form LIS IL-6 IFA after standard curve fitting was 0.5 to 156 pg mL^{-1} with the $R^2 > 0.97$. This dynamic range includes the required LOD sensitivities for oncological applications such as leukemia (1.45 pg mL^{-1} [82]) breast cancer (3-50 pg mL^{-1} [83]), prostate cancer (4-7 pg mL^{-1} [84,85]), ovarian cancer (10 pg mL^{-1} [86]), and liver cancer (12 pg mL^{-1} [2]). Importantly, the current dynamic range is also applicable for detection of Covid-19 (SARS-Cov2) infection (5.8-64 pg mL^{-1} [10]). Both buffer and plasma were also plotted with a quadratic (third degree polynomial) curve fit for the dynamic range of the LIS IL-6 IFA of 1 to 312.5 pg mL^{-1} shown in Figure S 5-6. IL-6 detection results in plasma and buffer demonstrated almost similar MFIs, indicating that the developed biosensor is capable of preventing non-specific binding and interference in plasma enabling detection of low concentrations of IL-6 in plasma. In Table S 5-3, the superior performance of the presented biosensor for IL-6 detection in human plasma is compared to the recent most well-known techniques along with their associated advantages and disadvantages. It is worth mentioning that the antibody-antigen interactions used as a based mechanism to capture IL-6 in this work, is intrinsically specific and it has been shown that there is not any non-specific interaction between the anti-IL-6 monoclonal antibody and other types of cytokine such as IL-2, IL-3, IL-4, IL-5, IL-8, IL-9, IL-11, TNF-α, TNF-β, IFN-α and IFN-γ.[33] Consequently, the specificity of our developed biosensor is adequately high for multiplex detection of cytokines.

In order to evaluate the performance of the developed biosensing surface in human whole blood, we examined the capability of the assay to recover IL-6 spiked into recalcified citrated blood. The calcified blood was spiked with IL-6 at the concentration of 312.5 pg mL^{-1} and incubated on the LIS sensing interface for an hour during blood coagulation process. Recovery of the spiked sample (n =9 replicates) on the plasma standard curve was 119.4% which is within the accuracy acceptance criteria of ± 20% bias. This corresponds the upper limit of quantitation of the LIS IL-6 IFA and indicates that the assay is able to detect IL-6 in whole blood (Figure S 5-7). We believe that this is the first report on performing biosensing in activated human whole blood while it coagulates.

In addition, a blood adhesion assay was conducted to evaluate the repellency of the surface treatment against fibrin-induced blood clot to the developed PMMA biosensing substrates. Figure 5-4 (f) depicts a representative optical microscope image of blood cells attached onto the plain PMMA surface, following clot formation after an hour of incubation with recalcified citrated blood. The substrates were washed three times with tris buffered saline (TBS) and TBS Tween 20 (TBST) before imaging. The inset image in Figure 5-4 (f) reveals the formed blood clots remaining on the plain PMMA surfaces after the washing steps. However, LIS coating significantly suppressed blood clot attachment to the surface (Figure 5-4 (g)). Owing to the omniphobic characteristic of

the treated PMMA surface, the clot that was formed during the blood incubation could readily be washed off the surface by the wash buffers used in the assay, while in the case of untreated PMMA surfaces, the clot remained stable onto the surface throughout the washing steps. Figure 5-4 (h) and (i) show the SEM images of the untreated PMMA surface compared to antibody embedded LIS after fixation of the remaining clot and fibrins.

Therefore, the antibody embedded lubricant-infused PMMA biosensor not only prevents non-specific adhesion of blood cells, but also enables IL-6 detection during the clot formation, facilitating accurate detection in non-anticoagulated whole blood, which could enable future *ex-vivo* and *in vivo* biosensing platforms as well as biosensing in blood-contacting wearable devices.[87]

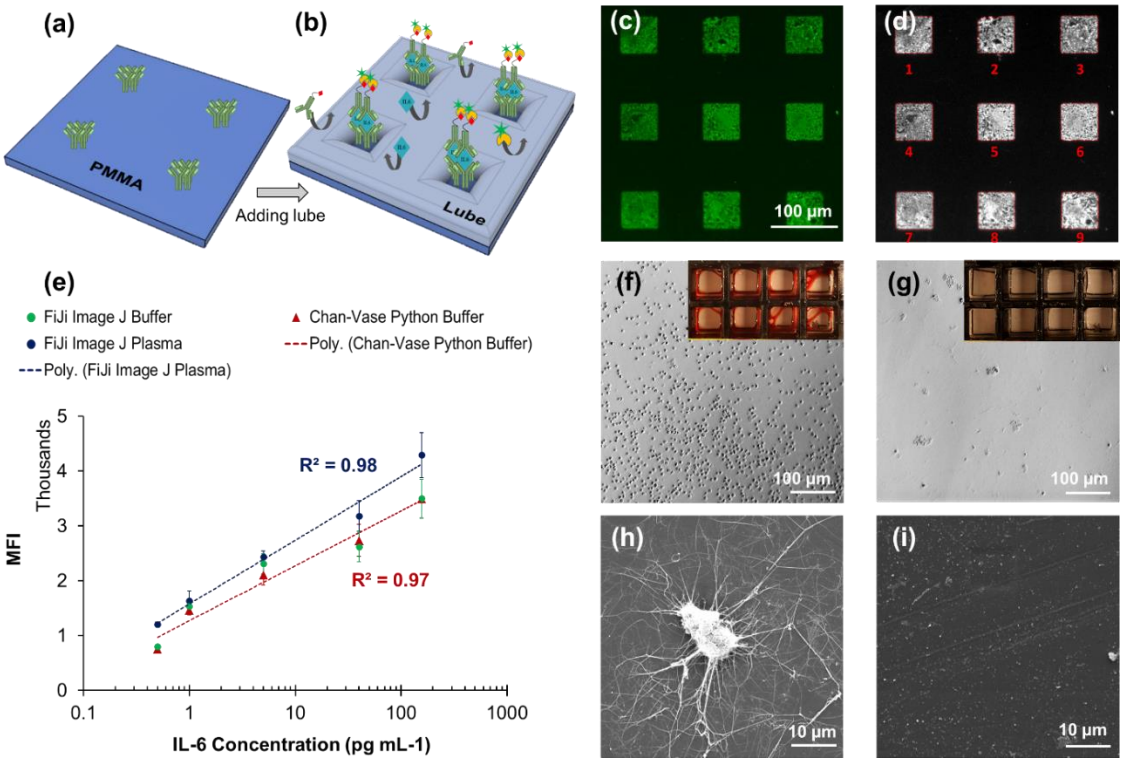

Figure 5-4. (a) Schematic representation of FS treated PMMA surface patterned with the capture antibodies. (b) Schematic representation of FS treated PMMA surface after adding the lubricant and performing the IFA. The lubricant layer repels all sorts of biofluids and proteins while capturing the target at the printed areas. (c) Raw image of the IL-6 microarrays at the concentration of 312.5 pg mL^{-1} in buffer. (d) Image (c) after the Chan-Vese image segmentation processing in Python. (e) Linear dynamic range of dose response curves of the IL-6 IFA using LIS. Graphical data are shown as mean (n = 18 replicates, $R^2 \geq 0.97$ for buffer and ≥ 0.98 for plasma) with linear range of 0.5 – 156 pg mL^{-1}. Error bars represent the $\pm$ standard deviation. (f) and (g) Optical microscope images of the blood cells attached to the untreated (plain) PMMA and LIS PMMA, respectively, following whole blood coagulation test. The inset images show the wells after the clotting assay. The area of each well is ~1cm^2. (h) SEM image of the blood clot attached to the plain PMMA surface. (i) SEM image of antibody-printed LIS PMMA surface after the clotting assay.

5.4 Conclusion

A unique biosensing interface was presented that enables sub picogram detection of IL-6 in human plasma as well as in coagulating human whole blood. This was achieved by

printing the developed bioink solution into a fluorosilanized PMMA substrate followed by infusion of a thin lubricant layer. The presented biosensing interface benefits from the repellency and omniphobicity of the LIS, which blocks non-specific attachment of interfering matrix components to the surface, thereby enhancing the sensitivity and specificity of the biosensor. Another factor contributing to the achieved low LOD, is the bioink, composed of epoxy-based silane-anti-IL-6 complexes, enabling covalent microcontact printing of the capture antibody onto the FS PMMA surface. The developed bio-interfaces promote covalent binding to the FS surface with various biomolecules through their amine moieties using this new bioink preparation technique. The presence of epoxy as a cross-linking agent in the bioink facilitates the transfer of the antibodies from the PDMS stamps to the FS treated PMMA substrate, leading to a higher yield of antibody patterned onto the surface..

The presented fabrication method is simple and scalable for mass production and can be applied to different substrates and for the detection of other disease markers. An important advantage of the developed biosensor is that since the substrate is covalently coated with a monolayer of fluorosilane, the repellency behavior of the surface is much more durable in comparison to common blocking agents that are physically or electrostatically attached to the surface. Furthermore, as we are able to covalently micro pattern the FS surface with the desired capture antibody, the stability of the immobilized

biomolecules is significantly increased. Future efforts will focus on design and optimization of a process for mass production of the developed biosensing interfaces as well as enabling multiplex detection of target biomarkers.

5.5 Experimental procedure

Materials: The following materials and reagents have been utilized for surface biofunctionalization and IL-6 sandwich immunoassay: trichloro(1*H*,1*H*,2*H*,2*H*-perfluorooctyl)silane (TPFS) (Sigma-Aldrich, Oakville, ON, Canada), (3-glycidyloxypropyl)trimethoxy-silane (GLYMO) (Sigma-Aldrich, Oakville, ON, Canada), perfluoroperhydrophenanthrene (PFPP) (Sigma-Aldrich, Oakville, ON, Canada), polydimethylsiloxane (PDMS) (Dow SYLGARD™ 184 Silicone Encapsulant, Ellsworth Adhesives, Stoney Creek, ON, Canada), albumin–fluorescein isothiocyanate conjugate (BSA-FITC) (Sigma-Aldrich, Oakville, ON, Canada), recombinant human (*E. Coli* derived) IL-6 (R&D Systems, Minnesota, US), IL-6 monoclonal antibody (MQ2-13A5, capture antibody) (ThermoFisher Scientific, ON, Canada), biotinylated IL-6 monoclonal antibody (MQ2-39C3, detector antibody) (ThermoFisher Scientific, ON, Canada), BV480 streptavidin (BD Horizon™, Mississauga, ON, Canada), and Poly(methyl methacrylate) plates (PMMA) (Beauty Glass, Hsin Hwa Chemical Co, Ltd, Taiwan). Human blood plasma, and citrated whole human blood were used as received without any modification and collected from

healthy donors who provided a signed consent for collecting their blood. The procedure was approved by the McMaster University Research Ethics Board.

Surface fluorosilanization: Before functionalization of PMMA, the substrates were cut to the size of a glass slide (75 mm x 25 mm), and carefully washed using water and ethanol to remove any traces of impurities. The PMMA surface was initially oxygen plasma treated for 15 min (Harrick Plasma) to hydroxylate the surface. Afterwards, the substrate was immediately transferred to a vacuum desiccator in order to perform fluorosilanization through CVD method using trichloro(1*H*,1*H*,2*H*,2*H*-perfluorooctyl)silane for 30 mins at -0.08 MPa pressure. Subsequently, the fluorinated surface was placed on a hot plate at 90°C for 30 mins to create FS SAM (Figure 5-1).

Preparation and microcontact printing of the bioink: (3-glycidyloxypropyl)trimethoxy-silane was diluted in PBS to achieve the concentration of 22.4 μM. Then, IL-6 monoclonal capture antibody was mixed with the epoxy solution at the concentration of 150 μg/mL. The prepared bioink was patterned on the fluorosilanized PMMA surface through microcontact printing. In order to make PDMS stamps, a silicon wafer mold with the desired patterns was fabricated using photolithography technique. PDMS was cast into a mold to produce stamps with an array of square protrusions (50×50 μm^2). The stamps were sonicated in ethanol and dried before use. The required amount of the capture antibody bioink (~ 5 μl) was added to each stamp to cover the entire features of

the stamps and incubated for 10 mins. Thereafter, the stamps were washed with PBS and then water and dried for a 2-4 seconds using a strong blast of compressed air. The stamps were immediately pressed onto the FS treated PMMA surface by placing a small amount of weight on top. After 2 mins, the stamps were removed, and the surfaces were incubated in a humidified atmosphere at 4 ℃ for around 1 hr and a half. To conjugate BSA-FITC with (3-glycidyloxypropyl)trimethoxy-silane, 100 mg/ml of BSA-FITC (diluted in PBS) was mixed with GLYMO at the same ratio as for the IL-6 capture antibody.

Lubricant-infusion of the fluorosilanized surface: Following the covalent antibody printing onto the fluorosilanized surface and assembly of the superstructure (Figure 5-1), PFPP lubricant was added to the wells and incubated for about 1-2 min. Then, the surface was flipped to remove the excess amount of the lubricant and washed with Tris buffered saline (TBS) and TBS Tween 20 (TBST) leaving a thin layer of lubricant trapped within the fluorine groups of the surface.

Surface characterization: High-resolution X-ray photoelectron spectroscopy (XPS) (PHI Quantera II, Biointerfaces Institute, McMaster University) was implemented to reveal the chemical bonds which appeared on the surface before and after the plasma treatment and after the fluorosilanization step. Worth mentioning that we decided to perform XPS 1 week after the surface treatment to ensure the chemicals and functional

groups of the modified surfaces remain stable. C1s, O1s, and F1s peaks were recorded in the high resolution XPS analysis and the raw data was deconvoluted incorporating CasaXPS application.

The hydrophobicity and surface tension of the PMMA substrates were quantified using contact angle and sliding angle techniques. The contact angles of plain, oxygen plasma treated, and fluorosilanized PMMA surfaces were measured via Future Digital Scientific OCA20 goniometer (Garden City, NY). In these experiments, 2 µl of deionized water was dropped onto the multiple spots of the surfaces and the contact angles were automatically calculated from the captured images of the droplets. A digital angle level (ROK, Exeter, UK) was adopted to measure the sliding angles of the plain and fluorosilanized PMMA samples. Before adding 2 µl of deionized water to the surfaces and obtaining the sliding angles, both plain and FS treated surfaces were lubricated with the PFPP lubricant and tilted to remove the excess amount of the lubricant. The droplets were placed onto the substrates at various angles, and the angle at which the droplet starts sliding off the surface was assigned as the sliding angle.

IL-6 immunofluorescence assay (IFA): Recombinant IL-6 solution was serially diluted in either sample diluent composed of 1% BSA in phosphate-buffered saline (PBS) or human blood plasma to produce the different concentrations of 2500 pg mL^{-1}, 312.5 pg mL^{-1}, 156 pg mL^{-1}, 40 pg mL^{-1}, 20 pg mL^{-1}, 5 pg mL^{-1}, 2 pg mL^{-1}, 1 pg mL^{-1}, 0.8 pg

mL^{-1}, and 0.5 pg mL^{-1}. 150 µl of the IL-6 solution was added to each well and incubated for an hour. Next, the wells were washed again using TBS and TBST, and biotinylated IL-6 monoclonal antibody (1:500 v:v diluted in the sample diluent buffer) was added to the wells and incubated for anhour. Finally, the wells were washed using both wash buffers, and the BV480 streptavidin dye (1:250 v:v diluted in the reporter buffer) was added to each well and incubated for 30 mins in complete darkness. The well plate was washed with the wash buffers before the imaging.

Fluorescence microscopy: Fluorescent imaging was conducted via a Zeiss inverted fluorescent microscope (AX10) using Fluorescein (FITC) filter set. The images were acquired via ZEN software under 10X magnification. In FiJi ImageJ software, the acquired 16-bit TIF images were first divided into individual colors (Image Color Split Channels). Next the Image Adjust Threshold function was used to define a printed square's positive signal. Square command was used to enclose a square around the PDMS stamped region. The pattern of squares for each well is replicated between images with the Take command of the ROI Manager. The median MFI signal intensities were then obtained by using the Measure command. Four smaller squares were then overlaid on the blank regions between the printed squares to obtain the background signal which was then subtracted from the MFI of the patterned areas for each well. The resulting raw data is processed by averaging the 9 positive and 4 negative spots for each

image. Duplicates of each sample, control or standard yielding 18 replicate squares for each measurement were evaluated on the IL-6 IFA PMMA slides,

In Chan-Vese segmentation image processing in Python, pixels within the red border demark the spot region while pixels outside the red border belong to local background. Spot signal is calculated as the MFI of spot region minus the median pixel value of local background (*i.e.*, background subtraction). For each level, a 'raw' mean and standard deviation are calculated from the signals of 18 replicates. In addition, Tukey Biweight algorithm has been applied on the raw data to obtain the robust mean and standard deviation (*i.e.*, weighted mean & STD) in order to minimize the influence of outliers.

The two-tailed student T-test assuming unequal variance was used for analysis of significant differences between IL-6 levels of the dose response curve. The fitting trendlines in the dose respond graph was done by a logarithmic relationship of Equation 1:

$$MFI = a \times \ln(x) + b \quad (1)$$

where x is the IL-6 concentration in pg mL^{-1}, and a and b are the fitting parameters. The number of tests for each concentration was 3.

Blood clot formation and scanning electron microscopy (SEM) imaging: By initiating blood clot formation onto PMMA substrates, we assessed the blood cells and proteins

interactions with our modified lubricant-infused surfaces compared to untreated PMMA surfaces. In order to initiate the clot, 100 µl of the citrated human blood was recalcified by 100 µl of 25 mM $CaCl_2$ (diluted in HEPES) and added to each of the wells with the treated and untreated PMMA bottom surfaces. After 1 hr incubation, the clot was gently removed, and the wells were washed several times with TBS and TBST wash buffers. Further, 2% glutaraldehyde (diluted in PBS) was added to the wells and incubated overnight to fix the clot. After proper washing, the surfaces were incubated for 1 hr with 1% osmium tetroxide in 0.1 m sodium cacodylate buffer to proceed with the post-fixation. The surfaces were dehydrated through a graded series of ethanol, and then critical point drying was performed on the samples by Leica EM CPD300 dryer (Leica Mikrosysteme GmbH, Wien, Austria) using liquid CO_2 flush. The samples were then sputtered with gold (Polaron Model E5100 sputter coater, Watford, Hertfordshire) and imaged via SEM (JSM-7000 F).

5.6 Acknowledgments

The authors acknowledge and thank Professor Zeinab Hosseinidoust for critically editing the paper. This work was supported by NSERC Discovery and CRD grants, Ontario Early Researcher Award grant and McMaster start-up funds to T.F.D.

5.7 References

[1] S. Grivennikov, M. Karin, *Cancer Cell* **2008**, *13*, 7.

[2] Y.-C. Chung, Y.-F. Chang, *J. Surg. Oncol.* **2003**, *83*, 222.

[3] Z. Culig, M. Puhr, *Mol. Cell. Endocrinol.* **2012**, *360*, 52.

[4] C. Dethlefsen, G. Højfeldt, *Breast Cancer Res. Treat.* **2013**, *138*, 657.

[5] H. Yanagawa, S. Sone, Y. Takahashi, T. Haku, S. Yano, T. Shinohara, T. Ogura, *Br. J. Cancer* **1995**, *71*, 1095.

[6] M. Lesina, M. U. Kurkowski, K. Ludes, S. Rose-john, M. Treiber, G. Kloppel, A. Yoshimura, W. Reindl, B. Sipos, S. Akira, R. M. Schmid, H. Algul, *Cancer Cell* **2011**, *19*, 456.

[7] N. Kumari, B. S. Dwarakanath, A. Das, A. N. Bhatt, *Tumor Biol.* **2016**, *37*, 11553.

[8] T. Tanaka, M. Narazaki, T. Kishimoto, *Cold Spring Harb Perspect Biol* **2014**, *6*, a016295.

[9] T. Herold, V. Jurinovic, C. Arnreich, J. C. Hellmuth, M. von Bergwelt-Baildon, M. Klein, T. Weinberger, *medRxiv* **2020**, 2020.04.01.20047381.

[10] X. Chen, B. Zhao, Y. Qu, Y. Chen, J. Xiong, Y. Feng, D. Men, Q. Huang, Y. Liu, B. Yang, J. Ding, F. Li, *Clin. Infect. Dis.* **2020**, ciaa449.

[11] F. Khosravi, S. M. Loeian, B. Panchapakesan, *Biosensors* **2017**, *7*, 17.

[12] M. Helle, L. Boeije, E. de Groot, A. de Vos, L. Aarden, *J. Immunol. Methods* **1991**, *138*, 47.

[13] J. Sabaté del Río, O. Y. F. Henry, P. Jolly, D. E. Ingber, *Nat. Nanotechnol.* **2019**, *14*, 1143.

[14] B. S. Munge, C. E. Krause, R. Malhotra, V. Patel, J. Silvio Gutkind, J. F. Rusling, *Electrochem. commun.* **2009**, *11*, 1009.

[15] T. Li, M. Yang, *Sensors Actuators B Chem.* **2011**, *158*, 361.

[16] R. Malhotra, V. Patel, J. P. Vaque, J. S. Gutkind, J. F. Rusling, J. P. Vaqué, J. S. Gutkind, J. F. Rusling, *Anal. Chem.* **2010**, *82*, 3118.

[17] M. A. Khan, M. Mujahid, *Sensors (Switzerland)* **2020**, *20*, 646.

[18] G. Wang, H. Huang, B. Wang, X. Zhang, L. Wang, *Chem. Commun.* **2012**, *48*, 720.

[19] M. Tertiş, B. Ciui, M. Suciu, R. Săndulescu, C. Cristea, *Electrochim. Acta* **2017**, *258*, 1208.

[20] C. Diacci, M. Berto, M. Di Lauro, E. Bianchini, M. Pinti, D. Simon, F. Biscarini, C. A. Bortolotti, *Biointerphases* **2017**, *12*, 10.1116.

[21] N. Liu, H. Yi, Y. Lin, H. Zheng, X. Zheng, D. Lin, H. Dai, *Microchim. Acta* **2018**, *185*, 277.

[22] X. P. Liu, X. L. Xie, Y. P. Wei, C. jie Mao, J. S. Chen, H. L. Niu, J. M. Song, B. K. Jin, *Microchim. Acta* **2018**, *185*, 52.

[23] T.-H. Chou, C.-Y. Chuang, C.-M. Wu, *Cytokine* **2010**, *51*, 107.

[24] J. F. Masson, *ACS Sensors* **2017**, *2*, 16.

[25] P. Chen, M. T. Chung, W. McHugh, R. Nidetz, Y. Li, J. Fu, T. T. Cornell, T. P. Shanley, K. Kurabayashi, *ACS Nano* **2015**, *9*, 4173.

[26] L. Luo, Z. Zhang, L. Hou, *Anal. Chim. Acta* **2007**, *584*, 106.

[27] L. Luo, Z. Zhang, L. Hou, J. Wang, W. Tian, *Talanta* **2007**, *72*, 1293.

[28] J. Wu, Y. Chen, M. Yang, Y. Wang, C. Zhang, M. Yang, J. Sun, M. Xie, X. Jiang, *Anal. Chim. Acta* **2017**, *982*, 138.

[29] J. Deng, M. Yang, J. Wu, W. Zhang, X. Jiang, *Anal. Chem.* **2018**, *90*, 9132.

[30] G. Liu, M. Qi, M. R. Hutchinson, G. Yang, E. M. Goldys, *Biosens. Bioelectron.* **2016**, *79*, 810.

[31] J. F. Djoba Siawaya, T. Roberts, C. Babb, G. Black, H. J. Golakai, K. Stanley, N. B. Bapela, E. Hoal, S. Parida, P. van Helden, G. Walzl, *PLoS One* **2008**, *3*, e2535.

[32] G. Liu, K. Zhang, A. Nadort, M. R. Hutchinson, E. M. Goldys, *ACS Sensors* **2017**, *2*, 218.

[33] X. Hun, Z. Zhang, *Biosens. Bioelectron.* **2007**, *22*, 2743.

[34] P. D'Orazio, *Clin. Chim. Acta* **2011**, *412*, 1749.

[35] T.-S. Wong, S. H. Kang, S. K. Y. Tang, E. J. Smythe, B. D. Hatton, A. Grinthal, J. Aizenberg, *Nature* **2011**, *477*, 443.

[36] M. Villegas, Y. Zhang, N. Abu Jarad, L. Soleymani, T. F. Didar, *ACS Nano* **2019**, *13*, 8517.

[37] M. Badv, S. M. Imani, J. I. Weitz, T. F. Didar, *ACS Nano* **2018**, *12*, 10890−10902.

[38] A. Hosseini, M. Villegas, J. Yang, M. Badv, I. W. Jeffrey, L. Soleymani, F. T. Didar, *Adv. Mater. Interfaces* **2018**, *5*, 1800617.

[39] M. Badv, I. H. Jaffer, J. I. Weitz, T. F. Didar, *Sci. Rep.* **2017**, *7*, 11639.

[40] N. Vogel, R. A. Belisle, B. Hatton, T. S. Wong, J. Aizenberg, *Nat. Commun.* **2013**, *4*, 1.

[41] D. C. Leslie, A. Waterhouse, J. B. Berthet, T. M. Valentin, A. L. Watters, A. Jain, P. Kim, B. D. Hatton, A. Nedder, K. Donovan, E. H. Super, C. Howell, C. P. Johnson, T. L. Vu, D. E. Bolgen, S. Rifai, A. R. Hansen, M. Aizenberg, M. Super, J. Aizenberg, D. E. Ingber, Donald E Ingber, *Nat. Biotechnol.* **2014**, *32*, 1134.

[42] J. Li, T. Kleintschek, A. Rieder, Y. Cheng, T. Baumbach, U. Obst, T. Schwartz, P. A. Levkin, *ACS Appl. Mater. Interfaces* **2013**, *5*, 6704.

[43] P. Wang, Z. Lu, D. Zhang, *Corros. Sci.* **2015**, *93*, 159.

[44] S. Yuan, S. Luan, S. Yan, H. Shi, J. Yin, *ACS Appl. Mater. Interfaces* **2015**, *7*, 19466.

[45] N. T. Darwish, S. D. Sekaran, Y. Alias, S. M. Khor, *J. Pharm. Biomed. Anal.*

2018, *149*, 591.

[46] S. M. Imani, M. Badv, A. Shakeri, H. Yousefi, D. Yip, C. Fine, T. F. Didar, *Lab Chip* **2019**, DOI 10.1039/C9LC00608G.

[47] P. Delfani, L. Dexlin Mellby, M. Nordström, A. Holmér, M. Ohlsson, C. A. K. Borrebaeck, C. Wingren, *PLoS One* **2016**, *11*, e0159138.

[48] S. Yatsushiro, R. Akamine, S. Yamamura, M. Hino, K. Kajimoto, K. Abe, H. Abe, J. Kido, M. Tanaka, Y. Shinohara, Y. Baba, T. Ooie, M. Kataoka, *PLoS One* **2011**, *6*, e18807.

[49] J. Foncy, A. Estève, A. Degache, C. Colin, J. C. Cau, L. Malaquin, C. Vieu, E. Trévisiol, in (Eds.: P. Ertl, M. Rothbauer), Springer New York, New York, NY, **2018**, pp. 83–95.

[50] R. Castagna, A. Bertucci, E. A. Prasetyanto, M. Monticelli, D. V. Conca, M. Massetti, P. P. Sharma, F. Damin, M. Chiari, L. De Cola, R. Bertacco, *Langmuir* **2016**, *32*, 3308.

[51] S. L. Seurynck-Servoss, A. M. White, C. L. Baird, K. D. Rodland, R. C. Zangar, *Anal. Biochem.* **2007**, *371*, 105.

[52] J. H. T. Luong, K. B. Male, J. D. Glennon, *Biotechnol. Adv.* **2008**, *26*, 492.

[53] L. Chen, P. Y. Qian, *Mar. Drugs* **2017**, *15*, 264.

[54] W. J. Yang, T. Cai, K. G. Neoh, E. T. Kang, S. L. M. Teo, D. Rittschof, *Biomacromolecules* **2013**, *14*, 2041.

[55] C. Rodriguez-Emmenegger, M. Houska, A. B. Alles, E. Brynda, *Macromol. Biosci.* **2012**, *12*, 1413.

[56] J. Jiang, L. Zhu, L. Zhu, H. Zhang, B. Zhu, Y. Xu, *ACS Appl. Mater. Interfaces* **2013**, *5*, 12895.

[57] S. Sathish, N. Ishizu, A. Q. Shen, *ACS Appl. Mater. Interfaces* **2019**, *11*, 46350.

[58] A. M. D. Wan, D. Devadas, E. W. K. Young, *Sensors Actuators B Chem.* **2017**, *253*, 738.

[59] A. C. Glavan, R. V. Martinez, A. B. Subramaniam, H. J. Yoon, R. M. D. Nunes, H. Lange, M. M. Thuo, G. M. Whitesides, Adv. Funct. Mater. **2014**, 24, 60.

[60] S. Oyola-Reynoso, I. D. Tevis, J. Chen, B. S. Chang, S. Çinar, J. F. Bloch, M. M. Thuo, J. Mater. Chem. A **2016**, 4, 14729.

[61] V. V. Naik, R. Städler, N. D. Spencer, Langmuir **2014**, 30, 14824.

[62] V. V. Naik, M. Crobu, N. V. Venkataraman, N. D. Spencer, J. Phys. Chem. Lett. **2013**, 4, 2745.

[63] S. Oyola-Reynoso, Z. Wang, J. Chen, S. çinar, B. Chang, M. Thuo, Coatings **2015**, 5, 1002.

[64] P. Samyn, J. Mater. Sci. **2013**, 48, 6455.

[65] G. Beamson, D. Briggs, *J. Chem. Educ.* **1993**, *70*, A25.

[66] S. Pletincx, K. Marcoen, L. Trotochaud, L. L. Fockaert, J. M. C. Mol, A. R. Head, O. Karslioğlu, H. Bluhm, H. Terryn, T. Hauffman, *Sci. Rep.* **2017**, *7*, 13341.

[67] V. Dugas, Y. Chevalier, *J. Colloid Interface Sci.* **2003**, *264*, 354.

[68] A. Shakeri, S. Rahmani, S. M. Imani, M. Osborne, H. Yousefi, T. F. Didar, in *Woodhead Publ. Ser. Electron. Opt. Mater.* (Eds.: K. Pal, H.-B. Kraatz, A. Khasnobish, S. Bag, I. Banerjee, U. Kuruganti), Woodhead Publishing, **2019**, pp. 635–699.

[69] X. Cui, Y. Gao, S. Zhong, Z. Zheng, Y. Cheng, H. Wang, *J. Polym. Res.* **2012**, *19*, DOI 10.1007/s10965-012-9832-6.

[70] T. Song, Q. Liu, J. Liu, W. Yang, R. Chen, X. Jing, K. Takahashi, J. Wang, *Appl. Surf. Sci.* **2015**, *355*, 495.

[71] C. S. Park, E. Y. Jung, H. J. Jang, G. T. Bae, B. J. Shin, H. S. Tae, *Polymers (Basel).* **2019**, *11*, DOI 10.3390/polym11030396.

[72] H. R. Tantawy, B. A. F. Kengne, D. N. McIlroy, T. Nguyen, D. Heo, Y. Qiang, D. E. Aston, *J. Appl. Phys.* **2015**, *118*, DOI 10.1063/1.4934851.

[73] L. Zhang, Y. Li, L. Zhang, D. W. Li, D. Karpuzov, Y. T. Long, *Int. J. Electrochem. Sci.* **2011**, *6*, 819.

[74] A. Shukla, S. D. Bhat, V. K. Pillai, *J. Memb. Sci.* **2016**, *520*, 657.

[75] G. Panomsuwan, N. Saito, T. Ishizaki, *J. Mater. Chem. A* **2015**, *3*, 9972.

[76] A. R. Barron, *Physical Methods in Chemistry and Nano Science*, Rice University, Houston, Texas, **2012**.

[77] M. Badv, J. I. Weitz, T. F. Didar, *Small* **2019**, *15*, 1905562.

[78] M. Badv, C. Alonso-Cantu, A. Shakeri, Z. Hosseinidoust, J. I. Weitz, T. F. Didar, *ACS Biomater. Sci. Eng.* **2019**, *5*, 6485.

[79] J. Schindelin, I. Arganda-Carreras, E. Frise, V. Kaynig, M. Longair, T. Pietzsch, S. Preibisch, C. Rueden, S. Saalfeld, B. Schmid, J.-Y. Tinevez, D. J. White, V. Hartenstein, K. Eliceiri, P. Tomancak, A. Cardona, *Nat. Methods* **2012**, *9*, 676.

[80] P. Getreuer, *Image Process. Line* **2012**, *2*, 214.

[81] S. Van Der Walt, J. L. Schönberger, J. Nunez-Iglesias, F. Boulogne, J. D. Warner, N. Yager, E. Gouillart, T. Yu, *PeerJ* **2014**, *2*, e453.

[82] L. Fayad, M. J. Keating, J. M. Reuben, S. O'Brien, B. N. Lee, S. Lerner, R. Kurzrock, *Blood* **2001**, *97*, 256.

[83] H. Knüpfer, R. Preiß, *Breast Cancer Res. Treat.* **2007**, *102*, 129.

[84] J. Nakashima, M. Tachibana, Y. Horiguchi, M. Oya, T. Ohigashi, H. Asakura, M. Murai, *Clin. Cancer Res.* **2000**, *6*, 2702 LP.

[85] D. J. George, S. Halabi, T. F. Shepard, B. Sanford, N. J. Vogelzang, E. J. Small, P. W. Kantoff, *Clin. Cancer Res.* **2005**, *11*, 1815 LP.

[86] M. Plante, S. C. Rubin, G. Y. Wong, M. G. Federici, C. L. Finstad, G. A. Gastl, *Cancer* **1994**, *73*, 1882.

[87] J. Kim, A. S. Campbell, B. E.-F. de Ávila, J. Wang, *Nat. Biotechnol.* **2019**, *37*, 389.

5.8 Supporting Information

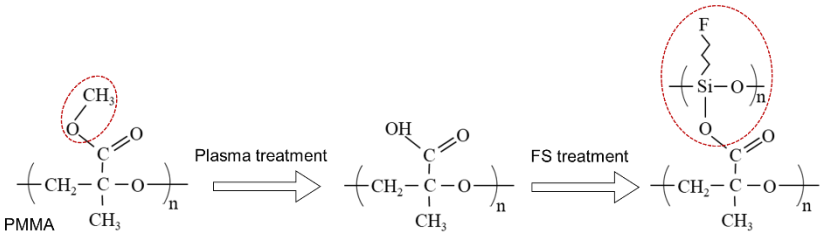

Figure S 5-1. Schematic representation of a potential approach for attachment of silanol groups to the PMMA substrate.

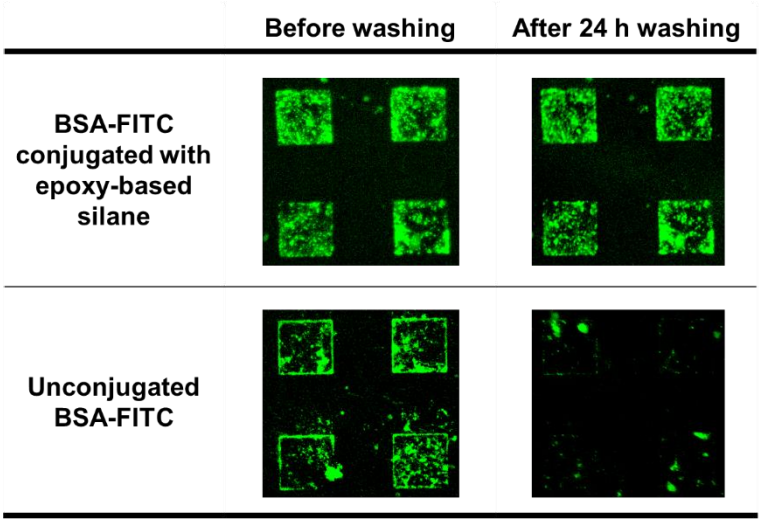

Figure S 5-2. BSA-FITC conjugated with GLYMO was microcontact printed onto an FS treated PMMA substrate and the obtained fluorescent patterns were compared to a control sample where unconjugated BSA-FITC was patterned. The "before washing" images show higher yield of the protein obtained by use of GLYMO. The samples were then shaken for 24 hours in TBST buffer at100 rpm to show the effect of conjugation in stability of the protein. In the unconjugated sample, the patterns were almost completely washed off due to the lack of covalent immobilization.

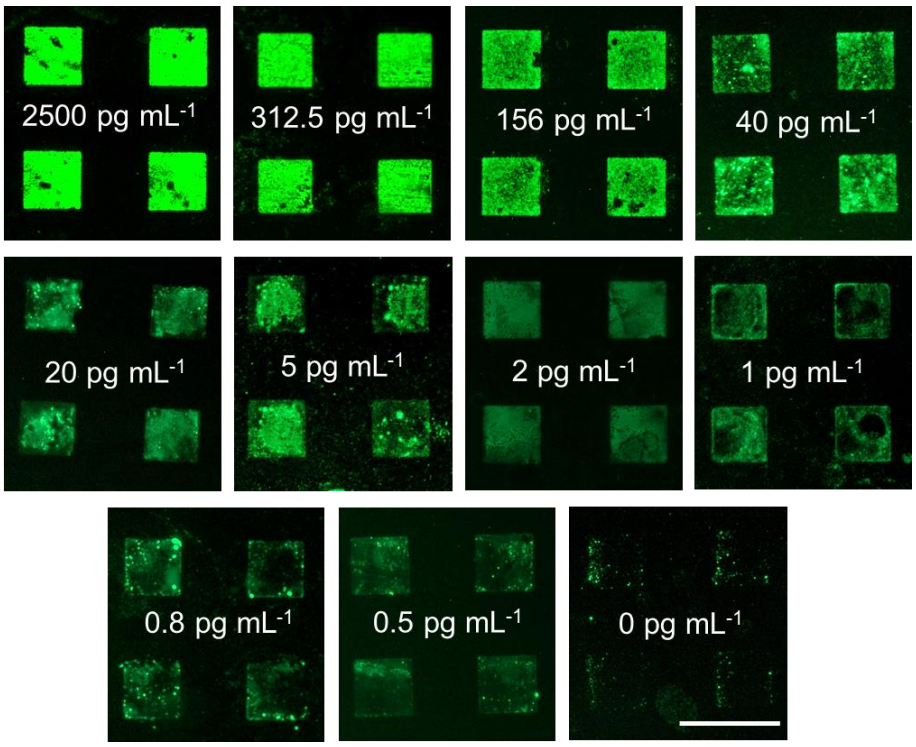

Figure S 5-3**.** IFA results of microarrays of IL-6 diluted in buffer at different concentrations. Scale bar is 100 μm.

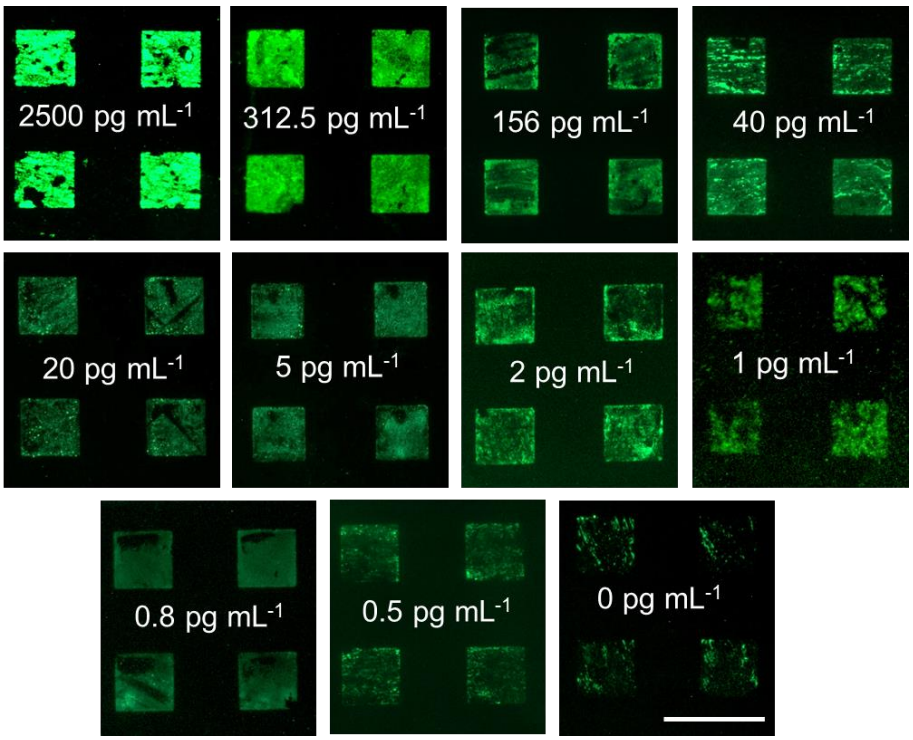

Figure S 5-4. IFA results of microarrays of IL-6 diluted in plasma at different concentrations. Scale bar is 100 µm.

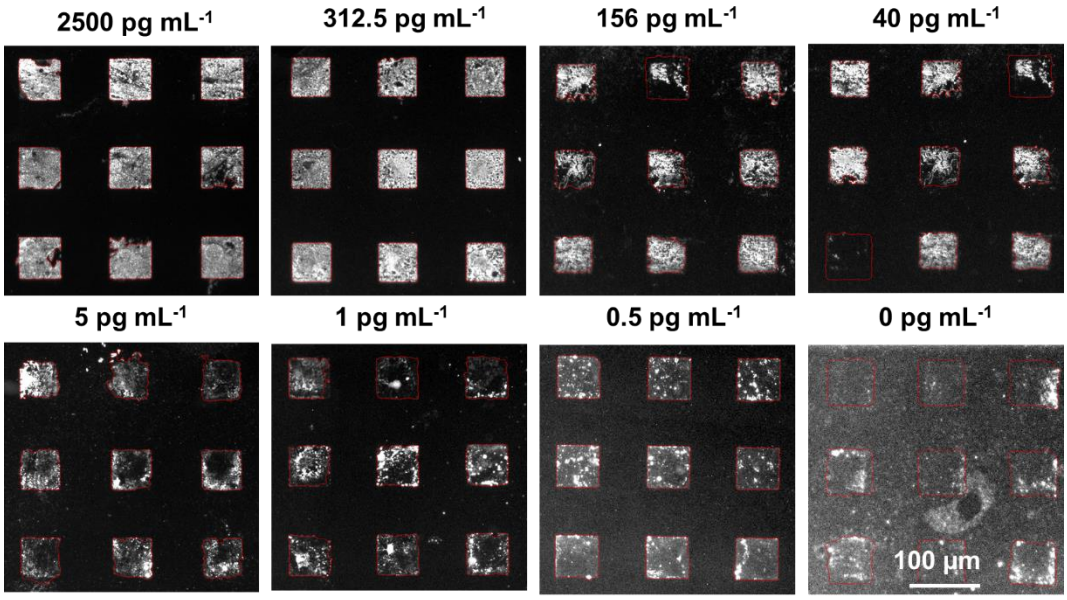

Figure S 5-5. Chan-Vese image segmentation processing of the LIS IL-6 IFA dose response in pg mL^{-1} of buffer.

Table S 5-1. Two-sample T-test assuming unequal variances for buffer LOD significance using Chan-Vese Python MFI values

Raw MFI	*0* pg mL^{-1}	*0.5* pg mL^{-1}
Mean	11543	14000
Observations	18	18
P(T<=t) two-tail	4.06E-18	
t Critical two-tail	2.07	
Background Subtracted MFI	*0* pg mL^{-1}	*0.5* pg mL^{-1}
Mean	106	793
Observations	18	18
P(T<=t) two-tail	2.47E-10	
t Critical two-tail	2.05	

Table S 5-2. Two-sample T-test assuming unequal variances for plasma LOD significance using FiJi ImageJ processing

Raw MFI	*0* pg mL^{-1}	*0.5* pg mL^{-1}
Mean	11350	14537
Observations	18	18
P(T<=t) two-tail	2.99E-20	
t Critical two-tail	2.04	
Background Subtracted MFI	*0* pg mL^{-1}	*0.5* pg mL^{-1}
Mean	338	1207
Observations	18	18
P(T<=t) two-tail	1.07E-06	
t Critical two-tail	2.04	

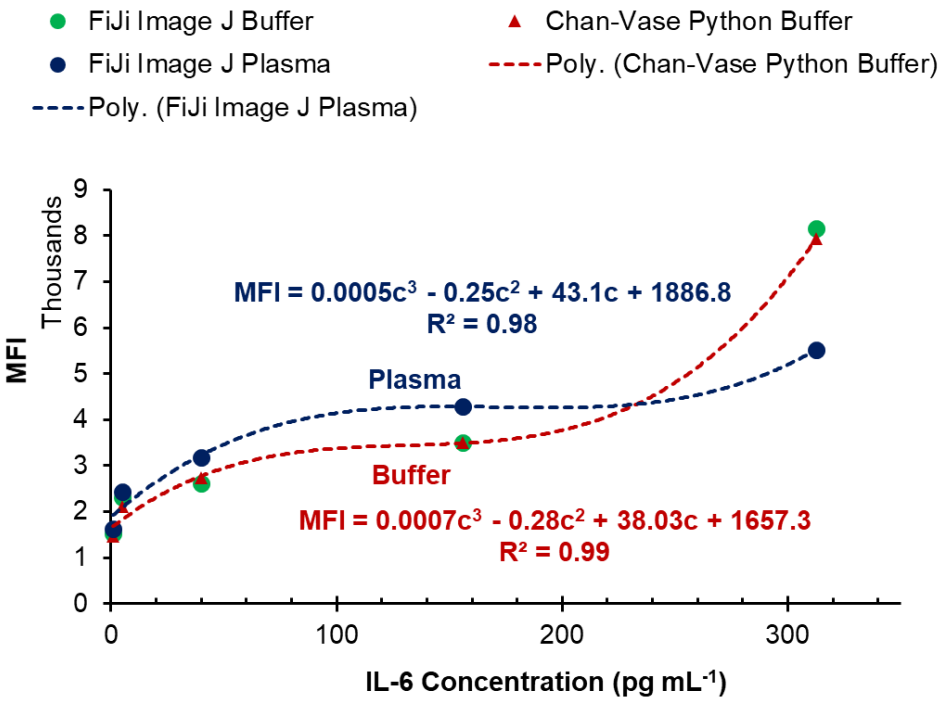

Figure S 5-6. Dose response curves of the LIS IL-6 IFA . Graphical data are shown as mean (n = 18 replicates) fitted by a quadratic trendline with goodness of fit $R^2 \geq 0.99$ for buffer and ≥ 0.98 for plasma. Reportable range is 1 – 312.5 pg mL^{-1}. There is a significant difference between the LOD of 0.5 and zero concentration with $P < 0.0005$. In the inset equations, c is the IL-6 concentration in pg mL^{-1}.

Table S 5-3. Comparison of our developed IL-6 biosensor with previously reported strategies

Ref.	*Method*	*Advantages*	*Disadvantages*	*LOD[a)]*	*Sample*
[1]	Surface plasmon resonance using a sandwich type immunoassay	The cell culture medium could be analyzed directly without any prior procedures.	Poor LOD and low sensitivity	1300	Cell media
[2]	Electrochemical immunosensor using CNTs	High sensitivity and good reproducibility	Complexity and time-consuming production, no LOD was shown in plasma	0.5	Calf serum
[3]	Chemiluminescence immunoassay combining ELISA and bis (2,4,6-trichlorophenyl) oxalate–hydrogen peroxide based CL	Good specificity and high emission intensity	Time consuming assay, lack of good sensitivity in complex biofluids	0.5	Buffer
[4]	Chemiluminescence assay using gold nanoparticles	Improved linear range and loading capability of the assay, good sensitivity	Complex design, low sensitivity in complex fluids	0.5	Buffer
[5]	Electrochemical sensor using polyelectrolyte, ferrocene and $CaCO_3$ nanoparticles	Good sensitivity and good reproducibility	Complex design, low sensitivity in complex fluids, 100 pg/ml IL-6 in serum was the lowest concentration shown with good recovery	1	Buffer
[6]	Localized SPR-based microfluidic optical biosensor	Rapid, capable of performing multiplex and low volume assays.	No LOD was assigned for biofluids	11.29	Buffer
[7]	Immunofluorescence assay using core-shell nanoparticles	Simplicity and reproducibility	Low sensitivity, use of beads	7	Buffer
[8]	Microfluidic immunoassay combined with the streptavidin-biotin-peroxidase (SA-B-HRP) nanocomplex-signal amplification system	Good sensitivity and linear dynamic range, good selectivity	Incapable of detecting IL-6 in complex biofluids (e.g. plasma)	1	Buffer

[9]	Electronic detection using liquid-gated field-effect transistor (FET) sensors and CNTs	Good stability and sensitivity	Incapable of detecting IL-6 in unprocessed biofluids. Detection only showed in 100 times diluted serum	1.37	Buffer
[10]	Sandwich-based IFA using gold nanoparticle modified silica optical fibers	Requires low sample volume, capable of spatially localized cytokine detection	Complex design, incapable of detecting IL-6 in complex fluids	1	Buffer
[11]	Electrochemical immunosensor using supersandwich multienzyme–DNA label	Very high sensitivity and low LOD in buffer	Complex design, Lack of sensitivity in complex biofluids	0.05	Buffer
[12]	Photoelectrochemical sensing using $LaFeO_3$ NPs deposited on FTO glass	Very low LOD in buffer	Lack of sensitivity in complex biofluids. 100 pg/ml in serum was the lowest detection trial done in the paper.	0.033	Buffer
[13]	Electrochemical aptasensor using a composite of polypyrrole and gold nanoparticles	High sensitivity in buffer, high analytical range	The device functionality in unprocessed biofluids is not shown	0.33	Buffer
[14]	Electrochemical sensor using porous composite of BSA, AuNWs, and CNTs or AuNPs	Good sensitivity and stability in complex liquids	Complex design	23	Plasma
This work	LIS-IFA using patterned capture antibodies on a functional lubricant infused surface	Low cost and simple design, low LOD in complex biofluids, ability to multiplex detection for high-throughput applications	Relatively longer time of detection due to using well plates. Can be improved in the future using microfluidic based assays	0.5	Plasma and Buffer

[a)]LOD is in pg mL^{-1}

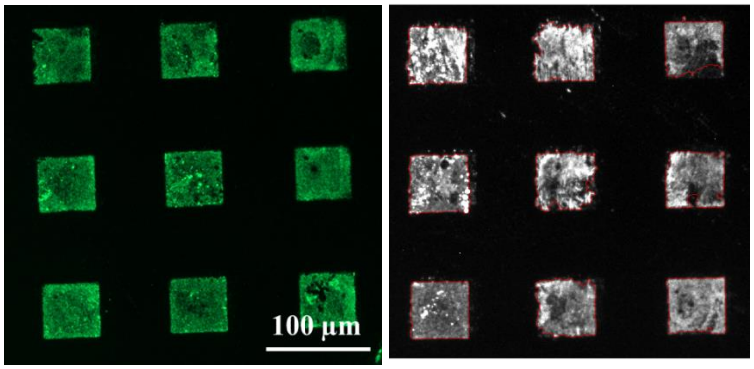

Figure S 5-7. Fluorescence microscopy image of IL-6 IFA patterns captured from recalcified citrated blood at the concentration of 312.5 pg mL^{-1} before and after Chan-Vese image segmentation processing. Recovery of the spiked sample (n =9 replicates) on the plasma standard curve was 119.4% indicating the functionality of LIS-IFA for detection of IL-6 in whole blood.

References

[1] T.-H. Chou, C.-Y. Chuang, C.-M. Wu, Cytokine 2010, 51, 107.

[2] R. Malhotra, V. Patel, J. P. Vaque, J. S. Gutkind, J. F. Rusling, J. P. Vaqué, J. S. Gutkind, J. F. Rusling, Anal. Chem. 2010, 82, 3118.

[3] L. Luo, Z. Zhang, L. Hou, J. Wang, W. Tian, Talanta 2007, 72, 1293.

[4] L. Luo, Z. Zhang, L. Hou, Anal. Chim. Acta 2007, 584, 106.

[5] T. Li, M. Yang, Sensors Actuators B Chem. 2011, 158, 361.

[6] P. Chen, M. T. Chung, W. McHugh, R. Nidetz, Y. Li, J. Fu, T. T. Cornell, T. P. Shanley, K. Kurabayashi, ACS Nano 2015, 9, 4173.

[7] X. Hun, Z. Zhang, Biosens. Bioelectron. 2007, 22, 2743.

[8] J. Wu, Y. Chen, M. Yang, Y. Wang, C. Zhang, M. Yang, J. Sun, M. Xie, X. Jiang, Anal. Chim. Acta 2017, 982, 138.

[9] H. Chen, T. K. Choo, J. Huang, Y. Wang, Y. Liu, M. Platt, A. Palaniappan, B. Liedberg, A. I. Y. Tok, Mater. Des. 2016, 90, 852.

[10] G. Liu, K. Zhang, A. Nadort, M. R. Hutchinson, E. M. Goldys, ACS Sensors 2017, 2, 218.

[11] G. Wang, H. Huang, B. Wang, X. Zhang, L. Wang, Chem. Commun. 2012, 48, 720.

[12] X. P. Liu, X. L. Xie, Y. P. Wei, C. jie Mao, J. S. Chen, H. L. Niu, J. M. Song, B. K. Jin, Microchim. Acta 2018, 185, 52.

[13] M. Tertiş, B. Ciui, M. Suciu, R. Săndulescu, C. Cristea, Electrochim. Acta 2017, 258, 1208.

[14] J. Sabaté del Río, O. Y. F. Henry, P. Jolly, D. E. Ingber, Nat. Nanotechnol. 2019, 14, 1143.

Chapter 6: Conclusions and Future Direction

6.1 Conclusions and contributions to knowledge

In this thesis, new surface functionalization techniques were described to create durable coatings amenable for biological and environmental applications such as self-cleaning systems, microfluidic cell culturing, biomolecule patterning, as well as biosensors and diagnostics. We showed that these strategies could result in covalent attachment of biomolecules and amine-conjugated nanoparticles while preserving the functionality of the immobilized entities. Covalent immobilization can promote robustness and durability of the final products, which are highly beneficial for long-term applications in harsh environmental conditions. In comparison to the reported biofunctionalization techniques, the introduced methods in this thesis do not require several wet chemistry steps and incubation times, making them more straightforward and expeditious for commercialization and scale-up manufacturing. We demonstrated that the new strategies are applicable to a variety of substrates including glass, PDMS, PMMA, and ceramic tiles. Moreover, one could use them to create micropatterns of different biomolecules covalently bound to the surface using simple microcontact printing techniques. Patterning the biomolecules is highly advantageous for high throughput applications and multiplex detections in biosensing industries. Furthermore, our novel techniques allow for covalent immobilization of antibody microarrays on lubricant-

infused surfaces (LISs). The presence of LISs could effectively suppress the non-specific adhesion of bio-species while the immobilized antibody can specifically capture the biomarker of interest. This led to an extraordinary sensitivity in detecting a very low molecular weight cytokine, namely interleukin 6, in complex biofluids such as human whole blood and plasma.

6.2 Recommendations for future work

Due to the versatile nature of our new biofunctionalization methods, they can be applied on different substrates for various applications. For instance, we recommend using our strategies for covalent immobilization of TiO_2 particles doped with elements such as nickel on different medical surfaces as well as other surfaces prone to be touched by public such as doorknobs, desks, workstations, and commonly touched surfaces in public transportation systems. As the doped TiO_2 particles possess photocatalytic activity in ambient light, it can annihilate viruses and bacteria resulting in durable antiviral and antibacterial coatings. Particularly, considering the ongoing COVID-19 pandemic which has recently become a serious global issue, the coated surfaces can effectively suppress rapid spread of coronavirus by preventing cross-contamination through the surfaces. To coat the already built-in substrates, we recommend plasma treating them by handheld plasma pens that could easily be transported to many different places, followed by spraying the functional particles onto the surfaces.

Moreover, in microfluidic devices, our surface functionalization technique can be used for cell culture and organs-on-chip applications, as well as cell patterning for high throughput studies such as effects of a drug on different cell lines. It could also be employed for investigating the effect of strong physiological forces on proteins activity in the microfluidic channels as high shear stresses do not lead to detachment of the biomolecules from the channel owing to our covalent immobilization techniques. In addition, the new micropatterning techniques could be utilized to create arrays of capture antibodies or DNAs on flexible surfaces embedded in food packages or wearable devices for detection of different bacterial and contamination. Furthermore, since the new biofunctional LISs could enable us to precisely detect IL-6 with, similar biosensing strategies could be used to detect other types biomarkers from patients' unprocessed blood or plasma making the whole detection process rapid and straightforward. Due to the capability of micropatterning, we also suggest multiplex detection of different analytes with the same platform to further expedite the process and enhance its efficacy.

We also recommend that the interested researchers examine combination of our new strategies to obtain some unique surface properties. For instance, the new antibody micropatterned on LISs strategy could be integrated with microfluidic functionalization technique to form a highly efficient biosensor for point-of-care diagnostic applications.

Moreover, immobilization of particles along with cells in microfluidic devices can open doors to further studies on cell biology such as radioembolization of cancer cells via radioactive particles. Combination of TiO_2 immobilization strategy with LISs could also result in a more efficient antiviral surfaces that are able to not only repel viruses but also annihilate them.

APPENDIX A

BIOMICROFLUIDICS **11**, 044111 (2017)

Generating 2-dimensional concentration gradients of biomolecules using a simple microfluidic design

Amid Shakeri,[1] Nick Sun,[1] Maryam Badv,[2] and Tohid F. Didar[1,2,a)]
[1]*Department of Mechanical Engineering, McMaster University, 1280 Main Street West, Hamilton, Ontario L8S 4L7, Canada*
[2]*School of Biomedical Engineering, McMaster University, 1280 Main Street West, Hamilton, Ontario L8S 4L8, Canada*

(Received 21 June 2017; accepted 26 July 2017; published online 2 August 2017)

This study reports a microfluidic device for generating 2-dimensional concentration gradients of biomolecules along the width and length of a chamber and conventional 1-dimensional gradients along the width of its lateral parallel channels. The gradient profile can be precisely controlled by the applied flow rate. The proposed design is simple and straightforward, has a small footprint size compared to previously reported devices such as tree-shape designs, and for the first time, provides capability of generating desired 2D and 1D gradients, simultaneously. The finite element simulation analysis proves the feasibility of the microfluidic device, and the fluorescently labelled IgG antibody is used to demonstrate generated chemical gradients. This simple microfluidic device can be implemented for a wide range of high-throughput concentration gradient applications such as chemotaxis, drug screening, and organs-on-chips. *Published by AIP Publishing.* [http://dx.doi.org/10.1063/1.4991550]

I. INTRODUCTION

Generating precise chemical concentration gradients is greatly momentous in several research areas such as cell migration and chemotaxis,[1] cancer metastasis,[2,3] stem cell,[4] drug screening,[5] and microfabrication.[6] From a biological perspective, it is quite challenging to create and control a consistent chemical gradient *in vitro* which can exactly mimic *in vivo* conditions—an enclosed environment introducing minute volumes of biomolecules which can adhere to creeping laminar flow while resisting diffusion forces. However, lab-on-a-chip (LOC) technology represents unique solutions to create stable and controlled gradients of different biomolecules by means of microfluidic principles and has been utilized for several applications such as drug screening and studying cell interactions.[7–12]

The free-diffusion of soluble molecules from the "source" to "sink" is one way to generate concentration gradients in microfluidic devices.[13–16] In this system, concentration gradients evolve as the molecules diffuse along the length of a microfluidic channel or a reservoir connecting source to sink and reach a steady state. These gradient generators are simple and can be used in high throughput applications requiring a low volume of reagents.[17] Nevertheless, gradients usually require a long time to be created inside the microfluidic channel and can be maintained for a limited time since the size of the source and sink is very small in microfluidic systems.[11] External pumping components may be required to address this problem, which brings about the complexity of the system.

Another gradient generation method is based on the diffusion of species across the interface of two adjacent laminar flows inside a microfluidic channel. Many of the flow-based microfluidic gradient generators have been relied on the tree-shape design introduced by Jeon *et al.* in 2000.[18–21] The main limitation of the tree-shape design is its considerably large footprint size

a)Author to whom correspondence should be addressed: didar@mcmaster.ca

which minimizes the space available for the targeted test. Moreover, long diffusion time is required to generate the desired gradient in channels, which limits either the flow rate or the channel length.[22–28]

Although the designs that produce one-dimensional (1D) gradients, a change in the concentration perpendicular to the fluid flow input, have been well established, there are very few studies on microfluidic devices generating two-dimensional (2D) gradients. For instance, Jang *et al.*[29] and Cooksey *et al.*[30] utilized micro-wells and multifaceted tree-shape design, respectively, to achieve microfluidic-based 2D gradient generators. These devices are not only demanding to fabricate but also involve a multilayer control for fluid handling which is complex to operate. Microfluidic devices with 2D chemical gradients could be powerful tools in a wide range of applications such as antibiotic susceptibility testing, characterization of cellular responses, and chemotaxis when high-throughput experiments with a low volume of reagents are required.

Here, we report a simple microfluidic design for generating both 2D and 1D concentration gradients of biomolecules based on the hydrodynamic resistances induced by channel geometries. The proposed design generates two-dimensional gradients of biomolecules across both the width and length of a main chamber which can be well controlled by the applied flow rate. The main chamber seeds five parallel channels with different hydrodynamic resistances. These parallel channels can also produce one-dimensional gradients. Table SI (supplementary material) highlights the novelty and advantages of our microfluidic design in comparison to those already reported in the literature.

II. MATERIALS AND METHODS

The microfluidic device was designed using AutoCAD® software (Autodesk Inc., CA, USA) and printed on a chrome mask. Standard photolithography was then applied to produce an SU-8 based mold on a silicon wafer using the printed mask. Next, soft lithography was applied to create the microfluidic channels on the polydimethylsiloxane (PDMS, Essex Chemical, Boston, MA) substrate. The PDMS layer was peeled off from the mold, and the inlet and outlet ports were punched. The protocol for covalently functionalizing the surface with generated concentration gradients and the assembly of the microfluidic device has been introduced elsewhere.[31,32] Briefly, both PDMS and glass substrates were oxygen plasma treated, and then, (3-Aminopropyl) triethoxysilane (APTES, Sigma-Aldrich) was micro-contact printed onto the glass substrates using a flat PDMS stamp. Instantly, the functionalized glass substrate was kept in contact with the PDMS layer to create irreversible bonds. The platform was then dried at 60 °C, and N-hydroxysuccinimide (NHS, Sigma-Aldrich) together with 1-ethyl-3–(3-dimethylaminopropyl) carbodiimide (EDC, Sigma-Aldrich) and phosphate buffered saline (PBS, Sigma-Aldrich) were used to activate the printed amine groups so as to covalently attach biomolecules onto the surface. To demonstrate generated gradients, fluorescein isothiocyanate (FITC) conjugated-IgG antibody and Cy3 conjugated IgG (Abcam, Cambridge, MA) were flown into the inlets by a multi-stage syringe pump. Furthermore, an inverted fluorescence microscope (ZEISS-Axio Observer Inverted Microscope) was used to image the generated gradients.

COMSOL software (COMSOL Inc., Burlington, MA) was used to perform the finite element simulation analysis. The 3D model of the microfluidic device was designed to process the full scale simulation of the experimental setup. The governing equations used for the computational fluid dynamic (CFD) analysis were Navier-Stokes and continuity equations assuming incompressible steady state conditions

$$\nabla\left[\eta(\nabla \mathrm{u} + (\nabla \mathrm{u}))\right] + \rho(\mathrm{u}.\nabla)\mathrm{u} + \nabla \mathrm{p} = 0, \tag{1}$$

$$\nabla.\mathrm{u} = 0, \tag{2}$$

where u is the velocity field, p is the pressure, η is the dynamic viscosity, and ρ is the liquid density. The fluid inside the channels was assumed to be a Newtonian fluid and to have the physical properties of water.

Species diffusion in the solution was modelled using multi-physics capabilities of COMSOL. The velocity components from the CFD results were simultaneously implemented for concentration distribution using the convection and diffusion module. Species diffusion in flow conditions was solved by applying Eq. (3)

$$\frac{\partial c}{\partial t} + \nabla.(-D\nabla c + cu) = 0, \tag{3}$$

where c represents each species concentration, t is the time, and D is the diffusion coefficient.

III. RESULTS AND DISCUSSION

Figure 1(a) shows the microfluidic design. It begins with two opposite inlet channels which then merge into a single channel perpendicular to the inlet axis. This channel joins the main chamber (1600 μm width $\times$ 800 μm length) which feeds into five parallel channels with different maximum widths as follows: channel 1st = 50 μm, channel 2nd = 100 μm, channel 3rd = 200 μm, channel 4th = 300 μm, and channel 5th = 500 μm. The entrance of all these channels is equal to 50 μm, and the height of all channels and chamber is 60 μm.

The size of the device has been optimized to be a minute footprint size of 4 mm $\times$ 8 mm, allowing us to fabricate a high throughput device by adding replicas of the same design in parallel for high throughput experiments (Fig. S1, supplementary material).

By imposing certain hydrodynamic resistances via 5 parallel channels, the microfluidic device is able to provide 2D gradients in the main chamber and 1D gradients inside channels 4 and 5 (Fig. 3). From the electronic-hydrodynamic analogy, the hydrodynamic resistance (R_h) of a straight microchannel in a laminar incompressible steady state flow with a rectangular cross section can be defined as follows:[33,34]

$$R_h = \frac{12\mu L}{wh^3}\left[1 - \frac{h}{w}\left(\frac{192}{\pi^5}\sum_{(n=1,3,5)}^{\infty}\left[\frac{1}{n^5}\tanh\left(\frac{n\pi w}{2h}\right)\right]\right)\right]^{-1}, \tag{4}$$

where L, w, and h are the length, width, and height of the channel, respectively, and μ is the dynamic viscosity. According to Eq. (4), changing the width of the microchannel results in

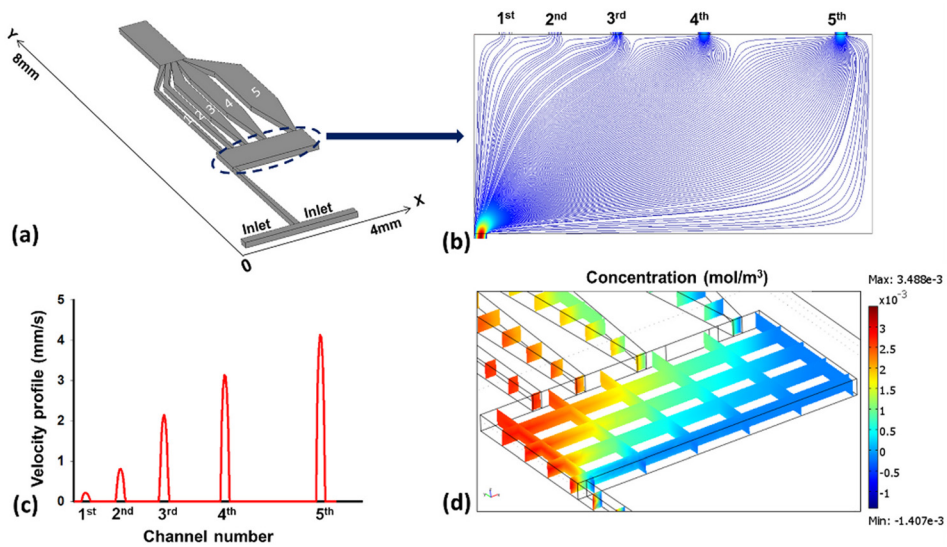

FIG. 1. (a) Schematic representation of the microfluidic design. (b) Simulation results for velocity streamlines throughout the chamber by applying the flow rate of 1 μl min^{-1}. (c) Velocity field at the entrance of the five parallel channels. (d) Simulation results for the concentration gradient inside the main chamber and side channels.

different hydrodynamic resistances. Consequently, in order to achieve the desired hydrodynamic resistance in our microfluidic design, the geometry of the channels was adjusted based on Eq. (4).

A corresponding computational fluid dynamics analysis and simulation of the concentration distribution were performed using COMSOL software. In the simulation process, to generate the 2D gradient, the biomolecule solution and buffer merge into the single channel until they enter the gradient chamber with applying desired flow rates. The biomolecule solution enters the chamber from the side that is furthest to the channel with the lowest resistance.

Figure 1(b) depicts the simulation results for streamlines inside the chamber applying a flow rate of 1 μl/min. It can be seen that the density of streamlines increases at the entrance of the chamber and at the entrance of the 5 parallel channels. Moreover, there is a gradual increase in the streamline density moving from the 1st channel to the 5th channel. The velocity field at the entrance of the five parallel channels is plotted in Fig. 1(c). Each of the parallel channels aspirates the fluid with different flow rates, which brings about the biomolecule distribution inside the chamber and inside the side channels.

Figure 1(d) demonstrates the simulation results for concentration distribution in the microfluidic device. As the width of the channel decreases, the channel hydrodynamic resistance increases. Thus, there is a higher concentration of biomolecules at the entrance of the first channel and the concentration is reduced along the length and width of the chamber due to lower hydrodynamic resistance and more fluid velocity. Moreover, Fig. 1(d) shows 1D gradients in the parallel channels perpendicular to the inlet flow. Furthermore, changing the arrangement and configuration of hydrodynamic resistances in these parallel channels leads to different gradient patterns shown in Figs. S2–S5 (supplementary material).

In addition to the 2D concentration gradient, there is a velocity gradient inside the main chamber as shown in Figs. 2(a) and 2(b) together with their arc-length directions. The directions of X and Y components of the velocity field are based on the coordinate systems shown in Fig. 1(a). According to Fig. 2(a), at the chamber's entrance (shown by a yellow line), there is a high velocity peak, which is due to the inlet flow rate. By getting far from the entrance and approaching the 5 parallel channels, the first sharp velocity peak decreases and other peaks gradually appear along the arc-length direction. Different fluid velocities inside the 5 parallel channels induced by their different hydrodynamic resistances are the main reason for the generation of these new velocity peaks. At the end side of the chamber close to the entrances of the 5 parallel channels, the velocity peaks related to each channel could be readily distinguished. Regarding the velocity pattern along the width directions [Fig. 2(b)], the velocity curve

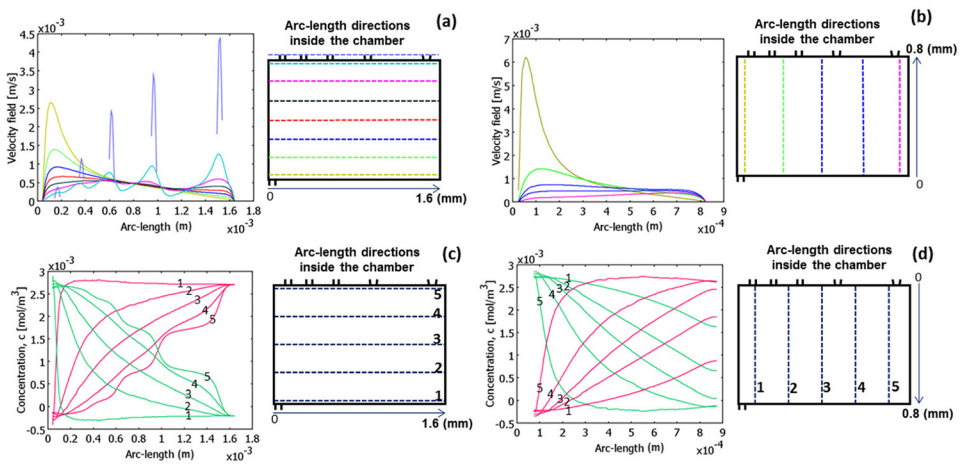

FIG. 2. Simulation results of velocity and concentration gradients. (a) Y-component of velocity fields along represented arc-length directions with different colors (right image) inside the main chamber. (b) X-component of velocity fields along represented arc-length directions (right image). (c) Concentration gradients of two separate biomolecular solutions along the length of the chamber with represented arc-length directions (right image). (d) Concentration gradients along the width of the chamber with represented arc-length directions (right image).

becomes smooth by getting far from the chamber's entrance since there are no channels at the width side of the chamber. Figures 2(c) and 2(d) illustrate the simulation outcome of the concentration along the length and width of the chamber when two different bimolecular solutions (indicated as green and red lines) enter through two opposite inlets of the microfluidic device. These patterns confirm the appropriate 2D concentration gradient of two different biomolecules throughout the chamber.

The CFD analysis was quite analogous to the experimental results demonstrated in Fig. 3. This experiment was performed via employing a FITC conjugated-IgG antibody and PBS solution flown into the microfluidic device through the two opposite inlets. Figures 3(a)–(3d) show the generated 2D gradients of the FITC conjugated IgG antibody inside the chamber at various inlet flow rates. The 3D fluorescence intensities of the generated chemical gradients are plotted in Figs. 3(e)–3(j) for the applied flow rates using Image J software. It is obvious that the inlet flow rate has a substantial effect on the generated gradient's pattern. At high flow rates of 8 and 2 μl min^{-1}, there was a steep slope of reduction in fluorescence intensity along the chamber's diagonal; however, at lower flow rates, the fluorescence intensity decreased more gently. Moreover, there was no significant gradient at a very low flow rate of 0.1 μl min^{-1}. Produced convection in the Y-direction, because of the varying hydrodynamic resistances in parallel channels, is the main factor in the formation of gradients, and the generated gradients could easily be covalently attached to the aminosilanized surface using EDC-NHS chemistry.[32]

The 1D gradients generated in the channels 4 and 5 are shown in Figs. 3(k)–3(p) at different inlet flow rates, and the related intensity diagrams are plotted in Figs. 3(q) and 3(r). The 1D gradient perpendicular to the parallel channel direction is due to the effect of the generated 2D-gradient in the main chamber. At a flow rate of 8 μl min^{-1}, very high fluid velocity of channel 5 caused a very low fluorescence concentration at the very left side of the channel. The generated 1D gradient is more distinct in channel 4 with higher hydrodynamic resistance compared to channel 5. At lower inlet flow rates, the laminar flow rates inside the channel 5 were in an appropriate range to create a 1D gradient. As a proof of concept, we immobilized *Escherichia coli* (ATCC8739) bacteria inside the microfluidic device and demonstrated successful gradient generation using FITC labelled IgG solution (Fig. S6, supplementary material). This provides a powerful tool for performing rapid and high-throughput antibiotic susceptibility tests.

To further demonstrate the design principle, we examined flowing two different fluorescently labelled IgG antibodies from two different inlets. Figure 4 illustrates these results where

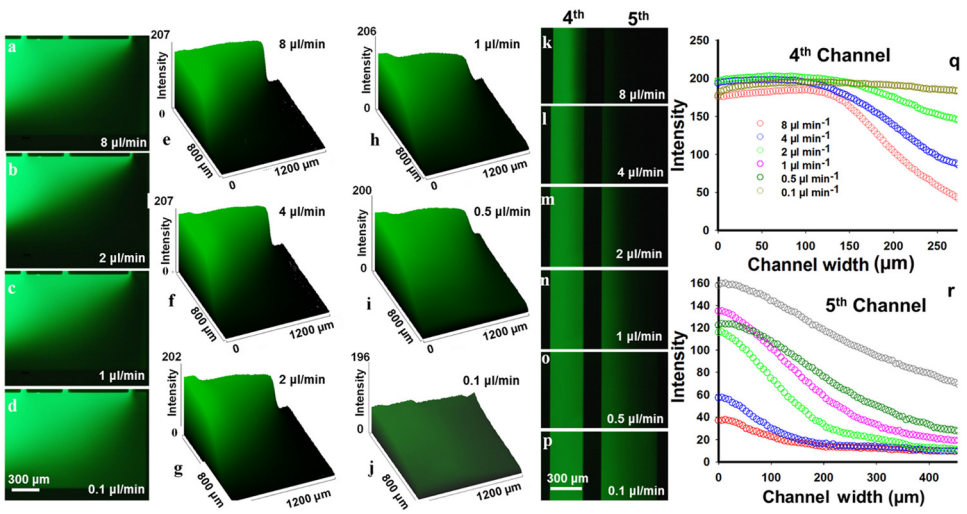

FIG. 3. Fluorescence microscopy results using FITC conjugated IgG at different inlet flow rates. (a)–(d) Generated 2D gradient patterns inside the chamber. (e)–(j) 3D intensity plots quantifying the fluorescence intensity of the 2D concentration gradients in the main chamber. (k)–(p) Generated 1D gradient in channels 4 and 5. (q) and (r) Intensity diagram of channels 4 and 5 as a function of the channel width showing the 1D gradient inside the channels.

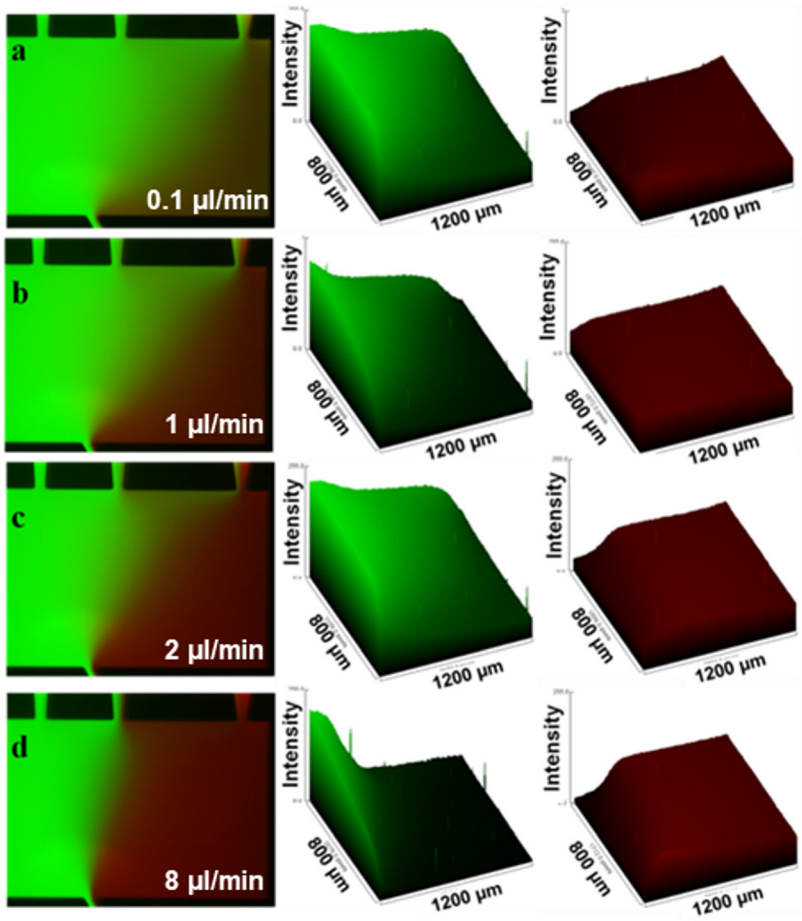

FIG. 4. Generated 2D gradients of FITC conjugated IgG and Cy3 conjugated IgG inside the chamber together with their 3D intensity plots at different inlet flow rates of (a) 0.1 μl min^{-1} (b) 1 μl min^{-1} (c) 2 μl min^{-1} and (d) 8 μl min^{-1}, obtained using Image J software.

FITC conjugated IgG and Cy3 conjugated IgG were flown into the opposite inlets and proceeded to the chamber through the entrance narrow channel as two coflowing streams—the Cy3 conjugated antibody stream on the right and the FITC conjugated antibody on the left side of the entrance channel. In this system, two conjugated antibodies entered the main chamber at the center of the chamber length. The low intensity of red fluorescence determines the minor generated 2D gradients of the Cy3 conjugated IgG, while the FITC conjugated IgG represents well-established 2D gradients, confirming the effect of implemented different hydrodynamic resistances in the design where a smooth 2D gradient is generated towards the channels with lower hydrodynamic resistance. At a flow rate of 8 μl min^{-1}, as the Cy3 conjugated antibody could rapidly reach the low hydrodynamic resistant channels 4 and 5, there is not enough time for antibodies to diffuse, thereby forming a steep concentration gradient pattern. Decreasing the flow rate, however, brought about more gradual 2D concentration gradients throughout the main chamber.

IV. CONCLUSIONS

In conclusion, a simple and straightforward microfluidic design was introduced to generate 2D and 1D gradients of biomolecules. Having remarkably small footprint size, the device is capable of generating two-dimensional concentration gradients throughout its chamber and one-dimensional gradients inside its parallel channels. The simulation results demonstrated the creation of 2D velocity field and particle concentration gradients inside the chamber owing to

various hydrodynamic resistances of the 5 parallel lateral channels. Fluorescence microscopy experiments successfully illustrated different 2D and 1D gradient patterns dependent on the inlet flow rates. Due to its small footprint, several designs can be integrated into a single chip (Fig. S1, supplementary material) for a wide range of high-throughput concentration gradient applications such as antibiotic susceptibility tests, chemotaxis, drug screening, and organs-on-chips where 2D or 1D chemical gradients of biomolecules are needed.

SUPPLEMENTARY MATERIAL

See supplementary material for more information on the proposed microfluidic design and other microfluidic gradient generators already published in the literature.

ACKNOWLEDGMENTS

The financial support for this work was provided by the Natural Science and Engineering Research Council of Canada (NSERC) Discovery Grant and start-up funds from McMaster Faculty of Engineering.

[1]N. L. Jeon, H. Baskaran, S. K. W. Dertinger, G. M. Whitesides, L. Van De Water, and M. Toner, Nat. Biotechnol. **20**, 826 (2002).
[2]S.-J. Wang, W. Saadi, F. Lin, C. M.-C. Nguyen, and N. Li Jeon, Exp. Cell Res. **300**, 180 (2004).
[3]W. Saadi, S.-J. Wang, F. Lin, and N. L. Jeon, Biomed. Microdevices **8**, 109 (2006).
[4]B. G. Chung, L. A. Flanagan, S. W. Rhee, P. H. Schwartz, A. P. Lee, E. S. Monuki, and N. L. Jeon, Lab Chip **5**, 401 (2005).
[5]B. Hong, P. Xue, Y. Wu, J. Bao, Y. J. Chuah, and Y. Kang, Biomed. Microdevices **18**, 21 (2016).
[6]P. J. A. Kenis, R. F. Ismagilov, S. Takayama, G. M. Whitesides, S. Li, and H. S. White, Acc. Chem. Res. **33**, 841 (2000).
[7]D. Barata, C. Van Blitterswijk, and P. Habibovic, Acta Biomater. **34**, 1 (2016).
[8]G. Du, Q. Fang, and J. M. J. den Toonder, Anal. Chim. Acta **903**, 36 (2016).
[9]S. Halldorsson, E. Lucumi, R. Gómez-Sjöberg, and R. M. T. Fleming, Biosens. Bioelectron. **63**, 218 (2015).
[10]Y. Du, J. Shim, M. Vidula, M. J. Hancock, E. Lo, B. G. Chung, J. T. Borenstein, M. Khabiry, D. M. Cropek, and A. Khademhosseini, Lab Chip **9**, 761 (2009).
[11]S. Kim, H. J. Kim, and N. L. Jeon, Integr. Biol. **2**, 584 (2010).
[12]A. G. G. Toh, Z. P. Wang, C. Yang, and N. T. Nguyen, Microfluid. Nanofluid. **16**, 1 (2014).
[13]V. V. Abhyankar, M. A. Lokuta, A. Huttenlocher, and D. J. Beebe, Lab Chip **6**, 389 (2006).
[14]H. Wu, B. Huang, and R. N. Zare, J. Am. Chem. Soc. **128**, 4194 (2006).
[15]Y. Saka, M. Macpherson, and C. V. Giuraniuc, Physica A **470**, 132 (2017).
[16]X. Luo, T. Vo, F. Jambi, P. Pham, and J. S. Choy, Lab Chip **16**, 3815 (2016).
[17]J. Atencia, J. Morrow, and L. E. Locascio, Lab Chip **9**, 2707 (2009).
[18]N. L. Jeon, S. K. W. Dertinger, D. T. Chiu, I. S. Choi, A. D. Stroock, and G. Whitesides, Langmuir **16**, 8311 (2000).
[19]X. Chen, D. Wu, X. Mei, Z. Zhou, L. Wang, Y. Zhao, G. Zheng, and D. Sun, in *2016 IEEE 10th International Conference on Nano/Molecular Medicine and Engineering* (2016), pp. 104–108.
[20]K.-Y. Ko and I.-H. Kim, Biotechnol. Bioprocess Eng. **21**, 453 (2016).
[21]H. Wang, C. Chen, Z. Xiang, M. Wang, and C. Lee, Lab Chip **15**, 1445 (2015).
[22]X. Shi, S. Ostrovidov, Y. Shu, X. Liang, K. Nakajima, H. Wu, and A. Khademhosseini, Langmuir **30**, 832 (2014).
[23]J. Ruan, L. Wang, M. Xu, D. Cui, X. Zhou, and D. Liu, Mater. Sci. Eng. C **29**, 674 (2009).
[24]P. J. Hung, P. J. Lee, P. Sabounchi, R. Lin, and L. P. Lee, Biotechnol. Bioeng. **89**, 1 (2005).
[25]S. Park, D. Kim, R. J. Mitchell, and T. Kim, Lab Chip **11**, 2916 (2011).
[26]H. J. Yoo, J. Park, and T. H. Yoon, Cytometry, Part A **83**, 356 (2013).
[27]K. Campbell and A. Groisman, Lab Chip **7**, 264 (2007).
[28]S. K. W. Dertinger, X. Jiang, Z. Li, V. N. Murthy, and G. M. Whitesides, Proc. Natl. Acad. Sci. U.S.A. **99**, 12542 (2002).
[29]Y.-H. Jang, M. J. Hancock, S. B. Kim, S. Selimović, W. Y. Sim, H. Bae, and A. Khademhosseini, Lab Chip **11**, 3277 (2011).
[30]G. A. Cooksey, C. G. Sip, and A. Folch, Lab Chip **9**, 417 (2009).
[31]T. F. Didar and M. Tabrizian, Lab Chip **12**, 4363 (2012).
[32]T. F. Didar, A. M. Foudeh, and M. Tabrizian, Anal. Chem. **84**, 1012 (2012).
[33]K. W. Oh, K. Lee, B. Ahn, and E. P. Furlani, Lab Chip **12**, 515 (2012).
[34]D. J. Beebe, G. A. Mensing, and G. M. Walker, Annu. Rev. Biomed. Eng. **4**, 261 (2002).

APPENDIX B

Biofunctional interfaces for cell culture in microfluidic devices

26

Amid Shakeri[1], Sara Rahmani[2], Sara M. Imani[2], Matthew Osborne[2], Hanie Yousefi[1,3] and Tohid F. Didar[1,2,]*

[1]Department of Mechanical Engineering, McMaster University, Hamilton, ON, Canada,
[2]School of Biomedical Engineering, McMaster University, Hamilton, ON, Canada,
[3]Department of Chemical Engineering, McMaster University, Hamilton, ON, Canada

Introduction

In vivo, there is a continuous spatially and temporally organized cross-talk between cells and their surrounding environment, consisting mainly of an underlying extracellular matrix (ECM), neighboring cells, and soluble factors (Abbott, 2003; Cartwright et al., 2016; El-Ali, Sorger, & Jensen, 2006; García, 2005; Hui & Bhatia, 2007). However, conventional cell culture models maintain cells in a static environment with very limited cell−cell interactions (El-Ali et al., 2006). Various technologies have emerged to develop more physiologically relevant microenvironments for cell cultures, among which microfluidic devices offer a microscale cell culture environment that more precisely resembles that of in vivo. The advantages of microfluidic devices over other three-dimensional (3D) cell culture models can be attributed not only to their size, elasticity, and microstructure but also to their ability to promote the continuous perfusion of media, which allows for the transferring of nutrient and chemical cues to the cells while removing waste products (Bauer, Su, Beebe, & Friedl, 2010; Meyvantsson & Beebe, 2008; Whitesides, 2006). Microfluidic devices offer a spatially and temporally well-controlled 3D microscaled environment for cell cultures that closely resembles the in vivo microenvironment. The 3D microstructure, perfusion of laminar flow, and the precise control over the microenvironment of the microfluidic channel promote cell−cell, cell−matrix, and cell−soluble factor interaction and functionality (Young & Beebe, 2010). The microenvironment is defined by the local chemical and mechanical characteristics present in the direct surroundings of the cells. The chemical cues are supplied by the cell medium and its soluble factors in addition to the underlying matrix. On the other hand, the mechanical cues are induced from the culture matrix as well as the shear forces exerted via the surrounding flow. Microfluidic devices create a platform to locally and dynamically control both these parameters (Li, Veres, Didar, & Tabrizian, 2016; Meyvantsson & Beebe, 2008).

* Corresponding author: didart@mcmaster.ca

Bioelectronics and Medical Devices. DOI: https://doi.org/10.1016/B978-0-08-102420-1.00033-9

Microfluidic-based devices offer new avenues for quantitative and fundamental biological studies including the manipulation and analysis of cultured cells. Additionally, advanced technology allows for the incorporation of on-chip sensors, detectors, and optical components, which facilitate the performance of cell culture, cell sorting, and biological assays on one chip.

Cross-linked polydimethylsiloxane (PDMS) is the most common material used to fabricate microfluidic devices as it provides high fidelity and feature resolution (Villegas, Cetinic, Shakeri, & Didar, 2018). PDMS is permeable to air and water and is transparent to ultraviolet (UV) light and visible light. Cured PDMS is compatible with cells; however, unmodified PDMS is hydrophobic, which restricts direct cell attachment and growth (Annabi et al., 2013). To address this shortcoming, various techniques have been adopted to induce hydrophilicity to PDMS to facilitate its application in cell culture.

The purpose of surface coating and functionalization is to engineer chemically reactive groups on surfaces such as PDMS-based microfluidic channels to increase the binding affinity and immobilization of the cells and small biomolecules within the channel (Khetani & Bhatia, 2008; Yousefi, Ali, Su, Filipe, & Didar, 2018). To prepare the surface of the channels for cell cultivation, different surface coating and functionalization strategies have been developed to modify the surfaces for cell culture applications (Annabi et al., 2013; Meyvantsson & Beebe, 2008).

In this section, we will give a brief overview of various surface functionalization and modification techniques within a channel of the microfluidic devices in order to prepare the surface for cell culture applications.

Approaches for creating biofunctional interfaces in microfluidics

Plasma treatment

Plasma treatment is being widely used to enhance physical and chemical characteristics of different surfaces such as glass and polymer. These characteristics are wettability, adhesion properties, and printability, as well as introducing new chemical groups to the surfaces (Notsu, Fukazawa, Tatsuma, Tryk, & Fujishima, 2001; Ozdemir, Yurteri, & Sadikoglu, 1999). Plasma treatment can be facilitated to gases such as Ar, N_2, O_2, NH_3, CO_2, and CF4 and can have the ability to insert or substitute chemical functionalities onto a substrate. These methods can also create radicals for cross-linking or subsequent surface modification. Recently, plasma-based approaches have gained considerable attention as they can be used in the creation of surfaces that can be in contact with biological samples, which are called biointerfaces (Siow, Britcher, Kumar, & Griesser, 2006). An important group of biointerfaces are the silane-based surfaces that are generally made of immobilizations of a silane group on plasma-treated substrates. Based on the silane molecule's design, the surfaces can have different characteristics such as

hydrophobicity and low nonspecific attachments. Depending on different plasma processes' conditions, such as the gas type, substrates, and process conditions, various reactions such as deposition, substitution, or etching can be done on the surfaces while silane-treating them (Inagaki, 1996). O_2, and CO_2 plasma treatments are commonly used methods that provide the treated surfaces with hydroxyl, aldehyde, and carboxylic groups (Landgraf, Kaiser, Posseckardt, Adolphi, & Fischer, 2009; Terlingen, Gerritsen, Hoffman, & Feijen, 1995). Amine-containing surfaces can be prepared with two methods: ammonia plasma treatment or by the plasma polymerization of alkylamine monomers. Although there are some reports of utilizing amine modified surfaces for cell colonisations (Griesser, Chatelier, Gengenbach, Johnson, & Steele, 1994), the large majority of literature introduces them as reactive surfaces for the covalent immobilization of other biologically active molecules (Dai et al., 2000). Plasma-carboxylated surfaces are another group of these surfaces. They have been found to be good options for immobilization for some anchorage-dependent cell lines (Daw, Brook et al., 1998; Haddow et al., 1999). Many different methods have been used with the goal of creating COOH groups on various substrates. The most common methods are plasma treatment with CO_2 or CO as of ease of functionalization and low prices (Inagaki, Tasaka, & Hibi, 1992; Ko, Lin, & Cooper, 1993). The COOH percentage on the surfaces can be controlled with plasma conditions. Also, there are some works done to prevent the dissolution of the plasma-treated regions in solutions (Daw, Candan et al., 1998). The ability to decrease dissolution is important, as it can prevent nonspecific binding to the substrate during cell adhesion or protein adsorption studies. Carboxylate copolymer surfaces have shown excellent ability to support the colonization of some human cell lines of clinical interest. Immobilization of proteins onto plasma-carboxylated surfaces is also well established. Moreover, hydroxy groups can be formed on the surfaces with O_2 plasma treatment. Hydroxy-coated surfaces have also been used for cell colonization (Dai et al., 2000; Hou, Hu, Park, & Lee, 2012). Although reductive amination of aldehyde surfaces is an attractive interfacial immobilization chemistry, in contrast to the various use of carboxy surfaces, there are a few reports on using plasma-fabricated aldehyde surfaces. Several bioactive molecules or spacer groups have been successfully grafted onto aldehyde groups on plasma polymers (Gong, Dai, Griesser, & Mau, 2000; Kühn, Weidner, Decker, Ghode, & Friedrich, 1999). These functional groups can be used to create self-assembled monolayers (SAMs) of different coatings that can be used in many cell culture applications, especially when nonspecific binding is important. These reactive surfaces are highly compatible with many chemical reactions for grafting of biomaterials to take advantage of their functional amine, carboxy, hydroxy, and aldehyde groups. Many bioactive moieties such as enzymes, antibodies, proteins, and glycosaminoglycans are shown to be successfully immobilized on plasma-treated surfaces (Delorme, Bardeau, Bulou, & Poncin-Epaillard, 2006). Specifically, these surface chemistries perform high biocompatibility for cell colonization, while the effectiveness seems to depend on the process gas and the plasma conditions.

Silanization

One of the most promising approaches to covalently bond a biospecies to a substrate is use of silane coupling agents. These agents could be readily deposited onto various substrates such as silicon wafers, PDMS, glass, and aluminum surfaces, where the hydroxyl groups on the surface can react with chemically active groups of the silane agent such as methoxysilane or chlorosilanes (Hoque, Derose, Hoffmann, Bhushan, & Mathieu, 2007; Krasnoslobodtsev & Smirnov, 2002; Ofner et al., 2017; Santini et al., 2017; Torres, Eland, Redfern, & Hedley, 2017) to create a crystalline or semicrystalline single molecular layer, called SAM, on the surfaces (Hosseini et al., 2018). A silane SAM comprises three parts: a head group that chemically reacts with the substrate leading to chemisorption of the silane agent to the substrate, a tail group that remains functional so as to covalently bond to the desired biomolecules and/or provides the substrate with appropriate chemical and physical properties, and a spacer (backbone) chain group linking the head and tale groups.

The silane head groups go through hydrolysis and condensation reactions and anchor the molecules to the substrate by means of oxane (Si_3O_3M) bond formation (Kango et al., 2013). The substrate−adsorbate interactions together with molecule−solvent interactions (in wet-chemical methods), nonbonded interactions between adsorbates, and intramolecular interactions can control the kinetics of the SAM formation (Cheng & Hu, 2012). The spacer chains, on the other hand, can interact with one another via nonbonded interactions such as van der Waals, steric, repulsive, and electrostatic forces (Cheng & Hu, 2012; Kind & Wöll, 2009; Sellers, Ulman, Shnidman, & Eilers, 1993). The packing and ordering of the SAMs is attributed to the chemisorption of the adsorbate as well as intra- and interchain interactions contributing to the stability and mechanical properties of the SAM (Kind & Wöll, 2009; Sellers et al., 1993; Wang, Liechti, Wang, & White, 2005). Other parameters including ambient humidity and temperature and the presence of impurities can also play a role.

Silane SAMs have several advantages such as mechanical robustness, thermal stability at temperatures up to 250°C, and immunity from swelling in the presence of solvents (Ding, Wong, & Yang, 2006; Helmy & Fadeev, 2002; Srinivasan, Houston, Howe, & Maboudian, 1998). More importantly, the distinct advantage of the silane SAM is its capability to create covalent bonds between the ligand of interest and the substrate where SAMs are used for biofunctionalization approaches. This comes in handy in microfluidic systems especially when biochemical assays should be carried out in harsh environment and under high shear rates, which can potentially detach any nonspecific and noncovalent interactions, thereby deteriorating the efficiency of the immunoassay.

Depending on the number of hydrolysable groups of the silane coupling agent, the topology of the silane SAMs can vary. Silane agents comprising one hydrolysable group can only create one oxane bond at the head group, while silane agents possessing two or three hydrolysable groups can undergo lateral siloxane (Si_3O_3Si) polymerization in addition to the possible multiple bonds formed with the substrate.

It has been shown that the trifunctional silane generally result in more ordered and packed SAM (Brzoska, Azouz, & Rondelez, 1994; Parikh, Allara, Azouz, & Rondelez, 1994). It is worth mentioning that although the trifunctional silanes possess three head groups, all of which can chemisorb to the hydroxyl groups of the surface, the reaction is usually incomplete. Since only reasonable values of bond lengths and angles of the silanol (Si_3OH) bonds can take, it is sometimes impossible for silane agents to bond to the substrate with all head groups, considering the fixed positions of the hydroxyl groups on a flat surface. One drawback to trifunctional silanes is that polycondensation of the hydrolyzed silanes may result in thick and rough final silane SAMs as well, if the hydrolyzation and condensation process is not delicately controlled (Dugas & Chevalier, 2003).

There are two models proposed for the formation of SAMs via di- or trifunctional silanes. In the continuous growth model, the well-ordered SAM is gradually formed out of a liquidlike disordered film. In the second model, distinct areas (islands) of SAM are first formed and then the islands grow until they reach each other and create a single uniform layer on the surface (Krasnoslobodtsev & Smirnov, 2002). Water content is a decisive factor in SAM preparation in such a way that the more the water content is, the more the silane polymerization is performed inside solution before deposition onto the surface causing island growth of SAM rather than continues growth (Krasnoslobodtsev & Smirnov, 2002; Vallant et al., 1998). Furthermore, other ambient parameters such as temperature and contaminants can also affect the formation of SAMs (Lessel et al., 2015).

There are a considerable number of silane coupling agents used in microfluidics including trimethoxysilane-based silanes such as 3-methacryloxypropyltrimethoxysilane (MEMO) (Nie et al., 2007; Xu, Takai, Konno, & Ishihara, 2007), 3-aminopropyltrimethoxysilane (APTMS) (Séguin, McLachlan, Norton, & Lagugné-Labarthet, 2010; Zhang, Zhao, & Xiao, 2009), 3-isocyanatopropyltrimethoxysilane (Baker, Sriram, & Miller, 2015), 3-mercaptopropyltrimethoxysilane (MPS) (Chen et al., 2010; Cheng et al., 2007; Wu et al., 2015; Xue et al., 2011), as well as triethoxysilane-based silanes such as 3-aminopropyltriethoxysilane (APTES) (Kim, Jensen, Megens, Boser, & Mathies, 2011; Tan & Desai, 2004; Wu, Zhao, Dai, Qin, & Lin, 2006; Zhang, Crozatier, Le Berre, & Chen, 2005).

APTES and APTMS are two of the most frequently used silane agents for functionalizing the surfaces and introducing amino groups, which is required to immobilize biomolecules (Didar et al., 2015). Both silane coupling agents have the same tail and spacer chain groups, but with two different head groups. This leads to release of ethanol and methanol as the products given by hydrolysis of APTES and APTMS, respectively. Usually, substrates are required to be pretreated before APTES or APTMS treatment so as induce hydroxyl (−OH) groups onto the surface. Typical ways to hydroxylate the surface include piranha etching (mixture of sulfuric acid and hydrogen peroxide), oxygen plasma treatment, UV irradiation (photooxidation), as well as UV with ozone (Glass, Tjeung, Chan, Yeo, & Friend, 2011; Kim et al., 2011; Tan & Desai, 2004). These methods are compatible with various substrates, however, in case of soft polymers, piranha solution may bring about significant corrosion, and plasma treatment or UV photooxidation may result in creation

of cracks, pitches, and overoxidized products (Yang & Yang, 2014). After the hydroxylation process, rinsing surfaces with deionized water could be beneficial for making the surfaces fully hydroxylated (Glass et al., 2011).

Subsequent to the hydroxylation step, APTES or APTMS monolayers are deposited using either chemical vapor deposition (CVD) or liquid phase deposition (LPD) method. LPD is the most widely used method due to its simplicity and low setup cost (Glass et al., 2011; Shakeri et al., 2018). This method comprises dilution of the silane agent in a proper solvent to usually obtain the final concentration of ~1 to ~5 vol.%. The common solvents for APTES and APTMS include toluene, ethanol, water, and acetone (Diéguez, Winter, Pocock, Bremmell, & Thierry, 2015; Jain et al., 2016; Sang, Chou, Pan, & Sheu, 2016; Tan et al., 2017). In order to perform the silanization, one could simply submerge the substrates inside the silane solution or perfuse the solution through the channels for microfluidic systems. The incubation time usually varies between ~20 minutes to a couple of hours depending on concentrations and substrates. Finally, the surfaces should be rinsed with either deionized water, toluene, methanol, 70% ethanol, or 100% ethanol (Fig. 26.1).

In the LPD method, the trace of water becomes a decisive factor. In many cases, excess amount of water induces rapid self-polymerization of the silane agent forming a disordered and irregular silane layer (Hu, Noda, Okubo, Yamaguchi, & Komiyama, 2001; Liu, Wang, Liu, & Bao, 2008). On the other hand, low water causes partial formation of the SAM decreasing the efficiency of the device (Glass et al., 2011). CVD is an alternative approach providing us with several advantages. The procedure has the capability of precise control on the moisture, which allows it to form close-packed homogeneous SAMs and reduces the possibility of self-polymerization. Moreover, it is reproducible and sample contamination is less likely to happen (Fiorilli et al., 2008; Zhang et al., 2010). However, it needs more-advanced equipment, and incorporation of this technique in microfluidic systems might be a bit challenging (Batz, Mellors, Alarie, & Ramsey, 2014; Tan & Desai, 2004).

In CVD process, the SAMs are produced through the deposition of silane vapor and following reduction in the surface-free energy. Transformation of the liquid to gas state can be done by means of a vacuum chamber to increase the presence of the silane partial pressure (Handa et al., 2008). The other way is heating the silane solution in a close chamber (Wang & Vaughn, 2008). More-advanced CVD systems are equipped with a plasma machine to hydroxylate the substrates before CVD

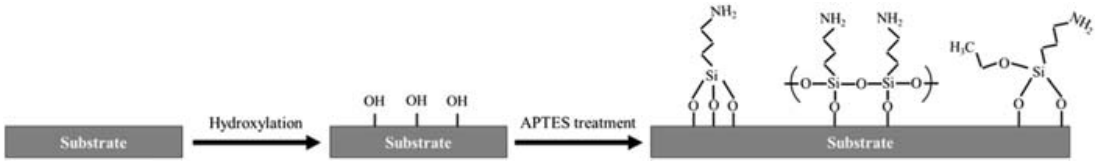

Figure 26.1 Schematic representation of three possible bond formation of APTES to a hydroxylated substrate. *APTES*, 3-Aminopropyltriethoxysilane.

treatment. Moreover, heating and vacuum could be performed simultaneously to shorten the process time and enhance the efficiency of CVD (Batz et al., 2014; Fiorilli et al., 2008; Zhang et al., 2010). Depending on the CVD system, the treatment time varies from 10 minutes to even 16 hours and the pressure is often kept between 2 and 5 Torr. Usually, concentrated amount of silane agent is used in CVD; nevertheless, it is possible to dilute APTES or APTEMS in a solvent and perform the CVD process (Wang & Vaughn, 2008). It is not required to rinse the samples after CVD treatment. A secondary CVD treatment with water vapor could also improve the siloxane formation (Fiorilli et al., 2008).

A baking step may be required after LPD treatment or CVD treatment (especially when the heating is not applied during the CVD) to promote the oxane and siloxane formation and enhance the quality of SAMs. APTES and APTMS SAMs possess amino groups at the tails out which could then be used to anchor ligands and biomolecules through their carboxyl groups. It is highly favorable to cross-link the antibodies through their carboxyl groups to the substrate rather than their amino groups, which occurs when the substrate is carboxylated. The reason for this is attributed to the fact that carboxyl groups are located on the fragment crystallizable region (tail region, Fc) of the antibodies; however, amino groups could be found everywhere on the antibodies including the antigen-binding (Fab) fragment. Thus amine functionalization of the surface causes the antibodies to bind to the surface with their tails. This proper orientation of antibody increases the antigen detection in immunoassays (Vashist, 2012).

To bind the ligands with amine moieties of the silane SAMs, the carboxyl groups of the ligands should first be activated. This could be happen using 1-ethyl-3-(-3-dimethylaminopropyl) carbodiimide (EDC or EDAC) hydrochloride (Didar, Foudeh, & Tabrizian, 2012; Guan, Zhang, Bi, Zhang, & Hao, 2010; Handa et al., 2008; Khnouf, Karasneh, & Albiss, 2016; Zhang et al., 2005). EDC is a popular water-soluble reactive to carboxyl groups producing *O*-acylisourea intermediate. The carbodiimide is zero-length cross-linker as its chemical structure in not included in the final carboxyl to amine (peptide) bond (Hermanson, 2013; Vashist, 2012). The reaction between *O*-acylisourea intermediate and amino group occurs very quickly producing isourea as a by-product. It should be mentioned that the *O*-acylisourea intermediate is very unstable in aqueous solution and the carboxyl group can be regenerated by hydrolysis of the intermediate and release of *N*-unsubstituted urea (Vashist, 2012). In order to make activated carboxyl groups more stable, usually *N*-hydroxysuccinimide (NHS) or sulfo-NHS is used along with EDC. NHS or sulfo-NHS reacts with the intermediate and produces NHS ester, which is stable for few hours at pH 7.4. It is still highly recommended to carry out the carboxyl to amine binding procedure as fast as possible to achieve the best efficiency. Furthermore, the most efficient EDC cross-linking happens at pH 4.5 using MES (4-morpholinoethanesulfonic acid) buffer (Carbodiimide Crosslinker Chemistry, n.d.) (Fig. 26.2).

In what follows, some examples of the microfluidic devices that have been used for cell associated applications and been functionalized using silanization method will be discussed.

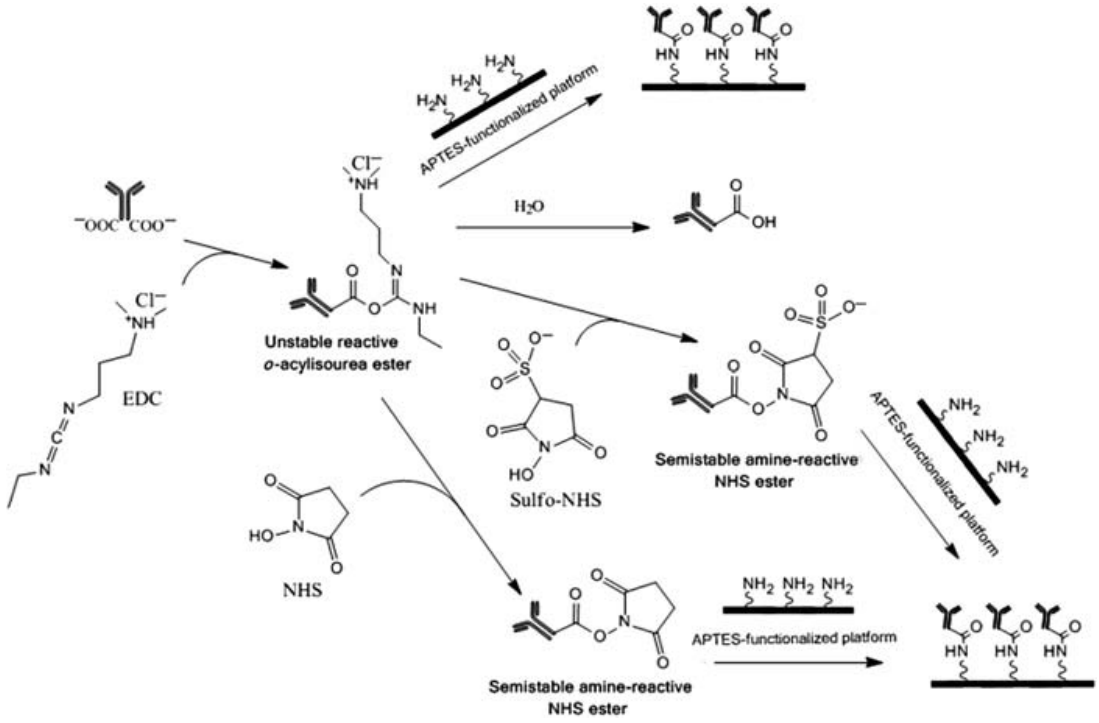

Figure 26.2 Schematic representation of EDC−NHS based chemistries for binding antibodies with APTES treated substrates. *APTES*, 3-Aminopropyltriethoxysilane; *EDC*, 1-ethyl-3-(-3-dimethylaminopropyl) carbodiimide; *NHS*, *N*-hydroxysuccinimide.
Source: Reproduced from Vashist, S. K. (2012). Comparison of 1-ethyl-3-(3-dimethylaminopropyl) carbodiimide based strategies to crosslink antibodies on amine-functionalized platforms for immunodiagnostic applications. *Diagnostics*, *2*(4), 23−33. Retrieved from <http://www.mdpi.com/2075-4418/2/3/23/> with permission from MDPI.

In research done by Guan et al. (2010), microbead-based immunoseparation technique was integrated with microfluidic technology to capture and quantify the *Escherichia coli* bacterial cells. The microfluidic device comprised a glass substrate and a PDMS cover with the microchannel cavities. The device contained a micro-chamber in which only a monolayer of glass beads with the diameter of 50 μm can fit. LPD APTES treatment was performed on the glass beads, which were piranha etched in advance. Then, the anti-*E. coli* antibodies were covalently bound to the beads using EDC/sulfo-NHS in MES buffer.

In another work done by Zhang et al. (2005), murine cancer cells, S180 cells, were immobilized on the surface of PDMS-PDMS and PDMS-glass microfluidic channels of 100 μm width and 50 μm height. The biofunctionalization of the channels was performed using plasma treatments of the channel pieces before binding and perfusion of 2% APTES in 95% acetone. The EDC−NHS method was used to activate the carboxyl groups of antifibronectin IgG in order to bind to the APTES treated channel. After that, fibronectin (FN) was used to make the channel functional for capturing the cancel cells.

Jain et al. (2016) lined fixed human endothelium inside a microfluidic device to investigate thrombus formation and platelet adhesion induced by perfusion the

human whole blood through the channel at a certain flow rate. The microfluidic device was oxygen plasma treated to hydroxylate the surface and then treated with 1% APTMS in ethanol via LPD method. The device was bake at 80°C for 2 hours and then coated with rat type I collagen. Human umbilical vein endothelial cells (ECs) were flowed to the channel and after proper incubation, 4% formaldehyde solution was flushed through the channel. Then, other required agent for blood coagulation such as tissue factor, and vascular endothelial-cadherin were perfused into the device.

Microcontact printing

In 1993 microcontact printing (μCP) was firstly introduced by Kumar and Whitesides (1993) to create micropatterns of alkanethiols on a gold substrate. A μCP is stamping an ink of a desired molecule on a substrate with an elastomer stamp, such as PDMS, which the stamp is generally fabricated by soft lithography (Didar, Bowey, Almazan, & Tabrizian, 2014; Kumar & Whitesides, 1993; Mrksich & Whitesides, 1995). As μCP does not require repetitive access to clean rooms, harsh solvents, and special equipment, and further it allows for rapid and easy production of micropatterns of desired molecules, therefore μCP has become an emerging field for generating patterns in a micron scale (James et al., 1998; Kumar & Whitesides, 1993; Mrksich & Whitesides, 1995; St. John et al., 1997).

μCP proteins on a solid substrate were initially introduced in 1997 (James et al., 1998), and since then, this method has been widely implemented for different biological applications. When comparing μCP proteins with conventional methods, such as photolithography, it is relatively straightforward, fast, and cost effective and does not require harsh solvents (Didar & Tabrizian, 2010; James et al., 1998; Mrksich, Dike, Tien, Ingber, & Whitesides, 1997; St. John et al., 1997). Moreover, μCP can be employed to print other molecules such as silanes, creating SAMs, which can contain different types of functional groups (Mrksich & Whitesides, 1995). Attachment of biomolecules to SAMs can lead to a possibility of designing sophisticated systems that can have precise control over the degree of cell adhesion and activities (Kane, Takayama, Ostuni, Ingber, & Whitesides, 1999; Mrksich et al., 1997; Mrksich & Whitesides, 1995; Singhvi et al., 1994; St. John et al., 1997; Zhanga et al., 1999). As an example for creating SAMs by μCP, microarrays of multiple antibodies were created by Didar et al. by means of μCP an aminosilane, APTES, on a glass substrate. APTES further provided an anchor site for antibodies through its amine functional group, which was activated by EDC and NHS, allowing for covalent attachment of antibodies to the APTES printed regions. Multiple laminar flow streams containing a specific biomarker were passed through the channel and created multiplex protein patterns on the APTES regions, which have the potential to be used in complex cell-based studies (Didar et al., 2012). Here, we will firstly discuss studies that have implemented μCP of biomolecules (e.g., antibodies) in a single step or multiple steps (with or without a chemical coupling agent), and μCP of blocking agents, in all cases cells have been incorporated in the microchannels for further research.

In a study by Thiébaud et al., laminin was directly microcontact printed on a polystyrene petri dish substrate to achieve structured cellular growth in vitro. Mouse embryonic carcinoma cells were seeded on the substrate, and through a microfluidic device called microinjector array system, localized and controlled drug application to cells cultures were studied (Thiébaud, Lauer, Knoll, & Offenhäusser, 2002).

Another example of direct μCP of biomolecules is an immunodetection study on cancer cells, which anti−epithelial cell adhesion molecules (anti-EpCAMs) were microcontact printed on a nanoporous silica substrate (Fig. 26.3). The nanoporous substrate was used in order to enhance the surface area in contact with the stamp with the intention of enriching the amount of the antibody deposited on the surface, which would contribute to the improvement of the sensitivity on this detection method. The nanoporous microcontact printed substrate was then incorporated in grooved microchannels, which act as a micromixer in such a way that the decrease in the height of the channel directs the flow downward. Therefore this geometrical enhanced microchannel brings cells closer to the substrate for a better cell−surface interaction. EpCAM positive and negative cells were studied in the channel, as well as patterned and non-micropatterned substrates to investigate the specificity of the detection system (Ng, Hoshino, & Zhang, 2013).

In a study, another way was introduced to pattern cells in microchannel, by having a microcontact printed substrate incorporated in a microfluidics device with microwells. For this end, a glass substrate was microcontact printed with poly-L-lysine (PLL) or laminin and then bonded to the channel similar to the methods mentioned in previous paragraphs. Cells were first loaded in the device with a negative pressure flow, and then the device was flipped with the microwell side on the bench and a positive pressure flow was applied to facilitate the cell capture in the

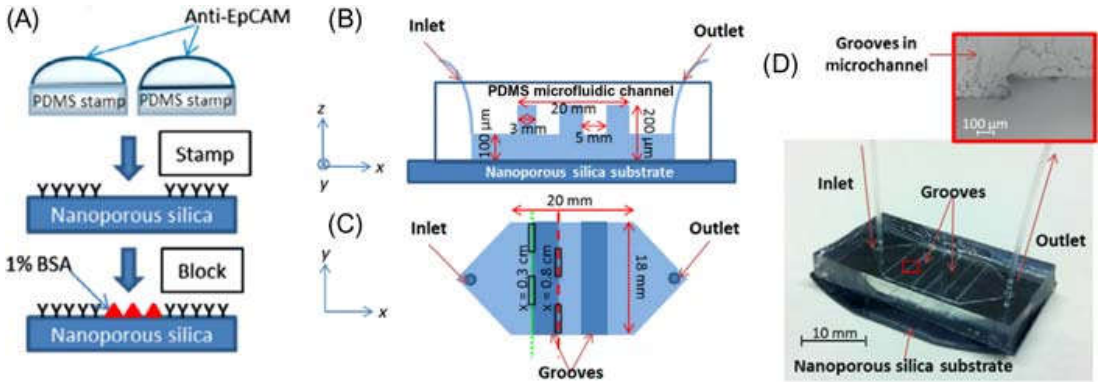

Figure 26.3 (A) Microcontact printing process of antibodies (anti-EpCAM) on nanoporous silica substrate. (B) Side and (C) top view of the grooved microfluidic device. The *black-boxed* areas are representatives of microcontact printed anti-EPCAM regions. (D) Image of the microfluidic device. *Anti-EPCAM*, Anti−epithelial cell adhesion molecule.
Source: Reproduced from Ng, E., Hoshino, K., & Zhang, X. (2013). Microfluidic immunodetection of cancer cells via site-specific microcontact printing of antibodies on nanoporous surface. *Methods*, *63*(3), 266−275 with permission from Elsevier.

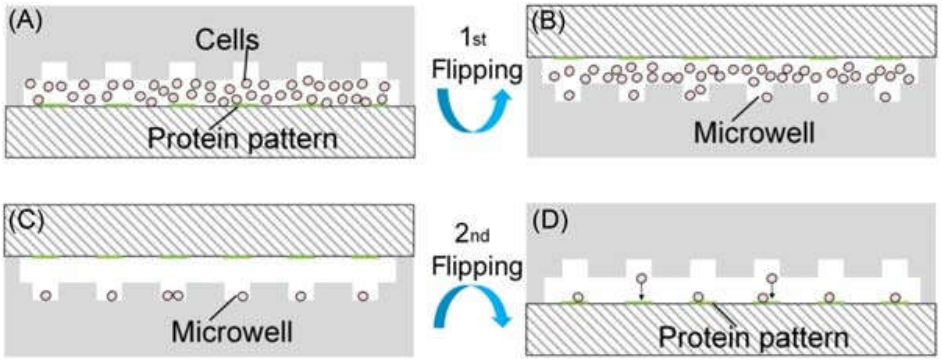

Figure 26.4 Cell loading processes in the grooved microfluidic channel on the patterned regions. (A) Cell suspension was flowed in the channel while the chip was facing up. (B) The device was flipped, allowing the cells to settle in the microwells. (C) After a fast flow of 20 μL/min, cells stayed in the microwells. (D) After the second flipping, cells dropped on the bottom side of the chip on the patterned regions.
Source: Reproduced from Tu, C., Huang, B., Zhou, J., Liang, Y., Tian, J., Ji, L., Liang, X., et al. (2017). A microfluidic chip for cell patterning utilizing paired microwells and protein patterns. *Micromachines*, *8*(1), 1−15 with permission from MDPI.

microwells (Fig. 26.4). The final step of the process was to flip the device again to allow the cells to settle down on the micropatterns on the substrate with gravitational force (Fig. 26.4). Furthermore, the cells were allowed to grow in a humidified petri dish while being in the device, and the cells lasted for 6 days as well as maintained the pattern even though no blocking chemicals were used (Tu et al., 2017).

To study local cell signaling, protein-micropatterned surfaces were employed in microfluidic channels to study axon guidance. Protein A was microcontact printed on a coverslip and incorporated in the axon chamber of a device where two separate chambers (one for axon and one for cell body) were connected by several microfluidics channels that limit diffusion between the chambers (Fig. 26.5). The patterned protein A region was then incubated with *N*-cadherin−Fc (cell adhesion protein) and able to specifically capture this biomolecule (a two-step patterning process). By incorporating embryoid bodies differentiated into spinal motor neurons, it was established that axon guidance was *N*-cadherin specific (Shi, Nedelec, Wichterle, & Kam, 2010).

For simultaneous cell separation and drug testing, a microfluidic device with a micropatterned substrate was used. The micropatterning was achieved in two steps: (1) neutravidin in Tris−HCl buffer was microcontact printed on a glass substrate, and then for the first study, the aim was to create two regions that have different antibodies; (2) each site was incubated with anti-CD19 and anti-CD71 (4×8 spots of anti-CD19 followed by 4×8 spots of anti-CD71). The channel was then bonded on the substrate and a 1:1 mixture of Ramos B cells (CD19 + and CD71 +) and HuT 78 T (CD71 +) cells was flowed inside. Anti-CD19 antibody sites revealed a 94% capture purity for CD19 + Ramos cells and anti-CD71 sites captured both cell types. The later one, 60% of the captured cells were Ramos B cells and the remaining 40% were HuT 78 T cells, which can be due to

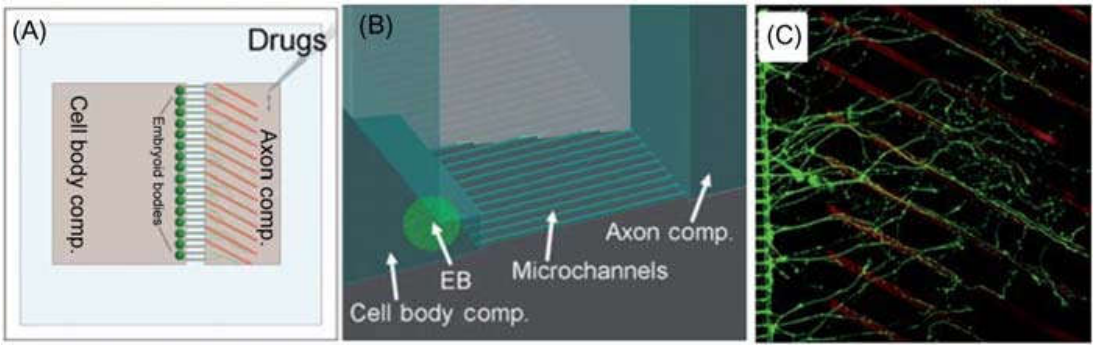

Figure 26.5 (A) Representation of the chamber design for the combination of cell body/axon isolation and outgrowth selectivity. (B) A microchannel barrier isolates the compartment. (C) Motor axons are guided by Ncad−Fc, which are captured on the protein A line patterns (shown in *red*).
Source: Reproduced from Shi, P., Nedelec, S., Wichterle, H., & Kam, L. C. (2010). Combined microfluidics/protein patterning platform for pharmacological interrogation of axon pathfinding. *Lab on a Chip*, *10*(8), 1005 with permission from Royal Society of Chemistry.

the antigen density of each cell type. Furthermore, through two separate streams of laminar flow, Ramos B and HuT 78 T cells were passed through the channel on an anti-CD71 region which results in a "north" and "south" separation of these two cell lines. For the second part of the study, apoptosis regulation was performed to simulate chemotherapy drugs with a cytotoxic compound, called staurosporine on the captured cells. For the third part, anti-CD95, a ligand which can capture cells, but at the same time induce a biochemical response, was used in the microfluidic channel. More precisely, anti-CD95 can capture T cells by binding to the Fas receptor on the cell surface and, subsequently, induces cell apoptosis (Liu, Germain, & Pappas, 2014).

Lovchik et al. demonstrate a method for μCP a compound to have patterned biomolecule-specific sites on an Au-coated Si substrate by microcontact printed 1-hexadecanethiol and further incubated the substrates with FN to promote cell arraying. As a blocking agent thiolated poly(ethylene glycol) (PEG) (HS-PEG) was used. The goal of this study was to ultimately have a system that stimulates cells and analyzes secreted analytes downstream. For this stage of the study, the FN patterned Au surface, having oval patterns in the size of the cell used for this study, was incorporated in a capillary-based microfluidic system, and a suspension of human breast cancer cells, type MCF-7, was flowed through the channel by capillary force and resulted in arrays of MCF-7 cells (Lovchik, Von Arx, Viviani, & Delamarche, 2008).

In another study, an intermediate chemical was used and the micropatterning steps were done afterwards. A microfluidics device was developed to investigate interfacial platelet-protein interactions in order to study the efficacy of antiplatelet drugs in whole blood. The substrate was cyclic olefin polymer sheets, which were treated with 3- APTES and further microcontact printed with a solution containing

fibrinogen, phosphate-buffered saline (PBS), Cy3-labeled bovine serum albumin (BSA) (facilitates visualization of the fibrinogen patterns) and blocked by BSA solution. The substrate was then bonded to self-pumped PDMS microchannels. The device comprised arrays of microfluidics channels, which after μCP and assembly was put in a vacuum chamber to evacuate the air and water vapor in the device (degas-driven flow) (Fig. 26.6A). The system worked in such a way that the inlet well was filled with blood, and the blood was slightly moved in by the self-pumped channel. Different designs and parameters were manipulated to have control over the shear force and flow rate. Ultimately, the effect of a $P2Y_{12}$ inhibitor, cangrelor, which is a drug used for cardiovascular disease patients, was studied through individual platelet assay. Adenosine-5′-diphosphate (ADP) induces $P2Y_{12}$ receptors on platelets, resulting in aggregation of the platelets (Fig. 26.6B). Individual platelets can bind individually to the fibrinogen microcontact printed dots, and the dot array occupancy (DAO) was measured as an indicator of platelet adhesion (Fig. 26.6D). Whole blood with ADP, ADP + cangrelor, or buffer was flowed through the system, and the DAO was measured, the results revealing a higher DAO for ADP + cangrelor than ADP, which demonstrates a potential application of these devices for assessment of $P2Y_{12}$ inhibitors (Fig. 26.6C and D) (Jose et al., 2016).

In a novel approach, patterns of non-biofouling molecules such as PEG-based copolymer or the polysaccharide hyaluronic acid (HA), were created on the surface in such a way that the stamp along with the non-biofouling ink was incubated on the surface and was further subject to oxygen plasma (Khademhosseini, Suh, et al., 2004; Khademhosseini, Yeh, et al., 2004). The regions which were not beneath the PDMS stamp were destroyed due to coming in contact with the plasma; on the other hand, stamp regions were left intact and transferred the non-biofouling ink to the surface and subsequently a PDMS microfluidic was bonded on top of the patterned surface. The nonpatterned regions were coated with proteins such as FN or BSA to further allow for biofunctionalization of the surface by the created microfluidics system. For cell attachment experiments, a solution of FN was flowed through the channel to create anchoring sites for cells, and then a suspension of cells in a medium was passed through the channel. The results revealed that cells can be patterned within microfluidic channels at high confluency and can be maintained up to 24 hours, which is adequate for biosensing applications (Khademhosseini, Suh, et al., 2004).

Microfluidic patterning

Microfluidic patterning is defined as using laminar flows to create functionalized regions patterned either on a flat surface or inside the microfluidic device. In general, three main techniques are employed to microfluidic pattern the biomolecules: reversibly bound microfluidic channels, combination of parallel laminar flows, and concentration gradient generators. In the following, some examples for each of the approaches will be provided to better understand these methods.

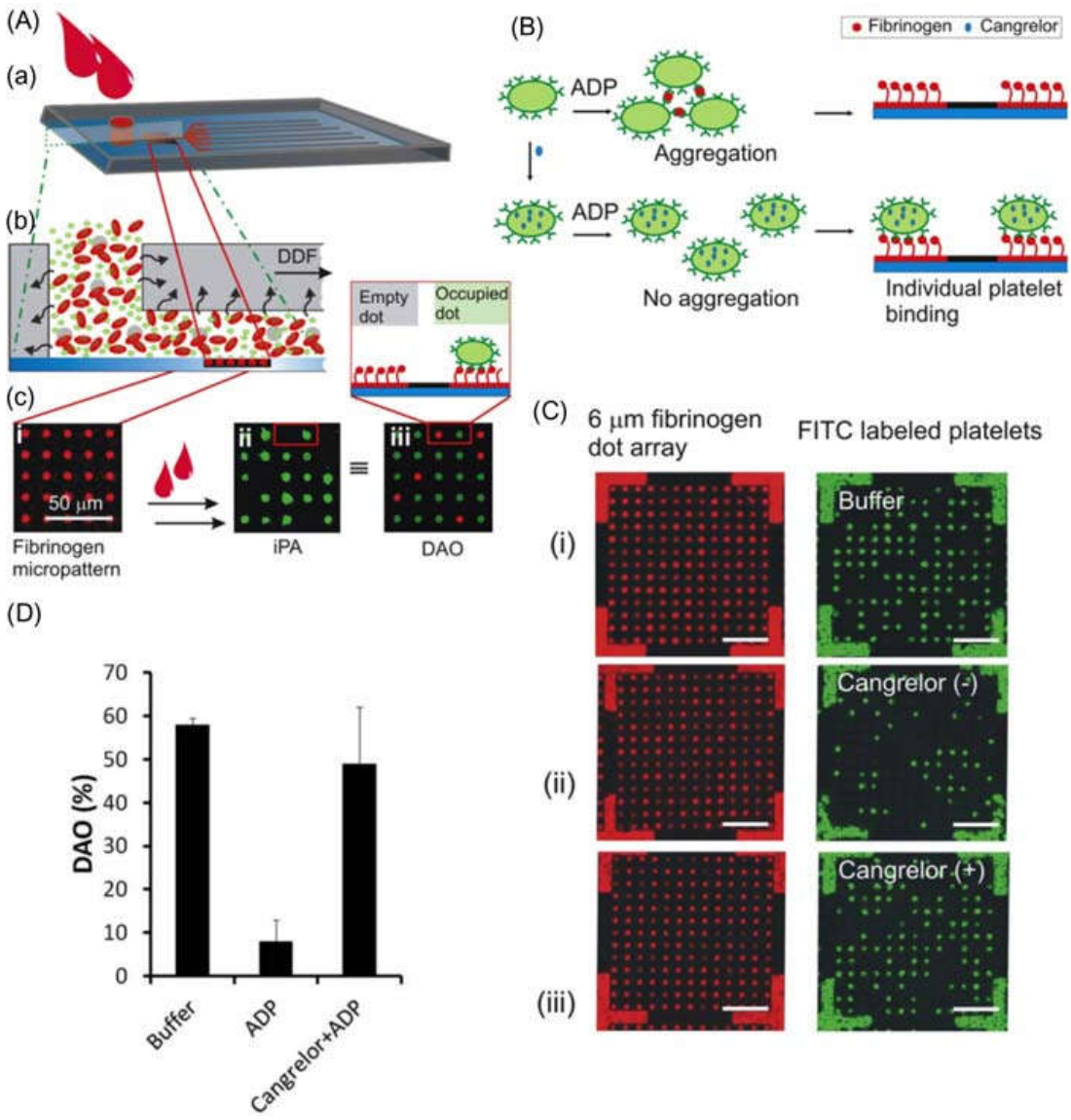

Figure 26.6 (A) Schematic representation of integrating the iPA assay on the device. The COP bottom side of the device is coated with fibrinogen dot array. Via DDF, whole blood is flowed through the device on the fibrinogen micropatterns. Each fibrinogen dot will be occupied by single platelets. To statistically compare the results, DAO was employed. (B) Schematic representation of the P2Y12 assay. A lower adhesion rate happens when ADP causes aggregation of platelets, whereas when the ADP is mitigated by a P2Y12 inhibitor, platelet adhesion will be similar to normal state. (C) Fluorescence images of Cy3-labeled fibrinogen-dot arrays (*red dots*) and of FITC-labeled platelets (*green dots*) which are in the device. Prior to flowing the whole blood in the chip, it was incubated with (i) buffer, (ii) 20 μM ADP ["Cangrelor (−)"], or (iii) 20 μM ADP plus 10 μM cangrelor ["Cangrelor (+)"]. White bars indicate 50 μm. (D) The effects of ADP and ADP + cangrelor were evaluated by DAO values. *COP*, Cyclic olefin polymer; *DAO*, dot array occupancy; *DDF*, degas-driven flow; *iPA*, individual platelet assay.
Source: Reproduced from Jose, B., McCluskey, P., Gilmartin, N., Somers, M., Kenny, D., Ricco, A. J., Kent, N. J., et al. (2016). Self-powered microfluidic device for rapid assay of antiplatelet drugs. *Langmuir*, *32*(11), 2820−2828 with permission from ACS Publications.

Reversible bound microfluidic channels

It consists three basic steps. First, a PDMS layer that contains the microchannels' cavities underneath is reversibly placed onto a flat substrate as it often forms a close channel. Second, the desired biospecies or gel is perfused inside the channel. Third, the PDMS is peeled off while the patterns remain on the surface.

Tan and Desai (2003) utilized this method to create 3D patterns of ECs, smooth muscle cells (SMCs), and fibroblasts (FBs). The procedure started with hydroxylation of glass slides or silicon wafers using piranha etch. Thereafter, APTES treatment was done on the surfaces through LPD method. The surfaces were placed inside a preheated vacuum oven together with a petri dish containing 600 μL of APTES. The APTES treatment was performed at 150°C for 1 hour. Then, in order to make the silanized substrates functional, the surfaces were immersed inside glutaraldehyde (GA) solution. APTES−GA activated surfaces can covalently bind to amino groups of the biomolecule of interest (Fig. 26.7). PDMS template with microchannel structure was laid on the substrates while the channel cavities were facing down. The PDMS could physically bind to the substrates, which provided

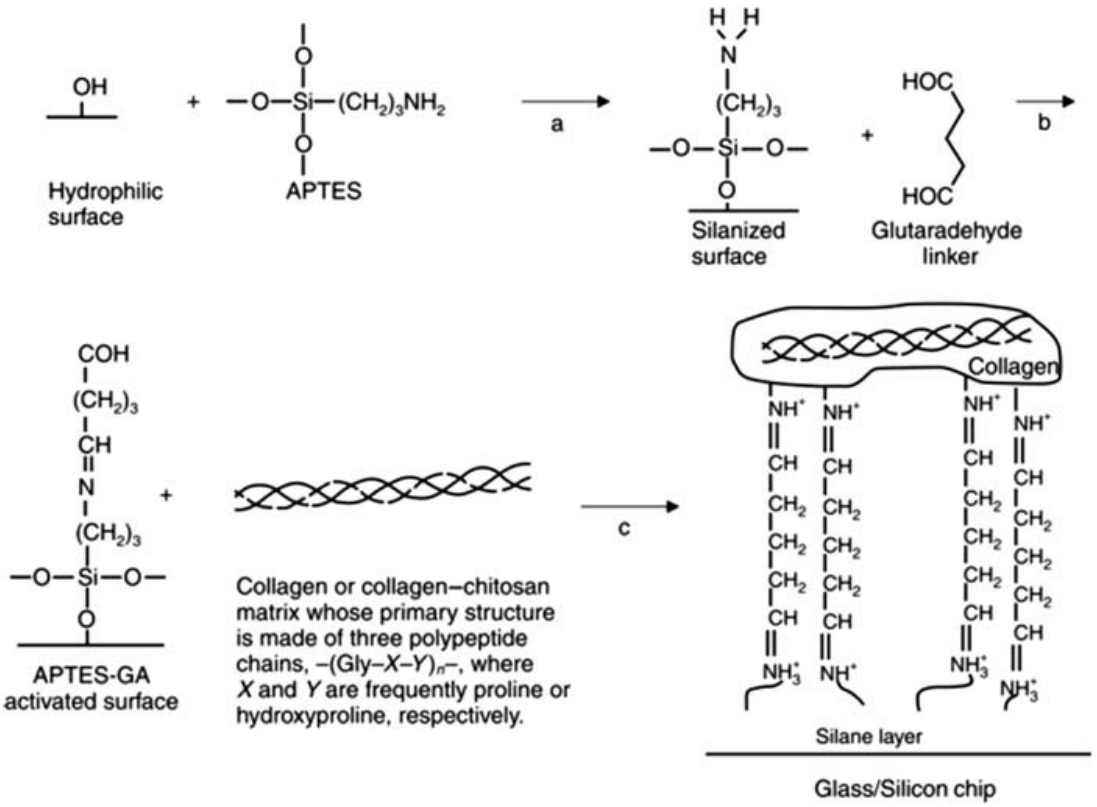

Figure 26.7 Schematic representation of surface modification procedure. (A) APTES treatment of the surface, (B) activation with glutaraldehyde, (C) cell-collagen adhesion. *APTES*, 3-Aminopropyltriethoxysilane.
Source: Reproduced from Tan, W., & Desai, T. A. (2003). Microfluidic patterning of cellular biopolymer matrices for biomimetic 3-D structures. *Biomedical Microdevices*, *5*(3), 235−244 with permission from Springer.

the bottom surface of the channels. The PDMS template was punched in advance to create the inlets and outlets. The channels were 350 μm in width and 300 μm in height. The suspension of cells together with ECM of collagen and collagen-chitosan were perfused inside the channels. As the collagen is made of polypeptide chains, they are able to covalently bond to the APTES−GA activated surface. In this research, three layers of FBs, SMCs, and ECs were formed on top of each other. The sample was incubated properly and then they peeled off the PDMS layer, leaving the 3D cell−matrix on the slides. Finally, the samples were rinsed with PBS buffer (Fig. 26.8).

Khademhosseini et al. (2007) used the related method to fabricate 3D patterns of contractile cardiac organoids. To pattern the cells on glass slides, PDMS with the

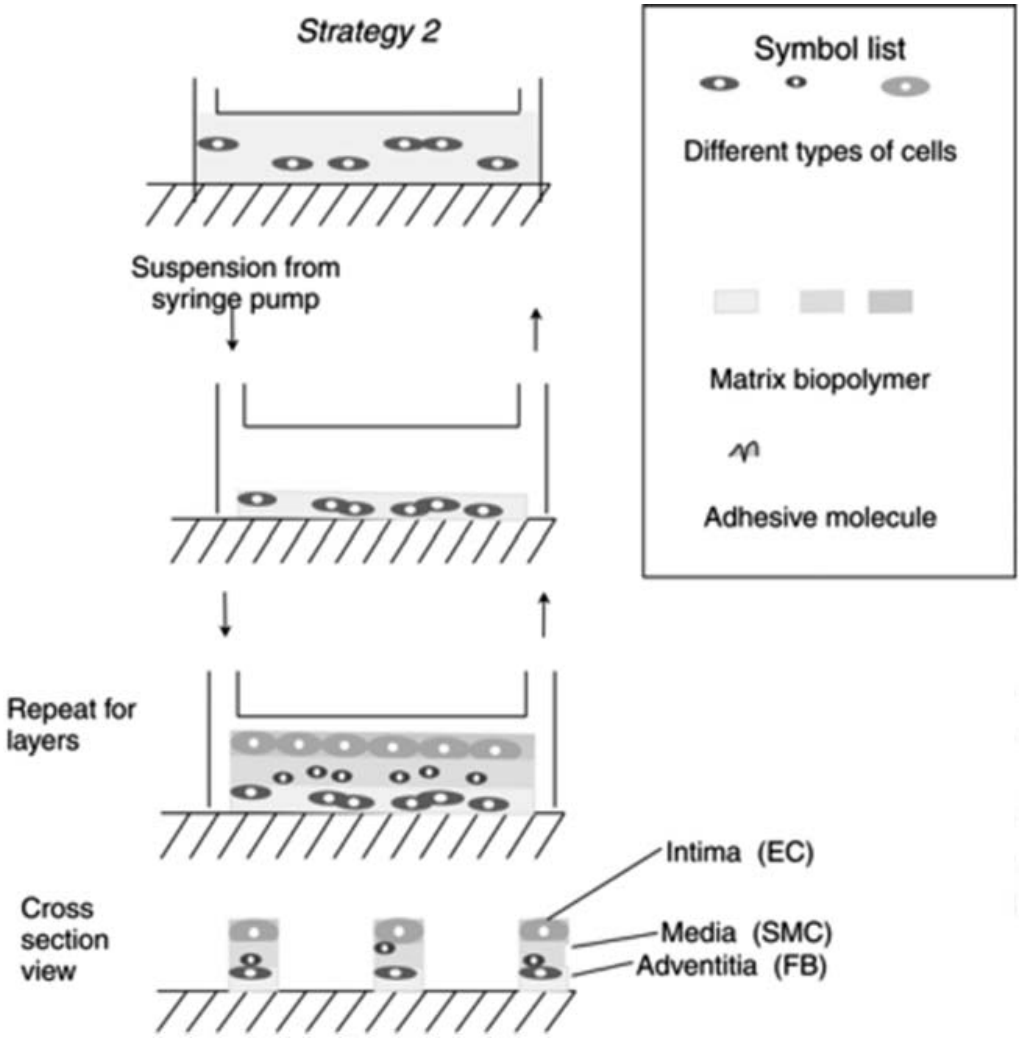

Figure 26.8 Schematic representation of 3D printed 3-layer of cells using reversible bound microfluidic approach. *3D*, Three-dimensional.
Source: Reproduced form Tan, W., & Desai, T. A. (2003). Microfluidic patterning of cellular biopolymer matrices for biomimetic 3-D structures. *Biomedical Microdevices*, *5*(3), 235−244 with permission from Springer.

array of microchannels were placed on the substrate. Afterwards, the channels were filled up with HA solution using capillary forces via placing droplets of the solution at the inlet. After 12 hours incubation and the following physisorption of the HA onto the substrate, the PDMS template was peeled off and the glass was rinsed with water. Then, the surface was treated with FN for cell-adhesion's sake. Since HA resists the protein adhesion, FN was formed on micro-lanes between the HA patterned strips. Further, the cardiomyocytes (cardiac muscle cells) were added to the glass substrates with HA and FN patterns by placing the substrates inside a well plate. The myocytes aligned along the HA cell-repulsive patterns attaching preferentially on the regions between the HA patterns. Cardiomyocytes spontaneously lifted off the surface and formed beating organoids. It is mentioned that presence of residual PDMS on the substrate is required for the myocyte lift-off (Fig. 26.9).

Berry et al. (2017) used an open microfluidic platform, called Monorail Device, to partition cell culture surfaces demarcated by hydrogel walls. This technique is different from the previous methods as the open microfluidic device is not detached from the workplace area. Their method can be incorporated in available well-plates and cell culturing petri dishes. The open microfluidic devices with different dimensions and feature arrays were fabricated using a 3D printer. The device could be inserted into a 24-well plate, in a way that the bottom surface of the 3D printed platform did not touch the substrate. Thus the platform provided some arrays of rails with a certain height to the substrate. After that, the hydrogel was pipetted into a specific region of the platform, called loading zone or inlet. Based on the spontaneous capillary flow (SCF) and Laplace pressure, the hydrogel flowed along the rails and covered the empty distances between the rails and the well plate surface. This resulted in the formation of small empty chambers enclosed by the hydrogel walls, which had access from top to pipette cells and biomolecules. The hydrogel flow within the rails depends on the height (h) and width (w) of the rail. The platform was optimized for use of Matrigel, fibrin, and collagen I. The advantage of having hydrogels walls that segregate culturing regions is the permeability of the hydrogel. While they allow soluble factors to diffuse through wall, they act as a barrier for the cells. Thus this technique can be employed in many cells' coculture systems. To obtain proper control on the hydrogel and ensure the hydrogel only flows along the rails on SCF, some modifications were done on the device. The loading zone was precisely designed to confine the hydrogel beneath the rails and prevent it from wetting the culture chamber. It was incorporated with a height gradient leading the hydrogel to pass along the rails. Moreover, a region with larger width (with the same height) was designed at the end of the flow path to increase the capillary favorability and better control the flow. Also, the rails were fabricated with trapezoidal cross-section to prevent the capillary rise of the hydrogel (Fig. 26.10).

Combination of parallel laminar flows

The patterning is performed by use of multiple microfluidic flows with low Reynolds number passing through a single channel. As the flow regime is laminar in this

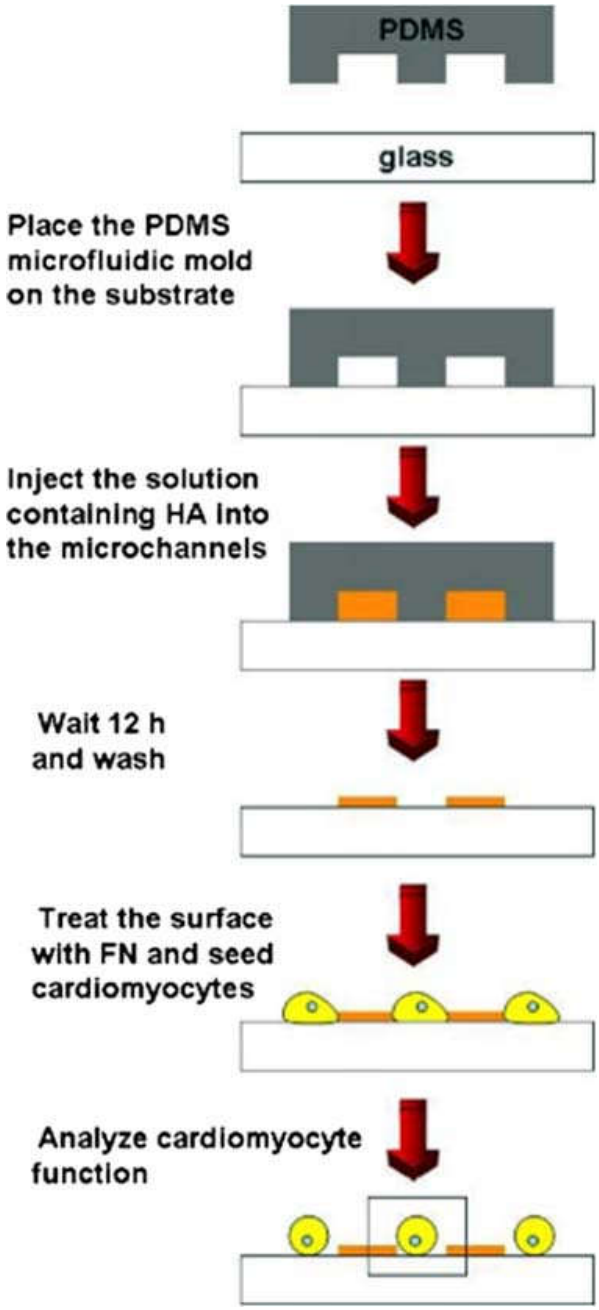

Figure 26.9 Schematic representation of fabricating cardiomyocyte organoids using bound microfluidic approach.
Source: Reproduced from Khademhosseini, A., Eng, G., Yeh, J., Kucharczyk, P. A., Langer, R., Vunjak-Novakovic, G., & Radisic, M. (2007). Microfluidic patterning for fabrication of contractile cardiac organoids. *Biomedical Microdevices*, *9*(2), 149−157 with permission from Springer.

system, turbulent mixing will not occur, and the parallel streams of different solutions will be sustained during the perfusion while the particles can diffuse in the adjacent streams across the interfaces. Modulating the flow rate, we are able to control the patterns arrangement (Duncombe, Tentori, & Herr, 2015; Takayama et al., 1999).

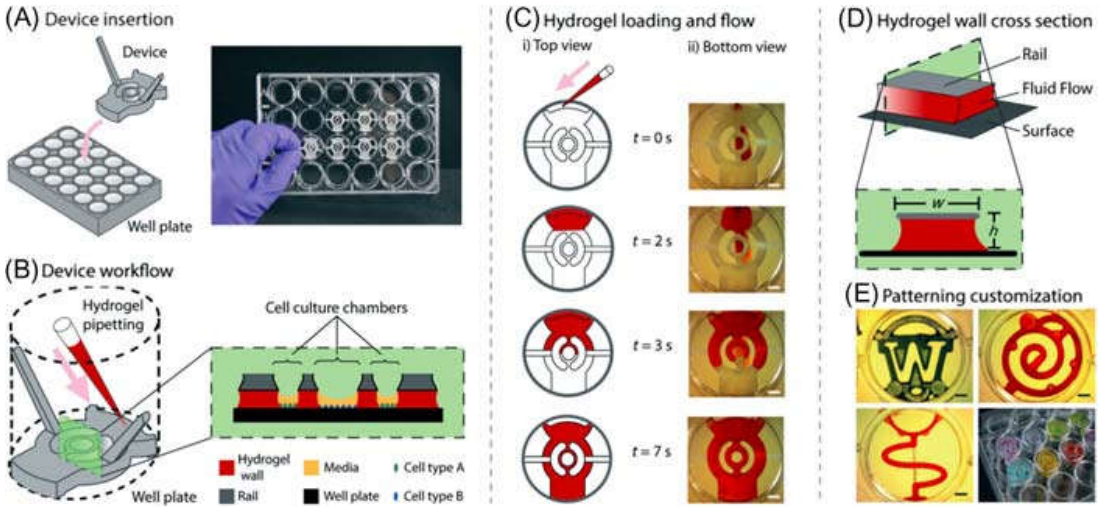

Figure 26.10 Illustration of the microfluidic rail system. (A) Insertion of the device into a well plate. (B) Pipetting the hydrogel at the specific loading zone, the hydrogen flows along the rails to fill the gap between the membrane and the substrate. (C) Schematic representation (i) and real images (ii) of the device at certain time points during the loading process. (D) Schematic of device's rail cross-section loaded with the fluid. (E) Different patterning achievable with the microfluidic rail system. Scale bars are 2 mm.
Source: Reproduced from Berry, S. B., Zhang, T., Day, J. H., Su, X., Wilson, I. Z., Berthier, E., & Theberge, A. B. (2017). Upgrading well plates using open microfluidic patterning. *Lab on a Chip*, *17*, 4253–4264. Retrieved from <http://www.xlink.rsc.org/?DOI = C7LC00878C> with permission from Royal Society of Chemistry.

Takayama et al. (1999) have patterned different cells and proteins using the parallel laminar flow approach. The device comprised a PDMS membrane bound to a petri dish by conformal contact. It had three inlet channels that merged into a main center channel. It was shown that perfusion of fluorescein isothiocyanate (FITC) mannopyranosyl phenylisothiocyante labeled BSA (man-FITC-BSA) through the side inlets channels and unlabeled BSA through the center inlet channel led to formation of fluorescent micro-lanes along the edges of the main channel. Indeed, the flows of the side inlets caused the center inlet flow to be squeezed while joining the main channel. Next, *E. coli* cells were injected inside all channels. The results demonstrated that *E. coli* cells only adhered to the mannose presenting strips of the channel. Different experiment with other combination of cells, proteins, as well as microchannel arrays could generate various kinds of patterns inside the device. It is stated that changing the flow rates, number of the inlet channels, and particle sizes or media that indicate the diffusion coefficient play a role in the pattern formation (Fig. 26.11).

Almost the same technique was used in a work done by Didar et al. (2012). They combined the parallel laminar flow concept with μCP method to fabricate the patterns of cells. The device was made of seven inlet microchannels that are converged into one main channels. The inlet channels fed the main channel at three separate intersections. Before binding the device, they microcontact printed APTES

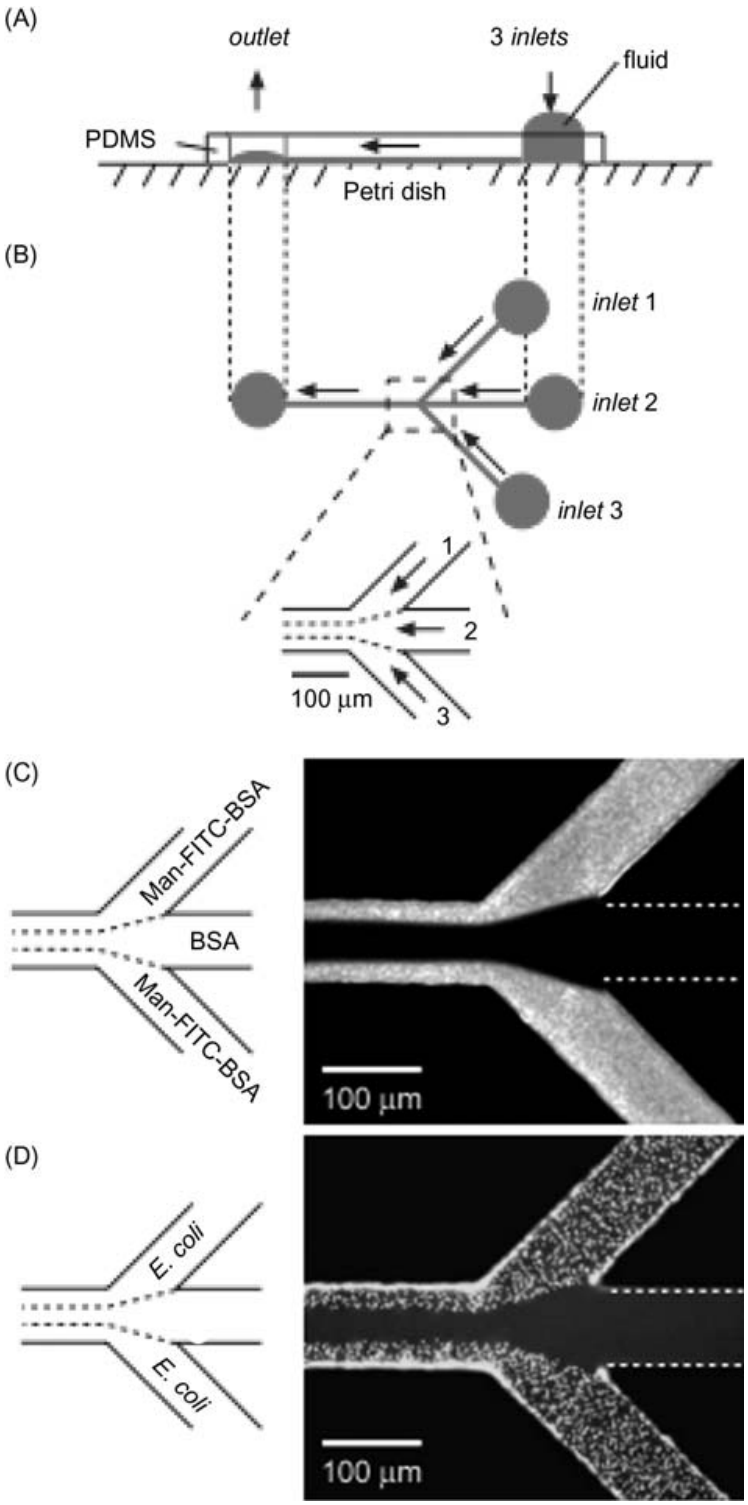

Figure 26.11 Schematic representation the microfluidic patterning using parallel laminar flow concept. (A) Side view and (B) top view of the microfluidic device with 3 inlet channels. Using the microfluidic device, patterns of (C) man−FITC−BSA and (D) *Escherichia coli (strain designated RB 128)* were formed inside the device.
Source: Reproduced from Takayama, S., McDonald, J. C., Ostuni, E., Liang, M. N., Kenis, P. J. A., Ismagilov, R. F., & Whitesides, G. M. (1999). Patterning cells and their environments using multiple laminar fluid flows in capillary networks. In *Proceedings of the National Academy of Sciences of the United States of America*, *96*(10), 5545−5548. Retrieved from <http://www.pnas.org/cgi/doi/10.1073/pnas.96.10.5545> with permission from National Academy of Sciences.

on an oxygen plasma treated glass slide. Immediately after the μCP, an oxygen plasma treated membrane containing the channel arrays was brought into contact with the glass slide to irreversibly bond together and form the device in such a way that the printed APTES was located within the main channel. EDC−NHS chemistry was incorporated to activate the printed amino groups inside the channel. Different fluorescently labeled antibody solutions were passed through the inlet channels to create the patterns by covalent bonding of the antibodies to the APTES printed areas while the functionality of the antibodies was maintained. The desired pattern outcome can be manipulated by controlling the flow rate and concentration of the proteins at each inlet channel (Fig. 26.12).

Concentration gradient generators

Microfluidic systems have been widely used in generating one-dimensional (1D) or two-dimensioanl (2D) chemical gradient inside microchamber or channels. Chemical gradients can control cell migrations as well as cell growth and could be used to study cancer metastasis (Chiang et al., 2012; Lee, Kim, Kang, Lee, & Chung, 2011; Mao, Cremer, & Manson, 2003; Nakashima & Yasuda, 2007; Shakeri, Sun, Badv, & Didar, 2017; Somaweera, Ibraguimov, & Pappas, 2016; Tourovskaia, Figueroa-Masot, & Folch, 2005). One of the common methods to create 1D gradient is source-sink method where free-diffusion of soluble molecules occurs from one high concentration end (source) to the low concentration end (sink) of the microfluidic channel. The concentration gradient generates along the length of the microchannel, and based on the Fick's law it continues until equilibrium between the source and sink concentrations is achieved. Abhyankar, Lokuta, Huttenlocher, and Beebe (2006) have used this method to generate chemoattractant concentration gradient required for migration of cells from sink toward the source (Fig. 26.13). The advantages of these gradient generators are simplicity and cost effectivity as they need low volume of reagents and can be employed for high throughput applications. However, these platforms can be used for a limited time due to the fact that the source and sink are not loaded progressively, and the diffusion makes the concentration of the source and sink the same over time (Kim, Kim, & Jeon, 2010; Somaweera et al., 2016). To tackle this problem, Diao et al. (2006) designed a three-channel microfluidic device to generate concentration gradient by based on the source-sink concept, except here it is possible to refresh the sink and source continuously (Fig. 26.14). They used nitro-cellulose membrane with the pore size of 0.45 μm as a platform for the device, and CO_2 laser was used to cut out the channels. The side channels were considered to be the source and sink, and the concentration gradient was formed in the middle channel via diffusion of the biomolecules through the porous membrane induced by the hydrostatic pressure at the inlet. Wildtype *E. coli* and mutant strains were added in the middle channel, and the migration of the cell toward the attractants such as L-aspartate gradients was shown inside the device.

In another protocol described by Shin et al. (2012), the same array of channels is utilized along with four individual channels located between the three channels (Fig. 26.15). Each channel has its own access separate from the other channels. The four interfacial channels are filled with a kind of hydrogel. The cells are usually

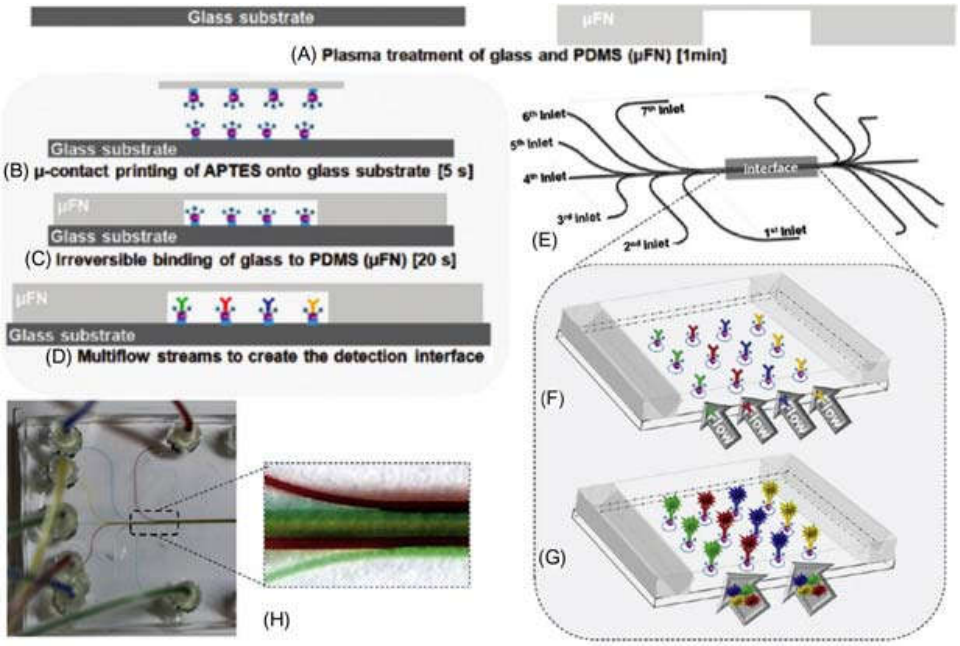

Figure 26.12 Schematic presentation of the device used by Didar et al. to generate microfluidic patterns. The procedure comprises (A) plasma treatment of the substrates, (B) microcontact printing of APTES onto the substrate, (C) binding the PDMS membrane with the substrate, (D) activation of the surfaces by EDC−NHS chemistry, and finally covalent bonding of biomolecules to the activated amino groups at the printed areas. (E) Schematic of the whole microfluidic design. (F) Laminar flows of multiple biomarker streams creating the multiplex patterns along the channel width. (G) Addition of secondary antibodies specific to the primary antibodies on the device. (H) The microfluidic device illustrating the multiple micro-lanes of laminar flows. *APTES*, 3-Aminopropyltriethoxysilane; *EDC*, 1-ethyl-3-(-3-dimethylaminopropyl) carbodiimide; *NHS*, *N*-hydroxysuccinimide; *PDMS*, polydimethylsiloxane.
Source: Reproduced from Didar, T. F., Foudeh, A. M., & Tabrizian, M. (2012). Patterning multiplex protein microarrays in a single microfluidic channel. *Analytical Chemistry*, *84*(2), 1012−1018 with permission from ACS publications.

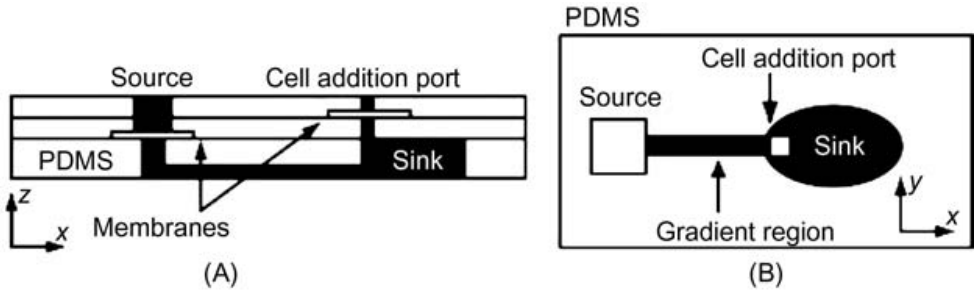

Figure 26.13 Schematic representations of (A) side and (B) top views of the sink-source-based gradient generator used by Abhyankar et al.
Source: Reproduced from Abhyankar, V. V., Lokuta, M. A., Huttenlocher, A., & Beebe, D. J. (2006). Characterization of a membrane-based gradient generator for use in cell-signaling studies. *Lab on a Chip*, *6*(3), 389−393. Retrieved from <http://dx.doi.org/10.1039/B514133H> with permission from the Royal Society of Chemistry.

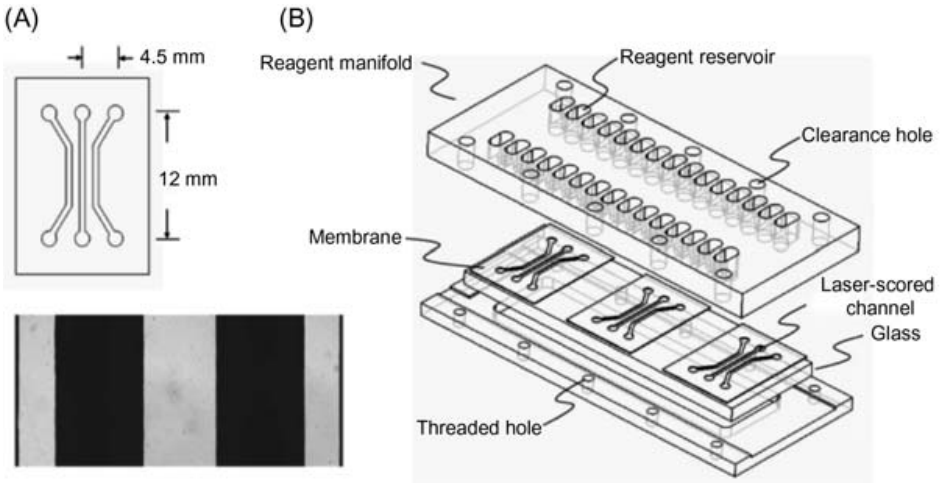

Figure 26.14 Schematic representation of the sink-source-based gradient generator device with the capability to refresh the source and sink during the gradient formation. (A) Top view. (B) The full device.
Source: Reproduced from Diao, J., Young, L., Kim, S., Fogarty, E. A., Heilman, S. M., Zhou, P., Shuler, M. L., et al. (2006). A three-channel microfluidic device for generating static linear gradients and its application to the quantitative analysis of bacterial chemotaxis. *Lab on a Chip*, *6*(3), 381–388. Retrieved from <http://www.xlink.rsc.org/?DOI = B511958H> with permission from the Royal Society of Chemistry.

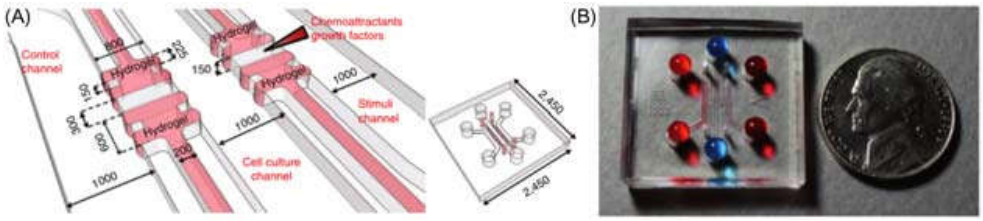

Figure 26.15 (A) Schematic and (B) photograph representation of the gradient generator microfluidic device. The two side channels are sink and source channels indicated with *red color* in part (B), and the central channel is indicated with *blue color*. Hydrogel is incorporated within the four microchannels between the two side channels and the central channel. All scale bars are represented as μm.
Source: Reproduced from Shin, Y., Han, S., Jeon, J. S., Yamamoto, K., Zervantonakis, I. K., Sudo, R., Kamm, R. D., et al. (2012). Microfluidic assay for simultaneous culture of multiple cell types on surfaces or within hydrogels. *Nature Protocols*, *7*(7), 1247–1259 with permission from Nature Publishing Group.

cultured in the center channel and the other two sides channel work as source and sink to generate the concentration gradient. In this way, cell can diffuse inside the hydrogel and form 3D concentration gradients. This method has been used in several other works (Jeong et al., 2011; Vickerman, Blundo, Chung, & Kamm, 2008). Nevertheless, the protocol suffers from some limitations including incapability of generating large gradients as well as lack of continuous flow of cell medium in the cell culture chambers (Somaweera et al., 2016).

The other common approach to generate concentration gradient is incorporating adjacent laminar flows and the following diffusion of molecules across the interfaces. Here, the design of the channels arrays is completely different from the previous section where we discussed parallel laminar flows; however, almost the same concept results in the gradient formation. This new design is introduced by Jeon et al. (2000) and is called tree-shape design and has been employed in many cell experiments (Chang et al., 2014; Chung et al., 2005). The channels array starts with a couple of inlet channels. Then these channels into more channels at several intersections on the device platform creating a complicated network of horizontal and vertical channels (Fig. 26.16). When a fluid with a certain concentration flows through the channels' network, it splits into several streams and then recombines at the next intersection. This cycle occurs several times while the fluid passes inside the channels bringing about the generation of different concentrations of the desired biomolecules at the final channels of the platform. The main disadvantages of this design are the large footprint size and long diffusion time required to generate the gradient. Moreover, the flow rate should be precisely controlled as large shear stresses induced by the device can damage cells.

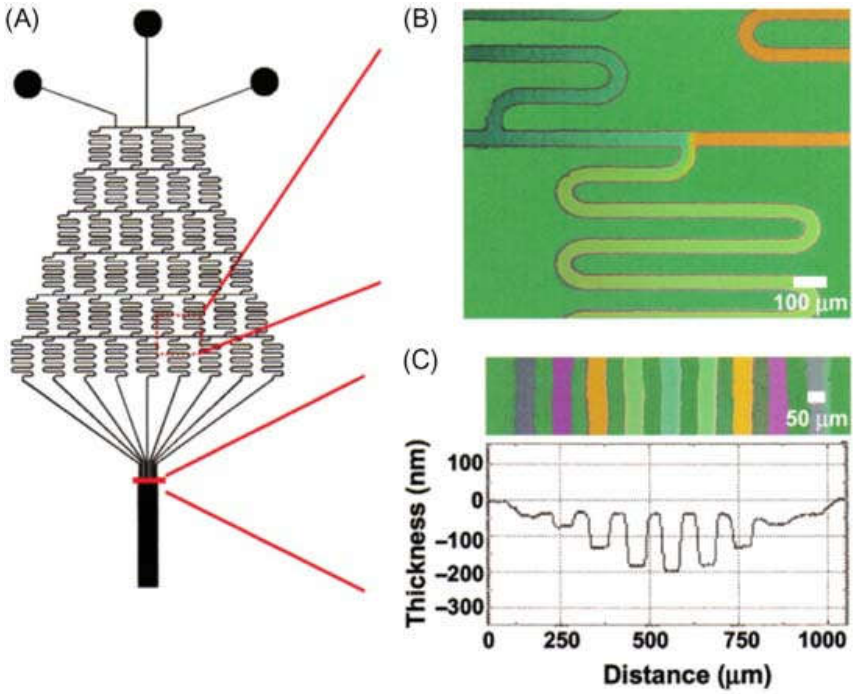

Figure 26.16 (A) Schematic representation of the tree-shape microfluidic gradient generator. (B) The optical photograph of one of the junctions in the device. It shows how the two flows with different concentrations can merge to one stream where the color is rapidly homogenized. (C) Optical micrograph and surface profilometer scan results across the branch channels before they combination. The thickness is correlated with amount of etching induced based on the HF acid concentration of the channel. *HF*, Hydrofluoric.
Source: Reproduced from Jeon, N. L., Dertinger, S. K. W., Chiu, D. T., Choi, I. S., Stroock, A. D., & Whitesides, G. M. (2000). Generation of solution and surface gradients using microfluidic systems. *Langmuir*, *16*, 8311−8316 with permission from ACS publications.

Graft polymerization

Surface graft polymerization is another technique applied to modify the surface of microfluidic microchannels. It is defined as the covalent binding of polymers onto different surfaces. There are two approaches for polymer grafting known as "grafting from" and "grafting to," which are categorized according to the reagents used and the experimental conditions. In the former approach, the polymerization reaction is conducted by the presence of a surface radical. The surface-free radicals that act as sites for graft polymerization are commonly formed via electron beam irradiation or UV. On the other hand, in the latter technique, the polymer chains with functional groups are covalently attached to the functional groups on the surface. The functionalization of the surface can be achieved by plasma treatment or silanization. One of the limiting factors of this approach is that limited grafting density can be achieved due to steric hindrance enforced by already-bonded polymers. Although the "grafting from" approach facilitates higher grafting densities, it leads to higher polydispersity because it is less possible to control the molecular mass of the polymer.

Polymer grafting techniques have been extensively used to functionalize the surface of the channel in the microfluidic device. For example, PEG-silane grafted onto oxidized surface of PDMS to generate an antifouling surface (Sui et al., 2006). (Kovach et al., 2014) for the first time were able to fabricate a long-term stable hydrophilic PDMS-based microfluidic device via covalently attaching PEG to an oxygen plasma-treated channel surface. When uncoated PDMS was used in blood-contacting applications, a high level of fibrinogen was absorbed onto PDMS and subsequently initiated platelet activation and led to the rapid augmentation of pressure across the channel, which made them useless for long-term applications. Thus through siloxane-bound PEG coating of the channel, Kovach et al. (2014) were able to remarkably decrease the fibrinogen adsorption and platelet adhesion for up to 28 days. The coagulation response in the presence of whole blood flow was also significantly reduced when assessed using this device. Therefore the PEG coating of a PDMS channel was able to enhance the hemocompatibility and the lifetime of the device by 16 times in comparison to an uncoated device. Demming et al. (2012) followed the same technique to integrate PEG-silane polymers onto the surface of plasma-treated PDMS, which yielded a coating with improved homogeneity and bonding ability in comparison to the commercially available PEGylation kit. This device maintained its hydrophilic stability in air and in different solvents long term. A batch cultivation of hydrophobic yeast cells, *Saccharomyces cerevisiae*, showed antiadhesive behavior of the cells to the surface. Thus this modification technique not only increased the emulsification of oil microdroplets in water but also decreased the adsorption of hydrophobic yeast cells. Later, this group developed a more improved approach, in which polyelectrolyte multilayers (PEMs) were deposited onto a microfluidic channel under continuous flow. In this technique, the pretreated PDMS surface was alternately exposed to a poly(diallyldimethylammonium chloride) solution and poly(acrylic acid) (PAA) solution, leading to the layer-by-layer assembly of each polymer onto the surface.

Although chemical grafting of PEG onto PDMS demonstrated superior mechanical and chemical robustness of the surface, the solution-phase nature of this polymer grafting technique not only needed complex processing steps to obtain high-quality functionalization, the organic solvents being used could also swell the PDMS device (Effenhauser, Bruin, Paulus, & Ehrat, 1997). Consequently, as described in the hydrogel section, studies have emerged to photo cross-linked PEG via UV irradiation onto the surface of microchannel (Kim, Jeong, Khademhosseini, & Suh, 2006; Sui et al., 2006), which led to the formation of PEG-based hydrogels.

Similar to PDMS, cyclic olefin copolymer (COC)-based lab-on-a-chip devices cannot be used without modifications due to the hydrophobic nature of COC (Faure et al., 2008). To address this shortcoming, Roy, Yue, Venkatraman, and Ma (2013) evaluated the UV-photografting of four different monomers, namely (acrylic acid, AA; acryl amide, AAm; hydroxyethylmethacrylate, HEMA; and *N*-vinylpyrrolidone, NVP) onto COC lab-on-a-chip devices. Various properties of each of the grafted polymers including their long-term stability, transparency, hydrophilicity, and platelet adhesion were assessed. It was concluded that UV-photografted NVP was a very effective approach for enhancing the hydrophilicity, hemocompatibility, bonding efficiency, and surface stability of COC microfluidic devices. Another example of the "grafting from" technique on COC devices was described by Jena and Yue (2012). To prevent protein adsorption and cell adhesion, Jena et al. proposed the conjugation of [2-(methacryloyloxy)ethyl]phosphorylcholine (MPC) monomer onto COC via sequential photografting with covalent attachment of the initiator. It was found that by increasing the irradiation time, the hydrophilicity and the thickness of the MPC was improved. Additionally, it was observed that the presence of a higher concentration of MPC led to a superior antifouling behavior on COC.

Moreover, graft polymerization through surface patterning has also been explored. Idota, Tsukahara, Sato, Okano, and Kitamori (2009) developed a patterned surface of Poly (*N*-isopropylacrylamide) (PNIPAM). They grafted PNIPAM onto a PAA-coated glass surface by means of electron beam lithography to induce the radical polymerization of PNIPAM onto the PAA-coated surface. With this approach, the use of a photomask was eliminated. This group further elucidated the successful thermally controlled cell attachment and detachment process. Ebara, Hoffman, Stayton, and Hoffman (2007) followed the same approach and reported the development of a smart microfluidic channel exhibiting a reversible hydrophobic-hydrophilic surface. They used UV-induced graft polymerization of temperature- and pH-responsive copolymers composed of PNIPAM-co-acrylic acid (AA), and a nonfouling PEG-diacrylate (PEGDA) hydrogel to modify the surface of the PDMS-based microchannels. This smart microchannel exhibited significant surface wettability variation depending on temperature and/or pH conditions.

Vu, Fouet, Gue, and Sudor (2014) revealed the grafting of 3,4-dihydroxy-L-phenylalanine-functionalized PAA brushes onto a PDMS surface via mussel-inspired chemistry. These surfaces showed a profoundly lower protein adsorption property; however, such surfaces maintained their protein adsorption property when unmodified or treated with dopamine film only.

SU-8 is a common photoresist used for microfluidic fabrication; however, it is chemically difficult to modify. Gao, Henthorn, and Kim (2008) adopted the "grafting from" technique to immobilize the photo-initiator on the surface of the negative-tone photoresist, SU-8. Then, a thin layer of either 2-HEMA-based hydrogel or PEG hydrogels were grown on the modified SU-8 substrate in the presence of UV irradiation. It was observed that the formation of PEG-based hydrogel dramatically increased the wettability of SU-8. Moreover, strategies have been explored to graft maleic anhydride (MA) copolymer films onto the surface of PDMS precoatings (Cordeiro, Zschoche, Janke, Nitschke, & Werner, 2009). The covalent grafting of MA to the surface of the PDMS was induced by incorporating amino groups to PDMS either via grafting an APTES precursor layer onto air plasma-treated PDMS or through low-pressure ammonia plasma treatment. The former PDMS activation technique led to a very rough and nonhomogeneously coated surface, whereas the latter approach formed a smooth and homogenous MA copolymer film onto PDMS.

Launiere et al. (2012) developed an in situ dual protein patterning methodology for immobilization of two proteins on a PDMS microchannel in order to fabricate a microfluidic capture device. PAA was photopolymerized onto the PDMS-based channel surface. The two proteins, anti-EpCAM) and anti-EpCAM plus E-selection, were then immobilized on the adjacent alternating modified surfaces to promote increased tumor cell capturing efficiency. In this technique, the photoresist behaved as a blocking agent and prevented the immobilization of proteins on the remaining surfaces.

Polydopamine hydrochloride (PDA) is a biocompatible material capable of strongly attaching to the surface and manipulating the surface property. The ability of PDA to undergo one-step LPD promoted the spatial patterning of the PDA onto the substrate via passing the dopamine solution through a microfluidic channel (Palchesko, Zhang, Sun, & Feinberg, 2012). In a recent study, Aghvami et al. (2017) rendered the surface of a COC device fluoro-philic. To induce fluorophilicity to the surface, PDA was flowed through the channel to self-polymerize and deposit a layer of hydrophilic PDA coating on the surface. Subsequently, a solution of *H*,1*H*,2*H*,2*H*-perfluorodecanethiol was passed and rendered the surface fluoro-philic. Chuah et al. (2015) coated the surface of a PDMS-based microchannel with PDA and further demonstrated the profound impacts of a PDA-coated surface on bone marrow stem cell adhesion, proliferation, and multipotency during a prolonged culture period. In another study, three types of cells, namely, mouse preosteoblast MC3T3-E1, FB NIH-3T3, and fibrosarcoma HT1080, were cultivated onto a PDA-patterned PDMS channel (Ku, Lee, & Park, 2010). All three cell types, while maintaining their normal morphology, revealed a strong affinity to grow and proliferate along the PDA-coated sections. Moreover, it was also confirmed that by manipulating the thickness of the PDA coating, the cell seeding density could be varied. Shi et al. (2014) generated various thicknesses of patterned PDA on a microfluidic concentration gradient generator. It was observed that the surface was rendered more hydrophilic when the PDA became thicker. Upon cultivation of human adipose mesenchymal stem cells (MSCs), lower cell density appeared on a

section with thicker PDA patterns. In addition, the cell number significantly reduced when the thickness of PDA was reduced.

Hydrogels

Hydrogel is defined as a 3D, cross-linked, hydrophilic, porous, polymeric network capable of absorbing and retaining significant amounts of aqueous solutions (Kumar, Srivastava, Galaev, & Mattiasson, 2007). The hydrated environment within hydrogels as well as its tissue-like elasticity, which closely resembles the properties of the natural ECM environment, make them a promising coating for the surface of the microchannel (Rahmani, 2011). Thus the use of hydrogels has emerged as an approach to regulate microchannel surface and cell interactions (Aubin et al., 2010; Liu & Bhatia, 2002). Hydrogels are synthesized from a variety of biocompatible material or ECM components such as collagen (Lee et al., 2009), HA (Collins & Birkinshaw, 2008; Khademhosseini et al., 2006), gelatin (Nichol et al., 2010), and elastin (Mithieux, Rasko, & Weiss, 2004; Patel, Fine, Sandig, & Mequanint, 2006).

Hydrogels that are utilized to coat the surface of microfluidic devices have to fulfill several requirements, including allowing the microfabrication of channels, sealing the channels, facilitating proper fluid flow through the channel, in addition to promoting the penetration of large or small molecules (Cabodi et al., 2005; Liu & Bhatia, 2002). Therefore the direct incorporation and assembly of hydrogels into sealed microfluidic devices is challenging because of the absence of surface chemical affinity between the hydrophobic PDMS-based microchannel surface and hydrogels (Cha et al., 2013; Greiner et al., 2014). To address this challenge, various approaches have emerged to generate supplementary interface material that behaves like an adhesive to attach these components.

Biocompatible hydrogels from both natural material (e.g., collagen, alginate, chitosan, agarose and dextran) and synthetic material PEG, polyacrylamide (PA) and PAA have been investigated for microchannel coating (Peppas, Hilt, Khademhosseini, & Langer, 2006).

Photopolymerizable polymers provide another approach to create in situ 3D cross-linked hydrogels. The in situ photopolymerization of a prepolymer solution to form a layer of microstructured hydrogel onto the supporting surface has been widely investigated. When working under a dynamic fluidic environment it is crucial to covalently attach the hydrogels network to the microfluidic channel walls to avoid detachment of the hydrogel by the shear flow (Lee, Arena, Beebe, & Palecek, 2010; Lee, Beebe, & Palecek, 2012). Annabi et al. (2013) engineered a photo-cross-linkable methacrylated gelatin and methacrylated tropoelastin hydrogel and introduced these prepolymers into the microfluidic channel under continuous flow. Upon UV irradiation to these photo-cross-linkable solutions, it was polymerized into a tubular-shaped cross-linked hydrogel inside the microfluidic channels. To examine the impact of this coating protocol on cell attachment, the primary cardiomyocytes were cultivated onto these hydrogels. It was observed that the softer and more elastic surface of tropoelastin-based hydrogels was more favorable for primary cardiomyocytes attachments and proliferation in contrast to a gelatin-coated

substrate. This group also concluded that by manipulating the flow rate of the injected prepolymer solution and its residence time within the channel solution during UV cross-linking, the thickness and homogeneity of the hydrogel can be controlled. The schematic of the hydrogel formation procedure is depicted in Fig. 26.17A.

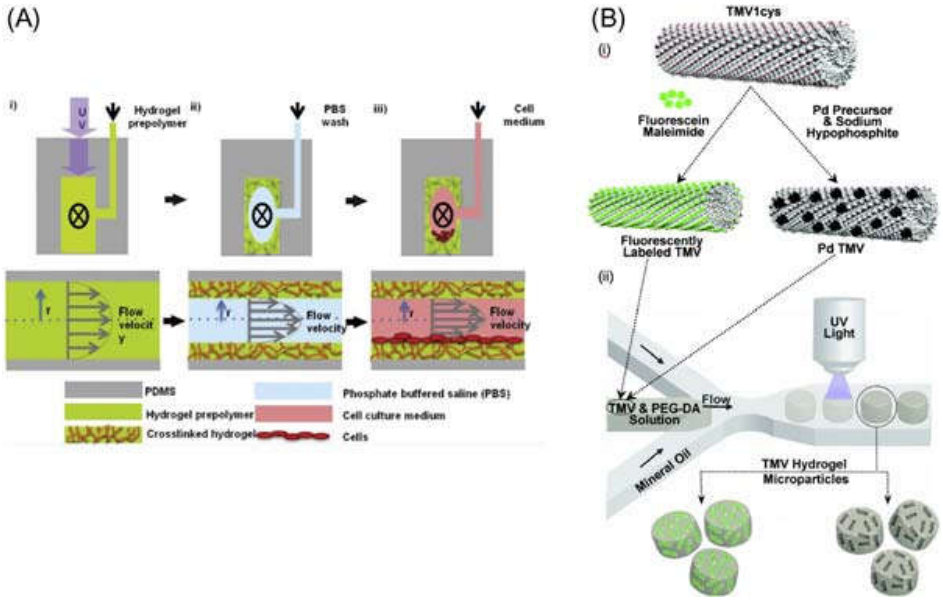

Figure 26.17 (A) Schematic representing the coating procedure: (i) A hydrogel prepolymer solution was introduced into channel and cross-linked by getting exposed to UV irradiation, (ii) The cross-linked hydrogel coated the surface of the PDMS channel, whereas the uncross-linked prepolymer was removed from the channel by PBS wash, (iii) The medium-loaded cell was introduced into the channel. The top figures presented the cross-section of a channel, perpendicular to the direction of the flow, while the bottom figures presented the cross-section of a channel, along the direction of the flow. (B) Schematic representing the fabrication procedure for microparticles composed of fluorescently labeled TMV or Pd−TMV complexes, (i) Schematic of chimera model showing approximately one-fifth of an entire TMV1cys virion. The cysteine residues genetically located on the outer surface of each coated protein were showed in red dots. TMV1cys via electroless plating was functionalized with fluorescein maleimide at the cysteines ormetalized with Pd nanoparticles, (ii) Schematic representing the fabrication procedure of microparticle within a microfluidic channel. The TMV-PEG solution was introduced into the channel as a dispersed droplet phase, while mineral oil was added into the channel as a continuous phase. In the presence of UV irradiation, the droplets are photopolymerized to generate PEG-based hydrogel microparticles with fluorescently labeled TMV. *PBS*, Phosphate-buffered saline; *Pd*, palladium; *PDMS*, polydimethylsiloxane; *PEG*, poly(ethylene glycol); *TMV*, tobacco mosaic virus; *UV*, ultraviolet.
Source: (A) Reproduced from Annabi, N., Selimović, Š., Acevedo Cox, J. P., Ribas, J., Afshar Bakooshli, M., Heintze, D., et al. (2013). Hydrogel-coated microfluidic channels for cardiomyocyte culture. *Lab on a Chip*, *13*, 3569−3577 with permission from the Royal Society of Chemistry. (B) Reproduced from Lewis, C. L., Lin, Y., Yang, C., Manocchi, A. K., Yuet, K. P., Doyle, P. S., & Yi, H. (2010). Microfluidic fabrication of hydrogel microparticles containing functionalized viral nanotemplates. *Langmuir*, *26*(16), 13436−13441 with permission from the American Chemical Society.

Synthetic hydrogels composed of PEGDA have been extensively used in a wide range of applications due to their highly cross-linked network, which allows for the capsulation of cells, DNA, protein, and drugs as well as their ability to readily cross-link with natural gels such as alginate, agarose, and chitosan (Koh & Pishko, 2005; Lee et al., 2012; Park et al., 2006; Shah et al., 2012). PEG hydrogels have been widely fabricated via photopolymerization in the presence of photoinitiators in closed microfluidic channels. In this polymerization process, UV light initiated the free-radical cross-linking of acrylate functional groups on PEGDA leading to the fabrication of highly cross-linked PEG hydrogel (Koh & Pishko, 2005). Gradient hydrogels incorporated within a microfluidic device were developed to explore the impact of RGD (arginine−glycine−aspartic acid) concentration gradient on MSC behavior (Liu et al., 2012). Cell adhesion RGD peptide was covalently immobilized into PEG molecules to create acryloyl−PEG−RGD. To facilitate the hydrogel formation process, a PDMS-based microfluidic gradient generator device was used consisting of two inlets. One inlet was used to inject PEGDA mixed with a photoinitiator and to another one to introduce PEGDA along with a different concentration of acryloyl−PEG−RGD. Subsequently, these two-polymer solutions solidified in the gradient chamber upon irradiation with UV light. In addition, to promote the covalent bonding of PEG hydrogel to the underlying glass slide, its surface was salinized with 3-(trimethoxysilyl) propyl methacrylate. MSCs were then cultured on an RGD immobilized PEG hydrogels surface. It was found that MSCs attachment and growth was directly correlated with the density of the incorporated RGD (Liu et al., 2012). In another study, in situ photopolymerization of PEGDA was done to design a microfluidic device as a biosensing tool. The ability of the device as a sensing application was assessed through a colorimetric protein assay. Bromophenol blue pH indicator dye was immobilized in the UV-irradiated hydrogel. When this dye interacted with the protein in the acidic environment, a color shift from blue to yellow occurred (Puchberger-Enengl, Krutzler, Keplinger, & Vellekoop, 2014).

Koh and Pishko (2005) conjugated a ratiometric pH sensitive carboxy seminaphthofluorescein (SNAFL-1)-labeled enzyme with a PEGDA solution in the presence of a photo-initiator. The deposition of the solution into a microfluidic device and the subsequent UV irradiation induce the formation of enzyme-loaded hydrogel microstructures within the microchannel. This device has the potential to be used as a biosensor or microreactor. The pH-responsive behavior of this device was confirmed with changes in the intensity and emission wavelength of these hydrogels when a solution with a different pH was injected into the channel. In situ formed PEG-based hydrogels were further used as a microparticle to encapsulate and carry genetically modified tobacco mosaic virus nanotemplates. The procedure is shown in Fig. 26.17B (Lewis et al., 2010).

Furthermore, patterned deposition of the hydrogel within the microfluidic devices has also been explored (He & Herr, 2010; Kim, Karns, Tia, He, & Herr, 2012; Tia, He, Kim, & Herr, 2011). Piao, Han, Azad, Park, and Seo (2015) investigated the use of a photomask to pattern the surface of plasma-treated and TMP salinized PDMS-based microfluidic devices with PEGDA hydrogels. Prior to the

photopolymerization of PEGDA, glucose oxidase was introduced to the prepolymer solution to make the device capable of sensing glucose. The capability of the device to detect small amounts of glucose, even from a urine sample, was attributed to the patterning of the surface of the device. Lee et al. (2010) fabricated photopatterned macroporous PA and PEGDA hydrogels within a microfluidic channel in the presence of PEG porogen. The induced-macroporosity in these hydrogels significantly improved the large macromolecules transport to the interior of the hydrogel. A PEG-based hydrogel-coated microchannel surface was further applied as a platform to create micropatterns of photo-immobilized cell binding protein FN on the surface of the channel. The spatially defined FN patterns remarkably increased the cell attachment. In another study, PEGDA hydrogels were embedded within the PDMS channel via a multilayer soft lithographic technique in which PDMS and PEGDA were serially replica molded to generate microfluidic hydrogel networks. The complete procedure is portrayed in Fig. 26.18F. It was concluded that these cell-laden microfluidic hydrogels were able to significantly improve cellular viability (Cuchiara, Allen, Chen, Miller, & West, 2010).

The pH-responsive behavior of chitosan, namely its positive charges at low pH, allowed the electro-deposition of a layer of chitosan onto a negatively biased electrode surface, as depicted in Fig. 26.18B. This procedure led to the formation of a biopolymer hydrogel network at the electrode surface with high spatial resolution. In addition, chitosan possesses a proper functional group for the covalent conjugation of cells and biomolecules (Park et al., 2006).

PA gels with various ranges of elastic moduli can be fabricated via manipulating the ratio of bisacrylamide cross-linker to the acrylamide (Cukierman, Pankov, & Yamada, 2002). Moreover, hydrogels consisting of different protein moieties were patterned onto the surface of microfluidic devices. Photopolymerization of PA through a photomask led to surface functionalization, followed by polymerization by benzophenone, which was absorbed by the PDMS substrate. This patterned microchannel was applied to improve the isolation, and further analysis of the circulating tumor cells (CTCs) under flow conditions (Cukierman et al., 2002). Olsen, Ross, and Tarlov (2002) described the photoinduced cross-linking of acrylamide-modified DNA probes in microchannels. They showed that single-stranded DNA modified with an acrylic acid can be conjugated into a PA, which can form a gel in the presence of UV light within a microfluidic channel. The porosity of the hydrogels facilitated the transportation and hybridization of the fluorescence-labeled DNA with the complementary DNA strands through the gel. Later, Zangmeister and Tarlov (2003) improved the mechanical breakdown and dislodgment of these DNA hydrogels under continuous electrophoretic conditions. They enhanced the stability of the PA hydrogels within a microchannel by performing UV/O_3/silane pretreatment of the surface followed by the UV graft polymerization of PA onto the chemically-modified surface of the channel. Moreover, the in situ photopatterning of the PA hydrogel within the microfluidic device also yielded the formation of an automated immunoblotting assay on chip. This PA-based hydrogel-patterned chip device resembled both a protein-binding membrane and a miniature slab gel (He & Herr, 2009, 2010). This one-chamber device was able to unify the PA gel

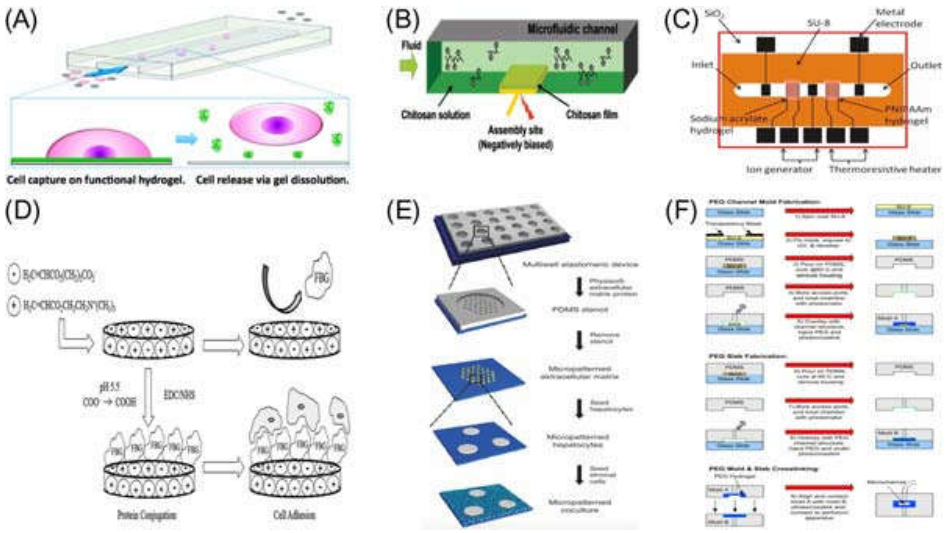

Figure 26.18 (A) Schematic representing covalently cross-linked alginate (*green*) hydrogel, biofunctionalized with biotin moieties to increase its affinity for cells and introduced into the channel to coat the surface of the microchannel. Exposing the hydrogel to the bacterial enzyme such as alginate lyase led to dissolution of the hydrogel and release of the cell. (B) Schematic showing the coating of chitosan onto the surface of the microfluidic channel at the assembly site. (C) Schematic of integrating temperature- and pH-responsive hydrogel microvalves into microfluidic device. (D) Schematic representing the deposition and conjugation of TMA/CAA hydrogel onto the surface of the channel, which induce resistant to nonspecific protein adsorption onto the surface of the channel. (E) Schematic representing the procedure to create micropatterned ECM-based hydrogel onto microchannel surface. Subsequently, primary hepatocytes selectively attached to ECM-coated areas, promoting supportive stromal cells to be seeded into the bare areas. (F) A PEGDA microchannel was created within a PDMS device through serial replica molding of PEGDA and PDMS onto the photoresist masters. To generate 3D microchannel environment, the PDMS/PEGDA mold, Mold A, can either attached to cover glass after step 5 or cross-linked to a PEGDA blank slab, Mold B (step 9). *3D*, Three-dimensional; *CAA*, 2-carboxyethyl acrylate; *ECM*, extracellular matrix; *PDMS*, polydimethylsiloxane; *PEGDA*, poly(ethylene glycol)-diacrylate. Source: (A) Reproduced from Shah, A. M., Yu, M., Nakamura, Z., Ciciliano, J., Ulman, M., Kotz, K., Stott, S. L., et al. (2012). Biopolymer system for cell recovery from microfluidic cell capture devices. *Analytical Chemistry*, *84*, 3682−8 with permission from the American Chemical Society. (B) Reproduced from Park, J. J., Luo, X., Yi, H., Valentine, T. M., Payne, G. F., Bentley, W. E., Ghodssi, R., et al. (2006). Chitosan-mediated in situ biomolecule assembly in completely packaged microfluidic devices. *Lab on a Chip*, *6*, 1315−1321. with permission from the Royal Society of Chemistry. (C) Reproduced from Bäcker, M., Raue, M., Schusser, S., Jeitner, C., Breuer, L., Wagner, P., et al. (2012). Microfluidic chip with integrated microvalves based on temperature- and pH-responsive hydrogel thin films. *Physica Status Solidi (A) Applications and Materials Science*, *209*, 839−845 with permission from Wiley-VCH. (D) Reproduced from Schroeder, M. E., Zurick, K. M., McGrath, D. E., & Bernards, M. T. (2013). Multifunctional polyampholyte hydrogels with fouling resistance and protein conjugation capacity. *Biomacromolecules*, 14, 3112−3122 with permission from the American Chemical Society. (E) Reproduced from Khetani, S. R., & Bhatia, S. N. (2008). Microscale culture of human liver cells for drug development. *Nature Biotechnology*, *26*, 120−126 with permission from Springer Nature. (F) Reproduced from Cuchiara, M. P., Allen, A. C. B., Chen, T. M., Miller, J. S., & West, J. L. (2010). Multilayer microfluidic PEGDA hydrogels. *Biomaterials*, 31, 5491−5497 with permission from Elsevier.

electrophoresis protein separation, electrophoretic transfer, and antibody-based in-gel blotting. Sung, Chen, Makamba, and Chen (2009) also studied the integration of a PA-based hydrogel with PDMS-based microchannels. This group covalently photopatterned 3D hydrogels composed of PA functionalized with protein G onto the microfluidic channel coated with PEMs. This protein G-immobilized hydrogel was further used for immune-assay application in which estrogen receptors α were detected quantitatively with enhanced specificity.

Shah et al. (2012) developed a biodegradable and photo-cross-linkable coating within microfluidic channels consisting of alginate and methacrylic groups. The schematic of this approach is portrayed in Fig. 26.18A. These hydrogels further elucidated the efficient delivery and release of the antibody-captured cells. The enzymatic degradation of the alginate with alginate lyase led to controlled release of the cells with $99 \pm 1\%$ efficiency in which $98.9 \pm 0.3\%$ of the cell remained viable and proliferative. In addition, it was observed that after 96 hours, single-cell colony formation could be achieved which was comparable to control cells.

Furthermore, the characteristics of hydrogel are defined by the prepolymer solution used. Thus the nature of the chosen monomer in addition to the presence of external stimuli such as changes in pH, temperature, magnetic field, light, ionic strength, and radiation forces can cause hydrogels to undergo phase transition (Bäcker et al., 2012; Launiere et al., 2012). Hydrogels that are responsive to external stimuli are known as smart polymer. PNIPAM is one of the well-investigated thermo-responsive polymers because of its capability to undergo conformational changes from hydrophilic to hydrophobic at about 32°C, which corresponds to its lower critical solution temperature. Bäcker et al. (2012) for the first time applied a poly(sodium acrylate) (PSA) hydrogel to form on chip integrated pH-responsiveness into a microfluidic device. They developed two types of microvalves consisting of temperature-responsive PNIPAM and a pH-responsive PSA hydrogel film fabricated by in situ photopolymerization within a microfluidic channel, as presented in Fig. 26.18C. The shrinking and swelling behavior in addition to the height change of the hydrogel films were also investigated.

Synthetic hydrogels with polyampholyte properties have also been integrated into microfluidic devices. Hydrogel synthesized from positively charged [2-(acryloyloxy)ethyl]trimethylammonium chloride (TMA) and negatively charged 2-carboxyethyl acrylate (CAA) monomer exhibited zwitterionic behavior. This hydrogel was disposed onto a microfluidic device to obtain nonfouling properties against lysozyme and fibrinogen, as depicted in Fig. 26.18D (Schroeder, Zurick, McGrath, & Bernards, 2013).

Natural ECM-derived hydrogels such as collagen, Matrigel, alginate, and agarose are the most commonly used polymers to coat the surface of microfluidic devices, particularly for cell culture applications. For example, agarose gel was laid on top of the NIH-3T3 and Hela cell seeded onto the microfluidic channel. To perform drug screening, different concentrations of the drug introduced on top of the agarose gel (Tran, Cho, & Min, 2013). Khetani and Bhatia (2008) generated a liver-cell micropatterned device. They fabricated a 24-well PDMS mold sealed against a polystyrene plate, and subsequently a microchannel surface micropatterned with

various collagen-I island diameters via photolithography and hepatocyte was seeded onto these collagen-patterned islands. The fabrication procedure was depicted in Fig. 26.18E. It was observed that micropatterned hepatocyte clustering on micro-scale islands were able to promote liver-specific functions and maintain their phenotypic function over several weeks.

In an organ-on-chip section, we will describe in more detail the application of other naturally derived ECM proteins including collagen, Matrigel, and FN as a coat hydrogel to modify the surface of the microfluidic microchannel for the development of the organo-on-a-chip devices.

Surface blocking strategies for controlled cell adhesion

The principal function of blocking agents is to prevent nonspecific adsorption (NSA) of biological or chemical molecules on surfaces. For decades, they have been extensively employed in ELISAs and Western blots to coat all interfaces between the working solution and the well plates or membranes, respectively (Julián, Cama, Martínez, & Luquin, 2001; Mahmood & Yang, 2012; Mohammad & Esen, 1989; Steinitz, 2000). Alternatively, they can be used to cover select nonfunctionalized areas of biosensing microarrays and microfluidic devices (Hsieh et al., 2009). The latter two applications are explored in further detail in the "Selected applications" section.

By reducing the NSA of untargeted molecules, blocking agents are improving the sensitivity and the specificity of the aforementioned diagnostics techniques, leading to more accurate and reliable measurements. Sensitivity is defined as the technique's output to input signal ratio. This parameter can be weakened by NSA if untargeted molecules disable the binding sites designated for molecules of interest, thereby weakening the signal output and potentially leading to false negative diagnoses. Specificity refers to the technique's ability to only measure targeted interactions. Untargeted interactions are seen as high background noise and can significantly impact the reliability of a reading (Hegde et al., 2000). For example, in the case of ELISAs or biosensors, fluorescently labeled identifiers complementary to the target molecule may adhere to unblocked surfaces, which could subsequently lead to inadvertent inflation of the fluorescent signal and false positive diagnoses. Blocking agents can also be applied to a surface in specific patterns, through contact printing or masks, for controlled biomolecular or cellular adhesion. This can be useful for normalizing cell shapes, thus reducing their dimensional and functional variability during culture (Guo & Wang, 2011).

Three adsorption conditions can be implemented to attach blocking agents to a designated surface: physisorption, chemisorption, and electrostatic adsorption.

- *Physisorption*, or the physical adherence of blocking agent to the surface, is attained through van der Waals forces (Autumn et al., 2000), resulting in lower interaction energy and adsorption stability. This may impact the efficiency of the blocking layer over long periods of time or in relatively harsh environments, such as high flow rates or acidity.

The application of the blocking agent is relatively simple: the blocking agent is suspended in a buffer (e.g., PBS, tris-buffered saline) (Mahmood & Yang, 2012), introduced to the surface, and left to adsorb over an incubation period. However, multiple layers of the blocking agent may occur as a result of physisorption.

- *Chemisorption* refers to the covalent binding of the blocking agent to the surface, usually in SAMs (Lavrich, Wetterer, Bernasek, & Scoles, 1998). Under this condition, the surface must have appropriate and accessible functional groups for the blocking agent to bind to; otherwise, a linking agent can be applied to bridge the two. While the covalent attachment of blocking agents leads to a superior stability, it often presents more challenges procedurally and monetarily. Specific thermodynamic (e.g., pressure, temperature) or chemical (e.g., molarity, pH) conditions are typically necessary for covalent bonds to occur, which in turn could require additional equipment or time.
- *Electrostatic adsorption* involves an electrostatic attraction between oppositely charged blocking agents and surfaces (Ferrari, Kaufmann, Winnefeld, & Plank, 2010; Serizawa, Kamimura, & Akashi, 2000). It is applied and may be perturbed similarly to physisorption.

A wide range of polymers have been employed as blocking agents in biomolecular detection. The most commonly used polymer in biomedical applications is PEG due to its low toxicity and high cellular and bacterial resistance. Furthermore, its high hydrophilicity increases surface wettability and protein repulsion (Riquelme et al., 2016). PEG is typically modified to improve adsorption stability, but at higher cost and complexity. For example, PEG chains can be grafted to a PLL backbone, and the resulting PLL−PEG molecules can be easily attached to a negatively charged surface using electrostatic adsorption (Bergstrand, Rahmani-Monfared, Östlund, Nydén, & Holmberg, 2009). Unmodified PEG has demonstrated adequate physisorption and surface blocking in low surface concentrations on plastics for biomolecular assays (Liu et al., 2013). Other blocking polymers are PA (PAA) (Guo & Wang, 2011), polyallylamine hydrochloride (Liu, Huang, Kelly, & Liu, 2016), polystyrene sulfonate (Liu et al., 2016), polyvinyl pyrrolidone (Haycock, 1993), and polyvinyl sulfonic acid (Liu et al., 2016).

In addition to polymers, proteins are often used as blocking agents. When selecting a protein, it must be enzymatically inert and must not otherwise chemically interact with any components of the working solution such as reactants, other proteins, or cells (Steinitz, 2000). Considering their larger size compared to polymers, proteins exert a higher degree of steric hindrance and may reduce the reactivity of a functionalized surface (Hsieh et al., 2009). Due to their chemical complexity compared to polymers (Julián et al., 2001), the number of proteins that can be used for surface blocking is more limited, and the contents of the working solution must be considered. The most popular blocking protein is BSA, due its limited reactivity with other proteins, relatively small size, and stability (Jeyachandran, Mielczarski, Mielczarski, & Rai, 2010). Chicken serum albumin is similar to BSA in size and can be used as a substitute (Riquelme et al., 2016). Nonfat dry milk, including the protein family casein (Esser, 1991; Mack et al., 2017), and gelatin (Haycock, 1993) consist of a wide variety of low-reactivity proteins and are favorable for their low cost and availability, but result in a heterogeneous blocking layer (Mohammad & Esen, 1989).

Surfactants are compounds used to lower the surface tension at the interface between a liquid and a gas, liquid, or solid. Principally, they are used as detergents

for removing nonspecifically adsorbed molecules from a surface or for increasing surface wettability (Rosen & Kunjappu, 2012). They have also been implemented as blocking agents; however, the principal drawbacks of surfactants are their cellular toxicity, tendency to denature proteins, and generation of bubbles (Liu et al., 2016). Surfactants with low reactivity, namely polysorbate (Tween) 20, can still be effective blocking agents at low concentrations or in conjunction with other agents (Liu et al., 2013; Riquelme et al., 2016; Steinitz, 2000), but they are not optimal for applications involving controlled cell adhesion. The following surfactants have also been implemented as blocking agents for noncellular applications: sodium dodecyl sulfate (Liu et al., 2016), cetrimonium bromide (Liu et al., 2016), and Triton X-100 (Haycock, 1993; Liu et al., 2013).

There exist a few other organic compounds that can be used as blocking agents but that are not associated with one of the three categories above:

- Succinic anhydride can be used to block amine-functionalized surfaces (Taylor, Smith, Windle, & Guiseppi-Elie, 2003), which can be used to easily anchor biomolecules in biosensors or microfluidic devices.
- Mercaptohexanol (Guo & Wang, 2011; Vikholm-Lundin & Piskonen, 2008) and mercaptoundecanol (Riquelme et al., 2016) are long-chain alkanes capable of forming dense and repellent SAMs via chemisorption.
- Ethanolamine and cysteine have been used to block carboxyl functional groups with additional cross-linkers (Frederix et al., 2004).

New developments in omniphobic lubricant-infused (OLI) coatings present a significantly different approach to surface blocking (Ingber et al., 2015). They are inspired by the *Nepenthes* pitcher plant, which is capable of locking a thin layer of water from rainfall to form a highly repellent and slippery surface. Insects are unable to adhere to its surface and fall into the plant's pit-like trap for digestion (Leslie et al., 2014). Similarly, OLI coatings rely on surface modification techniques to enhance a surface's affinity to a lubricant, a thin homogeneous layer of which can be subsequently immobilized on the surface and acts as a highly repellent barrier to prevent NSA of biomolecules and cells. While proteins generally have a high affinity for hydrophobic surfaces, the lubricant has proven to be effective at repelling high concentrations of biomolecules in complex solutions, namely blood (Leslie et al., 2014).

The two approaches used for establishing this affinity is through surface texturing and/or chemical modification. Microscale posts have been fabricated using soft-lithography (Leslie et al., 2014) and photolithography (Leslie et al., 2014), then subsequently silanized and perfused with lubricant to achieve superhydrophobic and slippery repellency (Anand, Paxson, Dhiman, Smith, & Varanasi, 2012; Daniel, Mankin, Belisle, Wong, & Aizenberg, 2013). Without surface texturing, the chemisorption of silane SAMs with tethered perfluorocarbon chains is capable of capturing fluorinated lubricants such as perfluorodecalin to comparable effect (Badv, Jaffer, Weitz, & Didar, 2017; Leslie et al., 2014). Through the formation of hybrid SAMs consisting of multiple types of silanes, OLI coatings can achieve simultaneous functionality and surface blocking. Functional biomolecules can then

penetrate through the lubricant to capture targets while maintaining an otherwise homogeneous slippery barrier to block NSA. They have demonstrated the added benefit of significantly reducing the rate of coagulation of blood (Badv et al., 2017), which can be critical for direct capture of biomolecules or cells from blood-based solutions.

To summarize, the selection of a blocking agent to minimize NSA is dependent on the surface and target in question. They can be adsorbed to the surface physically or electrostatically for simplicity, or covalently for added stability. Polymers, proteins, and surfactants are well-established categories of blocking agents in immunoassays and biosensors but are not all suitable for controlled cell adhesion due to toxicity and reactivity. OLI coatings are an emerging blocking strategy that employs covalent stability, hydrophobic and slippery repellency, and anticoagulant properties.

Selected applications

Affinity-based cell sorting and separation in microfluidic devices

In the past decades, sorting, isolating, and counting cells have been drastically under research due to their applications in clinical diagnostics or fundamental research (Autebert et al., 2012; Didar, Li, Veres, & Tabrizian, 2013; Fatanat-Didar, Li, Tabrizian, & Veres, 2013). With the advent of microfluidics and the growth publications and innovative ideas in the past decade (Autebert et al., 2012), researchers have the advantage of scaling the cell sorting system corresponding to the size of cells, as well as multiplexing assays, reduction in reagent amount, elimination of potential biohazard aerosols, and reduction in time and expenses (Autebert et al., 2012; Didar & Tabrizian, 2010; Kanaji, Fahs, Shi, Haberichter, & Montgomery, 2012). Microfluidic adhesion-based methods for cell sorting specifically capture cells based on the biochemical properties of cells membrane. These classes of devices generally depend on antibody−antigen interactions to promote the adhesion and sorting (affinity molecule-coated surfaces) (Autebert et al., 2012). However, there are other methods based on cell's specific biological markers, such as fluorescence-activated cell sorting and magnetic-activated cell sorting, as well as methods based on physical properties of cells such as size, which is not the focus of this section (Antfolk & Laurell, 2017; Choi, Karp, & Karnik, 2012). Initially reported by Nagrath et al., a design of a CTC chip to sort cells was firstly achieved. In their design, anti-EpCAM antibodies were coated on arrays of microposts in a microfluidic channel. In a few hours, this device was able to sort CTCs from whole blood (Nagrath et al., 2007). Since then, there has been numerous research on different cell types and sorting them through affinity-based methods. Here, the focus is mainly on sorting and separating cells other than cancer cells by affinity-based methods for both positive and negative separation and sorting (Fig. 26.19), which is primarily achieved by functionalizing microfluidic channels. Firstly, studies that have implemented antibody coatings are discussed, and then studies that have

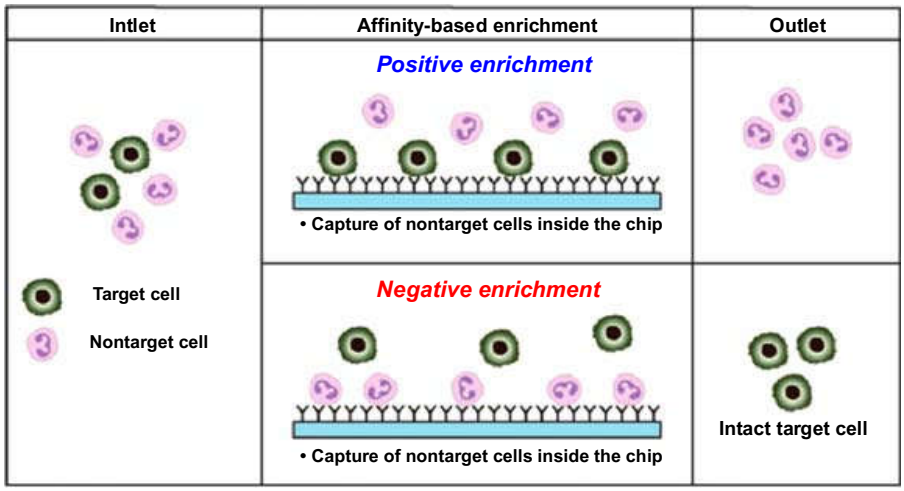

Figure 26.19 Affinity-based positive and negative separation and sorting of cells. In a positive enrichment, an antibody (another capture molecule) is implemented to capture the target cells, whereas in a negative separation, an antibody (or another capture molecule) is used to capture the nontarget cells and the target cells is enriched in the outlet.
Source: Reproduced from Hyun, K. A., & Jung, H. I. (2013). Microfluidic devices for the isolation of circulating rare cells: A focus on affinity-based, dielectrophoresis, and hydrophoresis. *Electrophoresis*, *34*(7), 1028–1041 with permission from Wiley Online Library.

implemented a coupling agent for immobilizing antibodies and peptides, and lastly, an electro-generated, protein-adsorptive device for cell capture is discussed.

Deterministic cell rolling, designed by Choi et al., sorted out cells based on the surface interactions with the microfluidic channel (Fig. 26.20). In their system, target cells interact with the P-selectin modified surface, allowing the cells to roll across the ridges on the channel, and furthermore displace laterally toward the gutter side on the device. Since the nontargeted cells do not interact with the surface, they flow over the ridges, and later on exit through the focusing side. As a negative control, the channel was completely block by BSA which resulted in no separation of the two different cell types as cell–surface interactions were negligible. Nevertheless, the two cell lines to validate this concept were leukemia cell lines, HL-60 [target cell, expresses P-selectin glycoprotein ligand-1 (PSGL-1, CD62P)] and K562 (nontarget cell, lack PSGL-1) (Choi et al., 2012).

A 3D microfluidic channel was implemented with multiple vertical inlets to an affinity surface to facilitate cell separations in an antibody coated channel (Fig. 26.21). The inside of the channel was functionalized with the antibody of interest and then the cells were flowed inside the device so that the target cell would be enriched in the outlet by negative selection of untargeted cells. For instance, using anti-CD19 coated chips, HuT 78 lymphocytes (target cells in this case and CD71 + CD19 −) were separated from Ramos cells (CD71 + CD19 +). In the inlet, the HuT 78 cell percentage was 35%, and after the separation, in the outlet, the percentage raised to 90% (Li, Gao, & Pappas, 2011).

In a recent study in 2017, a microfluidic device was fabricated with the aim of sepsis diagnostic. An affinity molecule-coated surface, in this case, anti-CD64

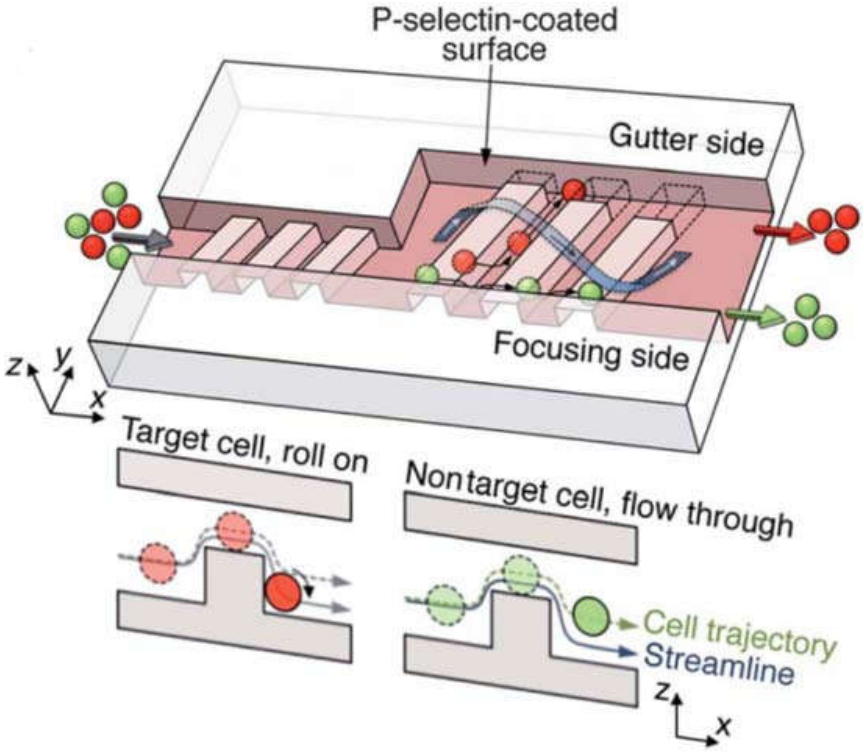

Figure 26.20 Schematic of a microfluidic channel which contains focusing ridges in the narrow channel and sorting ridges in the wide channel. The ribbon is a representative of the helical streamline. In the bottom side of the figure, cross-section views of the microchannel are shown, which depict the cell trajectories based on their surface interactions.
Source: Reproduces from Choi, S., Karp, J. M., & Karnik, R. (2012). Cell sorting by deterministic cell rolling. *Lab on a Chip*, *12*(8), 1427 with permission from Royal Society of Chemistry.

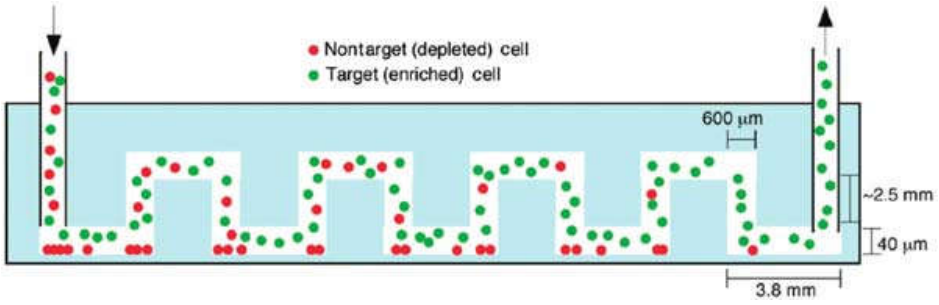

Figure 26.21 Schematic of the negative enrichment microfluidic device. A mixture of cells are flowed in through the inlet, allowing the nontarget cells to be captured in the channels due to the surface interaction. Furthermore, the target cells are passed through the microchannel and are enriched in the outlet.
Source: Reproduced from Li, P., Gao, Y., & Pappas, D. (2011). Negative enrichment of target cells by microfluidic affinity chromatography. *Analytical Chemistry*, *83*(20), 7863−7869 with permission from ACS publications.

antibody coated surface, was used in the microfluidic device, as the expression of CD64 in leukocytes increases in case of sepsis, and highly expressing CD64 + cells were captured and low-expressing CD64 + cells were not. Two different modules was tested in the device: one was using differentiated HL-60 cells (HL-60 cells can differentiate into various cell lines) to neutrophils, which were stimulated to upregulate CD64 expression, and the other was using blood samples from healthy volunteers and septic patients in the device as a validation step (Zhang et al., 2018).

A tandem affinity microfluidic was developed to positively separate and sort CD4 + /CD8 + T lymphocytes to further measure their ratio based on affinity separation (Fig. 26.22). CD4/CD8 ratio is an important factor, and it is measured to investigate human immunodeficiency virus infection and acquired immunodeficiency syndrome. The microfluidic device is composed of two sections, which were separately sealed by pneumatic actuated control layers to further facilitate CD4 and CD8 coatings in each region through the main channel. Subsequently, blood was flowed inside the main channel and allowing the cells to settle down on their respective affinity regions. Furthermore, antibodies were passed through the main channel to stain the captured cells and remove nonspecifically captured ones. Captured CD4 + and CD8 + T lymphocytes in each region matched the CD4 + / CD8 + T lymphocytes ratio in blood (Li, Gao, & Pappas, 2015).

Ligand–receptor interactions, in a form of peptide sequences such as Arg–Glu–Asp–Val (REDV) and Val–Ala–Pro–Gly (VAPG), which bind to ECs and SMCs, respectively, is another method used in microfluidic devices to achieve selective cell adhesion and sorting. The work done by Plouffe et al. utilized a microfluidics channel design, which allowed for the shear stress to decrease along the longitudinal axis of the device. The surface of the device was functionalized in three steps: (1) 3-mercaptopropyl trimethoxysilane solution, (2) *N-y*-maleimidobutyryloxy succinimide ester (GMBS) solution (coupling agent), (3) peptide solution (REDV or VAPG). Furthermore, adhesion of the cells was shown to be independent from the cell solution, as the device was able to capture cells from both a

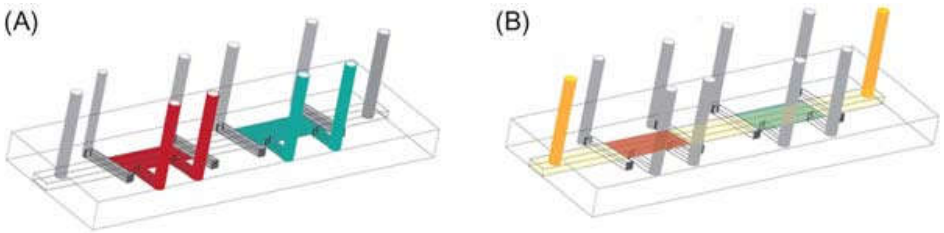

Figure 26.22 Schematic representative of the tandem affinity microfluidic device. (A) The antibody immobilization step. Initially pneumatic valves (*gray channels*) were closed, to keep the antibody solutions (*red* and *green*) in their affinity regions. (B) The separation step. The blood sample was flowed through from the inlet (*orange cylinder*) and then the cells were allowed to settle on the surface.
Source: Reproduced from Li, W., Gao, Y., & Pappas, D. (2015). A complementary method to CD4 counting: Measurement of CD4 + /CD8 + T lymphocyte ratio in a tandem affinity microfluidic system. *Biomedical Microdevices*, *17*(6), 113 with permission from Springer.

suspension of one cell type as well as a heterogeneous suspension containing ECs, SMCs, and FB with a purity as high as 83%. The adhesion of the cells were mainly a function of the amount of the shear stress, and the selectivity of the adhesion was primarily based on the peptide that had been used (Plouffe et al., 2007). Similar studies have implemented the same concept for cell sorting and capture with antibodies (Plouffe, Kniazeva, Mayer, Murthy, & Sales, 2009) and peptides (Plouffe, Radisic, & Murthy, 2008).

Hansmann et al. developed a disposable microfluidic platform to selectively capture circulating endothelial progenitor cells (EPCs) from human whole blood. The microchannel has microposts [similar to the study by Nagrath et al. (2007)], and was functionalized using 3-mercaptopropyl trimethoxysilane, followed by N-[γ-maleimidobutyryloxy] succinimide ester (GMBS) coupling agent and attachment of anti-CD34. After passing blood through the system, captured cells were counterstained with antibodies against characteristic EPC surface antigens, kinase insert domain (KDR), CD31, and CD45. The blood used for the experiments were from healthy and patients with pulmonary arterial hypertension (PAH). The results revealed that the patients with PAH had 50% lower EPCs than healthy people, and as a validation, results from the device were compared with conventional flow cytometry counts (Hansmann et al., 2011).

A microfluidic device was developed to separate a type of leukocytes from a suspension of different leukocytes within a specific region of the device (Fig. 26.23). Bottom side of the channel was blocked by PEG-dimethacrylate (PEGDM), and the upper side of the channel had arrays of platinum electrodes, which electro-generated HBrO, which subsequently allows the down side of the channel to became protein-adsorptive. Through this method, since the rest of the bottom side is blocked by PEGDM, the surface can become selectively adhesive toward proteins. Neutrophil- or eosinophil-specific antibodies were then immobilized on the created regions and the cells were flowed inside the channel. Furthermore, an AC voltage was applied to the microelectrode arrays for negative dielectrophoresis to concentrate the cells in the channel. The results revealed that the corresponding leukocyte type can be captured from the concentrated leukocytes within the channel (Hashimoto, Kaji, & Nishizawa, 2009).

Organ-on-a-chip

The 2D cell culture system is not able to closely recapitulate the complex biochemical and mechanical cell−cell, cell−matrix interactions, whereas cell cultures in 3D microfluidic systems exhibit more in vivo−like behavior (Griffith & Swartz, 2006; May, Evans, & Parry, 2017; Mueller-Klieser, 1997; Musah et al., 2017; Pampaloni, Reynaud, & Stelzer, 2007). Organ-on-a-chip technology has been emerged as a cell culture model within microfluidic channels capable of closely recapitulating physiologically relevant cellular microenvironment. This technology is a complex and integrated system that closely recapitulates the key aspects of organ structure and function in a miniaturized scale (Bhatia & Ingber, 2014; Ingber, 2016; Pampaloni et al., 2007; Verhulsel et al., 2014). Organ-on-a-chip devices facilitate

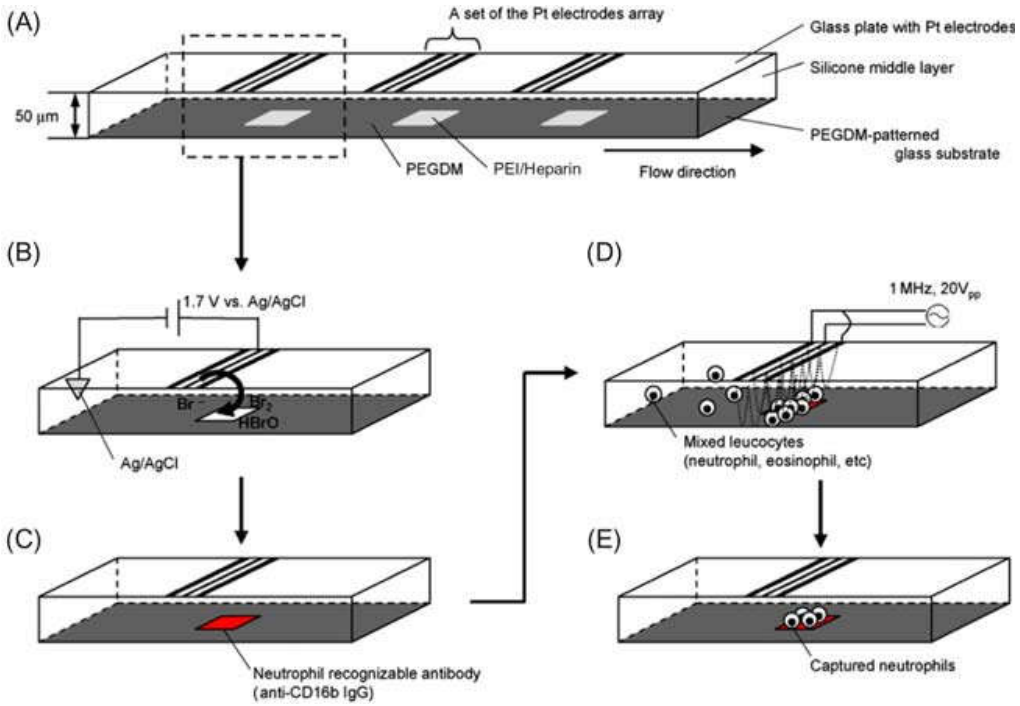

Figure 26.23 Schematic representations of neutrophils' specific capture from mixed leukocytes within a device. (A) Schematic of the microfluidic device. A region without the PEGDM coating was incubated with polyethyleneimine (PEI)/heparin to create a layer which is aligned under the Pt electrodes array. (B) The produced HBrO then removes the PEI/heparin to make the surface protein adsorptive. (C) Neutrophil-specific antibodies are then immobilized on the created regions. (D) Though negative DEP force, the leukocytes are enriched in the created protein adhesive regions. (E) Neutrophils are captured by the immobilized antibodies, and further on the unbounded cells are removed. *DEP*, Dielectrophoresis; *HBrO*, hypobromous acid; *PEGDM*, poly(ethylene glycol)-dimethacrylate; *Pt*, platinum.
Source: Reproduced from Hashimoto, M., Kaji, H., & Nishizawa, M. (2009). Selective capture of a specific cell type from mixed leucocytes in an electrode-integrated microfluidic device. *Biosensors and Bioelectronics*, *24*(9), 2892–2897 with permission from Elsevier.

compartmentalized culturing, in which different cell types can simultaneously culture with adequate intercellular interactions (Zhang, Zhao, Abdul Rahim, van Noort, & Yu, 2009).

Using a matrix that closely mimics native tissue and cell–ECM interaction is one of the major ingredients of designing a cell culture system. In vivo, ECM acts as a supporting network composed mainly of collagen, elastin, and laminin. This network gives the cells their mechanical characteristics and facilitates cross-talk between cells encapsulated in the matrix (Abbott, 2003). The binding of the cells to the ECM occurs via receptors presented on the surface of the cells such as integrin, which attaches to the ECM and promotes biochemical signaling from the surrounding environments. Therefore to closely recapitulate the cell–matrix interaction in the microfluidic device, the surface of the microchannel is commonly coated with ECM proteins (Ingber, 2016; Pampaloni et al., 2007).

Organ-on-a-chip devices have been extensively investigated and various organ- and body-on-a-chip devices have been developed. To closely mimic the native ECM environment on this device, the majority of the organ-on-a-chip devices were coated with naturally derived hydrogel including collagen, Matrigel, laminin, and FN to support cell growth and differentiation in vitro (Huh, Torisawa, Hamilton, Kim, & Ingber, 2012). Here, we examine different ECMs used to establish a 3D microfluidic cell culture environment.

A 3D microfluidic device that closely resembled the cellular microenvironment, diffusive properties, in addition to the expansion and compression of the lung was developed by Huh et al. (Schultze et al., 2010). This lung-on-a-chip device, Fig. 26.24A, was fabricated out of PDMS, consisted of two parallel microchannels, and was separated by a PDMS membrane. Human alveolar epithelial cells (NCI H441) were cultured onto a collagen or FN-coated membrane in the upper channel, whereas human pulmonary microvascular ECs were seeded to the lower channel. There were also two hollow microchannels on either side of the membrane responsible for creating a vacuum in order to mimic breathing movement. Both upper and lower chambers perfused with culture media, which allowed the apical and basolateral section of the cell to get exposed to fluid shear stress, which subsequently promoted the growth and differentiation of the seeded cells. To assess the functionality of a device, different inflammatory cytokines and bacteria were introduced into the air, while immune cells entered into the fluid. The innate cellular response to pulmonary infection of bacteria was identified in this lung-on-a-chip device.

Following the design of lung-on-a-chip, Kim, Huh, Hamilton, and Ingber (2012), Kim, Li, Collins, and Ingber (2016), and Kim, Hegde, and Jayaraman (2010) were able to develop a human-gut-on-a-chip device, Fig. 26.24B. The intestinal peristalsis-like motions were mimicked by applying cyclic strain through vacuum chambers located on the side of the two microchannels. In this device, Caco-2 cells, were cultivated on a collagen type I-coated PDMS semipermeable membrane, in which well-defined monolayers resembling intestinal epithelium were formed under dynamic continuous perfusion of media. The capillary endothelium cells, on the other hand, were cultured in the lower channel to mimic the neighboring vasculature in a native tissue. Under both mechanical distortion and continuous fluid flow, the Caco-2 cells were able to grow into a 3D intestinal crypt−villus microstructure. To examine the functionality of the device, both pathogenic and probiotic bacteria were introduced into the lower channel along with different inflammatory cytokines.

Most recently, Shah et al. (2016) established a modular microfluidics-based system, referred to as HuMiX, Fig. 26.24C. This chip closely recapitulated a human intestine-microbiome interface by culturing facultative anaerobe and obligate anaerobe bacteria under anaerobic conditions. This design consisted of three microchambers made of silicone rubber gaskets encased between two polycarbonate (PC) layers, with each microchamber containing a spiral-shaped microchannel. The upper microchamber was dedicated to culture commensal bacteria and was partitioned from the lower channel by a mucin-coated nanoporous membrane made of PC. The middle microchamber was dedicated to the culture of Caco-2 cells and was

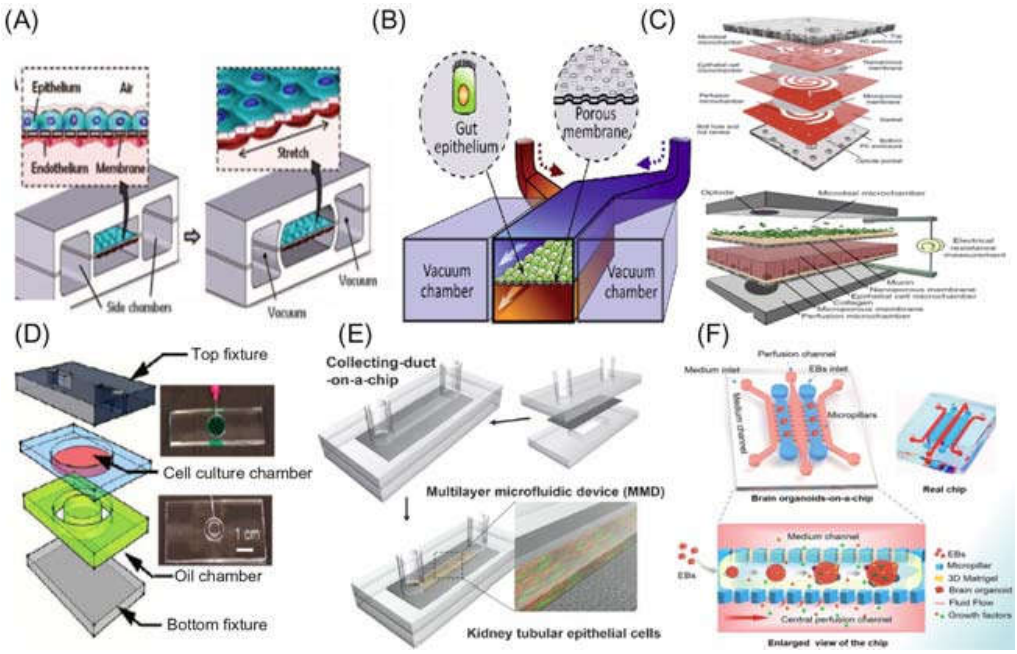

Figure 26.24 Schematic representing different organ-on-a-chip technologies, (A) Lung-on-a-chip device, (B) gut-on-a-chip device, (C) HuMix gut-on-chip device, (D) heart-on-a-chip device, (E) kidney-on-a-chip, (F) human brain organoid-on-a-chip.
Source: (A) Reproduced from Schultze, M., Fieß, M., Karpowicz, N., Gagnon, J., Korbman, M., Hofstetter, M., et al. (2010). Delay in photoemission. *Science*, *328*, 1658−1662 with permission from the American Association for the Advancement of Science. (B) Reproduced from Kim, D., Karns, K., Tia, S. Q., He, M., & Herr, A. E. (2012). Electrostatic protein immobilization using charged polyacrylamide gels and cationic detergent microfluidic western blotting. *Analytical Chemistry*, 84, 2533−2540; Kim, H. J., Huh, D., Hamilton, G., & Ingber, D. E. (2012). Human gut-on-a-chip inhabited by microbial flora that experiences intestinal peristalsis-like motions and flow. *Lab on a Chip*, *12*, 2165−2174 with permission from the Royal Society of Chemistry. (C) Reproduced from Shah, P., Fritz, J. V., Glaab, E., Desai, M. S., Greenhalgh, K., Frachet, A., et al. (2016). A microfluidics-based in vitro model of the gastrointestinal human-microbe interface. *Nature Communications*, *7*, 11535 with permission from Springer Nature. (D) Reproduced from Giridharan, G. A., Nguyen, M. D., Estrada, R., Parichehreh, V., Hamid, T., Ismahil, M. A., et al. (2010). Microfluidic cardiac cell culture model (μCCCM). *Analytical Chemistry*, *82*, 7581−7587 with permission from the Royal Society of Chemistry. (E) Reproduced from Jang, K. J., Cho, H. S., Kang, D. H., Bae, W. G., Kwon, T.-H., & Suh, K.-Y. (2011). Fluid-shear-stress-induced translocation of aquaporin-2 and reorganization of actin cytoskeleton in renal tubular epithelial cells. I*ntegrative Biology*, *3*(2), 134−141 with permission from the Oxford University Press. (F) Reproduced from Wang, Y., Wang, L., Guo, Y., Zhu, Y., & Qin, J. (2018). Engineering stem cell-derived 3D brain organoids in a perfusable organ-on-a-chip system. *RSC Advances*, 8, 1677−1685 with permission from the Royal Society of Chemistry.

comprised of a collagen-coated microporous membrane made of PC. The lower microchamber was devoted to perfusions of growing medium and immune cells, as depicted in Fig. 26.24C. This device was able to successfully recapitulate the in vivo human−bacteria interface.

Song et al. (2005) reported the fabrication of endothelium-on-a-chip to systematically investigate the impact of mechanical force including shear stress on ECs. The device is comprised of single compartment PDMS-based microchannels in which EC cells seeded onto FN-coated salinized glass slide. To replicate various shear stress, this group incorporated various microchannels with different contact area into the microfluidic device. This device was also able to induce the formation of pulsatile fluid flow representing the intrinsic nature of blood flow in the arterial vasculature, which is a crucial parameter for inducing the differentiation of ECs in vitro.

Giridharan et al. (2010) established cardiac cell culture system on a microfluidic device, Fig. 26.24D. This group cultured H9c2 cells, an embryonic cardiomyoblast cell lines, onto FN-coated PDMS membrane. This cell culture chip composed of a PDMS membrane sandwiched between two PC plates that were milled with microfluidic channel to generate perfusion through the membrane. A pulsatile valve was also accommodated in the device to induce mechanical strain, which promote the better differentiation and proliferation of the seeded cells. The device was further used to model different cardiac disorders.

Kidney-on-a-chip has also been developed by Jang et al. (2011) and Jang and Suh (2010), in the form of a multilayer microfluidic device that contained primary rat inner medullary collecting duct (IMCD) (Fig. 26.24E). This device was composed of two PDMS-based microchambers with a collagen-coated porous polyester membrane separating the two chambers. The IMCD were cultured on a membrane, and well-defined polarized monolayer of IMCD cells were formed after 3 days resembling in vivo cell polarity. The functionality of this collecting-duct-on-a-chip system was confirmed through assessing transportation of different protein across the membrane. In another study (Jang et al., 2013), this group fabricated the human proximal tubule-on-a-chip by seeding primary human kidney epithelial cells on the porous membrane.

Advances in stem cell and organoid culture system over the past decade have opened a new window to integrate organ-on-a-chip technology with stem cell research (Rahmani, Breyner, Su, Verdu, & Didar, 2019). Studies have emerged to develop stem cell-on-a-chip as a promising and predictive platform for drug screening and disease modeling and paving the path toward personalized medicine (Clevers, 2016; Drost & Clevers, 2017; Dutta, Heo, & Clevers, 2017). Very recently, Workman et al. (2017) established intestinal organoid on a microengineered chip. This microfluidic device was inspired by human-gut-on-a-chip device. It contained two PDMS layers that sandwiched a layer of a PDMS-based membrane. This group further developed human-induced pluripotent stem cell (hiPSCs)-derived human intestinal organoid (HIOs) and cultivated them in the form of a monolayer on an apical surface of a Matrigel-coated membrane. After 72 hours under dynamic condition, a continuous and fully confluent monolayer of intestinal epithelial cells was reported along the entire surface of the top channel. This HIO-derived epithelial cell was closely resembled the in vivo intestinal epithelium cell population. Permeability and cytotoxicity assays were confirmed the functionality of this device. Shortly after, Kasendra et al. (2018) engineered human small

intestine-on-a-chip device composed of intestinal stem cells isolated from intestinal biopsies. This group first developed 3D organoid from primary intestinal epithelial cells via spatial and temporal addition of the proper growth factors. This 3D organoid structure was then dissociated into a single stem cell and seeded on an apical surface of a PDMS-based porous membrane separating the two parallel microchannels and coated with a combination of collagen type I and Matrigel. In addition, the human intestinal endothelium cell was cultured in the basolateral surface of the membrane in a bottom microchannel. In the presence of cyclic mechanical strain and the continuous flow of growth media supplemented with pro-intestinal factors, the villi-like microstructures were formed. These projections were lined with a polarized monolayer of organoid-derived intestinal epithelial cells closely recapitulating human intestinal epithelium. It was concluding that this device is crucial to investigate and model human intestinal disease, development, and physiology.

In a recent study, Wang, Wang, Guo, Zhu, and Qin (2018) established a new approach to develop human brain organoid-on-chip, Fig. 26.24F. In this work, 3D brain organoids were derived from hiPSCs and embedded within 3D Matrigel network within a microfluidic device. The microfluidic system consisted of two top and bottom layers, the top layer contained two parallel chambers separated by a central channel that possesses ten pillar arrays structures at both sides of the channel acting as an interconnection to allow the flow of medium. The central channel was used to flow the medium, while the two parallel chambers were served as platform to culture 3D organoids. 3D organoid was embedded in Matrigel and introduced into the chamber. Upon Matrigel gelation, the 3D brain organoids immobilized within the microfluidic chamber in the presence of continuous medium perfusion. The engineered 3D organoids elucidated well-defined neural growth, differentiation, and organization, resembling the early human brain organogenesis in vivo.

These studies demonstrate the promising potential of organ-on-a-chip devices that serves not only as platform to promote long-term culture of stem cells but also offers a new window to investigate human development and disease.

Biosensing for cell detection

Biosensors are devices designed to convert biological activity to a measurable signal. They consist of two main components: bioreceptors and transducers. The bioreceptor, also known as a biorecognition element (BRE), can be a biomolecule (e.g., nucleic acids, enzymes, and proteins) or a microorganism. These elements are capable of sensing a target molecule or chemical (Yousefi, Su, Ali, Filipe, & Tohid, 2018). The transducer transforms the recognition of the analyte to a signal that can be detected by the BRE and transformed to a measurable signal (Luong, Male, & Glennon, 2008; Sethi, 1994). The biosensors' role is to combine the sensing and the reporting components together into a single integrated system (sensor). Therefore there is no need to do extra processing steps on the analyte. A crucial requirement for a biosensor is to use an appropriate platform and immobilize the BRE molecules on them (Prieto-Simín, Campàs, & Marty, 2008; Sassolas, Blum, & Leca-Bouvier,

2012). Recently, biosensors have been widely used for cell analysis (Cheng, Ding, Lei, Ding, & Ju, 2008; Qian, Bai, Wang, Xu, & Chen, 2010). Microfluidic devices have also recently being used, as they can provide precise fluid handling, low sample usage, and easy manipulation (Andersson & van den Berg, 2003; Fraser et al., 2018; Pratt, Huang, Hawkins, Gleghorn, & Kirby, 2011; Rivet, Lee, Hirsch, Hamilton, & Lu, 2011).

When aiming to adhere cells to the interior surface of a microfluidic device, the selection of an appropriate BRE is critical. The attachment between the BRE and the channel wall as well as that between the BRE and the target cell must be able to withstand relatively high shear stresses induced by fluid flow. Covalent immobilization of the BRE on the channel wall can be optimized using previously discussed strategies such as plasma treatment, silanization, and polymer grafting. On the other hand, the bond between the BRE and the target cell should be both stable and specific. In this regard, three categories of BREs have proven to be effective at cell capture: antibodies, aptamers, and DNAzymes.

Antibodies have been the most prevalent tool for molecular detection in the past half-century (Jayasena, 1999). These proteins appear naturally in the human body as a product of the immune system to target-specific ligand. Antibodies and ligands interact in a complementary lock-and-key manner. In the immune system, the ligand is typically a foreign organism called an antigen. The antibody is capable of neutralizing or flagging the antigen for destruction. As such, antibodies are identified and best produced in vivo. The use of animals in animal production leads to batch variation in antibody performance. In biosensing, antibodies are complementary to a target biomarker, whether it be an individual biomolecule or feature on a cellular membrane. For example, CD34 is a well-established transmembrane protein biomarker on progenitor cells (Krause, Fackler, Civin, & May, 2018) and CD34 antibodies have been used to capture EPCs on the surfaces of stents (Aoki et al., 2005). The principal drawback of proteins is the risk of denaturing (i.e., unfolding due to heat, pH, organic solvent, external force) that could render them nonfunctional during diagnosis and limits their shelf-life (Jayasena, 1999).

Aptamers are biomolecules consisting of a short sequence of nucleotides or peptides that are similarly capable of binding with high affinity and specificity to target molecules or cells (Jayasena, 1999). RNA- and DNA-based aptamers are typically single-stranded and thermally stable, making them more kinetically robust and longer lasting than antibodies (Ku et al., 2015). Even in the case where an aptamer is denatured, it can be regenerated within minutes, whereas a protein's denaturation is irreversible. Since they are chemically synthesized, aptamers are made with higher reproducibility and compositional flexibility than antibodies (Jayasena, 1999). Aptamers have been used in conjunction with antibodies to simultaneously capture multiple biomarkers on CTCs (Zhang, Sheng, & Fan, 2014). As shown in Fig. 26.25, they are not only capable of being immobilized on surfaces for cell capture but can also be labeled with a reporter molecule, such as a fluorophore, for specifically identifying captured targets (Jayasena, 1999).

DNAzymes are similar to aptamers in structure and function but are additionally capable of performing catalytic reactions upon interaction with the target

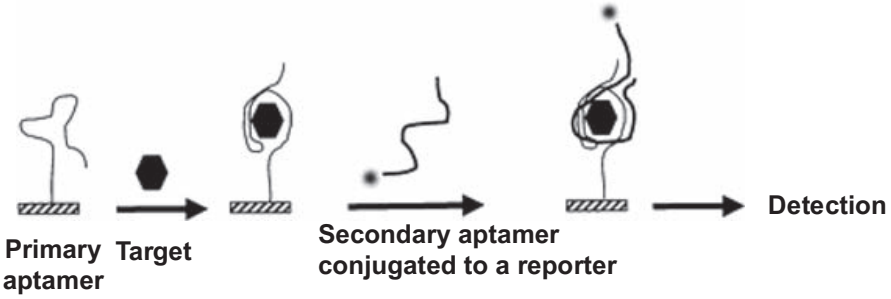

Figure 26.25 Pairs of aptamers, one immobilized and one labeled with a reporter molecule (e.g., fluorophore), can be used to simultaneously capture target biomolecules or cells and output readable signals.
Source: Reproduced from Jayasena, S. D. (1999). Aptamers: An emerging class of molecules that rival antibodies in diagnostics. *Clinical Chemistry*, *45*(9), 1628−1650 with permission from the American Association for Clinical Chemistry.

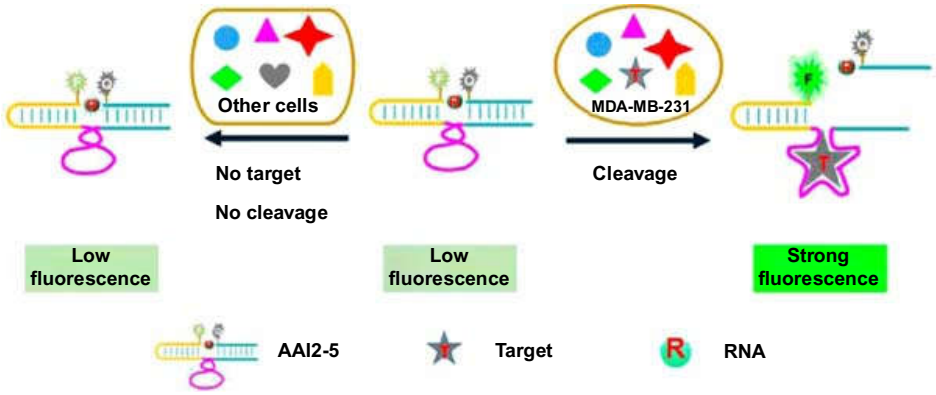

Figure 26.26 RFD probe can specifically react with target cells, resulting in RNA-cleaving and increase in fluorescence (right). Other cells have no effect on the probe, and the fluorescence remains low (left). *RFD*, RNA-cleaving fluorogenic DNAzyme.
Source: Reproduced form Xue, P., He, S., Mao, Y., Qu, L., Liu, F., Tan, C., et al. (2017). The optimization and characterization of an RNA-cleaving fluorogenic DNAzyme probe for MDA-MB-231 cell detection. *Sensors*, *17*(3), 650 with permission from MDPI.

biomarker. A common configuration is the RNA-cleaving fluorogenic DNAzyme (RFD). A RFD probe includes two deoxyribonucleotides, each labeled with one of a fluorophore and a quencher, linked by a single ribonucleotide. Upon interaction with the target, the ribonucleotide is cleaved, and the quencher is jettisoned as shown in Fig. 26.26 (Xue et al., 2017). The resulting surge in fluorescence is a simple and intuitive signal for successful biomarker detection. DNAzyme are synthetically derived and can be designed for both specific targets and output signals. However, they can be very expensive and complicated to produce.

A prominent application of biosensing is point-of-care (POC) diagnostics. By designing an integrated and compact device capable of capturing targeted biomolecules and cells and outputting an easily discernible signal, medical staff can make

diagnoses outside of a laboratory space and without large specialized equipment. Furthermore, since biomolecule and cell capture are near instantaneous, biosensors do not require the long periods of time that are necessary for traditional cell culturing methods. Faster diagnoses lead to more effective treatments and have the potential to save lives. Alternatively, POC biosensors can be designed for remote monitoring. Noninvasive wearable biosensors allow patients to recover outside of the hospital bed and gather medical data that can be monitored by the patient or transmitted to health care professionals (Noah et al., 2017). For noninvasive biosensors, the analyte solution is typically limited to sweat, urine, tears, or saliva. However, common target cells are found in the bloodstream and require the use of minimally invasive biosensors, which are not suitable for remote monitoring.

Conclusion

In this chapter, we have explored a variety of biofunctionalization techniques for homogeneous coating or patterning of solid−liquid interfaces in microfluidic devices. The stable immobilization of biomolecules for specific cell capture and promoting proliferation is foundational in the design of many devices, including microfluidic cell sorting, organs-on-chips, and biosensors. Moreover, biomolecular−cellular interactions are an active area of interest for researchers, and the diversity of applications is likely to continue growing with the discovery of new interactions.

References

Abbott, A. (2003). Biology's new dimension. *Nature*, *424*, 870.

Abhyankar, V. V., Lokuta, M. A., Huttenlocher, A., & Beebe, D. J. (2006). Characterization of a membrane-based gradient generator for use in cell-signaling studies. *Lab on a Chip*, *6*(3), 389−393. Available from https://doi.org/10.1039/B514133H, Retrieved from.

Aghvami, S. A., Opathalage, A., Zhang, Z. K., Ludwig, M., Heymann, M., Norton, M., et al. (2017). Rapid prototyping of cyclic olefin copolymer (COC) microfluidic devices. *Sensors and Actuators, B: Chemical*, *247*, 940−949.

Anand, S., Paxson, A. T., Dhiman, R., Smith, J. D., & Varanasi, K. K. (2012). Enhanced condensation on lubricant-impregnated nanotextured surfaces. *ACS Nano*, *6*, 10122−10129.

Andersson, H., & van den Berg, A. (2003). Microfluidic devices for cellomics: A review. *Sensors and Actuators B: Chemical*, *92*(3), 315−325.

Annabi, N., Selimović, Š., Acevedo Cox, J. P., Ribas, J., Afshar Bakooshli, M., Heintze, D., et al. (2013). Hydrogel-coated microfluidic channels for cardiomyocyte culture. *Lab on a Chip*, *13*, 3569−3577.

Antfolk, M., & Laurell, T. (2017). Continuous flow microfluidic separation and processing of rare cells and bioparticles found in blood − A review. *Analytica Chimica Acta*, *965*, 9−35.

Aoki, J., Serruys, P. W., van Beusekom, H., Ong, A. T. L., McFadden, E. P., Sianos, G., et al. (2005). Endothelial progenitor cell capture by stents coated with antibody against CD34: The HEALING-FIM (Healthy Endothelial Accelerated Lining Inhibits

Neointimal Growth-First In Man) Registry. *Journal of the American College of Cardiology*, *45*(10), 1574–1579. Retrieved from <http://www.sciencedirect.com/science/article/pii/S073510970500481X>.

Aubin, H., Nichol, J. W., Hutson, C. B., Bae, H., Sieminski, A. L., Cropek, D. M., et al. (2010). Directed 3D cell alignment and elongation in microengineered hydrogels. *Biomaterials*, *31*, 6941–6951.

Autebert, J., Coudert, B., Bidard, F. C., Pierga, J. Y., Descroix, S., Malaquin, L., & Viovy, J. L. (2012). Microfluidic: An innovative tool for efficient cell sorting. *Methods*, *57*(3), 297–307.

Autumn, K., Liang, Y. A., Hsieh, S. T., Zesch, W., Chan, W. P., Kenny, T. W., et al. (2000). Adhesive force of a single gecko foot-hair. *Nature*, *405*, 681. Available from https://doi.org/10.1038/35015073, Retrieved from.

Bäcker, M., Raue, M., Schusser, S., Jeitner, C., Breuer, L., Wagner, P., et al. (2012). Microfluidic chip with integrated microvalves based on temperature- and pH-responsive hydrogel thin films. *Physica Status Solidi (A) Applications and Materials Science*, *209*, 839–845.

Badv, M., Jaffer, I. H., Weitz, J. I., & Didar, T. F. (2017). An omniphobic lubricant-infused coating produced by chemical vapor deposition of hydrophobic organosilanes attenuates clotting on catheter surfaces. *Scientific Reports*, *7*(1), 11639. Available from https://doi.org/10.1038/s41598-017-12149-1, Retrieved from.

Baker, J. E., Sriram, R., & Miller, B. L. (2015). Two-dimensional photonic crystals for sensitive microscale chemical and biochemical sensing. *Lab on a Chip*, *15*(4), 971–990. Available from https://doi.org/10.1039/C4LC01208A, Retrieved from.

Batz, N. G., Mellors, J. S., Alarie, J. P., & Ramsey, J. M. (2014). Chemical vapor deposition of aminopropyl silanes in microfluidic channels for highly efficient microchip capillary electrophoresis-electrospray ionization-mass spectrometry. *Analytical Chemistry*, *86*(7), 3493–3500.

Bauer, M., Su, G., Beebe, D. J., & Friedl, A. (2010). 3D microchannel co-culture: Method and biological validation. *Integrative Biology*, *2*, 371–378.

Bergstrand, A., Rahmani-Monfared, G., Östlund, Å., Nydén, M., & Holmberg, K. (2009). Comparison of PEI-PEG and PLL-PEG copolymer coatings on the prevention of protein fouling. *Journal of Biomedical Materials Research—Part A*, *88*, 608–615.

Berry, S. B., Zhang, T., Day, J. H., Su, X., Wilson, I. Z., Berthier, E., & Theberge, A. B. (2017). Upgrading well plates using open microfluidic patterning. *Lab on a Chip*, *17*, 4253–4264. Retrieved from <http://xlink.rsc.org/?DOI = C7LC00878C>.

Bhatia, S. N., & Ingber, D. E. (2014). Microfluidic organs-on-chips. *Nature Biotechnology*, *32* (8), 760–772. Retrieved from <http://www.nature.com/doifinder/10.1038/nbt.2989>.

Brzoska, J. B., Azouz, I. B., & Rondelez, F. (1994). Silanization of solid substrates: A step toward reproducibility. *Langmuir*, *10*(11), 4367–4373.

Cabodi, M., Choi, N. W., Gleghorn, J. P., Lee, C. S. D., Bonassar, L. J., & Stroock, A. D. (2005). A microfluidic biomaterial. *Journal of the American Chemical Society*, *127*, 13788–13789.

Carbodiimide Crosslinker Chemistry. (n.d.). Retrieved from <https://www.thermofisher.com/ca/en/home/life-science/protein-biology/protein-biology-learning-center/protein-biology-resource-library/pierce-protein-methods/carbodiimide-crosslinker-chemistry.html>.

Cartwright, M., Rottman, M., Shapiro, N. I., Seiler, B., Lombardo, P., Gamini, N., et al. (2016). A broad-spectrum infection diagnostic that detects pathogen-associated molecular patterns (PAMPs) in whole blood. *EBioMedicine*, *9*, 217–227. Available from https://doi.org/10.1016/j.ebiom.2016.06.014, Retrieved from.

Cha, C., Antoniadou, E., Lee, M., Jeong, J. H., Ahmed, W. W., Saif, T. A., et al. (2013). Tailoring hydrogel adhesion to polydimethylsiloxane substrates using polysaccharide glue. *Angewandte Chemie—International Edition*, *52*, 6949−6952.

Chang, C.-W., Cheng, Y.-J., Tu, M., Chen, Y.-H., Peng, C.-C., Liao, W.-H., & Tung, Y.-C. (2014). A polydimethylsiloxane-polycarbonate hybrid microfluidic device capable of generating perpendicular chemical and oxygen gradients for cell culture studies. *Lab on a Chip*, *14*(19), 3762−3772. Available from https://doi.org/10.1039/C4LC00732H, Retrieved from.

Chen, C., Skog, J., Hsu, C.-H., Lessard, R. T., Balaj, L., Wurdinger, T., et al. (2010). Microfluidic isolation and transcriptome analysis of serum microvesicles. *Lab on a Chip*, *10*(4), 505−511. Retrieved from <http://xlink.rsc.org/?DOI = B916199F>.

Cheng, H., & Hu, Y. (2012). Influence of chain ordering on frictional properties of self-assembled monolayers (SAMs) in nano-lubrication. *Advances in Colloid and Interface Science*, *171−172*, 53−65. Available from https://doi.org/10.1016/j.cis.2012.01.003, Retrieved from.

Cheng, W., Ding, L., Lei, J., Ding, S., & Ju, H. (2008). Effective cell capture with tetrapeptide-functionalized carbon nanotubes and dual signal amplification for cytosensing and evaluation of cell surface carbohydrate. *Analytical Chemistry*, *80*(10), 3867−3872.

Cheng, X., Irimia, D., Dixon, M., Sekine, K., Demirci, U., Zamir, L., et al. (2007). A microfluidic device for practical label-free CD4 + T cell counting of HIV-infected subjects. *Lab on a Chip*, *7*(2), 170−178. Retrieved from <http://xlink.rsc.org/?DOI = B612966H>.

Chiang, H. C., Wang, Y. S., Chou, C. H., Liao, A. T., Chu, R. M., & Lin, C. S. (2012). Overexpression of chemokine ligand 7 is associated with the progression of canine transmissible venereal tumor. *BMC Veterinary Research*, *8*(1), 1, Retrieved from BMC Veterinary Research.

Choi, S., Karp, J. M., & Karnik, R. (2012). Cell sorting by deterministic cell rolling. *Lab on a Chip*, *12*(8), 1427.

Chuah, Y. J., Koh, Y. T., Lim, K., Menon, N. V., Wu, Y., & Kang, Y. (2015). Simple surface engineering of polydimethylsiloxane with polydopamine for stabilized mesenchymal stem cell adhesion and multipotency. *Scientific Reports*, *5*, 18162.

Chung, B. G., Flanagan, L. A., Rhee, S. W., Schwartz, P. H., Lee, A. P., Monuki, E. S., & Jeon, N. L. (2005). Human neural stem cell growth and differentiation in a gradient-generating microfluidic device. *Lab on a Chip*, *5*(4), 401−406. Available from https://doi.org/10.1039/B417651K, Retrieved from.

Clevers, H. (2016). Modeling development and disease with organoids. *Cell*, *165*, 1586−1597.

Collins, M. N., & Birkinshaw, C. (2008). Physical properties of crosslinked hyaluronic acid hydrogels. *Journal of Materials Science: Materials in Medicine*, *19*, 3335−3343.

Cordeiro, A. L., Zschoche, S., Janke, A., Nitschke, M., & Werner, C. (2009). Functionalization of poly(dimethylsiloxane) surfaces with maleic anhydride copolymer films. *Langmuir*, *25*, 1509−1517.

Cuchiara, M. P., Allen, A. C. B., Chen, T. M., Miller, J. S., & West, J. L. (2010). Multilayer microfluidic PEGDA hydrogels. *Biomaterials*, *31*, 5491−5497.

Cukierman, E., Pankov, R., & Yamada, K. M. (2002). Cell interactions with three-dimensional matrices. *Current Opinion in Cell Biology*, *14*(5), 633−640.

Dai, L., StJohn, H. A. W., Bi, J., Zientek, P., Chatelier, R. C., & Griesser, H. J. (2000). Biomedical coatings by the covalent immobilization of polysaccharides onto gas-plasma-activated polymer surfaces. *Surface and Interface Analysis*, *29*(1), 46−55.

Daniel, D., Mankin, M. N., Belisle, R. A., Wong, T. S., & Aizenberg, J. (2013). Lubricant-infused micro/nano-structured surfaces with tunable dynamic omniphobicity at high temperatures. *Applied Physics Letters*, *102*(23), 231603.

Daw, R., Brook, I. M., Devlin, A. J., Short, R. D., Cooper, E., & Leggett, G. J. (1998). A comparative study of cell attachment to self assembled monolayers and plasma polymers. *Journal of Materials Chemistry*, *8*(12), 2583–2584.

Daw, R., Candan, S., Beck, A. J., Devlin, A. J., Brook, I. M., MacNeil, S., et al. (1998). Plasma copolymer surfaces of acrylic acid/1,7 octadiene: Surface characterisation and the attachment of ROS 17/2.8 osteoblast-like cells. *Biomaterials*, *19*(19), 1717–1725.

Delorme, N., Bardeau, J. F., Bulou, A., & Poncin-Epaillard, F. (2006). Controlled modification of octadecyltrichlorosilane self-assembled monolayer by CO_2 plasma. *Thin Solid Films*, *496*(2), 612–618.

Demming, S., Peterat, G., Llobera, A., Schmolke, H., Bruns, A., Kohlstedt, M., et al. (2012). Vertical microbubble column—A photonic lab-on-chip for cultivation and online analysis of yeast cell cultures. *Biomicrofluidics*, *6*, 34106.

Diao, J., Young, L., Kim, S., Fogarty, E. A., Heilman, S. M., Zhou, P., et al. (2006). A three-channel microfluidic device for generating static linear gradients and its application to the quantitative analysis of bacterial chemotaxis. *Lab on a Chip*, *6*(3), 381–388. Retrieved from <http://xlink.rsc.org/?DOI = B511958H>.

Didar, T. F., Bowey, K., Almazan, G., & Tabrizian, M. (2014). A miniaturized multipurpose platform for rapid, label-free, and simultaneous separation, patterning, and in vitro culture of primary and rare cells. *Advanced Healthcare Materials*, *3*(2), 253–260.

Didar, T. F., Cartwright, M. J., Rottman, M., Graveline, A. R., Gamini, N., Watters, A. L., et al. (2015). Improved treatment of systemic blood infections using antibiotics with extracorporeal opsonin hemoadsorption. *Biomaterials*, *67*, 382–392. Retrieved from <http://www.sciencedirect.com/science/article/pii/S0142961215006341>.

Didar, T. F., Foudeh, A. M., & Tabrizian, M. (2012). Patterning multiplex protein microarrays in a single microfluidic channel. *Analytical Chemistry*, *84*(2), 1012–1018.

Didar, T. F., Li, K., Veres, T., & Tabrizian, M. (2013). Separation of rare oligodendrocyte progenitor cells from brain using a high-throughput multilayer thermoplastic-based microfluidic device. *Biomaterials*, *34*(22), 5588–5593. Retrieved from <http://www.sciencedirect.com/science/article/pii/S0142961213004584>.

Didar, T. F., & Tabrizian, M. (2010). Adhesion based detection, sorting and enrichment of cells in microfluidic lab-on-chip devices. *Lab on a Chip*, *10*(22), 3043–3053.

Diéguez, L., Winter, M. A., Pocock, K. J., Bremmell, K. E., & Thierry, B. (2015). Efficient microfluidic negative enrichment of circulating tumor cells in blood using roughened PDMS. *The Analyst*, *140*(10), 3565–3572. Retrieved from <http://xlink.rsc.org/?DOI = C4AN01768D>.

Ding, J. N., Wong, P. L., & Yang, J. C. (2006). Friction and fracture properties of polysilicon coated with self-assembled monolayers. *Wear*, *260*(1), 209–214. Retrieved from <http://www.sciencedirect.com/science/article/pii/S0043164805001766>.

Drost, J., & Clevers, H. (2017). Translational applications of adult stem cell-derived organoids. *Development*, *144*, 968–975.

Dugas, V., & Chevalier, Y. (2003). Surface hydroxylation and silane grafting on fumed and thermal silica. *Journal of Colloid and Interface Science*, *264*(2), 354–361.

Duncombe, T. A., Tentori, A. M., & Herr, A. E. (2015). Microfluidics: Reframing biological enquiry. *Nature Reviews Molecular Cell Biology*, *16*(9), 554–567. Available from https://doi.org/10.1038/nrm4041, Retrieved from.

Dutta, D., Heo, I., & Clevers, H. (2017). Disease modeling in stem cell-derived 3D organoid systems. *Trends in Molecular Medicine*, *23*, 393−410.

Ebara, M., Hoffman, J. M., Stayton, P. S., & Hoffman, A. S. (2007). Surface modification of microfluidic channels by UV-mediated graft polymerization of non-fouling and "smart" polymers. *Radiation Physics and Chemistry*, *76*, 1409−1413.

Effenhauser, C. S., Bruin, G. J. M., Paulus, A., & Ehrat, M. (1997). Integrated capillary electrophoresis on flexible silicone microdevices: Analysis of DNA restriction fragments and detection of single dna molecules on microchips. *Analytical Chemistry*, *69*, 3451−3457.

El-Ali, J., Sorger, P. K., & Jensen, K. F. (2006). Cells on chips. *Nature*, *442*, 403.

Esser, P. (1991). Blocking agent and detergent in ELISA. *Nunc Bulletin*, *6*(9), 1−4.

Fatanat-Didar, T., Li, K., Tabrizian, M., & Veres, T. (2013). High throughput multilayer microfluidic particle separation. *Lab on a Chip*, *13*, 2615−2622.

Faure, K., Albert, M., Dugas, V., Crétier, G., Ferrigno, R., Morin, P., & Rocca, J. L. (2008). Development of an acrylate monolith in a cyclo-olefin copolymer microfluidic device for chip electrochromatography separation. *Electrophoresis*, *29*, 4948−4955.

Ferrari, L., Kaufmann, J., Winnefeld, F., & Plank, J. (2010). Interaction of cement model systems with superplasticizers investigated by atomic force microscopy, zeta potential, and adsorption measurements. *Journal of Colloid and Interface Science*, *347*, 15−24.

Fiorilli, S., Rivolo, P., Descrovi, E., Ricciardi, C., Pasquardini, L., Lunelli, L., et al. (2008). Vapor-phase self-assembled monolayers of aminosilane on plasma-activated silicon substrates. *Journal of Colloid and Interface Science*, *321*(1), 235−241.

Fraser, L. A., Kinghorn, A. B., Dirkzwager, R. M., Liang, S., Cheung, Y. W., Lim, B., et al. (2018). A portable microfluidic aptamer-tethered enzyme capture (APTEC) biosensor for malaria diagnosis. *Biosensors and Bioelectronics*, *100*, 591−596.

Frederix, F., Bonroy, K., Reekmans, G., Laureyn, W., Campitelli, A., Abramov, M. A., et al. (2004). Reduced nonspecific adsorption on covalently immobilized protein surfaces using poly(ethylene oxide) containing blocking agents. *Journal of Biochemical and Biophysical Methods*, *58*(1), 67−74. Retrieved from <http://www.sciencedirect.com/science/article/pii/S0165022X03001507>.

Gao, Z., Henthorn, D. B., & Kim, C. S. (2008). Enhanced wettability of SU-8 photoresist through a photografting procedure for bioanalytical device applications. *Journal of Micromechanics and Microengineering*, *18*, 450131−450137.

García, A. J. (2005). Get a grip: Integrins in cell-biomaterial interactions. *Biomaterials*, *26*, 7525−7529.

Giridharan, G. A., Nguyen, M.-D., Estrada, R., Parichehreh, V., Hamid, T., Ismahil, M. A., et al. (2010). Microfluidic cardiac cell culture model (μCCCM). *Analytical Chemistry*, *82*, 7581−7587.

Glass, N. R., Tjeung, R., Chan, P., Yeo, L. Y., & Friend, J. R. (2011). Organosilane deposition for microfluidic applications. *Biomicrofluidics*, *5*(3), 1−7.

Gong, X., Dai, L., Griesser, H. J., & Mau, A. W. H. (2000). Surface immobilization of poly (ethylene oxide): Structure and properties. *Journal of Polymer Science, Part B: Polymer Physics*, *38*(17), 2323−2332.

Greiner, A. M., Hoffmann, P., Bruellhoff, K., Jungbauer, S., Spatz, J. P., Moeller, M., et al. (2014). Stable biochemically micro-patterned hydrogel layers control specific cell adhesion and allow long term cyclic tensile strain experiments. *Macromolecular Bioscience*, *14*, 1547−1555.

Griesser, H. J., Chatelier, R. C., Gengenbach, T. R., Johnson, G., & Steele, J. G. (1994). Growth of human cells on plasma polymers: Putative role of amine and amide groups. *Journal of Biomaterials Science, Polymer Edition*, *5*(6), 531−554.

Griffith, L. G., & Swartz, M. A. (2006). Capturing complex 3D tissue physiology in vitro. *Nature Reviews Molecular Cell Biology*, *7*, 211–224.

Guan, X., Zhang, H. J., Bi, Y. N., Zhang, L., & Hao, D. L. (2010). Rapid detection of pathogens using antibody-coated microbeads with bioluminescence in microfluidic chips. *Biomedical Microdevices*, *12*(4), 683–691.

Guo, W. H., & Wang, Y. L. (2011). Micropatterning cell-substrate adhesions using linear polyacrylamide as the blocking agent. *Cold Spring Harbor Protocols*, *2011*, prot5582.

Haddow, D. B., France, R. M., Short, R. D., MacNeil, S., Dawson, R. A., Leggett, G. J., & Cooper, E. (1999). Comparison of proliferation and growth of human keratinocytes on plasma copolymers of acrylic acid/1,7-octadiene and self-assembled monolayers. *Journal of Biomedical Materials Research*, *47*(3), 379–387.

Handa, H., Gurczynski, S., Jackson, M. P., Auner, G., Walker, J., & Mao, G. (2008). Recognition of *Salmonella typhimurium* by immobilized phage P22 monolayers. *Surface Science*, *602*(7), 1392–1400.

Hansmann, G., Plouffe, B. D., Hatch, A., von Gise, A., Sallmon, H., Zamanian, R. T., & Murthy, S. K. (2011). Design and validation of an endothelial progenitor cell capture chip and its application in patients with pulmonary arterial hypertension. *Journal of Molecular Medicine (Berlin, Germany)*, *89*(10), 971–983.

Hashimoto, M., Kaji, H., & Nishizawa, M. (2009). Selective capture of a specific cell type from mixed leucocytes in an electrode-integrated microfluidic device. *Biosensors and Bioelectronics*, *24*(9), 2892–2897.

Haycock, J. W. (1993). Polyvinylpyrrolidone as a blocking agent in immunochemical studies. *Analytical Biochemistry*, *208*(2), 397–399. Retrieved from <http://www.sciencedirect.com/science/article/pii/S0003269783710687>.

He, M., & Herr, A. E. (2009). Microfluidic polyacrylamide gel electrophoresis with in situ immunoblotting for native protein analysis. *Analytical Chemistry*, *81*, 8177–8184.

He, M., & Herr, A. E. (2010). Polyacrylamide gel photopatterning enables automated protein immunoblotting in a two-dimensional microdevice. *Journal of the American Chemical Society*, *132*, 2512–2513.

Hegde, P., Qi, R., Abernathy, K., Gay, C., Dharap, S., Gaspard, R., et al. (2000). A concise guide to cDNA microarray analysis. *Biotechniques*, *29*, 548–550.

Helmy, R., & Fadeev, A. Y. (2002). Self-assembled monolayers supported on TiO_2: Comparison of $C_{18}H_{37}SiX_3$ (X = H, Cl, OCH_3), $C_{18}H_{37}Si(CH_3)_2Cl$, and $C_{18}H_{37}PO(OH)_2$. *Langmuir*, *18*(23), 8924–8928.

Hermanson, G. T. (2013). *Bioconjugate techniques* (3rd ed.). Academic Press.

Hoque, E., Derose, J. A., Hoffmann, P., Bhushan, B., & Mathieu, H. J. (2007). Alkylperfluorosilane self-assembled monolayers on aluminum: A comparison with alkylphosphonate self-assembled monolayers. *Journal of Physical Chemistry C*, *111*(10), 3956–3962.

Hosseini, A., Villegas, M., Yang, J., Badv, M., Jeffrey, I. W., Soleymani, L., & Tohid, F. D. (2018). Conductive electrochemically active lubricant-infused nanostructured surfaces attenuate coagulation and enable friction-less droplet manipulation. *Advanced Materials Interfaces*, *5*, 1800617. Retrieved from https://doi.org/10.1002/admi.201800617.

Hou, Y., Hu, J., Park, H., & Lee, M. (2012). *Journal of Biomedical Materials Research A. Growth (Lakeland)*, *100*(1), 1–7.

Hsieh, H. Y., Wang, P. C., Wu, C. L., Huang, C. W., Chieng, C. C., & Tseng, F. G. (2009). Effective enhancement of fluorescence detection efficiency in protein microarray assays: Application of a highly fluorinated organosilane as the blocking agent on the

background surface by a facile vapor-phase deposition process. *Analytical Chemistry*, *81*, 7908−7916.

Hu, M., Noda, S., Okubo, T., Yamaguchi, Y., & Komiyama, H. (2001). Structure and morphology of self-assembled 3-mercaptopropyltrimethoxysilane layers on silicon oxide. *Applied Surface Science*, *181*(3), 307−316. Retrieved from <http://www.sciencedirect.com/science/article/pii/S0169433201003993>.

Huh, D., Torisawa, Y., Hamilton, G. A., Kim, H. J., & Ingber, D. E. (2012). Microengineered physiological biomimicry: Organs-on-chips. *Lab on a Chip*, *12*, 2158−2164.

Hui, E. E., & Bhatia, S. N. (2007). Micromechanical control of cell-cell interactions. *Proceedings of the National Academy of Sciences of the United States of America*, *104*, 5722−5726.

Hyun, K. A., & Jung, H. I. (2013). Microfluidic devices for the isolation of circulating rare cells: A focus on affinity-based, dielectrophoresis, and hydrophoresis. *Electrophoresis*, *34*(7), 1028−1041.

Idota, N., Tsukahara, T., Sato, K., Okano, T., & Kitamori, T. (2009). The use of electron beam lithographic graft-polymerization on thermoresponsive polymers for regulating the directionality of cell attachment and detachment. *Biomaterials*, *30*, 2095−2101.

Inagaki, N. (1996). *Plasma surface modification and plasma polymerization, CRC Press*.

Inagaki, N., Tasaka, S., & Hibi, K. (1992). Surface modification of Kapton film by plasma treatments. *Journal of Polymer Science Part A: Polymer Chemistry*, *30*(7), 1425−1431.

Ingber, D., Super, M., Leslie, D. C., Didar, T., Watters, A. L., Berthet, J. B., & Waterhouse, A. (2015). Modification of surfaces for simultaneous repellency and targeted binding of desired moieties. United States.

Ingber, D. E. (2016). Reverse engineering human pathophysiology with organs-on-chips. *Cell*, *164*, 1105−1109.

Jain, A., van der Meer, A. D., Papa, A. L., Barrile, R., Lai, A., Schlechter, B. L., et al. (2016). Assessment of whole blood thrombosis in a microfluidic device lined by fixed human endothelium. *Biomedical Microdevices*, *18*(4), 1−7. Retrieved from https://doi.org/10.1007/s10544-016-0095-6.

James, C. D., Davis, R. C., Kam, L., Craighead, H. G., Isaacson, M., Turner, J. N., & Shain, W. (1998). Patterned protein layers on solid substrates by thin stamp microcontact printing. *Langmuir*, *14*(4), 741−744.

Jang, K.-J., Cho, H. S., Kang, D. H., Bae, W. G., Kwon, T.-H., & Suh, K.-Y. (2011). Fluid-shear-stress-induced translocation of aquaporin-2 and reorganization of actin cytoskeleton in renal tubular epithelial cells. *Integrative Biology*, *3*(2), 134−141.

Jang, K.-J., Mehr, A. P., Hamilton, G. A., Mcpartlin, L. A., Chung, S., Suh, K.-Y., & Ingber, D. E. (2013). Human kidney proximal tubule-on-a-chip for drug transport and nephrotoxicity assessment. *Integrative Biology*, *5*(5), 1119−1129.

Jang, K.-J., & Suh, K.-Y. (2010). A multi-layer microfluidic device for efficient culture and analysis of renal tubular cells. *Lab on a Chip*, *10*, 36−42.

Jayasena, S. D. (1999). Aptamers: An emerging class of molecules that rival antibodies in diagnostics. *Clinical Chemistry*, *45*(9), 1628−1650.

Jena, R. K., & Yue, C. Y. (2012). Cyclic olefin copolymer based microfluidic devices for biochip applications: Ultraviolet surface grafting using 2-methacryloyloxyethyl phosphorylcholine. *Biomicrofluidics*, *6*, 12822−1282212.

Jeon, N. L., Dertinger, S. K. W., Chiu, D. T., Choi, I. S., Stroock, A. D., & Whitesides, G. M. (2000). Generation of solution and surface gradients using microfluidic systems. *Langmuir*, *16*, 8311−8316.

Jeong, G. S., Han, S., Shin, Y., Kwon, G. H., Kamm, R. D., Lee, S. H., & Chung, S. (2011). Sprouting angiogenesis under a chemical gradient regulated by interactions with an endothelial monolayer in a microfluidic platform. *Analytical Chemistry*, *83*(22), 8454–8459.

Jeyachandran, Y. L., Mielczarski, J. A., Mielczarski, E., & Rai, B. (2010). Efficiency of blocking of non-specific interaction of different proteins by BSA adsorbed on hydrophobic and hydrophilic surfaces. *Journal of Colloid and Interface Science*, *341*(1), 136–142.

Jose, B., McCluskey, P., Gilmartin, N., Somers, M., Kenny, D., Ricco, A. J., et al. (2016). Self-powered microfluidic device for rapid assay of antiplatelet drugs. *Langmuir*, *32*(11), 2820–2828.

Julián, E., Cama, M., Martínez, P., & Luquin, M. (2001). An ELISA for five glycolipids from the cell wall of *Mycobacterium tuberculosis*: Tween 20 interference in the assay. *Journal of Immunological Methods*, *251*, 21–30.

Kanaji, S., Fahs, S. A., Shi, Q., Haberichter, S. L., & Montgomery, R. R. (2012). Contribution of platelet versus endothelial VWF to platelet adhesion and hemostasis. *Journal of Thrombosis and Haemostasis*, *10*(8), 1646–1652.

Kane, R. S., Takayama, S., Ostuni, E., Ingber, D. E., & Whitesides, G. M. (1999). Patterning proteins and cells using soft lithography. *Biomaterials*, *20*(23–24), 2363–2376.

Kango, S., Kalia, S., Celli, A., Njuguna, J., Habibi, Y., & Kumar, R. (2013). Surface modification of inorganic nanoparticles for development of organic-inorganic nanocomposites—A review. *Progress in Polymer Science*, *38*(8), 1232–1261. Available from https://doi.org/10.1016/j.progpolymsci.2013.02.003, Retrieved from.

Kasendra, M., Tovaglieri, A., Sontheimer-Phelps, A., Jalili-Firoozinezhad, S., Bein, A., Chalkiadaki, A., et al. (2018). Development of a primary human small intestine-on-a-chip using biopsy-derived organoids. *Scientific Reports*, *8*, 2871.

Khademhosseini, A., Eng, G., Yeh, J., Fukuda, J., Blumling, J., Langer, R., & Burdick, J. A. (2006). Micromolding of photocrosslinkable hyaluronic acid for cell encapsulation and entrapment. *Journal of Biomedical Materials Research Part A*, *79*, 522–532.

Khademhosseini, A., Eng, G., Yeh, J., Kucharczyk, P. A., Langer, R., Vunjak-Novakovic, G., & Radisic, M. (2007). Microfluidic patterning for fabrication of contractile cardiac organoids. *Biomedical Microdevices*, *9*(2), 149–157.

Khademhosseini, A., Suh, K. Y., Jon, S., Eng, G., Yeh, J., Chen, G. J., & Langer, R. (2004). A soft lithographic approach to fabricate patterned microfluidic channels. *Analytical Chemistry*, *76*(13), 3675–3681.

Khademhosseini, A., Yeh, J., Jon, S., Eng, G., Suh, K. Y., Burdick, J. A., & Langer, R. (2004). Molded polyethylene glycol microstructures for capturing cells within microfluidic channels. *Lab on a Chip*, *4*(5), 425.

Khetani, S. R., & Bhatia, S. N. (2008). Microscale culture of human liver cells for drug development. *Nature Biotechnology*, *26*, 120–126.

Khnouf, R., Karasneh, D., & Albiss, B. A. (2016). Protein immobilization on the surface of polydimethylsiloxane and polymethyl methacrylate microfluidic devices. *Electrophoresis*, *37*(3), 529–535.

Kim, D., Karns, K., Tia, S. Q., He, M., & Herr, A. E. (2012). Electrostatic protein immobilization using charged polyacrylamide gels and cationic detergent microfluidic western blotting. *Analytical Chemistry*, *84*, 2533–2540.

Kim, H. J., Huh, D., Hamilton, G., & Ingber, D. E. (2012). Human gut-on-a-chip inhabited by microbial flora that experiences intestinal peristalsis-like motions and flow. *Lab on a Chip*, *12*, 2165–2174.

Kim, H. J., Li, H., Collins, J. J., & Ingber, D. E. (2016). Contributions of microbiome and mechanical deformation to intestinal bacterial overgrowth and inflammation in a human gut-on-a-chip. *Proceedings of the National Academy of Sciences of the United States of America*, *113*, E7–E15.

Kim, J., Hegde, M., & Jayaraman, A. (2010). Co-culture of epithelial cells and bacteria for investigating host–pathogen interactions. *Lab on a Chip*, *10*, 43–50.

Kim, J., Jensen, E. C., Megens, M., Boser, B., & Mathies, R. A. (2011). Integrated microfluidic bioprocessor for solid phase capture immunoassays. *Lab on a Chip*, *11*(18), 3106–3112. Retrieved from <http://www.ncbi.nlm.nih.gov/pubmed/21804972>.

Kim, P., Jeong, H. E., Khademhosseini, A., & Suh, K. Y. (2006). Fabrication of non-biofouling polyethylene glycol micro- and nanochannels by ultraviolet-assisted irreversible sealing. *Lab on a Chip*, *6*, 1432–1437.

Kim, S., Kim, H. J., & Jeon, N. L. (2010). Biological applications of microfluidic gradient devices. *Integrative Biology*, *2*(11–12), 584–603. Available from https://doi.org/10.1039/C0IB00055H, Retrieved from.

Kind, M., & Wöll, C. (2009). Organic surfaces exposed by self-assembled organothiol monolayers: Preparation, characterization, and application. *Progress in Surface Science*, *84*(7), 230–278. Retrieved from <http://www.sciencedirect.com/science/article/pii/S0079681609000471>.

Ko, T. M., Lin, J. C., & Cooper, S. L. (1993). Surface characterization and platelet adhesion studies of plasma-carboxylated polyethylene. *Journal of Colloid And Interface Science*, *156*(1), 207–217.

Koh, W. G., & Pishko, M. (2005). Immobilization of multi-enzyme microreactors inside microfluidic devices. *Sensors and Actuators, B: Chemical*, *106*, 335–342.

Kovach, K. M., Capadona, J. R., Gupta, A. S., & Potkay, J. A. (2014). The effects of PEG-based surface modification of PDMS microchannels on long-term hemocompatibility. *Journal of Biomedical Materials Research Part A*, *102*, 4195–4205.

Krasnoslobodtsev, A. V., & Smirnov, S. N. (2002). Effect of water on silanization of silica by trimethoxysilanes. *Langmuir*, *18*(8), 3181–3184.

Krause, B. D. S., Fackler, M. J., Civin, C. I., & May, W. S. (2018). CD34: Structure, biology, and clinical utility. *Blood*, *87*(1), 1–13.

Ku, S. H., Lee, J. S., & Park, C. B. (2010). Spatial control of cell adhesion and patterning through mussel-inspired surface modification by polydopamine. *Langmuir*, *26*, 15104–15108.

Ku, T. H., Zhang, T., Luo, H., Yen, T. M., Chen, P. W., Han, Y., & Lo, Y. H. (2015). Nucleic acid aptamers: An emerging tool for biotechnology and biomedical sensing. *Sensors (Switzerland)*, *15*(7), 16281–16313.

Kühn, G., Weidner, S., Decker, R., Ghode, A., & Friedrich, J. (1999). Selective surface functionalization of polyolefins by plasma treatment followed by chemical reduction. *Surface and Coatings Technology*, *116–119*, 796–801.

Kumar, A., Srivastava, A., Galaev, I. Y., & Mattiasson, B. (2007). Smart polymers: Physical forms and bioengineering applications. *Progress in Polymer Science*, *32*(10), 1205–1237.

Kumar, A., & Whitesides, G. M. (1993). Features of gold having micrometer to centimeter dimensions can be formed through a combination of stamping with an elastomeric stamp and an alkanethiol "ink" followed by chemical etching. *Applied Physics Letters*, *63*(14), 2002–2004.

Landgraf, R., Kaiser, M. K., Posseckardt, J., Adolphi, B., & Fischer, W. J. (2009). Functionalization of polymer sensor surfaces by oxygen plasma treatment. *Procedia Chemistry*, *Vol. 1*, 1015–1018.

Launiere, C., Gaskill, M., Czaplewski, G., Myung, J. H., Hong, S., & Eddington, D. T. (2012). Channel surface patterning of alternating biomimetic protein combinations for enhanced microfluidic tumor cell isolation. *Analytical Chemistry*, *84*, 4022−4028.

Lavrich, D. J., Wetterer, S. M., Bernasek, S. L., & Scoles, G. (1998). Physisorption and chemisorption of alkanethiols and alkyl sulfides on Au(111). *The Journal of Physical Chemistry B*, *102*, 3456−3465.

Lee, A. G., Arena, C. P., Beebe, D. J., & Palecek, S. P. (2010). Development of macroporous poly(ethylene glycol) hydrogel arrays within microfluidic channels. *Biomacromolecules*, *11*, 3316−3324.

Lee, A. G., Beebe, D. J., & Palecek, S. P. (2012). Quantification of kinase activity in cell lysates via photopatterned macroporous poly(ethylene glycol) hydrogel arrays in microfluidic channels. *Biomedical Microdevices*, *14*, 247−257.

Lee, J. M., Kim, J., Kang, E., Lee, S., & Chung, B. G. (2011). An integrated microfluidic culture device to regulate endothelial cell differentiation from embryonic stem cells. *Electrophoresis*, *32*(22), 3133−3137.

Lee, W., Debasitis, J. C., Lee, V. K., Lee, J. H., Fischer, K., Edminster, K., et al. (2009). Multi-layered culture of human skin fibroblasts and keratinocytes through three-dimensional freeform fabrication. *Biomaterials*, *30*, 1587−1595.

Leslie, D. C., Waterhouse, A., Berthet, J. B., Valentin, T. M., Watters, A. L., Jain, A., et al. (2014). A bioinspired omniphobic surface coating on medical devices prevents thrombosis and biofouling. *Nature Biotechnology*, *32*, 1134. Available from https://doi.org/10.1038/nbt.3020, Retrieved from.

Lessel, M., Bäumchen, O., Klos, M., Hähl, H., Fetzer, R., Paulus, M., et al. (2015). Self-assembled silane monolayers: An efficient step-by-step recipe for high-quality low energy surfaces. *Surface and Interface Analysis*, *47*, 557−564.

Lewis, C. L., Lin, Y., Yang, C., Manocchi, A. K., Yuet, K. P., Doyle, P. S., & Yi, H. (2010). Microfluidic fabrication of hydrogel microparticles containing functionalized viral nanotemplates. *Langmuir*, *26*(16), 13436−13441.

Li, K., Veres, T., Didar, T. F., & Tabrizian, M. (2016). Peristaltic pump mcrofluidc separator field. United States.

Li, P., Gao, Y., & Pappas, D. (2011). Negative enrichment of target cells by microfluidic affinity chromatography. *Analytical Chemistry*, *83*(20), 7863−7869.

Li, W., Gao, Y., & Pappas, D. (2015). A complementary method to CD4 counting: Measurement of CD4 + /CD8 + T lymphocyte ratio in a tandem affinity microfluidic system. *Biomedical Microdevices*, *17*(6), 113.

Liu, B., Huang, P. J. J., Kelly, E. Y., & Liu, J. (2016). Graphene oxide surface blocking agents can increase the DNA biosensor sensitivity. *Biotechnology Journal*, *11*, 780−787.

Liu, B., Huang, P. J. J., Zhang, X., Wang, F., Pautler, R., Ip, A. C. F., & Liu, J. (2013). Parts-per-million of polyethylene glycol as a non-interfering blocking agent for homogeneous biosensor development. *Analytical Chemistry*, *85*, 10045−10050.

Liu, V. A., & Bhatia, S. N. (2002). Three-dimensional photopatterning of hydrogels containing living cells. *Biomedical Microdevices*, *4*(4), 257−266.

Liu, Y., Germain, T., & Pappas, D. (2014). Microfluidic antibody arrays for simultaneous cell separation and stimulus. *Analytical and Bioanalytical Chemistry*, *406*(30), 7867−7873.

Liu, Z., Xiao, L., Xu, B., Zhang, Y., Mak, A. F. T., Li, Y., et al. (2012). Covalently immobilized biomolecule gradient on hydrogel surface using a gradient generating microfluidic device for a quantitative mesenchymal stem cell study. *Biomicrofluidics*, *6*, 24111−2411112.

Liu, Z.-Z., Wang, Q., Liu, X., & Bao, J.-Q. (2008). Effects of amino-terminated self-assembled monolayers on nucleation and growth of chemical vapor-deposited copper films. *Thin Solid Films*, *517*(2), 635−640. Retrieved from <http://www.sciencedirect.com/science/article/pii/S0040609008007748>.

Lovchik, R., Von Arx, C., Viviani, A., & Delamarche, E. (2008). Cellular microarrays for use with capillary-driven microfluidics. *Analytical and Bioanalytical Chemistry*, *390*(3), 801−808.

Luong, J. H. T., Male, K. B., & Glennon, J. D. (2008). Biosensor technology: Technology push versus market pull. *Biotechnology Advances*, *26*, 492−500.

Mack, J. D., Yehualaeshet, T., Park, M. K., Tameru, B., Samuel, T., & Chin, B. A. (2017). Phage-based biosensor and optimization of surface blocking agents to detect *Salmonella typhimurium* on romaine lettuce. *Journal of Food Safety*, *37*, e12299.

Mahmood, T., & Yang, P. C. (2012). Western blot: Technique, theory, and trouble shooting. *North American Journal of Medical Sciences*, *4*, 429−434.

Mao, H., Cremer, P. S., & Manson, M. D. (2003). A sensitive, versatile microfluidic assay for bacterial chemotaxis. *Proceedings of the National Academy of Sciences of the United States of America*, *100*(9), 5449−5454. Retrieved from <http://www.pnas.org/content/100/9/5449.abstract>.

May, S., Evans, S., & Parry, L. (2017). Organoids, organs-on-chips and other systems, and microbiota. *Emerging Topics in Life Sciences*, *1*, 385−400.

Meyvantsson, I., & Beebe, D. J. (2008). Cell culture models in microfluidic systems. *Annual Review of Analytical Chemistry*, *1*, 423−449.

Mithieux, S. M., Rasko, J. E. J., & Weiss, A. S. (2004). Synthetic elastin hydrogels derived from massive elastic assemblies of self-organized human protein monomers. *Biomaterials*, *25*, 4921−7927.

Mohammad, K., & Esen, A. (1989). A blocking agent and a blocking step are not needed in ELISA, immunostaining dot-blots and Western blots. *Journal of Immunological Methods*, *117*, 141−145.

Mrksich, M., Dike, L. E., Tien, J., Ingber, D. E., & Whitesides, G. M. (1997). Using microcontact printing to pattern the attachment of mammalian cells to self-assembled monolayers of alkanethiolates on transparent films of gold and silver. *Experimental Cell Research*, *235*(2), 305−313.

Mrksich, M., & Whitesides, G. M. (1995). Patterning self-assembled monolayers using microcontact printing: A new technology for biosensors?. *Trends in Biotechnology*, *13*(6), 228−235.

Mueller-Klieser, W. (1997). Three-dimensional cell cultures: From molecular mechanisms to clinical applications. *American Journal of Physiology*, *273*, C1109−C1123.

Musah, S., Mammoto, A., Ferrante, T. C., Jeanty, S. S. F., Hirano-Kobayashi, M., Mammoto, T., et al. (2017). Mature induced-pluripotent-stem-cell-derived human podocytes reconstitute kidney glomerular-capillary-wall function on a chip. *Nature Biomedical Engineering*, *1*, 69. Available from https://doi.org/10.1038/s41551-017-0069, Retrieved from.

Nagrath, S., Sequist, L. V., Maheswaran, S., Bell, D. W., Irimia, D., Ulkus, L., et al. (2007). Isolation of rare circulating tumour cells in cancer patients by microchip technology. *Nature*, *450*(7173), 1235−1239.

Nakashima, Y., & Yasuda, T. (2007). Cell differentiation guidance using chemical stimulation controlled by a microfluidic device. *Sensors and Actuators A: Physical*, *139*(1), 252−258. Retrieved from <http://www.sciencedirect.com/science/article/pii/S0924424707004414>.

Ng, E., Hoshino, K., & Zhang, X. (2013). Microfluidic immunodetection of cancer cells via site-specific microcontact printing of antibodies on nanoporous surface. *Methods*, *63*(3), 266−275.

Nichol, J. W., Koshy, S. T., Bae, H., Hwang, C. M., Yamanlar, S., & Khademhosseini, A. (2010). Cell-laden microengineered gelatin methacrylate hydrogels. *Biomaterials*, *31*, 5536–5544.

Nie, F. Q., Yamada, M., Kobayashi, J., Yamato, M., Kikuchi, A., & Okano, T. (2007). On-chip cell migration assay using microfluidic channels. *Biomaterials*, *28*(27), 4017–4022.

Noah, B., Keller, M. S., Mosadeghi, S., Stein, L., Johl, S., Delshad, S., et al. (2017). Impact of remote patient monitoring on clinical outcomes: An updated meta-analysis of randomized controlled trials. *npj Digital Medicine*, *1*(1), 2. Retrieved from <http://www.nature.com/articles/s41746-017-0002-4>.

Notsu, H., Fukazawa, T., Tatsuma, T., Tryk, D. A., & Fujishima, A. (2001). Hydroxyl groups on boron-doped diamond electrodes and their modification with a silane coupling agent. *Electrochemical and Solid-State Letters*, *4*(3), H1.

Ofner, A., Moore, D. G., Rühs, P. A., Schwendimann, P., Eggersdorfer, M., Amstad, E., et al. (2017). High-throughput step emulsification for the production of functional materials using a glass microfluidic device. *Macromolecular Chemistry and Physics*, *218*(2), 1–10.

Olsen, K. G., Ross, D. J., & Tarlov, M. J. (2002). Immobilization of DNA hydrogel plugs in microfluidic channels. *Analytical Chemistry*, *74*, 1436–1441.

Ozdemir, M., Yurteri, C. U., & Sadikoglu, H. (1999). Physical polymer surface modification methods and applications in food packaging polymers. *Critical Reviews in Food Science and Nutrition*, *39*(5), 457–477.

Palchesko, R. N., Zhang, L., Sun, Y., & Feinberg, A. W. (2012). Development of polydimethylsiloxane substrates with tunable elastic modulus to study cell mechanobiology in muscle and nerve. *PLoS One*, *7*, e51499.

Pampaloni, F., Reynaud, E. G., & Stelzer, E. H. K. (2007). The third dimension bridges the gap between cell culture and live tissue. *Nature Reviews Molecular Cell Biology*, *8*, 839–845.

Parikh, A. N., Allara, D. L., Azouz, I. B., & Rondelez, F. (1994). An intrinsic relationship between molecular structure in self-assembled *n*-alkylsiloxane monolayers and deposition temperature. *The Journal of Physical Chemistry*, *98*(31), 7577–7590.

Park, J. J., Luo, X., Yi, H., Valentine, T. M., Payne, G. F., Bentley, W. E., et al. (2006). Chitosan-mediated in situ biomolecule assembly in completely packaged microfluidic devices. *Lab on a Chip*, *6*, 1315–1321.

Patel, A., Fine, B., Sandig, M., & Mequanint, K. (2006). Elastin biosynthesis: The missing link in tissue-engineered blood vessels. *Cardiovascular Research*, *71*, 40–49.

Peppas, N. A., Hilt, J. Z., Khademhosseini, A., & Langer, R. (2006). Hydrogels in biology and medicine: From molecular principles to bionanotechnology. *Advanced Materials*, *18*, 1345–1360.

Piao, Y., Han, D. J., Azad, M. R., Park, M., & Seo, T. S. (2015). Enzyme incorporated microfluidic device for in-situ glucose detection in water-in-air microdroplets. *Biosensors and Bioelectronics*, *65*, 220–225.

Plouffe, B. D., Kniazeva, T., Mayer, J. E., Murthy, S. K., & Sales, V. L. (2009). Development of microfluidics as endothelial progenitor cell capture technology for cardiovascular tissue engineering and diagnostic medicine. *The FASEB Journal*, *23*(10), 3309–3314.

Plouffe, B. D., Njoka, D. N., Harris, J., Liao, J., Horick, N. K., Radisic, M., & Murthy, S. K. (2007). Peptide-mediated selective adhesion of smooth muscle and endothelial cells in microfluidic shear flow. *Langmuir*, *23*(9), 5050–5055.

Plouffe, B. D., Radisic, M., & Murthy, S. K. (2008). Microfluidic depletion of endothelial cells, smooth muscle cells, and fibroblasts from heterogeneous suspensions. *Lab on a Chip*, *8*(3), 462.

Pratt, E. D., Huang, C., Hawkins, B. G., Gleghorn, J. P., & Kirby, B. J. (2011). Rare cell capture in microfluidic devices. *Chemical Engineering Science*, *66*(7), 1508–1522.

Prieto-Simín, B., Campàs, M., & Marty, J.-L. (2008). Biomolecule immobilization in biosensor development: Tailored strategies based on affinity interactions. *Protein and Peptide Letters*, *15*(8), 757–763.

Puchberger-Enengl, D., Krutzler, C., Keplinger, F., & Vellekoop, M. J. (2014). Single-step design of hydrogel-based microfluidic assays for rapid diagnostics. *Lab on a Chip*, *14*, 378–383.

Qian, Z., Bai, H. J., Wang, G. L., Xu, J. J., & Chen, H. Y. (2010). A photoelectrochemical sensor based on CdS-polyamidoamine nano-composite film for cell capture and detection. *Biosensors and Bioelectronics*, *25*(9), 2045–2050.

Rahmani, S. (2011). *Design of coated magnetic iron-oxide nanogels for drug delivery systems, University of Waterloo, Canada (MASc's thesis)*.

Rahmani, S., Breyner, N. M., Su, H.-M., Verdu, E. F., & Didar, T. F. (2019). Intestinal organoids: A new paradigm for engineering intestinal epithelium in vitro. *Biomaterials*, *194*, 195–214.

Riquelme, M. V., Zhao, H., Srinivasaraghavan, V., Pruden, A., Vikesland, P., & Agah, M. (2016). Optimizing blocking of nonspecific bacterial attachment to impedimetric biosensors. *Sensing and Bio-Sensing Research*, *8*, 47–54. Retrieved from <http://www.sciencedirect.com/science/article/pii/S2214180416300356>.

Rivet, C., Lee, H., Hirsch, A., Hamilton, S., & Lu, H. (2011). Microfluidics for medical diagnostics and biosensors. *Chemical Engineering Science*, *66*(7), 1490–1507.

Rosen, M. J., & Kunjappu, J. T. (2012). *Surfactants and interfacial phenomena* (4th ed.). John Wiley & Sons.

Roy, S., Yue, C. Y., Venkatraman, S. S., & Ma, L. L. (2013). Fabrication of smart COC chips: Advantages of *N*-vinylpyrrolidone (NVP) monomer over other hydrophilic monomers. *Sensors and Actuators, B: Chemical*, *178*, 86–95.

Sang, C. H., Chou, S. J., Pan, F. M., & Sheu, J. T. (2016). Fluorescence enhancement and multiple protein detection in ZnO nanostructure microfluidic devices. *Biosensors and Bioelectronics*, *75*, 285–292. Retrieved from <http://www.sciencedirect.com/science/article/pii/S0956566315303754>.

Santini, G. C., Potrich, C., Lunelli, L., Vanzetti, L., Marasso, S. L., Cocuzza, M., et al. (2017). miRNA purification with an optimized PDMS microdevice: Toward the direct purification of low abundant circulating biomarkers. *Biophysical Chemistry*, *229* (March), 142–150.

Sassolas, A., Blum, L. J., & Leca-Bouvier, B. D. (2012). Immobilization strategies to develop enzymatic biosensors. *Biotechnology Advances*, *30*, 489–511.

Schroeder, M. E., Zurick, K. M., McGrath, D. E., & Bernards, M. T. (2013). Multifunctional polyampholyte hydrogels with fouling resistance and protein conjugation capacity. *Biomacromolecules*, *14*, 3112–3122.

Schultze, M., Fieß, M., Karpowicz, N., Gagnon, J., Korbman, M., Hofstetter, M., et al. (2010). Delay in photoemission. *Science*, *328*, 1658–1662.

Séguin, C., McLachlan, J. M., Norton, P. R., & Lagugné-Labarthet, F. (2010). Surface modification of poly(dimethylsiloxane) for microfluidic assay applications. *Applied Surface Science*, *256*(8), 2524–2531.

Sellers, H., Ulman, A., Shnidman, Y., & Eilers, J. E. (1993). Structure and binding of alkanethiolates on gold and silver surfaces: Implications for self-assembled monolayers. *Journal of the American Chemical Society*, *115*(21), 9389–9401.

Serizawa, T., Kamimura, S., & Akashi, M. (2000). Electrostatic adsorption of polystyrene particles with different surface charges onto the surface of an ultrathin polymer film. *Colloids and Surfaces A: Physicochemical and Engineering Aspects*, *164*(2), 237–245. Retrieved from <http://www.sciencedirect.com/science/article/pii/S0927775799003994>.

Sethi, R. S. (1994). Transducer aspects of biosensors. *Biosensors and Bioelectronics*, *9*(3), 243–264.

Shah, A. M., Yu, M., Nakamura, Z., Ciciliano, J., Ulman, M., Kotz, K., et al. (2012). Biopolymer system for cell recovery from microfluidic cell capture devices. *Analytical Chemistry*, *84*, 3682–3688.

Shah, P., Fritz, J. V., Glaab, E., Desai, M. S., Greenhalgh, K., Frachet, A., et al. (2016). A microfluidics-based in vitro model of the gastrointestinal human-microbe interface. *Nature Communications*, *7*, 11535.

Shakeri, A., Sun, N., Badv, M., & Didar, T. F. (2017). Generating 2-dimensional concentration gradients of biomolecules using a simple microfluidic design. *Biomicrofluidics*, *11* (4), 044111. Retrieved from http://aip.scitation.org/doi/10.1063/1.4991550.

Shakeri, A., Yip, D., Badv, M., Imani, S. M., Sanjari, M., & Didar, T. F. (2018). Self-cleaning ceramic tiles produced via stable coating of TiO_2 nanoparticles. *Materials (Basel)*, *11*, 1003.

Shi, P., Nedelec, S., Wichterle, H., & Kam, L. C. (2010). Combined microfluidics/protein patterning platform for pharmacological interrogation of axon pathfinding. *Lab on a Chip*, *10*(8), 1005.

Shi, X., Ostrovidov, S., Shu, Y., Liang, X., Nakajima, K., Wu, H., & Khademhosseini, A. (2014). Microfluidic generation of polydopamine gradients on hydrophobic surfaces. *Langmuir*, *30*(3), 832–838.

Shin, Y., Han, S., Jeon, J. S., Yamamoto, K., Zervantonakis, I. K., Sudo, R., et al. (2012). Microfluidic assay for simultaneous culture of multiple cell types on surfaces or within hydrogels. *Nature Protocols*, *7*(7), 1247–1259.

Singhvi, R., Kumar, A., Lopez, G. P., Stephanopoulos, G. N., Wang, D. I. C., Whitesides, G. M., et al. (1994). Engineering cell shape and function. *Science*, *264*(5159), 696–698. <http://www.jstor.org/stable/2883517>.

Siow, K. S., Britcher, L., Kumar, S., & Griesser, H. J. (2006). Plasma methods for the generation of chemically reactive surfaces for biomolecule immobilization and cell colonization—A review. *Plasma Processes and Polymers*, *3*, 392–418.

Somaweera, H., Ibraguimov, A., & Pappas, D. (2016). A review of chemical gradient systems for cell analysis. *Analytica Chimica Acta*, *907*, 7–17. Available from https://doi.org/10.1016/j.aca.2015.12.008, Retrieved from.

Song, J. W., Gu, W., Futai, N., Warner, K. A., Nor, J. E., & Takayama, S. (2005). Computer-controlled microcirculatory support system for endothelial cell culture and shearing. *Analytical Chemistry*, *77*, 3993–3999.

Srinivasan, U., Houston, M. R., Howe, R. T., & Maboudian, R. (1998). Alkyltrichlorosilane-based self-assembled monolayer films for stiction reduction in silicon micromachines. *Journal of Microelectromechanical Systems*, *7*(2), 252–260.

St. John, P. M., Kam, L., Turner, S. W., Craighead, H. G., Issacson, M., Turner, J. N., & Shain, W. (1997). Preferential glial cell attachment to microcontact printed surfaces. *Journal of Neuroscience Methods*, *75*(2), 171–177.

Steinitz, M. (2000). Quantitation of the blocking effect of Tween 20 and bovine serum albumin in ELISA microwells. *Analytical Biochemistry*, *282*, 232–238.

Sui, G., Wang, J., Lee, C. C., Lu, W., Lee, S. P., Leyton, J. V., et al. (2006). Solution-phase surface modification in intact poly(dimethylsiloxane) microfluidic channels. *Analytical Chemistry*, *78*, 5543–5551.

Sung, W.-C., Chen, H.-H., Makamba, H., & Chen, S.-H. (2009). Functionalized 3D-hydrogel plugs covalently patterned inside hydrophilic poly(dimethylsiloxane) microchannels for flow-through immunoassays. *Analytical Chemistry*, *81*, 7967–7973.

Takayama, S., McDonald, J. C., Ostuni, E., Liang, M. N., Kenis, P. J. A., Ismagilov, R. F., & Whitesides, G. M. (1999). Patterning cells and their environments using multiple laminar fluid flows in capillary networks. *Proceedings of the National Academy of Sciences of the United States of America*, *96*(10), 5545–5548. Retrieved from http://www.pnas.org/cgi/doi/10.1073/pnas.96.10.5545.

Tan, W., & Desai, T. A. (2003). Microfluidic patterning of cellular biopolymer matrices for biomimetic 3-D structures. *Biomedical Microdevices*, *5*(3), 235–244.

Tan, W., & Desai, T. A. (2004). Layer-by-layer microfluidics for biomimetic three-dimensional structures. *Biomaterials*, *25*(7–8), 1355–1364.

Tan, X., Khaing Oo, M. K., Gong, Y., Li, Y., Zhu, H., & Fan, X. (2017). Glass capillary based microfluidic ELISA for rapid diagnostics. *Analyst*, *142*(13), 2378–2385. Available from https://doi.org/10.1039/C7AN00523G, Retrieved from.

Taylor, S., Smith, S., Windle, B., & Guiseppi-Elie, A. (2003). Impact of surface chemistry and blocking strategies on DNA microarrays. *Nucleic Acids Research*, *31*(16). Available from https://doi.org/10.1093/nar/gng086, e87–e87. Retrieved from.

Terlingen, J. G. A., Gerritsen, H. F. C., Hoffman, A. S., & Feijen, J. (1995). Introduction of functional groups on polyethylene surfaces by a carbon dioxide plasma treatment. *Journal of Applied Polymer Science*, *57*(8), 969–982.

Thiébaud, P., Lauer, L., Knoll, W., & Offenhäusser, A. (2002). PDMS device for patterned application of microfluids to neuronal cells arranged by microcontact printing. *Biosensors and Bioelectronics*, *17*(1–2), 87–93.

Tia, S. Q., He, M., Kim, D., & Herr, A. E. (2011). Multianalyte on-chip native western blotting. *Analytical Chemistry*, *83*, 3581–3588.

Torres, I., Eland, L., Redfern, C., & Hedley, J. (2017). Design of a mems device for studying cell migration and differentiation. *Sensors*, *2*(1), 17–19.

Tourovskaia, A., Figueroa-Masot, X., & Folch, A. (2005). Differentiation-on-a-chip: A microfluidic platform for long-term cell culture studies. *Lab on a Chip*, *5*(1), 14–19. Available from https://doi.org/10.1039/B405719H, Retrieved from.

Tran, T. B., Cho, S. B., & Min, J. (2013). Hydrogel-based diffusion chip with electric cell-substrate impedance sensing (ECIS) integration for cell viability assay and drug toxicity screening. *Biosensors and Bioelectronics*, *50*, 453–459.

Tu, C., Huang, B., Zhou, J., Liang, Y., Tian, J., Ji, L., et al. (2017). A microfluidic chip for cell patterning utilizing paired microwells and protein patterns. *Micromachines*, *8*(1), 1–15.

Vallant, T., Brunner, H., Mayer, U., Hoffmann, H., Leitner, T., Resch, R., & Friedbacher, G. (1998). Formation of self-assembled octadecylsiloxane monolayers on mica and silicon surfaces studied by atomic force microscopy and infrared spectroscopy. *Journal of Physical Chemistry B*, *102*(37), 7190–7197.

Vashist, S. K. (2012). Comparison of 1-ethyl-3-(3-dimethylaminopropyl) carbodiimide based strategies to crosslink antibodies on amine-functionalized platforms for immunodiagnostic

applications. *Diagnostics*, *2*(4), 23−33. Retrieved from <http://www.mdpi.com/2075-4418/2/3/23/>.

Verhulsel, M., Vignes, M., Descroix, S., Malaquin, L., Vignjevic, D. M., & Viovy, J. L. (2014). A review of microfabrication and hydrogel engineering for micro-organs on chips. *Biomaterials*, *35*, 1816−1832.

Vickerman, V., Blundo, J., Chung, S., & Kamm, R. (2008). Design, fabrication and implementation of a novel multi-parameter control microfluidic platform for three-dimensional cell culture and real-time imaging. *Lab on a Chip*, *8*(9), 1468−1477. Available from https://doi.org/10.1039/B802395F, Retrieved from.

Vikholm-Lundin, I., & Piskonen, R. (2008). Binary monolayers of single-stranded oligonucleotides and blocking agent for hybridisation. *Sensors and Actuators B: Chemical*, *134* (1), 189−192. Retrieved from <http://www.sciencedirect.com/science/article/pii/S0925400508003018>.

Villegas, M., Cetinic, Z., Shakeri, A., & Didar, T. F. (2018). Fabricating smooth PDMS micro fl uidic channels from low-resolution 3D printed molds using an omniphobic lubricant-infused coating. *Analytica Chimica Acta*, *1000*, 248−255. Available from https://doi.org/10.1016/j.aca.2017.11.063, Retrieved from.

Vu, T. T., Fouet, M., Gue, A. M., & Sudor, J. (2014). A new and easy surface functionalization technnology for monitoring wettability in heterogeneous nano- and microfluidic devices. *Sensors and Actuators, B: Chemical*, *196*, 64−70.

Wang, M., Liechti, K. M., Wang, Q., & White, J. M. (2005). Self-assembled silane monolayers: Fabrication with nanoscale uniformity. *Langmuir*, *21*(5), 1848−1857.

Wang, W., & Vaughn, M. W. (2008). Morphology and amine accessibility of (3-aminopropyl) triethoxysilane films on glass surfaces. *Scanning*, *30*(2), 65−77.

Wang, Y., Wang, L., Guo, Y., Zhu, Y., & Qin, J. (2018). Engineering stem cell-derived 3D brain organoids in a perfusable organ-on-a-chip system. *RSC Advances*, *8*, 1677−1685.

Whitesides, G. M. (2006). The origins and the future of microfluidics. *Nature*, *442*, 368−373.

Workman, M. J., Gleeson, J. P., Troisi, E. J., Estrada, H. Q., Kerns, S. J., Hinojosa, C. D., et al. (2017). Enhanced utilization of induced pluripotent stem cell-derived human intestinal organoids using microengineered chips. *Cellular and Molecular Gastroenterology and Hepatology*, *5*, 669−677.e2.

Wu, D., Zhao, B., Dai, Z., Qin, J., & Lin, B. (2006). Grafting epoxy-modified hydrophilic polymers onto poly(dimethylsiloxane) microfluidic chip to resist nonspecific protein adsorption. *Lab on a Chip*, *6*(7), 942−947. Available from https://doi.org/10.1039/B600765A, Retrieved from.

Wu, J., Wang, R., Yu, H., Li, G., Xu, K., Tien, N. C., et al. (2015). Inkjet-printed microelectrodes on PDMS as biosensors for functionalized microfluidic systems. *Lab on a Chip*, *15*(3), 690−695. Available from https://doi.org/10.1039/C4LC01121J, Retrieved from.

Xu, Y., Takai, M., Konno, T., & Ishihara, K. (2007). Microfluidic flow control on charged phospholipid polymer interface. *Lab on a Chip*, *7*(2), 199−206. Available from https://doi.org/10.1039/B616851P, Retrieved from.

Xue, M., Xie, Z., Zhang, L., Ma, X., Wu, X., Guo, Y., et al. (2011). Microfluidic etching for fabrication of flexible and all-solid-state micro supercapacitor based on MnO_2 nanoparticles. *Nanoscale*, *3*(7), 2703−2708. Available from https://doi.org/10.1039/C0NR00990C, Retrieved from.

Xue, P., He, S., Mao, Y., Qu, L., Liu, F., Tan, C., et al. (2017). The optimization and characterization of an RNA-cleaving fluorogenic DNAzyme probe for MDA-MB-231 cell detection. *Sensors*, *17*(3), 650.

Yang, P., & Yang, W. (2014). Hydroxylation of organic polymer surface: Method and application. *ACS Applied Materials & Interfaces*, *6*(6), 3759−3770. Retrieved from http://pubs.acs.org/doi/abs/10.1021/am405857m.

Young, E. W. K., & Beebe, D. J. (2010). Fundamentals of microfluidic cell culture in controlled microenvironments. *Chemical Society Reviews*, *39*, 1036−1048.

Yousefi, H., Ali, M. M., Su, H.-M., Filipe, C. D. M., & Didar, T. F. (2018). Sentinel Wraps: Real-time monitoring of food contamination by printing DNAzyme probes on food packaging. *ACS Nano*, *12*(4), 3287−3294.

Yousefi, H., Su, H.-M., Ali, M., Filipe, C. D. M., & Tohid, F. D. (2018). Producing covalent microarrays of amine-conjugated DNA probes on various functional surfaces to create stable and reliable biosensors. *Advanced Materials Interfaces*, *5*, 1800659. Available from https://doi.org/10.1002/admi.201800659, Retrieved from.

Zangmeister, R. A., & Tarlov, M. J. (2003). UV graft polymerization of polyacrylamide hydrogel plugs in microfluidic channels. *Langmuir*, *19*, 6901−6904.

Zhang, C., Zhao, Z., Abdul Rahim, N. A., van Noort, D., & Yu, H. (2009). Towards a human-on-chip: Culturing multiple cell types on a chip with compartmentalized microenvironments. *Lab on a Chip*, *9*, 3185−3192.

Zhang, F., Sautter, K., Larsen, A. M., Findley, D. A., Davis, R. C., Samha, H., & Linford, M. R. (2010). Chemical vapor deposition of three aminosilanes on silicon dioxide: Surface characterization, stability, effects of silane concentration, and cyanine dye adsorption. *Langmuir*, *26*(18), 14648−14654.

Zhang, J., Sheng, W., & Fan, Z. H. (2014). An ensemble of aptamers and antibodies for multivalent capture of cancer cells. *Chemical Communications*, *50*(51), 6722−6725. Available from https://doi.org/10.1039/C4CC02002B, Retrieved from.

Zhang, Y., Li, W., Zhou, Y., Johnson, A., Venable, A., Hassan, A., et al. (2018). Detection of sepsis in patient blood samples using CD64 expression in a microfluidic cell separation device. *The Analyst*, *143*(1), 241−249.

Zhang, Z., Zhao, P., & Xiao, G. (2009). The fabrication of polymer microfluidic devices using a solid-to-solid interfacial polyaddition. *Polymer*, *50*(23), 5358−5361. Available from https://doi.org/10.1016/j.polymer.2009.09.053, Retrieved from.

Zhang, Z. L., Crozatier, C., Le Berre, M., & Chen, Y. (2005). In situ bio-functionalization and cell adhesion in microfluidic devices. *Microelectronic Engineering*, *78−79*(1−4), 556−562.

Zhanga, S., Lin, Y., Altman, M., Lässle, M., Nugent, H., Frankel, F., et al. (1999). Biological surface engineering: A simple system for cell pattern formation. *Biomaterials*, *20*(13), 1213−1220.

This page intentionally left blank